Mechanostimulation of integrin αvβ6 and fibronectin in DCIS-myoepithelial cells

Thesis submitted in partial fulfilment of the requirements of the Degree of Doctor of Philosophy

Mary-Kate Hayward

Queen Mary University of London
2018

ACKNOWLEDGEMENTS

To Prof Louise Jones; for all the opportunities ahead, for which without your continued support and kindness, would not be possible. Thank you so much.

To Dr Michael Allen; for all your support in the laboratory.

To the cell bank; Jenny Gomm, Iain Goulding, Linda Haywood and Adrienne Morgan, for the endless supply of primary breast cells.

To the tissue bank; for access to breast tissue - particularly Sally Smith, thank you for your support throughout.

To the breast group babes; Rachel Nelan, Natalie Allen, Kathryn Hawkesford and Alastair Ironside, for taking me under your wing, and making me laugh endlessly.

To my colleague Ed Carter; for your scientific support, and to my other colleagues in tumour biology and those at Barts; thank you for making this fun.

To my friends, for distracting me throughout my studies.

Most importantly, to my incredible parents; always my biggest supporters. I can never thank you enough.

STATEMENT OF ORIGINALITY

I, Mary-Kate Hayward, confirm that the research included within this thesis is my own work or that where it has been carried out in collaboration with, or supported by others, that this is duly acknowledged below and my contribution indicated. Previously published material is also acknowledged below.

I attest that I have exercised reasonable care to ensure that the work is original, and does not to the best of my knowledge break any UK law, infringe any third party's copyright or other Intellectual Property Right, or contain any confidential material.

I accept that the College has the right to use plagiarism detection software to check the electronic version of the thesis.

I confirm that this thesis has not been previously submitted for the award of a degree by this or any other university.

Signature: Mary Kate Hayward
Date: 14.11.18

Details of collaborations:

- FFPE tissue sections were cut and H&E stained by G. Elia, Barts Cancer Institute, London.
- Immunohistochemical staining of ER, PR and HER2 to identify breast cancer subtypes was performed by Dr N. Allen, Barts Cancer Institute, London.
- Parental myoepithelial cell line (Myo-1089) was obtained from Prof M. O'Hare and Prof P. Jat, Institute of Neurology, University College London, London.
- Myoepithelial cell lines; N-1089 and β6-1089 were generated by Dr M. Allen, Barts Cancer Institute, London.
- Primary normal breast cells were isolated by magnetic bead isolation by Dr J. Gomm and Mr I. Goulding, Barts Cancer Institute, London.
- Access to the Flexcell tension system was provided by Prof M. Knight, Queen Mary University of London, London.

Details of publications:

- Nelan R., **Hayward M**. and Jones JL. The growth of molecular diagnostics: stratified medicine programme, the 100,000 genomes project and the future. Diagnostic histopathology. 2017; 23(10):458-467.
- Dreger S., Allen MD., **Hayward M**., Payne SJ., Reynolds L., Robinson S., Hodivala-Dilke K. and Jones JL. Myoepithelial cells in ductal carcinoma *in situ* (DCIS) of the breast promote angiogenesis through TGFβ-mediated upregulation of MMP9. (In preparation).
- **Hayward M**., Allen MD., Gomm JJ., Knight MM., Marshall JF. and Jones JL. Mechanostimulation of integrin αvβ6 in DCIS-myoepithelial cells. (In preparation).

Details of invited oral presentations:

- Gordon research seminar: fibronectin, integrins and related molecules – California USA, 2017, 'Functional significance of integrin αvβ6 and fibronectin in DCIS-myoepithelial cells: role in progression to invasion'.
- Pathological society of Great Britain and Ireland, Belfast pathology – Belfast UK, 2017, 'Myoepithelial cell phenotype in DCIS progression: functional significance of integrin αvβ6 and fibronectin'.

Details of awards:

- Sir Alastair Currie poster prize (1st) - Pathological society of Great Britain and Ireland, Nottingham Pathology – Nottingham, UK, 2016, 'Investigating the functional significance of integrin αvβ6 and fibronectin expression in myoepithelial cells: role in the progression of DCIS'.
- Student poster prize (1st) – PhD day, Barts Cancer Institute – London, UK, 2016, 'Altered microenvironment in the progression of DCIS'.

This work was funded by the Pathological Society of Great Britain and Ireland Studentship.

ABSTRACT

Alterations to the tumour microenvironment is a common feature of many cancers, including breast cancer, and there is increasing evidence that alterations to the microenvironment, including; increased integrin expression, ECM deposition and protease activity, promote cancer progression. Most invasive breast cancers arise from a preinvasive stage, ductal carcinoma *in situ* (DCIS). Previous work in our laboratory has shown the microenvironment of DCIS is altered, such that myoepithelial cells (MECs) switch to a tumour-promoting phenotype, associated with upregulation of integrin αvβ6 and fibronectin (FN) expression. Mechanisms by which integrin αvβ6 and FN expression are regulated is unclear. We show DCIS progression into invasion is accompanied by an increase in MEC expression of integrin αvβ6 and periductal FN deposition, and their expression were associated in DCIS. These findings were modelled in isolated primary DCIS-MECs, primary normal MECs and MEC lines, with and without integrin αvβ6 expression, where integrin αvβ6-positive MECs upregulating FN expression. We identified integrin αvβ6-positive DCIS ducts were larger than integrin αvβ6-negative DCIS ducts, and mechanical stretching of primary normal MECs and a normal MEC line led to upregulation of integrin αvβ6 expression and FN deposition in a TGFβ-dependent manner. We further show upregulation of integrin αvβ6 and FN by MECs mediate TGFβ-dependent upregulation of MMP13 which promotes breast cancer cell invasion *in vitro*. These data show altered tissue mechanics in DCIS and MEC expression of integrin αvβ6 and FN deposition are linked, and implicate TGFβ in their activation. These findings suggest integrin αvβ6 and FN may be used as markers to stratify DCIS patients.

CONTENTS

LIST OF FIGURES

LIST OF TABLES

LIST OF ABBREVIATIONS

β1	I-like domain
βME	beta-mercaptoethanol
βTD	Membrane proximal beta tail domain
IIICS	Type III connecting segment
ABC	Avidin-biotin complex
aCGH	Array-comparative genomic hybridisation
ADAM	A disintegrin and metalloproteinase
ADAMT	ADAM with thrombospondin domain
ADH	Atypical ductal hyperplasia
AFM	Atomic force microscopy
AKT	Protein kinase B
ALH	Atypical lobular hyperplasia
AMH	Anti-Mullerian hormone
APC	Allophycocyanin
APS	Ammonia persulphate
BM	Basement membrane
BMP	Bone morphogenic protein
BPE	Bovine pituitary extract
BSA	Bovine serum albumin
CAR	Cell adhesion recognition
CBD	Cell binding domain
cCM	Concentrated conditioned media
CD	Cluster of differentiation
CDK	Cyclin-dependent kinase
cDNA	Complementary DNA
cFN	Cellular fibronectin
CGH	Comparative genomic hybridisation
CK	Cytokeratin
CM	Conditioned media
COL	Collagen
Co-SMAD	Common mediator-SMAD
CT	Cycle threshold
CTGF	Connective tissue growth factor
DAPI	4’,6-diamidino-2-phenylindole
DAPK	Death associated protein kinase
DCIS	Ductal carcinoma *in situ*
DDR	Discoidin domain receptor
DMEM	Dulbecco’s modified eagle medium
DMSO	Dimethyl sulphoxide
dNTP	Deoxynucleotide
DOC	Deoxycholate
DPX	Distyene-tricresyl phosphate-xylene
DSC	Desmocollin

DSG	Demoglein
ECL	Enhanced chemiluminescence
ECM	Extracellular matrix
EDA	Extradomain A
EDB	Extradomain B
EDGIHEL	Glu-Asp-Gly-Ile-His-Glu-Leu
EDTA	Ethylenediaminetetraacetic acid
EE	Early endosome
EEA	Early endosome antigen
EGF	Epidermal growth factor
EGFR	Epidermal growth factor receptor
EMT	Epithelial-to-mesenchymal transition
EpCAM	Epithelial cell adhesion molecular
ER	Oestrogen receptor
ERK	Extracellular signal-regulated protein kinase
ESA	Epithelial specific antigen
F-12	Nutrient mixture hams F-12
FA	Focal adhesion
FACS	Fluorescence-activated cell sorting
FAK	Focal adhesion kinase
FAS	First apoptosis signal
FB	Fibrillar adhesion
FBN	Fibrillin
FBS	Foetal bovine serum
FEA	Flat epithelial atypia
FFPE	Formalin-fixed paraffin-embedded
FGF	Fibroblast growth factor
FGFR	Fibroblast growth factor receptor
FN	Fibronectin
FX	Focal complex
GADD45β	Growth arrest and DNA damage inducible 45β
GDF	Growth and differentiation factor
GFFKR	Gly-Phe-Phe-Lys-Arg
GPI	Glycosylphosphatidylinositol
HDR(R/K)E	His-Asp-Arg(Arg/Lys)Glu
H&E	Haematoxylin and eosin
HER2	Human epidermal growth factor receptor 2
HPV	Human papilloma virus
HRP	Horse radish peroxidase
HSC70	Heat shock cognate 70
IAC	Integrin adhesion complex
IDC	Invasive ductal carcinoma
I-domain	Insertion domain
IGF	Insulin-like growth factor

IGFBP	Insulin-like growth factor-binding protein
ILC	Invasive lobular carcinoma
IMP	Inhibitor of metalloproteinase
I-SMAD	Inhibitory-SMAD
ISH	*In situ* hybridisation
LAP	Latency associated peptide
LCM	Laser capture microdissection
LDV	Leu-Asp-Val
LEC	Luminal epithelial cell
LCIS	Lobular carcinoma *in situ*
LIMP	Large inhibitor of metalloproteinase
LLC	Large latent complex
LN	Laminin
LOH	Loss of heterozygosity
LOX	Lysyl oxidase
lrECM	Laminin-rich extracellular matrix
LTBP	Latent TGFβ binding protein
MAPK	Mitogen-activated protein kinase
MEC	Myoepithelial cell
Mg	Magnesium
MIDAS	Metal-ion dependent adhesion site
M-MLV	Moloney-murine leukaemia virus
MMP	Matrix metalloproteinase
Mn	Manganese
MSI	Microsatellite instability
MT-MMP	Membrane-type matrix metalloproteinase
MUC	Mucin
MWCO	Molecular weight cut off
ns	Not significant
NSCLC	Non-small cell lung cancer
NTC	Non-targeting control
PBS	Phosphate buffered saline
PE	Phycoerythrin
pFN	Plasma fibronectin
PHSRN	Pro-His-Ser-Arg-Asn
PI3K	Phosphoinositide 3-kinase
PR	Progesterone receptor
PSI	Plexin/semaphorin/integrin
p-SMAD	Phosphorylated SMAD
PTB	Phosphotyrosine-binding
PTHrH	Parathyroid hormone-related protein
qRT-PCR	Quantitative real-time polymerase chain reaction
RANK	Receptor activation of nuclear factor kappa-beta
RANKL	Receptor activation of nuclear factor kappa-beta ligand

REDV	Arg-Glu-Asp-Val
RGD	Arg-Gly-Asp
RIPA	Radio-immunoprecipitation assay
R-SMAD	Receptor regulated-SMAD
rt	Room temperature
RT	Reverse transcription
SAGE	Serial analysis of gene expression
SARA	SMAD2 anchor for receptor activation
SBE	SMAD binding element
SDS	Sodium dodecyl sulphate
SEM	Standard error of the mean
SGF	Serum and growth factor-free
SIMP	Small inhibitor of metalloproteinase
siRNA	Small interfering RNA
SLC	Small latent complex
SMA	Smooth muscle actin
SMAD	Small mothers against decapentaplegic
SM-MHC	Smooth muscle-myosin heavy chain
SMURF	SMAD ubiquitin regulatory factor
SNP	Single nucleotide polymorphism
TB	TGFβ-binding protein like
TBS	Tris buffered saline
TBS-T	Tris buffered saline-tween
TD	Terminal duct
TDLU	Terminal-ductal lobular unit
TEMED	Tetramethylethylenediamine
TFN	Total fibronectin
TGFβ	Transforming growth factor-beta
TGFβR	Transforming growth factor-beta receptor
TIMP	Tissue inhibitor of metalloproteinase
TMD	Transmembrane domain
TME	Tumour microenvironment
TMEPAI	Transmembrane TGFβ-inducible protein
TN	Triple negative
TNC	Tenascin-C
TNF	Tumour necrosis factor
UDH	Usual ductal hyperplasia
uPA	Urokinase-type plasminogen-activator
uPAR	Urokinase-type plasminogen-activator receptor
V	Variable region
VEGF	Vascular endothelial growth factor
VO	Orthovanadate
ZEB	Zinc-finger/homeodomain protein

1. INTRODUCTION

1.1 NORMAL BREAST

1.1.1 Structure of normal breast

The normal breast is composed of a ductal network that originates at the nipple and ends in one of many terminal ductal-lobular units (TDLUs) - the smallest functional unit of the breast. A TDLU is composed of a single terminal duct (TD) and multiple end ductules, known as acini, which form the lobule (Figure 1a). This ductal network is lined by two epithelial cell layers: the apically located luminal epithelial cell (LEC) layer that consists of polarised columnar cells of the ducts and cuboidal cells of the lobules, and the basally located myoepithelial cell (MEC) layer which lies in contact with the laminin (LN)-rich basement membrane (BM) (Figure 1b) [1]. The organisation of MECs differs between ducts and lobules. In the duct, MECs are elongated and arranged in an almost continuous layer which lies in direct contact with the BM, thereby separating LECs from the BM. While in the lobules, MECs are stellate-shaped and form a basket-like structure, this discontinuous layer exposes the basal surface of some LECs to the BM [2, 3]. Therefore, interaction between LECs and the surrounding stroma is mediated by the organisation of the MEC layer [4]. This ductal network is directly surrounded by a highly vascularised stroma, separated from the adipose tissue by fibrous connective tissue [1].

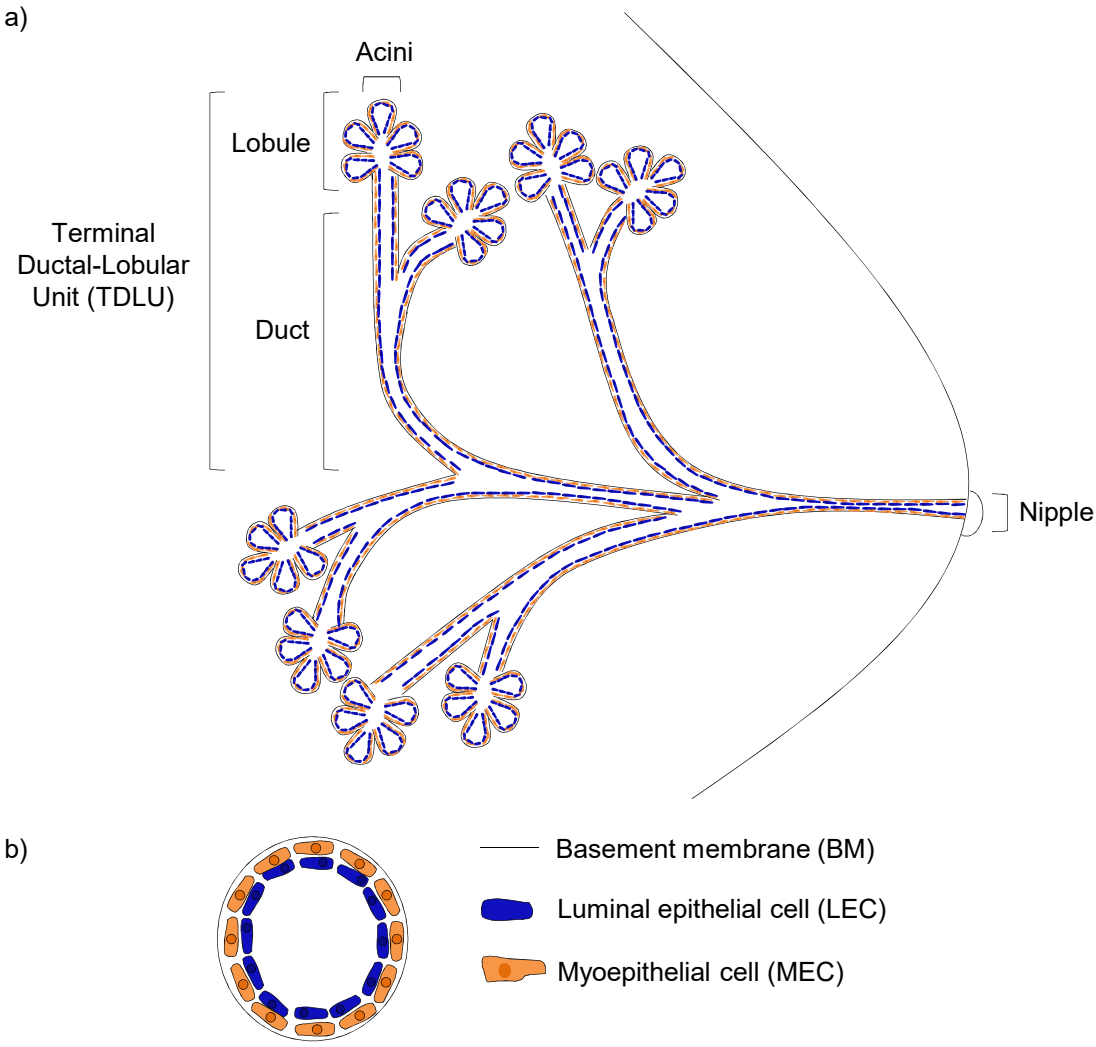

Figure 1. Structure of normal breast. a) The normal breast is composed of a ductal network that originates at the nipple and ends in one of many terminal ductal-lobular units (TDLUs). Each TDLU is composed of a terminal duct and multiple end ductules, known as acini, which form the lobule. This structure resides in a highly vascularised stroma which is separated from the adipose tissue by dense fibrous tissue. b) The ductal system is lined by two epithelial cell layers: the inner luminal epithelial cell (LEC) layer and the outer myoepithelial cell (MEC) layer, which lies in contact with the basement membrane (BM). Figure 1a adapted from [22] and 1b adapted from [16].

1.1.2 Development of normal breast

Development of the normal breast is a progressive process which begins during embryogenesis; in humans, males and females have a similar rudimentary ductal structure at birth [5, 6]. This consists of organised ducts, which are connected to the nipple but lack TDLUs. Development in the two sexes is identical until the onset of puberty. In puberty, under the action of the ovarian steroid hormone oestrogen, the ductal network undergoes branching morphogenesis in females, while the male ductal network remains rudimentary with some involution [5, 6]. Branching morphogenesis involves the growth and division of ducts and the development of early lobular structures, which are more primitive than the terminal structures of the mature resting breast [7]. Branching morphogenesis is accompanied by an increase in the volume of adipose and fibrous tissue [7]. Further development of the lobules continues with the onset of menstruation and pregnancy, with full terminal differentiation occurring only if lactation occurs [6].

1.1.3 Cyclical variations to normal breast

The breast undergoes cycles of growth and involution, regulated by steroid hormone activity in the menstrual cycle, and pregnancy and lactation [8]. In the mature breast, LECs and MECs are represented in equal numbers [9]. In the premenstrual phase, increased steroid hormone levels induce LEC proliferation and increase the number of acini per lobule. At the end of the cycle the levels of steroid hormones decrease and the breast involutes by apoptosis. In pregnancy, LECs proliferate and expand in response to steroid hormones, in order to prepare for lactation, during which prolactin allows LECs to synthesise milk proteins [8]. Following birth, the level of these steroid hormones decreases, and milk is ejected by the systemic contraction of MECs in response to suckling-mediated release of oxytocin [10]. After weaning, the breast involutes by apoptosis resulting in a decrease in breast size to the pre-pregnancy state. Involution occurs in response to decreased steroid hormone levels, as seen at the end of the menstrual cycle and post-pregnancy, and also with the decreased ovarian function that accompanies ageing [8]. In ageing, the lobules involute, with a reduction in the number and size of acini per lobule, and the glandular and fibrous tissue is progressively replaced by adipose tissue, resulting in a reduction in breast density [11]. Lobule involution is particularly pronounced after menopause [12].

1.2 BREAST CANCER

1.2.1 Classification of breast cancer

Histological types of breast cancer

Breast cancers may be classified into subgroups according to histological type and grade to provide prognostic value. Histological type refers to the cellular morphology of the lesion, and in general, breast cancers are classified as lobular and ductal histological subtypes [13]. The lobular subtype consists of small, nonpolarised cells which resemble cuboidal cells of the normal breast acini, while the ductal subtype consists of moderate to large, polarised cells that resemble columnar cells of the normal breast ducts [13]. The terms ‘ductal’ and ‘lobular’ were previously used to classify lesions based on their origin and localisation to either the duct or lobules respectively, however most breast cancers ultimately arise in the same anatomical site - the TDLU [14, 15]. Ductal and lobular lesions of the breast are further classified into *in situ* and invasive lesions. *In situ* lesions are characterised by tumour cell proliferation confined within the ductal-lobular network by an intact or focally disrupted MEC-BM interface, while invasive lesions are characterised by the loss of the MEC population, the degradation of the BM and the invasion of tumour cells into the surrounding stroma [16]. *In situ* precursor lesions in the development of invasive lobular carcinoma (ILC) include: atypical lobular hyperplasia (ALH) and lobular carcinoma *in situ* (LCIS), whereas precursor lesions in the development of invasive ductal carcinoma (IDC) include: usual epithelial ductal hyperplasia (UDH), flat epithelial atypia (FEA), atypical ductal hyperplasia (ADH) and ductal carcinoma *in situ* (DCIS) [13].

Histological grades of breast cancer

Histological grade refers to the degree of differentiation and proliferation of a tumour. These characteristics have been incorporated in multiple prognostic algorithms to determine the clinical management of DCIS, particularly to identify patients at risk of recurrence. The Van Nuys classification system is based on age at diagnosis and tumour features; size, margins, nuclear grade and necrosis. These factors are used to score DCIS lesions between 4 and 12 to determine risk of recurrence. Patients least likely to recur, score 4 and include older patients with small, low-grade, well-excised lesions, while patients most likely to recur, score 12 and include younger patients with large, high-grade, poorly-excised lesions [17]. The National Coordinating Group for Breast Screening Pathology has proposed a classification system based on growth pattern, nuclear morphology and necrosis [18]. These factors are used to subclassify DCIS into low-, intermediate- and high-grade. Low-grade DCIS consists of small, cohesive, polarised, uniform cells of low proliferative capacity, while high-grade DCIS consists of large, pleomorphic cells of high proliferative capacity with necrosis. Intermediate-grade DCIS shares characteristics of both grades [18]. Both classification systems demonstrate an association with high-scoring or high-grade DCIS and recurrence [19, 20]. However, these classification systems have limited reproducibility due to subjective interpretation of breast histology [21], particularly as individual DCIS lesions demonstrate heterogeneity in grade [22], and therefore are unable to inform on appropriate treatment alone [23]. With this, no single classification system for DCIS has been universally accepted [24]. Molecular characterisation of DCIS may improve the prognostic stratification of patients using such classification systems.

1.2.2 Model of progression of breast cancer

Progression to invasive breast cancer has been suggested to follow a step-wise transition through clinical and pathologically defined stages [25]. For the ductal subtype, two models have been proposed. The classical model suggests breast cancer arises from the transformation of a TDLU into FEA; to ADH; to DCIS, which progresses into IDC [26]. This model was proposed following the identification of a single anatomical site for the origin of breast cancer, and it was based on the speculation that these lesions are biologically related due to the gradual histological continuity between them [14, 15, 27]. This model is supported by the elevated risk of developing invasive disease with the progressive lesion [28]. Such that, patients with FEA have a 2-fold increased risk of developing invasive breast cancer, whereas patients with ADH and DCIS have a 5-fold and 10-fold increased risk, respectively [29-31]. However, these studies did not classify DCIS into histological grade, and therefore a correlation between DCIS grade and subsequent invasive development was not assessed. Moreover, these earlier lesions more frequently coexist in breasts with synchronous invasive breast cancer than normal breasts [27]. An alternative model, also supported by histomorphological and epidemiological observations, suggests UDH, instead of FEA, as a direct precursor to ADH [28, 29]. UDH carries a 1.5-fold increased risk of invasive development [28]. However, subsequent studies have suggested this model is likely invalid [13]. For the lobular subtype, similar to the classical model for the ductal subtype, a normal TDLU transforms into ALH, which progresses to LCIS and culminates as ILC [13].

1.2.3 Management of breast cancer

In the symptomatic setting, DCIS accounts for 3-5% of breast cancer diagnoses, while in the screening setting, DCIS accounts for 20-25% [32, 33]. Screening programmes aim to prevent disease-specific mortality through detection and treatment of disease at its earliest stages, suggesting DCIS as an ideal target in the prevention of invasive breast cancer [34]. The expected benefit of screening to reduce mortality depends on existence of an effective treatment. Current management of DCIS involves treatment of all cases by surgical excision, by mastectomy if the DCIS is extensive, which has a risk of recurrence of 1-2% or, for more limited disease, breast conserving surgery with adjuvant radiotherapy, which has a risk of recurrence of 12% [35, 36]. However, it is estimated that if left untreated, over half of DCIS cases will not progress into invasion within a patient's lifetime [37, 38]. A study followed 28 patients diagnosed with low-grade DCIS on biopsy, who received no further treatment. 11 patients developed invasive disease, with a variable time of progression up to 40 years, while 17 remained breast-cancer free [37]. In all cases, the site of recurrence was within the same quadrant of the same breast the biopsy had been taken, this supports disease progression rather than *de novo* disease [37]. A comparable study followed 13 patients diagnosed with varying grades of DCIS on biopsy, who received no further treatment. 10 patients recurred, 6 patients developed invasive disease, of those 2 low-grade DCIS recurred within 12 years, 2 intermediate-grade DCIS recurred within 10 years, and 2 high-grade DCIS recurred within 5 years, post-biopsy [38]. Together, these studies suggest, all DCIS grades have progressive potential, with high-grade DCIS progressing into invasion more rapidly. With no current markers to predict progression into, or recurrence as, invasive disease, there are concerns surrounding overdiagnosis and overtreatment of DCIS [39-41]. Overdiagnosis is the detection of a cancer which otherwise would not cause symptoms or death, while overtreatment relates to the treatment of any overdiagnosed cases or the unnecessary administration of more aggressive therapies than is necessary [42]. The main challenge in the management of DCIS is to determine the invasive capabilities and recurrence probabilities of DCIS cases, in order to generate robust prognostic and therapeutic stratification [40].

1.2.4 Molecular analysis of the progressive stages of breast cancer

1.2.4.1 Invasive breast cancer

Genomic analysis of invasive breast cancer

To understand breast cancer progression, molecular studies focused on the relationship between the genetic alterations in tumour cells and histological grade, as the histological grade is related to the clinical behaviour [19]. These studies demonstrated that specific DCIS grades exhibit distinct genomic differences, whereby low-grade IDCs displayed fewer overall chromosomal aberrations as compared to high-grade IDCs [43-45]. More specifically, low-grade IDCs display reoccurring chromosomal loss of 16q and gains of 1q, 16p and 8q, whereas high-grade IDCs exhibit recurrent losses of 8q, 11q, 13q, 1p and 18q, recurrent gains of 8q, 17q, 20q and 16q, and frequent high-level amplifications of 17q12 and 11q13 [43-45]. Intermediate-grade IDC shares genomic alterations of both grades [46]. The pattern of 16q loss in low-grade and gain high-grade IDC strongly argues against the hypothesis that low-grade IDCs progress to high-grade IDCs through accumulation of genetic alterations [47]. This suggests low-grade IDC and high-grade IDC have distinct pathways of progression.

Gene-expression analysis of invasive breast cancer

Gene-expression profiling has contributed to the understanding of biological and clinical heterogeneity of breast cancer [48]. A study by Perou and colleagues used complementary DNA (cDNA) microarrays to investigate gene-expression profiles of 65 breast cancer samples from 42 individuals (36 IDC, 1 DCIS, 2 LCIS and 3 normal) [49]. This study aimed to characterise breast cancers by alterations to a specific set of genes, known as the intrinsic gene set. Invasive breast cancers were classified into four intrinsic subtypes, including two ER positive; luminal A and luminal B, and two ER negative; HER2 and basal [49]. Luminal A and luminal B are the most common subtypes, usually representing low- to intermediate-grade, characterised by the expression of genes characteristic of normal LECs, including; cytokeratin 8 (CK8) and 18 (CK18). Luminal A subtype show high expression of ER and PR-related genes and lack HER2 expression, with a low-grade and low expression of proliferation-related genes. Luminal B subtype show a decreased expression of ER and PR and overexpress HER2, have a higher grade and higher expression of proliferation-related genes. Luminal subtypes show a better responsiveness to endocrine treatment and clinical outcome [50, 51]. HER2 and basal subtypes usually represent high-grade, and are associated with poor prognosis. HER2 subtype show expression of HER2, as well as other genes on the HER2 amplicon (17q12-q21), and lack expression of ER and PR. Basal subtype show expression of genes characteristic of normal MECs, including; CK5/6 and epidermal growth factor receptor (EGFR), and are most commonly characterised by the lack of ER, PR and HER2 expression, and are therefore frequently known as triple negative (TN) subtype. However, the basal and TN subtype are not identical, and their distinction is made on five markers; ER, PR, HER2, EGFR and CK5/6. Basal subtype are negative for ER, PR, HER2 and positive for EGFR and CK5/6, whilst TN subtype are negative for all five markers (Table 1) [52]. Subsequent follow-up studies demonstrated these subtypes were associated with distinct clinical outcomes, however, despite their clinical relevance, molecular characterisation of breast cancers using gene-expression profiling is not routine in clinical practice, and breast cancer management depends on the use of conventional classification systems analysing histological features [51, 53].

Intrinsic subtype	Expression profile	Histological grade	Outcome
Luminal A	ER+/PR+/HER2-	Low	Good
Luminal B	ER+/PR+/HER2+	Intermediate	Intermediate
HER2	ER-/PR-/HER2+	High	Poor
Basal	ER-/PR-/HER2- EGFR+/CK5/6+	High	Poor
Triple negative	ER-/PR-/HER2- EGFR-/CK5/6-	High	Poor

Table 1. Intrinsic subtypes of invasive breast cancer. Table adapted from [54].

1.2.4.2 *In situ* breast cancer

Genomic analysis of *in situ* breast cancer

Several genomic studies have demonstrated that DCIS exhibits distinct alterations associated with histological grade [44-46]. Using CGH, Buerger and colleagues demonstrated the frequent loss of 16q in low-grade DCIS, whereas more complex genomic alterations including, loss of 8p, 11q, 13q and 14q, gains of 1q, 5p, 8q and 17q, and high level amplification of 17q12 and 11q13 in high-grade DCIS [45]. As seen in IDC, intermediate-grade DCIS shares genomic alterations of both grades [45]. Analysis of CGH data generated from synchronous DCIS and IDC revealed a near-identical pattern of genomic alterations supporting the direct precursor relationship between DCIS and IDC [44-46]. Yao and colleagues utilised CGH in conjunction with serial analysis of gene expression (SAGE) to demonstrate an overall trend towards an increase in the number and amplitude of gains and losses during breast cancer progression [55]. Together, these data support DCIS as a direct precursor to IDC, and that distinct genetic pathways between low-grade and high-grade disease exists.

In the low-grade pathway, FEA is suggested as the precursor to ADH, and ADH as the precursor to low-grade DCIS, this notion is supported by shared histomorphological features and epidemiological data [14, 15, 27, 29-31]. Extending this, several loss-of-heterozygosity (LOH) studies identified loss of 16q in ADH, an alteration which is frequently observed in low-grade DCIS [56-58]. Moreover, the genetic profile of FEA overlaps with ADH and low-grade DCIS. Specifically, Moinfar and colleagues reported loss of 16q in FEA [59], and these were further supported by similar studies [26]. Notably, these common genomic alterations are not observed in UDH. This lesion displays rare and randomly distributed chromosomal alterations, or no changes at all, that are no different from normal breast tissue [57], thereby discounting UDH as a precursor to ADH, and therefore do not support the alternative model of ductal breast cancer progression. Identification of the precursor lesion of high-grade DCIS, with 17q12 amplification, remains elusive [13]. These observations support the role of FEA as the precursor to ADH, and ADH as the precursor to low-grade DCIS.

Gene-expression analysis of *in situ* breast cancer

Gene-expression analysis of DCIS demonstrated that like IDC, DCIS can also be categorised into the intrinsic subtypes [60]. Hannemann and colleagues used microarray analysis to compare the gene-expression profile of 40 DCIS and 40 IDC cases. By performing two-dimensional hierarchical clustering, they demonstrated these subtypes are observable in DCIS [60]. However, the relative frequency of these subtypes between DCIS and IDC are different [61]. Such that, there is a higher frequency of the HER2 subtype in DCIS (14.9%) compared to IDC (3-6%), and a lower frequency of the TN and basal subtypes in DCIS (7.5% and 4.2%) compared to IDC (11-20% TN/basal) [61-63]. To account for the differential frequencies of HER2-positivity in DCIS and IDC, two hypotheses have been suggested; HER2 overexpression may be lost during the transition to invasion, or HER2-positive DCIS may not develop into IDC. To investigate this, Park and colleagues compared HER2 levels between DCIS and DCIS with invasion (DCIS/IDC), and between the DCIS and invasive components within the same case of DCIS/IDC [63]. They demonstrated that HER2 amplification is more frequently detected in DCIS, and it is maintained in DCIS and invasive-component of DCIS/IDC. Moreover, HER2 expression is maintained in metastatic lesions. This suggests DCIS differs in the presence of invasive disease [63]. These data support that the intrinsic subtypes exist within DCIS however, these subtypes are unable to determine which DCIS cases will or will not progress.

Together, these studies support the classical model of breast cancer progression, through identifying shared alterations between DCIS and IDC. Furthermore, distinct genomic features found in different grades of IDC are also mirrored in DCIS lesions of comparable grade, whereas it was previously thought that low-grade DCIS can progress into high-grade DCIS through accumulation of genetic alterations. In simplistic terms it is accepted that, low-grade DCIS tends to progress to low-grade IDC, and high-grade DCIS tends to progress to high-grade IDC by accumulation of these specific gene alterations. Furthermore, FEA and ADH share identical genetic profiles as seen in low-grade DCIS, supporting FEA and ADH as the precursors to low-grade DCIS. The evolution of intermediate-grade DCIS remains unknown. With this, these two models of progression are widely supported however, it may oversimplify a complex process.

1.2.5 Identifying markers of the progression of breast cancer

1.2.5.1 Analysis of breast cancer cells

Early models of cancer progression suggest tumour cells acquire hallmarks of malignancy through the accumulation of advantageous genomic alterations as they progress to invasion [64]. Initial studies to understand the progression of breast cancer focused on identifying gene-expression changes within the tumour cells that constitute the progressive stages; ADH, DCIS and IDC [65, 66]. Identifying stage-specific gene-signatures may allow for the prediction of the progressive potential of the lesion and inform on treatment. In a study by Ma and colleagues, the epithelium from 36 tissue samples with synchronous lesions, and matched normal breast epithelium were isolated by laser capture microdissection (LCM) and analysed using gene-expression microarrays [66]. This study identified the most pronounced alterations occur in ADH, and are maintained in later stages of progression, with no major alterations between DCIS and IDC [66]. These data support the concept that there is a clonal relationship between the pathological stages, and that the gene-expression patterns of early lesions reflect the progressive potential. However, this study is that it reflects low-grade disease and therefore may not be relevant to high-grade disease, which has a poorer prognosis [19, 20]. These finding are supported by other studies [55, 67-69]. A study by Castro and colleagues analysed 4 normal, 5 DCIS, 22 DCIS/IDC, and 10 IDC cases in a similar manner [70]. This study demonstrated that tumour cells from DCIS exhibited the most divergent gene-expression changes, while gene-expression changes in tumour cells from the DCIS-component of DCIS/IDC were very similar to tumour cells isolated from IDC [70]. Therefore, these studies suggest that genetic alterations occur before the morphological changes associated with invasion. A further study supported the predictive potential of early lesions. This study demonstrated the prediction of breast cancer metastatic potential from the gene-expression profile of the primary tumour [71].

Although such studies did not identify gene-expression differences that were able to differentiate DCIS and IDC, unique gene-expression alterations were associated with different histological grades [66]. In which, ADH, low-grade DCIS and low-grade IDCs share a common gene-expression signature that is distinct from the gene-expression signature in high-grade DCIS and high-grade IDCs. Notably, intermediate-grade DCIS exhibited a hybrid of these signatures [66]. These data support the different pathological grades of DCIS progress to IDC by two distinct pathways. In the low-grade arm, tumours are of low nuclear grade, are usually ER and PR positive, negative for HER2 and basal markers, and harbour low genetic instability and recurrent 16q loss. While those in the high-grade arm, show a higher degree of nuclear atypia, are frequently ER and PR negative, frequently positive for HER2 or basal markers, and are genetically advanced lesions demonstrating a combination of common genomic alterations, including 16q gain [13]. These observations have been supported by several other breast cancer gene-expression profiling studies [67, 72]. Therefore, it has been demonstrated that histological grade, rather than stage, is associated with distinct gene-expression patterns and that changes in gene-expression required for invasive progression are already present in the early stages of breast cancer. Further studies are required to identify markers that may be used to develop a prognostic signature for patients with DCIS.

1.2.5.2 Analysis of the tumour microenvironment

The breast microenvironment comprises the extracellular matrix (ECM) as well as numerous stromal cell types, including endothelial and immune cells, MECs, fibroblasts, and adipocytes [99]. Early studies demonstrated the ability of the normal breast microenvironment to regulate the growth and differentiation of tumour cells [73, 74], and multiple *in vitro* and *in vivo* studies have demonstrated that stromal cells have profound effects on the growth, differentiation, polarity and invasion of tumour cells [75-77]. For example, normal primary MECs reduced the invasion of breast cancer cell lines *in vitro*, when they were cultured alone or in the presence of fibroblasts, which are well-known promoters of tumour cell invasion [78]. Similarly, it was shown that mammary tumours only arise following the treatment of the microenvironmental components with carcinogen, regardless of whether the epithelial cells were treated with carcinogen *in vitro* [79]. Furthermore, certain histopathological features of breast cancers, including fibrosis, lymphocytic infiltration, lymphogenesis and angiogenesis have prognostic significance [80]. To investigate the role of stromal cell types in breast cancer progression, Polyak and colleagues performed gene-expression analysis of the cell types comprising normal, DCIS and IDC tissue [80]. This identified altered gene-expression of all cell types in DCIS and IDC, suggesting a role in development and progression into invasion [80]. In particular, DCIS-MECs showed the most significant differences, as compared with their normal counterpart. Interestingly, DCIS-MECs downregulated MEC-specific differentiation markers, including; oxytocin receptor, CK7, CK14, CK17, and LN [80]. This suggests DCIS-MECs are phenotypically altered. This study however, does not recapitulate all the diversity seen in breast cancer due to a low number of tissue samples used. However, in support of these findings, several studies have shown that DCIS-MECs show immunophenotypic differences from normal MECs [81]. Hilson and colleagues demonstrated that expression of MEC markers such as SMA, SM-MHC, CK5/6, CD10 and calponin were reduced in DCIS-MECs compared to normal [82]. Furthermore, Sotiriou and colleagues analysed the expression profiles of DCIS with clinical follow-up and demonstrated that decreased expression of CD10, a MEC-specific differentiation marker, was associated with decreased disease-free survival [83].

While the function of MECs and their role in breast cancer is not well understood, normal MECs have been demonstrated to exert anti-proliferative, anti-invasive and anti-angiogenic effects on tumour cells in a paracrine manner [84]. With this, Polyak and colleagues focused their follow-up studies on the secreted proteins and cell-surface receptors abnormally expressed in DCIS-MECs. Several BM components (collagen; COL), proteases (cathepsins F, K and L), chemokines (CXCL12 and CXCL14) and protease inhibitors (thrombospondin 2) were highly upregulated in DCIS-MECs suggesting a role for MECs in ECM remodelling, and an alteration to their autocrine- and paracrine-mediated effects [80]. A study by Orimo and colleagues suggested that the secretion of CXCL12 by stromal cells promotes the growth of breast cancer cells [85]. Moreover, Polyak and colleagues observed an increase in the proliferation of tumour cells adjacent to MECs as compared with other regions of DCIS that were not in contact with MECs, as identified by Ki67 immunoreactivity [80]. With this, it was previously reported that tumour cells adjacent to a disrupted MEC layer in DCIS are molecularly and genetically different from their more distant counterpart, with loss of ER expression [86]. This was supported in a study by Zhu and colleagues, in which the gene-expression profile of tumour cells located at the periphery and the centre of DCIS ducts were significantly different [87]. In particular, they identified that gene-expression differences at the periphery were in genes associated with invasion [87]. These findings suggest that DCIS-MECs are altered, and these alterations may promote DCIS progression through ECM remodelling.

To determine whether changes in gene-expression were due to underlying genetic alterations, Polyak and colleagues performed comprehensive array-CGH-based (aCGH) analysis to investigate the genetic profile of LECs and MECs from normal, DCIS and IDC tissue [80]. As expected, they detected no genetic alterations in LECs and MECs from normal breast tissue [80], while there were significant chromosomal gains and losses in tumour cells, as supported by other studies [44, 45, 88], with no changes in MECs from DCIS or IDC. However, as aCGH is thought to be more sensitive to the detection of copy number gains rather than losses, Polyak and colleagues also performed a comprehensive genome-wide single nucleotide polymorphism (SNP) array analysis of these cell types from a set of breast cancer samples. As expected, tumour cells demonstrated a large degree of LOH on the majority of chromosomes, while MECs appeared to be mostly normal [80]. These data demonstrate, that although DCIS-MECs are phenotypically different from normal MECs, genomic changes are restricted to tumour cells.

In support of these data, Ma and colleagues conducted a comparative analysis of gene-expression changes in the epithelial and stromal cells during DCIS progression [69]. Following previous observations, they demonstrated significant gene-expression changes in both epithelial cells and stromal cells in the transition from normal to DCIS, while no major gene-expression differences were identified in epithelial cells in the transition to invasion. However, dramatic gene-expression changes were observed in stromal cells in the transition from DCIS to IDC. Specifically, 3 epithelial genes were differentially regulated at the transition to invasion, while 76 genes were upregulated and 229 genes were downregulated at this stage in stromal cells. Ma and colleagues next performed gene-enrichment analysis to identify biological processes associated with the transition to invasion, the genes upregulated included components of the extracellular matrix (ECM) and matrix metalloproteinases (MMPs; 2, 11 and 14), supporting ECM remodelling by stromal cells as a key step in invasion [69]. Together, these data support the role of tumour and stromal cell types in the progression of DCIS.

1.3 MYOEPITHELIAL CELLS

1.3.1 Characteristics of myoepithelial cells

MECs are defined by their shared properties with smooth muscle cells and location. MECs morphologically resemble smooth muscle cells as they express microfilaments and smooth muscle-specific cytoskeletal proteins such as alpha-smooth muscle actin (α-SMA), smooth muscle-myosin heavy chain (SM-MHC), α-actinin, vinculin and calponin [89], which are responsible for MEC contraction. MECs however are epithelial cells, as they express CKs such as CK5, CK14 and CK17, which are characteristic for the basal layer of stratified epithelium, and form the major component of the intermediate filament system [90]. The CK network, specifically CK5 and CK14, maintains MEC cytoarchitecture [91]. MECs are located between LECs and the BM. MECs interact with adjacent LECs and MECs through desmosomes and interact with the BM through hemidesmosomes [92]. Desmosomes which exist between MECs and LECs are composed of desmocollin-2 (DSC2) and desmoglein-2 (DSG2), whereas those that exist between adjacent MECs are composed of DSC3 and DSG3. Therefore, DSC2 and DSG2 are present in both MECs and LECs, while DSC3 and DSG3 are specific to MECs [91]. Treatment with function-blocking peptides to the cell adhesion recognition (CAR) sites in the MEC-specific DSC3 and DSG3 disrupts cell polarity, and formation of an acinar-like structure [91]. Hemidesmosomes which exist between MECs and the BM are composed of integrin $\alpha6\beta4$ and LN322. MECs express integrin $\alpha6\beta4$ which acts as a BM receptor for LN322 [93, 94]. Loss of hemidesmosomes leads to the detachment of MECs from the BM. MECs also express classical cadherin-mediated interactions, connecting MECs to coordinate the contractile release of milk from the duct [95]. These structural features of MECs, are indistinguishably linked to function.

1.3.2 Function of myoepithelial cells

In the breast, the main function of MECs is contractile, in order to release milk during lactation [2]. This function is reflected by MEC expression of α-SMA and SM-MHC, and oxytocin receptor to respond to the release of oxytocin during lactation. MECs have also been shown to provide important regulatory signals, in addition to structural features, essential for the maintenance of normal breast structure and function. MECs contribute to the synthesis and organisation of the BM, which is rich in COL4, LN and other molecules, as well contributing to the remodelling of the ECM through production of ECM-degrading enzymes and inhibitors [2, 96, 97]. Specifically, MECs produce the BM component, LN1, which induces apicobasal polarity of LECs [98]. This was identified through culturing LECs within a 3D COL1 gel versus a LN-rich ECM (lrECM). LECs cultured in COL1 gels formed acinus-like structures with reversed polarity, with apical marker – mucin-1 (MUC1) expressed on the external surface while basal marker - epithelial specific antigen (ESA) expressed on the luminal surface. Culture in lrECM led to the formation of acini with an organised BM at the basal pole. The addition of MECs prior to embedding in COL, resulted in correct LEC polarity and lumen formation. The effect of MECs was cell-type specific, since co-cultures of LECs with other breast cells; fibroblasts or non-breast cells; osteosarcoma cells did not lead to the correction of LEC polarity. Interestingly MECs isolated from invasive breast cancers were unable to exert this effect, suggesting a loss of normal function. Furthermore, the LN isoforms which constitute the BM (LN-1, -5 and -10/11) were tested since Matrigel, reconstituted BM material, was initially shown to be sufficient for acini formation. LN1 was found to reverse the polarity of LECs when added to COL gels, even in the absence of MECs. Moreover, in comparing LECs and MECs in the production of BM components, LN1 expression was lacking in LECs [98]. Thereby, MECs produce LN1 to induce the correct polarity of LECs in 3D COL1 gels. It remains to be shown whether desmosomes or LN1 are sufficient for polarity or whether both are required. Coordination of MEC functions is necessary to maintain normal breast function; accordingly, it is not surprising that MEC function is compromised in breast cancer, and the loss of the MEC population is universally associated with invasive breast cancer.

Tumour suppressive function of myoepithelial cells

MEC location suggests they may influence tumour progression through inhibiting the invasion of tumour cells by acting as a physical barrier. *In vitro* and *in vivo* studies demonstrate that MECs exert a wider suppressive effect on tumour cells [99], exerting anti-proliferative [100], anti-invasive [78] and anti-angiogenic [101] in an autocrine- and paracrine manner [102]. This tumour suppressive phenotype was originally based on the ability of MECs to inhibit the growth and invasion of breast cancer cells in coculture assays *in vitro* and inhibit tumour growth in xenograft assays [101, 103]. The mechanisms specifically underlying the invasion of tumour cells are incompletely understood however, matrix degradation by matrix metalloproteinases (MMPs), in particular the gelatinase enzymes, have been implicated in invasion of multiple tumour types, including breast cancer. Therefore, it was suggested MECs modulate MMP activity to inhibit invasion. Jones and colleagues demonstrated coculture of primary normal MECs with breast cancer cells decreased MMP expression, specifically MMP2, MMP9 and MT1-MMP, in breast cancer cells was observed [78]. In this manner, conditioned media (CM) isolated from primary normal MECs inhibited the invasion of breast cancer cells in coculture assays *in vitro*, even in the presence of fibroblasts, which are known promoters of tumour cell invasion. This supports the notion that MECs induce a tumour suppressor effect through paracrine mechanisms [78]. Moreover, normal MECs constitutively express high levels of tissue inhibitor of metalloproteinase 1 (TIMP1) and maspin [102]. These proteinase inhibitors act by blocking the activity of the released enzyme rather than by inhibiting proteolytic enzyme synthesis [102]. In this way, MECs release paracrine factors that inhibit protease activity however, MECs may also exert anti-invasive properties through direct modulation of tumour and stromal cell gene transcription, though these mechanisms are unclear [78]. This work demonstrates the dominance of MECs in tumour suppression, and this function is due to paracrine downregulation of MMP expression in tumour cells.

MECs also express a variety of recognised tumour suppressor proteins such as p63, p73 and maspin [76]. The ability of MECs to inhibit breast cancer cell growth and invasion may in part be attributed to their expression of maspin. Overexpression of maspin in the breast cancer cell line MDA-MB-435 resulted in inhibition of tumour growth, invasion and angiogenesis [104]. Subsequent studies revealed that MECs inhibited the growth through induction of growth arrest (G2/M status) in breast cancer cells [100]. In order to experimentally test the role of MECs in the inhibition of growth and invasion of tumour cells, an experimental model of DCIS that is reproducible is essential, as analysis of human tissues allows only for correlative studies. The MCF10A series is one of few human models of breast cancer progression, although it is likely to reflect basal subtype tumours. A derivative of MCF10A cells is the MCF10ADCIS.com (MCFDCIS) cell line xenograft model, which reproducibly gives rise to comedo DCIS-like structures; surrounded by a cell layer which shows positivity for MEC markers such as p63, and a BM rich in LN332, that spontaneously progress to invasion [105]. This xenograft model highly resembles human disease with respect to histopathology and natural history. Using this xenograft model and coinjection with normal MECs, and normal and tumour-associated fibroblasts, Hu and colleagues identified that normal MECs suppress tumour growth and progression to invasion. In contrast, normal and cancer-associated fibroblasts promoted progression to invasion [106]. This model supports the progression of DCIS into invasion is accompanied by the loss of normal MEC function.

Collective evidence suggests that MECs also function as autocrine tumour suppressors by their resistance to transformation and their tendency to transform to benign or low-grade myoepitheliomas when they do [107]. Angèle and colleagues identified differences in the DNA repair capacity of LECs and MECs, and this may contribute to the lower rate of transformation in MECs [108]. Moreover, myoepitheliomas are able to secrete and accumulate an abundant ECM composed of both BM and non-BM components, which suppressed breast cancer cell invasion compared to Matrigel [109, 110]. These myoepitheliomas produced ECM components including; COL, fibronectin (FN) and LN [110]. In addition, MECs secreted large amounts of proteinase inhibitors including maspin, TIMP1, protease nexin II and α1-antitrypsin, and many of these accumulated within the MEC-derived ECM [103, 109, 110]. Transwell invasion assays with these cell lines inhibited breast cancer cell invasion, partly by a maspin-dependent mechanism. These observations suggest an anti-invasive property of the MEC-derived ECM, which likely contributes to their low-grade biological behaviour. The caveat to this study, is that these immortalised MEC lines were derived from benign and low-grade human myoepitheliomas of the salivary gland and breast, and therefore may not reflect the function of normal breast MECs *in vivo*. However, they were shown to maintain the expression of MEC-specific differentiation markers, including; maspin, SMA and CK14, even following prolonged passaging *in vitro* [109, 111].

Tumour promoting function of myoepithelial cells

Correlating with the loss of the MEC layer in the transition of DCIS to invasion, studies have suggested that DCIS-MECs lose their tumour suppressive phenotype, and switch to promote breast cancer progression. Gene-expression profiles demonstrate that DCIS-MECs exhibit a phenotype distinct from normal MECs [80]. Consistent with gene-expression profiling, DCIS-MECs exhibit alterations in many of their normal markers, such as reduced expression of oxytocin receptor [80]. Functionally, tumour-derived MECs differ from their normal counterpart, and are unable to polarise LECs in 3D COL1 assays due to a loss of their ability to synthesis sufficient or functional LN1 [98]. Consistently, MECs present in breast cancer tissue demonstrated little or no expression of LN1 [98]. This suggests that cancer-associated MECs are unable to transmit the necessary signals to induce the correct polarity of LECs. Such that DCIS-MECs demonstrate a loss in hemidesmosome formation, and thereby are unable to interact with the BM [112], and demonstrate an alteration in ECM isoform expression. A study by Adams and colleagues identified that normal MECs express a truncated form of tenascin-C (TNC) in contrast, DCIS-MECs upregulate the expression of exon 14 in TNC, which was associated with progression to invasion [113]. These data support the notion that the loss of normal MEC function in DCIS may play a key role in the progression to invasion however, the prognostic and functional relevance of such changes is not yet established.

Work within our laboratory has identified alterations to DCIS-MECs including: *de novo* expression of the integrin $\alpha v\beta 6$ and upregulation of FN. Expression of integrin $\alpha v\beta 6$ was seen in a subset of pure DCIS and is almost universal in DCIS/IDC. Its presence is significantly associated with progression and recurrence. *In vitro* studies found integrin $\alpha v\beta 6$ promoted breast cancer cell invasion via TGFβ-dependent upregulation of MMP9, suggesting altered MECs participate in the transition to invasion [114]. In a separate unpublished study, using gene-expression microarray analysis on laser dissected normal versus DCIS-MECs identified further changes, including significant upregulation of FN in DCIS-MECs as compared with their normal counterpart. Currently, the relationship between integrin $\alpha v\beta 6$ and FN in DCIS-MECs is unclear.

1.4 INTEGRINS

1.4.1 Classification of integrins

Integrins are a family of adhesion receptors, mediating cell-cell and cell-matrix interactions through their extracellular domains, and cytoskeletal interactions through their intracellular domains. In this way, integrins derive their name from their ability to 'integrate' the external and internal cell environment [115]. Integrins are heterodimeric type I transmembrane proteins consisting of an α and β subunit [116]. Each subunit contains a relatively large extracellular domain, a single transmembrane domain (TMD) and a short cytoplasmic domain [116]. All three domains are required to regulate integrin activity. In humans, there are 18 α subunits and 8 β subunits, which non-covalently associate into 24 different receptors with different binding specificity and distribution [117]. Integrins are classified based on their binding properties to distinct, although partially overlapping, subsets of ligand including; COL, LN or RGD (Arg-Gly-Asp) amino acid sequences or based on their expression on leukocytes (Figure 2) [118].

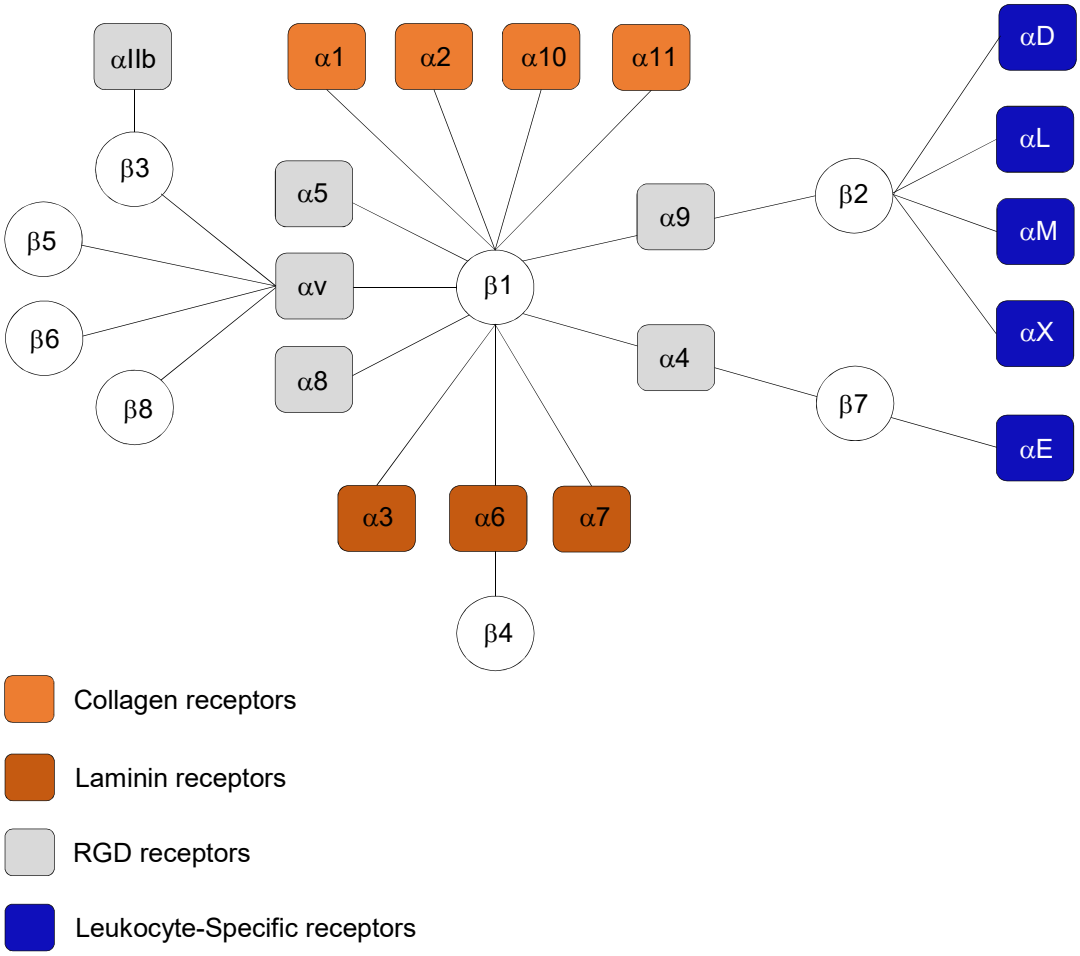

Figure 2. Classification of integrins. In humans, the integrin family contains 24 heterodimers, composed of 18 α and 8 β subunits. Integrins are classified according to their binding properties to ligands; collagen, laminins or RGD amino acid sequences, or according to their expression on leukocytes. Figure 2 adapted from [118].

1.4.2 Structure of Integrins

Extracellular domain

Integrin extracellular domains are relatively large structures (approximately 800 amino acids) responsible for ligand binding. The extracellular domain of the α and β subunits are comprised of several subdomains organised into a globular ligand-binding N-terminal head domain which sit on two C-terminal legs that connect to the TMD and cytoplasmic domain of each respective subunit (Figure 3) [119]. The extracellular domain of the α subunit forms the head, a thigh domain, and two calf domains; calf-1 and calf-2 [120, 121]. Half of α subunits contain an additional domain, known as the insertion (I)-domain [122]. The presence of the α I-domain represents an exclusive binding site for ligands. Within this domain is a conserved metal-ion dependent adhesion site (MIDAS) that binds to the divalent metal cations; calcium (Ca^{2+}), magnesium (Mg^{2+}) and manganese (Mn^{2+}) required for ligand binding [123]. These integrin-binding sites in ligands all contain a critical residue D (Asp) which interacts with the metal cation to facilitate this interaction [124]. Specifically, ligand binding alters the coordination of the metal cation in the MIDAS and shifts the I-domain from a closed, inactive conformation to an open, active conformation which results in integrin activation [125]. The extracellular domain of the β subunit contains a an I-like domain (β1), a PSI (plexin/semaphorin/integrin) domain, a hybrid domain, four epidermal growth factor (EGF) domains; and a membrane proximal β tail domain (βTD) [124]. The βI domain allows integrins which lack the I-domain to bind ligands. The ligand interacts with a metal cation in the MIDAS within the β subunit and the propeller domain of the α subunit to result in integrin activation [124].

Transmembrane domain

Integrin TMDs are single membrane-spanning structures (approximately 20 amino acids). In inactive integrin heterodimers, the α and β subunits are tightly packed through GxxxG dimerisation motifs within the TMDs, thereby forming glycine-glycine interactions [126].

Cytoplasmic domain

Integrin cytoplasmic domains are relatively small structures (10 to 70 amino acids, with the exception of the β4 subunit which contains over 1000 amino acids) which lack enzymatic activity. Nonetheless, the cytoplasmic domains of integrins play a key role in their activity through recruitment of scaffolding proteins, that couple the ECM to the actin cytoskeleton, and adaptor proteins, that are involved in intracellular signalling [124]. β subunit cytoplasmic domains are highly homologous, while α subunit cytoplasmic domains are highly divergent except for a single conserved sequence. The conserved GFFKR (Gly-Phe-Phe-Lys-Arg) and HDR(R/K)E (His-Asp-Arg(Arg/Lys)Glu) sequences located in the membrane proximal region of the α and β subunit, respectively, are suggested to form a salt bridge between R (Arg) and D (Asp) from the α and β subunit, respectively [127, 128]. This has been suggested to maintain integrins in the low-affinity, inactive state and its disruption may play a key role in the regulation of integrin activation. Within the β subunit cytoplasmic domain are two motifs; the membrane proximal NpxY motif and the membrane distal NxxY motif. These motifs represent recognition sequences for phosphotyrosine-binding (PTB) domains and serve as binding sites for integrin-binding proteins [129].

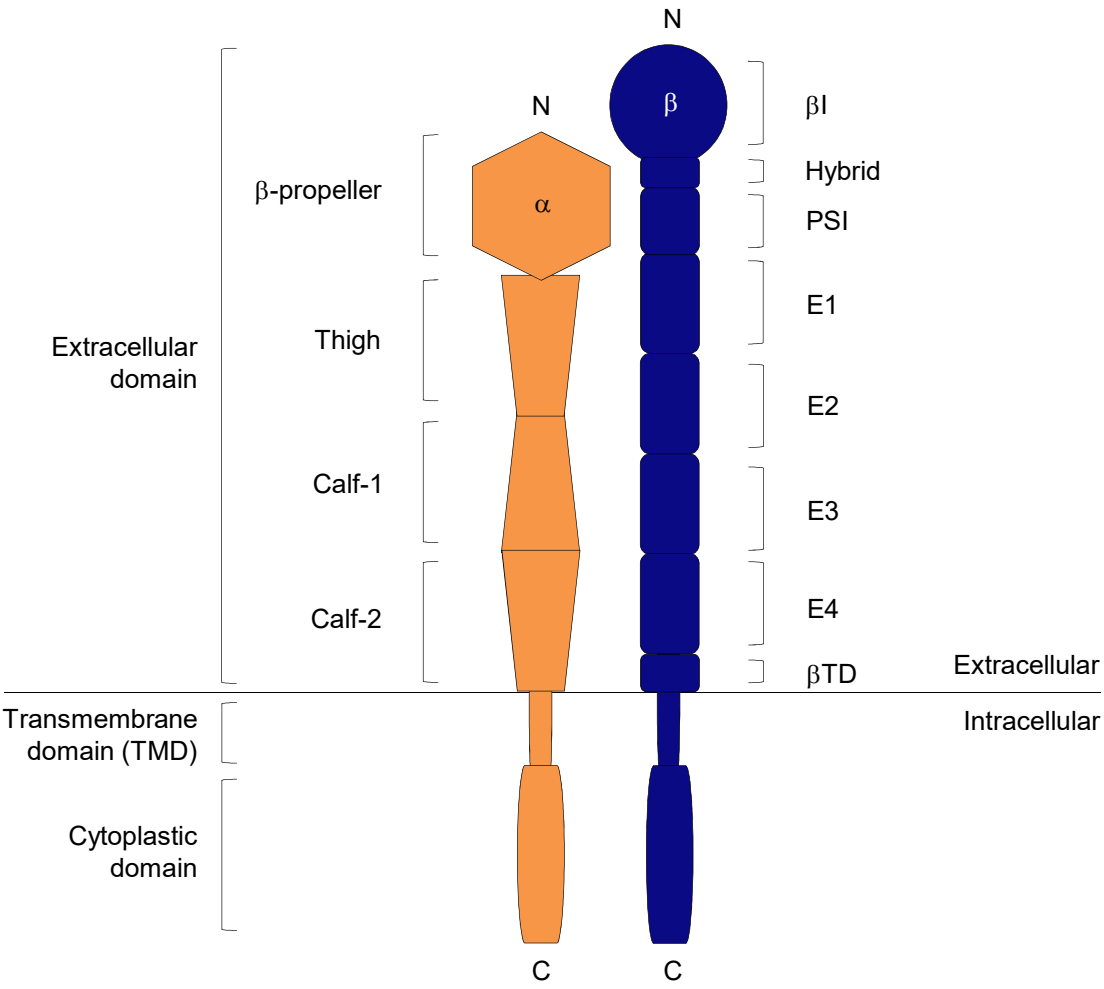

Figure 3. Structure of integrins. Integrins are formed by non-covalently associated α and β subunits. Each subunit has an extracellular domain, a single transmembrane domain (TMD), and a cytoplasmic domain. The extracellular domain of the α and β subunits are comprised of several subdomains organised into a globular ligand-binding N-terminal head domain which rest on two extended C-terminal legs that connect to the TMD and cytoplasmic domain of each respective subunit. The extracellular domain of the α subunit consists of a folded seven-bladed β-propeller that forms the head domain, a thigh domain and two calf domains; calf-1 and calf-2. The extracellular domain of the β subunit consists of a hybrid domain that connects to the I-like domain (β1) and a PSI (plexin/semaphoring/integrin) domain, four epidermal growth factor (EGF) domains (E1, E2, E3 and E4), and a membrane proximal β tail domain (βTD). Figure adapted from [118].

1.4.3 Signalling mechanisms of integrins

Integrins are adhesion receptors; the specific binding of the extracellular domain of integrins to ECM proteins or, to counter-receptors on adjacent cells in some cases, supports cell adhesion, which is crucial for embryonic development and tissue homeostasis. In addition to their physical role in adhesion, integrin-mediated interactions on either side of the cell-surface are dynamically linked; such that there is bi-directional signalling between the extracellular environment and the intracellular cytoskeleton mediated by integrin cytoplasmic tails. Through binding to the cytoskeleton, integrins transduce signals from inside out of the cell, in order to regulate their affinity for extracellular ligand. They do this by undergoing conformational changes in their extracellular domains that occur in response to signals that impinge upon the integrin cytoplasmic tail. This process is known as inside-out signalling or integrin activation [116]. In turn, through binding to the ECM, integrins transduce biochemical and biophysical extracellular properties from outside in of the cell, in order to regulate cellular responses such as cell adhesion, polarity, proliferation, differentiation, migration and ECM remodelling [117, 118, 130]. This process is known as outside-in signalling (Figure 4) [116]. Inside-out and outside-in signalling require dynamic, and spatially and temporally regulated assembly and disassembly of multiprotein complexes that form around the cytoplasmic tails of integrins. While conceptually these signalling pathways are considered separate, they are closely linked. Such that, integrin activation can increase ligand binding, resulting in outside–in signalling [116]. Conversely, ligand binding can generate signals that cause inside–out signalling [130]. In this way, these dynamic signalling pathways allow cells to sense and adapt to the extracellular environment.

Inside-out signalling

In inside-out signalling, integrins regulate their affinity for ligands by undergoing conformational changes in their extracellular domains. In the normal resting, low-affinity, inactive state, integrin extracellular domains are unbound to ligands and exist in a bent conformation. Activation signals from within the cell induce the extension of the extracellular domain and stabilise the high-affinity, active conformation. This conformational change exposes the external ligand-binding site to which ligands bind, allowing the transmission of signals from outside in [131]. The TMD plays a key role in integrin activation; such that interactions between the TMDs of α and β subunits maintain integrins in an inactive conformation and disruption of these TMD interactions is essential for integrins to adopt the active conformation [132]. Most integrin β subunits contain a positively charged K (Lys) or R (Arg) amino acid residue near the TMD. These positively charged amino acid residues 'snorkel' near negatively charged phospholipid head groups, and are thereby membrane-embedded. A stable $\alpha\beta$ TMD association requires the simultaneous formation of two discrete assemblies, an inner and outer membrane clasp. Mutation to K/R residues causes the dissociation of $\alpha\beta$ TMD clasp interactions and integrin activation [133]. In this manner, snorkelling residues in TMDs help maintain membrane-embedding, thereby regulating integrin activation state. Integrin cytoplasmic domains also play a key role in the regulation of integrin activation, in particular through interaction with the anchoring proteins - talin and kindlin. Talin and kindlin both bind to the β subunit cytoplasmic domain, although to distinct regions; talin binds to the membrane proximal NpxY motif [129], while kindlin binds to the membrane distal NxxY motif [135]. Together, they cooperate to regulate the affinity of integrins. Integrin activation follows the simultaneous binding of talin to the β subunit and actin cytoskeleton. However, to achieve complete integrin activation, the cooperation of kindlin is essential [135]. Furthermore, the synergistic effect of talin and kindlin on integrin activation is enhanced by the binding of vinculin to talin. Vinculin leads to the conformational transition of integrins to their active state capable of high-affinity interactions with ECM ligands [136]. In contrast to promoting integrin activation, on the basis of the existing data discussed here, it appears integrin activation may be prevented or diminished by interfering with TMD interactions and/or competition with talin and kindlin binding.

Outside-in signalling

In outside-in signalling, integrins bind to an ECM ligand to transduce signals into the cell. In this way, cells are connected to the extracellular microenvironment through integrins at focal adhesions (FAs), to translate mechanical signals from the outside into biochemical signals, a process known as mechanotransduction [137]. Ligation to an ECM ligand induces integrin clustering. Integrin clustering drives the formation of FAs, followed by phosphorylation of focal adhesion kinase (FAK) at tyrosine 397, to stabilise FAs and drive activation of RhoGTPase-dependent actomyosin-based cell contractility and cytoskeleton reinforcement [122]. Consequently, cell-generated contractile forces transmitted through integrins can remodel the surrounding matrix and alter matrix stiffness. This process is known as mechanoreciprocity [124]. In normal tissue homeostasis, this reciprocal interaction between cell contractility and matrix stiffness is balanced. Such that, cells sense external forces via integrin adhesions and respond through actomyosin contractile forces that are equal to that of the surrounding matrix to maintain normal tissue architecture. An imbalance in these reciprocal force interactions between the cell and matrix can result in pathological conditions such as fibrosis and cancer. These pathological conditions are associated with progressive matrix stiffening. Studies have shown that matrix stiffness strengthens integrin-cytoskeletal linkages and integrin clustering, as well as integrin expression, activity and FA formation. These changes have been shown to enhance cell growth and proliferation through integrin-mediated mechanisms [137]. Together, these bidirectional signalling events and the repertoire of integrins on a cells surface, integrins can dictate ECM sensing and cellular response. Consequently, disruption to these may promote cancer development and progression.

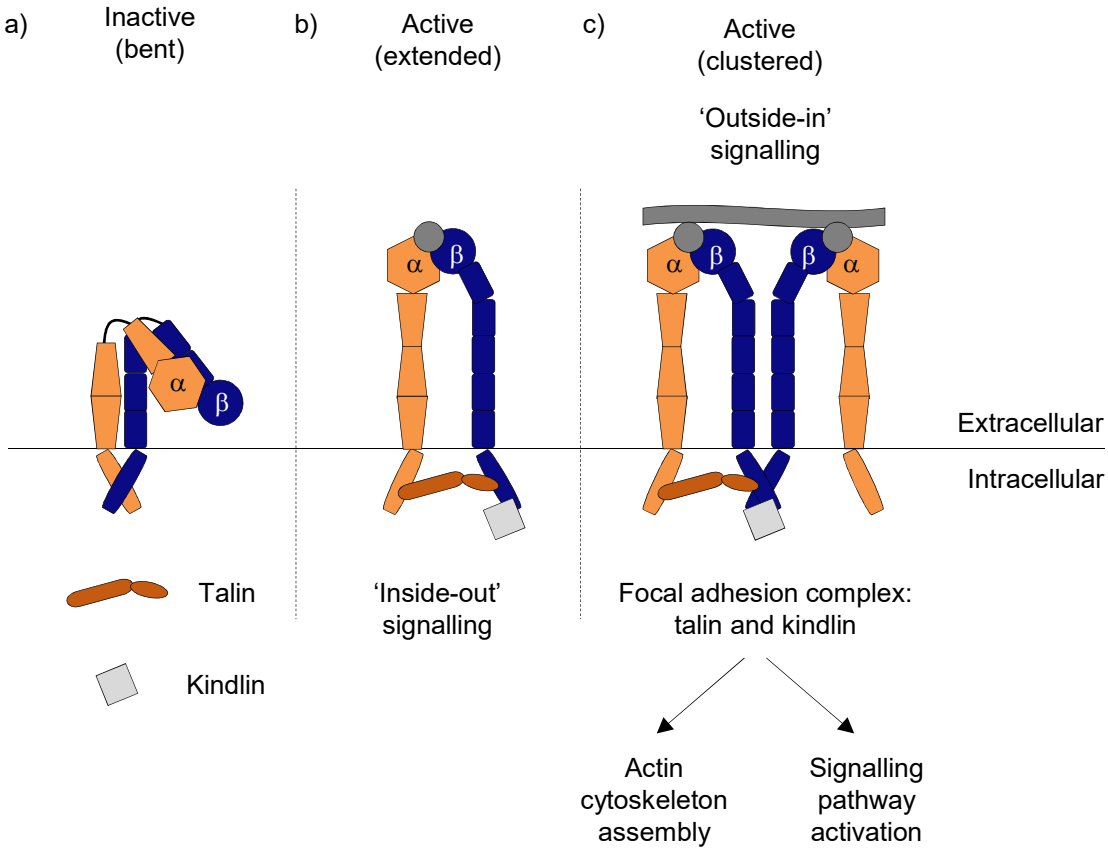

Figure 4. Signalling mechanisms of integrins. a) In the inactive resting state, integrins exist in a bent conformation and the TMD and cytoplasmic domain of the α and β subunits are closely associated. b) Integrins are activated by the binding of the cytoplasmic proteins, talin and kindlin, to the integrin cytoplasmic domain a process known as inside-out signalling. This leads to the separation of the TMD and cytoplasmic domain of the α and β subunits, and extension of the integrins extracellular domain. Ligand binding can occur in this conformation. c) Integrin binding to ligand results in the clustering of integrins at the cell membrane. This transmits intracellular signals into the cell, a process known as outside-in signaling. This leads to formation of focal adhesions (FAs), which are essential for reorganisation of the actin cytoskeleton and activation of downstream signaling to control various cellular responses. Figure adapted from [129].

1.4.4 Expression of integrins

Mechanisms regulating integrin expression at the cell surface include regulation of protein levels by transcriptional or post-transcriptional mechanisms, and mobilisation from preexisting intracellular stores [138]. Integrins are expressed in a cell-specific manner, and the expression of certain integrins is restricted to cells of a particular lineage, such as the expression of integrin β2 is restricted to leukoctyes [117]. The expression of integrins is regulated at the transcriptional level, such that each subunit is encoded by a different gene [138]. The expressed proteins then compete for compatible pairs in the endoplasmic reticulum, and only intact heterodimer αβ integrins are expressed on the cell surface [139, 140]. Excess unpaired α or β subunits are retained in the endoplasmic reticulum and degraded [140]. This mechanism is dynamically regulated such that the composition of integrins at the cell surface can be rapidly altered [140]. The number of integrins expressed at the cell surface often does not correlate with the expression levels of integrins as the production of α and β subunit binding partners may be unbalanced [141], such as αv and β1 subunits are produced in abundance relative to other subunits [142], which may be due to their ability to pair with multiple different subunits. For example, integrin αv can be found on the cell surface paired to any one of five different β subunits, and integrin β1 with any one of twelve different α subunits [118]. Each integrin heterodimer is also subject to post-translational modifications, which may alter their transport to the cell surface or alter their stability [138]. The repertoire of integrins on the cell surface is also altered in response to specific environmental cues [138]. Together, these alterations to integrin expression allows cells to respond dynamically to microenvironmental changes.

In the normal breast, integrin expression can vary however, a set of integrins are normally expressed and are restricted to either LECs or MECs, or their expression may be shared [143]. In general, MECs have higher levels of integrin expression as they interact with the surrounding ECM [144]. The α subunits most abudantly expressed by LECs and MECs include α1, α2, α3, α5, αv, α6 and α9 while the expression of α1, α5, αv and α9 are restricted to MECs [94, 144, 145]. The β1 and β4 integrin subunits are expressed in both cell types, while the β3 subunit exhibits a more restricted expression pattern [94, 144, 146]. Therefore, LECs and MECs in the breast are capable of assembling at least eight functional integrin receptors including two COL receptors (α1β1, and α2β1), three LN receptors (α3β1, α6β1, and α6β4) and four integrins (αvβ1, αvβ3, α5β1 and α9β1) which recognise RGD sequences present in ECM proteins [118]. Moreover, integrin expression may be polarised to distinct membrane surfaces. For example, α6β4 is predominantly expressed on the basal surface of MECs as it functions to connect MECs to the LN-rich BM through hemidesmosomes [94].

In cancer, integrin expression profiles appear to be altered in comparison to their normal counterparts [147-150]. In general, tumour cells demonstrate a loss of integrins involved in polarity and differentiation; and overexpress integrins involved in proliferation and invasion [143, 151]. These changes in integrin expression are complex and depend on tissue type, histological subtype, and stage [151]. Changes in the expression pattern of integrins in breast cancer have been reported in several studies. On one hand, α6 [152], β4 [153] and αv [154] are generally overexpressed in breast cancer cells, while on the other hand, the expression of α2β1 is lost in breast cancer [155]. Whilst these studies focus on alterations in the integrin repertoire on tumour cells, such changes also occur on stromal cells. It is likely that features of tumour cells influence the ability to interact with stromal cells through alterations to the integrin repertoire on these cells, which may be an important determinant of cancer behaviour. Work in our laboratory identified the *de novo* expression of the integrin αvβ6 by DCIS-MECs. It was shown that the expression of integrin αvβ6 by MECs promoted breast tumour cell invasion in a TGFβ-dependent upregulation of MMP9 [114].

1.4.5 Function of integrins

Adhesion

The adhesion of cells to the matrix via integrins plays a major role in tissue formation, cellular migration and induction of adhesion-mediated signalling. Integrin-mediated adhesions are complex structures, with over ~150 associated molecules, termed the integrin adhesome complex (IAC) [158]. These adhesions are categorised as 'classical' integrin-mediated adhesions including; focal complexes (FXs), FAs, and fibrillar adhesions (FBs); podosomes and invadosomes; and hemidesmosomes [159]. The molecular steps involved in the formation of these 'classical' integrin-mediated adhesions, involves the sequential formation of FXs, FAs and FBs [160]. FXs are small, dynamic, dot-like adhesions, which form under the protrusive lamellipodium of migrating cells and mediate signals that promote actin polymerisation [160]. These are transient structures which may disassemble and new FXs are assembled in front of them as the leading edge of the cell advances [160]. These cycles of FX assembly and disassembly persist as long as the lamellipodium advances. When the lamella retracts, or stops protruding, FXs disassemble and a subset of these adhesions grow and develop into FAs [159]. This transformation is accompanied by growth of the adhesion site and changes in its molecular composition [159]. Such that the conversion of FXs to FAs is characterised by the recruitment of zyxin to the membrane and the concomitant assembly of an actin bundle [161]. This transition depends on actomyosin-driven contractility, which applies force at cell–matrix adhesions [161]. The disassembly of FAs often occurs at the cell trailing edge.

This process involves microtubule-mediated destabilisation of the adhesions and plays an important role during cell migration [162]. Another mechanism leading to loss of FAs involves the transformation of these adhesion sites into stable FBs. FBs are elongated adhesions located around the cell centre, where integrin $\alpha5\beta1$ binds to FN fibrils [163]. FBs differ from classical FAs as the primary integrin receptors are integrin $\alpha5\beta1$ and integrin $\alpha v\beta3$, respectively [164]. In this way, different integrins promote distinct modes of cellular migration and cells may alter their motility by expressing different integrins. FAs and FBs also differ in the composition of the cytoplasmic complex. Such that, FAs contain high levels of phosphotyrosine but display only low levels of tensin; FBs, on the other hand, contain none or little phosphotyrosine but high levels of tensin [164]. Highly migratory and invasive cells form specialised types of integrin-mediated adhesions; podosomes and invadopodia [159]. These differ in that they are not associated with large actin filament bundles and instead contain an actin-rich core, in which the actin polymerising machinery and actin regulatory proteins rapidly drive actin polymerisation to drive membrane protrusion [165]. In podosomes, this core is surrounded by a ring structure composed of scaffolding and signalling proteins, and form in immune cells and osteoclasts [166], while invadosomes, contain actin-rich protrusive structures, and form in invasive tumour cells [165]. In contrast, hemidesmosomes are non-migration-related adhesions [167]. In these adhesions the cytoplasmic tail of the $\beta4$ subunit connects the integrin $\alpha6\beta4$ to the keratin cytoskeleton via plectin, rather than the adhesion molecules associated with other cell-matrix interactions [168].

Polarity

Integrin-mediated adhesions play a key role in tissue formation and cellular migration, which require correct cellular polarity [169]. Loss of polarity, and subsequent tissue disorganisation, and altered cellular migration are key features of tumours [169]. In tissues, at the lateral surface, tight and adheren junctions connect adjacent epithelial cells, whilst at the basal surface, integrins connect epithelial cells to the ECM to establish cellular polarity [169]. Initially, individual contact naïve cells have no surface polarity and express apical and basolateral surface proteins at all surfaces [170]. These contact naïve cells adhere to the surrounding collagenous ECM via integrin β1 to form initial cell-matrix interactions [171]. Maturation of these interactions initiates distinct membrane targeting and endocytic recycling pathways to direct proteins involved in apical and basolateral connections to the correct surface [172]. This interaction acts as a signal to orchestrate the polarised secretion and assembly of LNs forming the epithelial cell-specific BM, and also contributes to the asymmetric targeting of intracellular polarity protein complexes; Crumbs, Par, and Scribble [173]. The basally assembled BM, together with polarity complexes reinforces the alignment of cytoskeletal networks and thereby polarised organisation of the membrane trafficking networks [174]. Together, these mechanisms create a fully polarised epithelial cell. In cellular migration, integrins adhere to the ECM to form a leading edge that protrudes forward, whilst these adhesions disassemble at the trailing edge of the cell [159]. Currently it is unclear how the spatial organisation of signals that control polarity of a migrating cell is established, but similarly concentration of distinct protein complexes at sites of integrin-mediated adhesions at the asymmetrical edges of migrating cells, is likely [169].

Migration

Cell migration is a dynamic process, in which intracellular and extracellular signals merge to produce a coordinated response [175-177]. The migratory cycle consists of well-defined, integrated steps that include: front-to-back polarisation in response to extracellular cues, which are often chemotactic; membrane extension by protrusion and adhesion formation at the leading edge of the cell; cell-body translocation; adhesion disassembly; and retraction at the trailing edge of the cell [178]. Integrin-mediated adhesions serve two major functions in the migration cycle. It generates traction at the leading edge for cell-body translocation by linking the extracellular substratum to actomyosin filaments, and it organises the signalling networks, in particular Rho GTPases, that regulate actin and actomyosin polymerisation and organisation [159]. In this way, adhesion formation and actin polymerisation are linked. Adhesions provide nucleation points that support actin polymerisation; conversely, actin polymerisation determines the rate of adhesion assembly and potentially nucleates adhesions that contain activated integrins [179]. Adhesions and actin are physically linked, and this link coordinates adhesion assembly and disassembly, and the processes they regulate [178]. While integrin-dependent migration is important, integrin-independent mechanisms of migration also exist in some cell types, such as neuronal cells in the brain and tumour cells, under certain conditions [178].

Extracellular matrix remodelling

The ECM serves as a substratum to which cells attach via cell–matrix adhesions, but it is also initially constructed and remodelled by such adhesions. Integrins participate in the assembly of various ECM components. In BM synthesis, integrin β1 cooperates with the dystroglycan receptor to promote synthesis and polymerisation of LN chains into a multivalent network which subsequently incorporates COL and other components [180]. In FN matrix synthesis, integrin α5β1 cooperates with syndecans to promote the polymerisation of FN fibrils into a fibrillar network [181]. Integrins also contribute to ECM remodelling through regulating the expression, localisation, activation and activity of matrix-degrading proteases, in particular MMPs [130, 182]. Integrin ligation to the ECM can activate MMP synthesis, and thereby expression. Some αV [183-187] and β1 [188, 189] integrins have been shown to promote the expression of several MMPs. For example, integrin αvβ6 has been shown to promote the expression of MMP2 and MMP9 in cancer [183-186]. In invasive breast cancer cells, increased expression of integrin αvβ3 upregulates MMP2 expression following integrin binding to RGD peptides [187]. The localisation of MMPs also dictates their function. Localisation to cell membrane through the interaction with integrins has been demonstrated for multiple MMPs, including binding of MMP2 and MMP9 to integrin αvβ3 [190, 191]. Specifically, MMP2 is recruited to the cell surface via binding to integrin αvβ3, which results in the ECM degradation to promote cancer cell invasion [190]. MMP activation is also regulated by integrins. MMPs are initially synthesised as inactive zymogens known as pro-MMPs, which is then converted into an active protease [182]. For example, integrin αvβ3 promotes cancer cell invasion through activating MMP2 [151]. MMPs are also inhibited by integrins in order to prevent excessive ECM degradation. A study by Brooks and colleagues found the hemopexin domain of MMP2 in association with integrin αvβ3 in cancers. This domain competed with MMP2 binding to integrin αvβ3, serving as an inhibitor of MMP2 activity to prevent excess angiogenesis [192]. Together, integrins play a diverse role in cellular functions.

1.5 TRANSFORMING GROWTH FACTOR-β

1.5.1 Isoforms of TGFβ

Transforming growth factor-β (TGFβ) is a multifunctional cytokine involved in embryogenesis, development and normal tissue homeostasis as it effects the regulation of proliferation, differentiation, apoptosis, inflammation, ECM production, integrin expression and protease activity [193]. TGFβ consists of a group of three isoforms; TGFβ1, TGFβ2 and TGFβ3, which belong to a superfamily that also includes; activins, inhibins, bone morphogenic proteins (BMPs), growth and differentiation factors (GDFs) and anti-Mullerian hormone (AMH) [194]. TGFβ's functional diversity may be attributed to several features: three different isoforms of TGFβ exist, and all are secreted in a latent form either bound or unbound to a latent TGFβ binding protein (LTBP); three of four different isoforms of LTBP bind to latent TGFβ, and function to facilitate its secretion and localisation to the ECM; multiple mechanisms exist to liberate mature TGFβ from the latent complex and downstream signalling of TGFβ is complex, including both canonical and non-canonical pathways. Therefore, the different expression of TGFβ and LTBPs, combined with different activators, result in multiple mechanisms regulating TGFβ's bioavailability [195].

1.5.2 Synthesis and secretion of TGFβ

TGFβ isoforms are synthesised as precursor proteins that are proteolytically processed. The signal peptide is removed from the pre-pro-TGFβ during transit through the ER. Two pro-TGFβ molecules dimerise via disulphide-bond formation. Following dimerisation, another cleavage occurs by the convertase family of endoproteases [196]. These proteases cleave the precursor into an N-terminal propeptide homodimer, also known as latency associated peptide (LAP), and C-terminal mature growth factor homodimer. After cleavage, LAP and mature TGFβ remain associated via non-covalent bonds, this assembly is known as the small latent complex (SLC) [196]. LAP shields the receptor-interacting epitopes in mature TGFβ, maintaining TGFβ in its latent form [197]. LAP of the SLC can covalently attach to a LTBP via disulphide-bond formation, this assembly is known as the large latent complex (LLC) [198]. Specifically, LTBP1 and 3 associate with all three LAP-β isoforms, whereas LTBP4 associates with LAP-β1 and LTBP2 does not bind to any LAP-β isoforms. Most cell types secrete TGFβ as part of the LLC however, some cells secrete the SLC without bound LTBP [199]. In turn, LTBP1 and 4 may be secreted free of the SLC, much like LTBP2 which cannot interact with the SLC, suggesting that these LTBPs perform roles independent of TGFβ. LTBP3 on the other hand, is not secreted unless bound to the SLC [200]. Following secretion, LTBP then facilitates the localisation of the LLC in the ECM through interactions with various ECM proteins (Figure 5) [201]. Specifically, LTBP3 and LTBP4 are dependent on fibrillin (FBN), while LTBP1 is dependent on FN for incorporation into the ECM [202]. TGFβ is sequestered in the matrix until required.

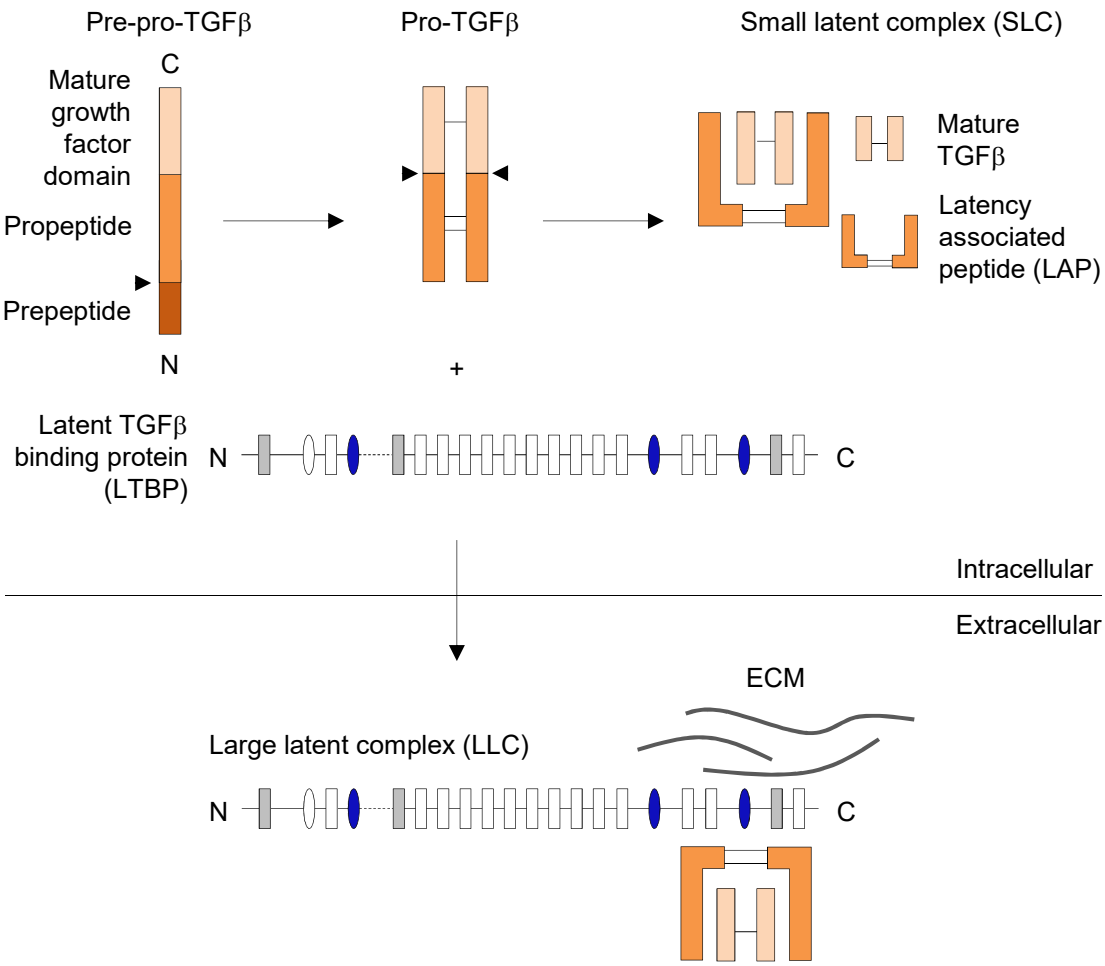

Figure 5. Synthesis and secretion of TGFβ. TGFβ is synthesised as a precursor protein that is proteolytically processed. The signal peptide is removed from pre-pro-TGFβ. Two pro-TGFβ molecules dimerise. Following dimerisation, another cleavage occurs. Pro-TGFβ is cleaved into the propeptide domain, also know as the latent associated peptide (LAP), and mature TGFβ. These homodimers remain associated to form the small latent complex (SLC). LAP of the SLC then associates with a LTBP (structure of LTBP1 shown) to form the large latent complex (LLC), allowing TGFβ to be secreted from the cell. LTBP of the LLC then localises latent TGFβ to the extracellular matrix (ECM). Figure adapted from [195].

1.5.3 Activation of TGFβ

For latent TGFβ to be activated and function at adjacent or neighbouring cells, TGFβ must be released from LAP. An indirect mechanism of TGFβ activation involves the liberation of the LLC from the ECM. Release of the LLC can be initiated with the displacement of LTBP from the ECM. Such that, the release of the LLC can be initiated with the displacement of LTBP bound to FBN [203]. The degradation of FBN by proteolytic enzymes, such as elastase, releases fragments of FBN, including a fragment which binds to FBN and displaces LTBP. This releases the LLC from FBN and contributes to localised TGFβ activation [203]. Degradation of ECM components by several proteolytic enzymes, including; plasmin and thrombin, releases the LLC from the ECM [204]. Cleavage of LTBP1 occurs in a sensitive hinge region, in this way an N-terminal fragment remains bound to the ECM, whilst the remaining LLC is released. BMP1-like MMPs were shown to cleave LTBP1 at two specific sites in the hinge region to release the LLC and facilitate subsequent MMP-dependent LAP cleavage [205]. Through these mechanisms, proteolysis indirectly activates TGFβ through ECM digestion, releasing truncated LLCs which may be further processed to release active TGFβ [195].

A direct mechanism of TGFβ activation involves targeting LAP (Figure 6) [204]. Activation can occur through proteolytic release of active TGFβ through cleavage of LAP by proteases, such as MMP2, MMP9, MMP13 and MMP14 [204]. Another important mechanism of TGFβ activation is via integrins. LAP of TGFβ1 (LAP-β1) and TGFβ3 (LAP-β3), but not LAP of TGFβ2 (LAP-β2), contain an RGD motif [195]. Several integrins including all five αv integrins, as well as α8β1 and α5β1 have been shown to interact with the RGD-containing LAPs. Specifically, LAP-β1 binds the RGD-binding integrins αvβ1, αvβ3, αvβ5, αvβ6, αvβ8 and α8β1, and LAP-β3 binds αvβ6 and αvβ8 [206]. Through this interaction, integrins induce a conformational change that leads to the liberation or exposure of active TGFβ [207-209]. This mechanism depends on the binding of the integrin to LAP via the RGD-motif and simultaneously to the cytoskeleton via the β subunit cytoplasmic domain, which then releases active TGFβ by LAP conformational modification [209]. Integrins αvβ1, αvβ5 [209] and αvβ6 [207, 210] have been shown to activate TGFβ in this way. The binding of LAP to the ECM through interactions with LTBP is a structural precondition for mechanical activation by integrins [207, 209, 211]. Specifically, activation of TGFβ by integrin αvβ6 is resistant to MMP inhibitors and requires a direct interaction of FN with LTBP1 which targets the LLC to the ECM [212]. As a result, TGFβ is inefficiently activated in cells which lack FN or the FN receptor, integrin α5β1. In contrast, activation of TGFβ by integrin αvβ8 is sensitive to MMP inhibitors as it requires MMP14. This mechanism depends on the binding of integrin αvβ8 to LAP-β1 and simultaneously to MMP14, which then releases active TGFβ by proteolytic cleavage of LAP [213]. The β8 subunit has a cytoplasmic domain is distinct, such that it does not interact with the cytoskeleton, and cells expressing a β8 mutant protein lacking the cytoplasmic domain retain the ability to activate TGFβ [206, 213]. It remains to be identified if other integrins active TGFβ in a similar manner.

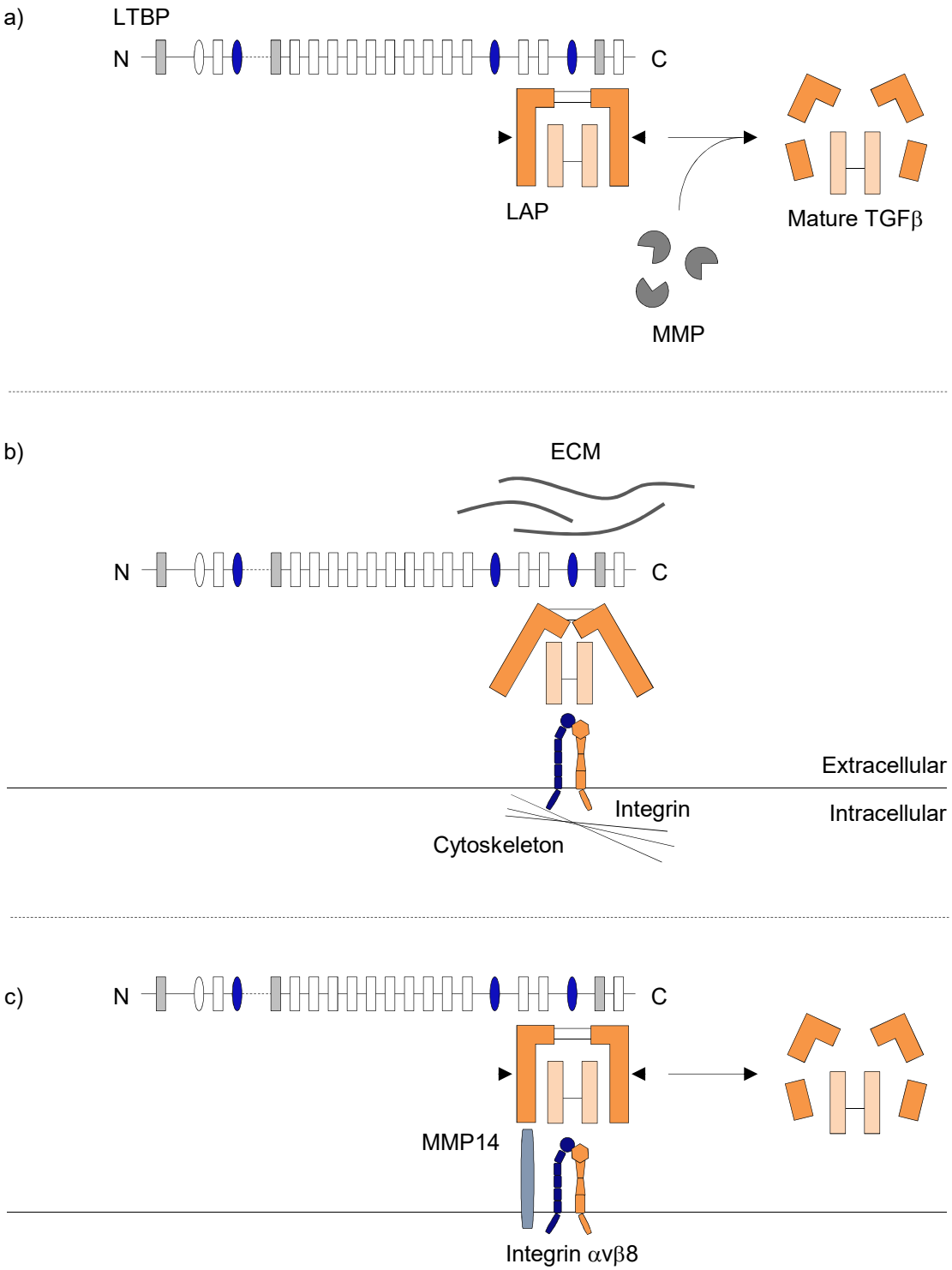

Figure 6. Activation of TGFβ. a) Activation of TGFβ can occur through proteolytic release of mature TGFβ through cleavage of LAP by proteases, including MMPs. b) Activation of TGFβ can also occur through conformational modification of LAP that leads to the release or exposure of mature TGFβ. This mechanism requires the localisation of the LLC to the ECM, the binding of the integrin to LAP via the RGD-motif and simultaneously to the cytoskeleton via the β subunit cytoplasmic domain, which then releases active TGFβ from LAP by conformational modification induced by tension. c) Activation of TGFβ by integrin αvβ8 requires the binding of αvβ8 to LAP1 and simultaneously to MMP14, which then releases active TGFβ by proteolytic cleavage of LAP. Figure adapted from [204].

1.5.4 Signalling pathways of TGFβ

Canonical signalling pathways of TGFβ

All TGFβ isoforms function through the same signalling pathways (Figure 7) [214]. In some cells, TGFβ binds to a transmembrane proteoglycan, known as type III TGFβ receptor (TGFβRIII), which promotes presentation of TGFβ to type II TGFβ receptor (TGFβRII). In other cells, TGFβ binds to directly to TGFβRII, a dimeric transmembrane protein with a constitutively active and phosphorylated serine/threonine kinase in the cytoplasmic domain [215]. TGFβ-bound TGFβRII then recruits type I TGFβ receptor (TGFβRI), a dimeric transmembrane protein with an inactive serine/threonine kinase [216]. The formation of this heterodimeric receptor complex leads to the phosphorylation and activation of TGFβRI by the constitutively active TGFβRII [217]. Active TGFβRI then phosphorylates serine residues in receptor-regulated SMADs, (R-SMADs); SMAD2 and SMAD3. This phosphorylation exposes the nuclear localisation signal (NLS) in the R-SMAD, and permits the binding of importin β to the NLS [218]. Simultaneously, a complex containing two molecules of R-SMAD, associates with a common mediator SMAD (Co-SMAD, SMAD4) [214]. The bound importin β mediates the translocation of this complex to the nucleus [214]. After importin β dissociates in the nucleus, the SMAD complexes bind to specific CAGA nucleotide repeats, known as the SMAD binding element (SBE) [219]. These SMAD complexes have a weak binding affinity for the SBE, and therefore DNA-binding transcription factors are required to regulate such interactions [220]. SMADs and associated cofactors bind in concert to recognition sites on DNA, allowing specific selection of the targeted gene and therefore, TGFβ-mediated transcription [221].

Non-canonical signalling pathways of TGFβ

In addition to SMAD-mediated canonical signalling, other SMAD-independent non-canonical signalling pathways may also be activated by TGFβ [214, 222]. These pathways bypass SMAD signalling and activate p38, JNK, Ras-ERK, PI3K-Akt, and small GTPases such as RhoA and Cdc42, among others [223, 224]. Through these pathways, TGFβ controls the transcription of many genes, including; ECM proteins, integrins and proteases [225].

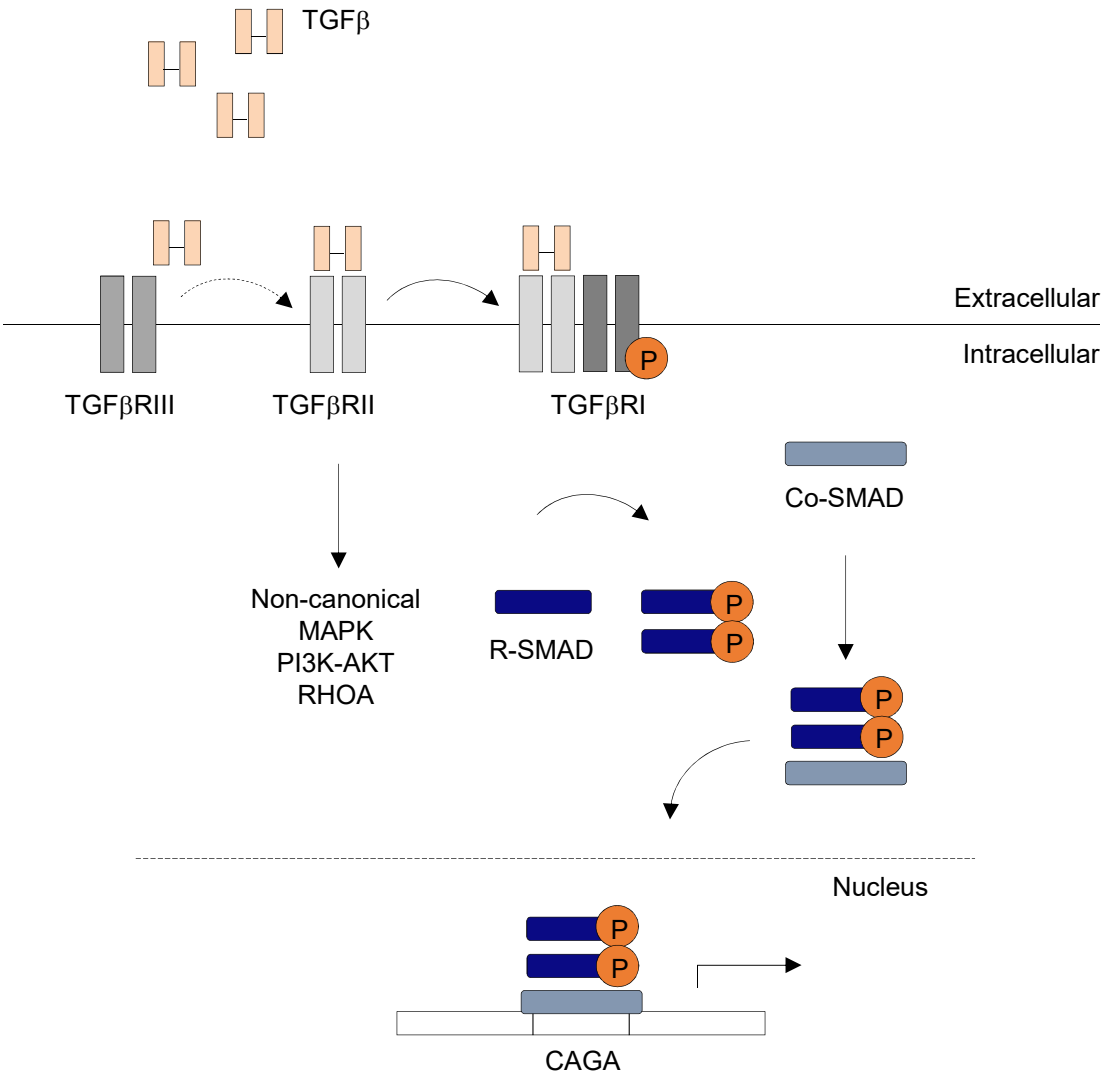

Figure 7. Signalling pathways of TGFβ. Canonical TGFβ signalling is initiated through the phosphorylation of TGFβRI by TGFβRII following ligand binding. TGFβRII may bind directly to TGFβ or indirectly through presentation by TGFβRIII. Active TGFβRI then induces the phosphorylation of the receptor-regulated SMADs (R-SMAD); SMAD2 and SMAD3, which transmit TGFβ signals to the nucleus by association with the common mediator SMAD (Co-SMAD, SMAD4) and binding to specific CAGA nucleotide repeats to control the transcriptional activation or repression of these genes. Non-canonical TGFβ signalling bypasses SMAD proteins and includes activation of: MAPK; PI3K-AKT; RHOA and other pathways. Figure adapted from [238].

Regulation of signalling pathways of TGFβ

TGFβ signalling is regulated in many ways (Figure 8) [219]. Presentation of R-SMADs to the active TGFβR complex is promoted by the SMAD2 anchor for receptor activation (SARA), leading to the promotion of SMAD2-mediated TGFβ signalling [226]. In contrast, R-SMADs are sequestered from the TGFβR by a transmembrane TGFβ-inducible protein (TMEPAI), preventing their phosphorylation [227]. TMEPAI also sequesters phosphorylated R-SMADs, preventing the formation of the R-SMAD/Co-SMAD complex [227]. Activated R-SMADs are also counteracted by phosphatases [228], or by ubiquitin-mediated degradation [229, 230]. In addition, inhibitory SMADs (iSMADs), SMAD6 and SMAD7 are transcriptionally induced upon BMP and TGFβ signalling [231]. While SMAD6 mainly inhibits BMP signalling [232], SMAD7 inhibits both BMP and TGFβ signalling. Mechanistically, SMAD7 can inhibit TGFβ signalling by interacting with the active TGFβRI to prevent the phosphorylation of R-SMADs or by inhibiting the formation of the R-SMAD/Co-SMAD complex [233]. In addition, SMAD7 may target the TGFβR complex for ubiquitin-mediated degradation. In this manner, SMAD7 recruits SMAD ubiquitin regulatory factors (SMURF1 and SMURF2) to the activated TGFβR complex, which leads to the ubiquitination of SMAD7 and results in both SMAD7 and receptor degradation [234]. Receptor internalisation is another essential mechanism in regulating TGFβ signalling [235]. TGFβRs can be constitutively internalised by clathrin-dependent or clathrin-independent mechanisms [235]. TGFβR internalisation via clathrin-dependent endocytosis into EEA1-positive early endosomes (EE), where SARA is localised, promotes TGFβ signalling [235-237]. Here, the TGFβR can be recycled back to the plasma membrane for further signalling. In contrast, TGFβR internalisation via clathrin-independent endocytosis into caveolin-positive compartments, where the SMAD7/SMURF complex is localised, leads to the inhibition of TGFβ signalling [235]. In this manner, segregation of TGFβRs into these distinct endocytic compartments regulates signalling and receptor turnover, however the mechanisms regulating receptor segregation are unknown.

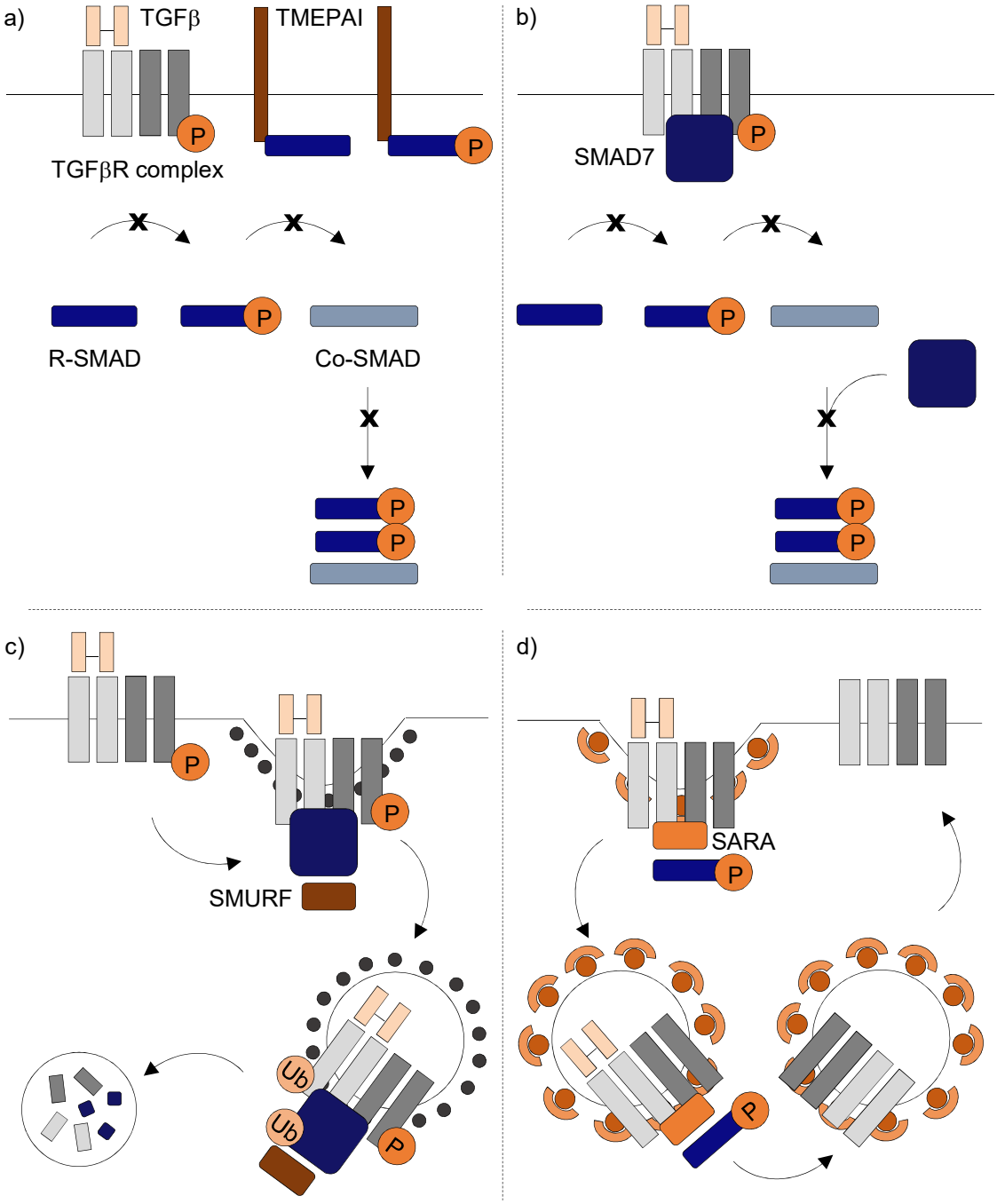

Figure 8. Regulation of signalling pathways of TGFβ. a) Transmembrane TGFβ-inducible protein (TMEPAI) inhibits TGFβ signalling by sequestering R-SMADs from the active TGFβR complex to prevent their phosphorylation or by binding to phosphorylated R-SMADs to prevent their interaction with Co-SMAD. b) Inhibitory SMAD (SMAD7) inhibits TGFβ signalling by interacting with the active TGFβR complex to prevent R-SMAD phosphorylation or by inhibiting the formation of the R-SMAD/Co-SMAD complex. c) SMAD7 may also target the TGFβR complex for ubiquitin-mediated degradation by recruiting SMAD ubiquitin regulatory factors (SMURFs) to the active TGFβR complex. The binding of SMAD7/SMURF to the TGFβR complex leads to internalisation via clathrin-independent endocytosis into caveolae-positive compartiments. SMURFs ubiquitinate (Ub) SMAD7 and TGFβR complex, resulting in their degradation by lyososomes. d) SMAD2 anchor for receptor activation (SARA) promotes the presentation of R-SMADs to the active TGFβR complex, facilitating their phosphorylation at the plasma membrane. TGFβR may be internalised via clathrin-dependent endocytosis into early endosomes, where SARA is localised, to promote TGFβ signalling. From here the TGFβR complex can then be recycled back to the plasma membrane. Figure adapted from [227, 235].

1.5.5 Function of TGFβ

In cancer, TGFβ can act paradoxically as both a tumour suppressor and tumour promoter [238]. At early stages of cancer development, TGFβ acts directly on tumour cells to suppress proliferation and activate apoptosis. With progression, however, TGFβ switches to stimulate the later stages of cancer progression through pleiotropic activities on both tumour and stromal cells. In this manner, TGFβ promotes the proliferation, survival, migration and invasion of tumour cells, while promoting angiogenesis, inflammation and fibroblast activation in the stroma [238]. The cues that drive the tumour suppressor and tumour promoter roles of TGFβ, as well as the switch between these phenotypes is not well known.

Tumour suppressive functions of TGFβ

The tumour suppressive functions of TGFβ are demonstrated by the disruption to components of the TGFβ signalling pathway in several cancers. Commonly, TGFβRII and SMAD4 are inactivated through mutation and LOH. TGFβRII-inactivating mutations are frequently found in colon cancers that are associated with microsatellite instability (MSI) [239]. TGFβRI-inactivating mutations are less frequent; however, they been observed in pancreatic, ovarian and breast cancers [240-242]. Decreased SMAD4 expression has been found in various cancers, including pancreatic, colorectal and head and neck cancers [243]. These studies provide evidence that TGFβ signalling pathways may function as tumour suppressive, and cancers must evade these pathways in order to progress [244].

Cytostatic mechanism. TGFβ exerts cellular cytostatic effects, and functions mechanistically to inhibit cell cycle progression through arrest in G1 phase through two mechanisms: mobilisation of cyclin-dependent kinase (CDK) inhibitors such as p15 (INK4B) and p21 (WAF1), and suppression of c-Myc. The expression of p15 and p21 are induced by SMAD3/SMAD4 complexes with FoxO and Sp1 transcription factors [245-247]. p15 functions to inhibit cell cycle progression in the late G1 phase by interacting with CDK4/6 and preventing their interaction with cyclin D [248]. Consequently, the CDK inhibitor p27 is relocated from cyclin D-CDK4 complexes to interact with and inhibit cyclin E-CDK2 complexes [248]. p21 also functions to inhibit cyclin E-CDK2 complexes [248]. The inactivity of these CDK complexes prevents phosphorylation of pRb, which mediates progression through G1 into S phase [249]. Simultaneously, with the activation of CDK inhibitors, TGFβ functions to repress the c-Myc oncogene that promotes cell proliferation. c-Myc is a transcription factor that may activate or repress gene transcription; such that, it inhibits the transcriptional activation of p15 and p21 [250-252]. In this manner, TGFβ induces cell cycle arrest in G1 and thereby, prevents cell proliferation [253].

Proapoptotic mechanism. TGFβ can also induce apoptosis, however, the mechanisms remain poorly characterised. Candidates that contribute to the proapoptotic functions of TGFβ include; death receptor FAS [254], growth arrest and DNA damage inducible 45β (GADD45β) [255], proapoptotic effector BIM [256] and death-associated protein kinase (DAPK) [257].

Tumour promoting functions of TGFβ

TGFβ is also known to function as a tumour promoter. While inactivating mutations in components of the TGFβ signalling pathway is one mechanism to evade its tumour suppressive effects, the majority of cancers do not exhibit such mutations and retain a functional signalling pathway [258]. Analysis of clinical tumour samples revealed that TGFβ signalling is strongly implicated in cancer progression. Such that increased TGFβ1 expression by tumour cells correlates with colorectal and prostate cancer progression [259, 260]. Positive TGFβ1 immunostaining also correlates with metastases in colorectal, prostate and breast cancers [260-262]. Moreover, TGFβ1 staining is stronger in invading local lymph node metastases than in the primary tumour sites in colorectal and breast cancers [263, 264]. These studies provide evidence that excessive TGFβ signalling is a prerequisite for cancer progression.

Proinvasive mechanism. TGFβ can promote tumour cell invasion and metastasis. For tumour cells to migrate to metastatic sites, they must lose their epithelial characteristics, such as cellular polarity and cell-cell interactions, in favour for mesenchymal characteristics, such as increased motility; a process known as epithelial-to-mesenchymal transition (EMT) [265]. The identification of TGFβ as an inducer of EMT was initially demonstrated *in vitro*. Treatment of normal mammary epithelial cells with TGFβ induced a morphological change, such that their cell shape was altered from cuboidal to an elongated spindle, and this was accompanied by a decreased expression of epithelial markers and increased expression of mesenchymal markers [266]. A hallmark of EMT is the disintegration and disassembly of epithelial cell-cell junctions [266-268]. During TGFβ-mediated EMT, occludins and claudins, and E-cadherin are downregulated, leading to the degradation of tight and adheren junctions, respectively [266-268]. Also during EMT, the actin cytoskeleton is also reorganised into actin stress fibres anchored to FA complexes that contribute to filopodia and promote cell motility [266-268]. *In vivo*, this is likely to be a transient differentiation event, which results in increased cellular plasticity to allow cancer cells to migrate from the primary tumour and disseminate to distant metastatic sites. It remains to be observed the extent to which EMT occurs in humans.

Prometastatic mechanism. TGFβ at the primary tumour site may initiate EMT, resulting in invasion however, once distant metastases have developed, the local production of TGFβ can affect metastatic growth [269]. Studies have suggested a prominent role for TGFβ in bone metastasis, a common site for breast cancer cell dissemination [269]. The bone microenvironment contains sequestered growth factors in the matrix, including TGFβ. MDA-MB-231 breast cancer cells metastasise to the bone, and activate osteoclasts which function to degrade the bone matrix and release activate TGFβ. Expression of a dominant-negative mutant of TGFβRII rendered MDA-MB-231 cells unresponsive to TGFβ. Using a mouse model, these cells led to the development of fewer tumours, with less osteoclast recruitment, less bone destruction at metastatic sites and prolonged survival [269]. TGFβ stimulates the secretion of parathyroid hormone-related protein (PTHrP) by these cells [269, 270]. TGFβ-induced expression of PTHrP in turn stimulated the production of RANK ligand (RANKL) in osteoblasts to promote the differentiation of osteoclast precursors and bone resorption [271]. Administration of anti-PTHrP neutralising antibodies inhibits TGFβ-mediated osteolytic bone metastasis in mice [272]. This is a significant finding as women with PTHrP-positive breast cancer are more likely to develop bone metastasis than those with PTHrP-negative breast cancers [273].

Proangiogenic mechanism. TGFβ can induce a proangiogenic environment. The ability of tumour cells to induce blood vessel formation is essential for tumour growth and blood-borne metastasis. In multiple cancers, elevated circulating plasma levels of TGFβ1 and enhanced tumour angiogenesis correlates with poor patient prognosis [274-276]. More specifically, in breast and non-small cell lung cancers (NSCLCs), high levels of TGFβ1 have been associated with increased microvessel density, which also correlates with poor patient prognosis [274, 275]. The mechanisms of angiogenesis stimulation by TGFβ are both direct and indirect. Such that TGFβ functions to induce the expression of key angiogenic factors including vascular endothelial growth factor (VEGF) and connective tissue growth factor (CTGF) in endothelial cells and fibroblasts [277-280]. TGFβ also directly induces capillary formation of endothelial cells cultured on a COL matrix [281]. TGFβ functions indirectly by acting as a potent chemoattractant for monocytes, which release angiogenic cytokines [282]. TGFβ also induces the expression of MMPs; MMP2 and MMP9, and downregulates the expression of TIMPs in tumour and endothelial cells, to provide a protease-rich microenvironment to enhance the migratory and invasive properties of angiogenically active endothelial cells [283]. Moreover, TGFβ represses the expression of angiopoietin-1 in fibroblasts, which functions to maintain vessel integrity, thereby contributing to the permeability of cancer-associated blood vessels [284]. In this manner, TGFβ promotes tumour angiogenesis.

Microenvironmental mechanism. A common feature of cancers that overexpress TGFβ1 is a desmoplastic stromal response, which is characterised by excessive ECM remodelling, usually through the enhanced activation of stromal fibroblasts [238]. TGFβ can induce the fibroblast-to-myofibroblast transition. Myofibroblasts, also known as 'cancer-associated fibroblasts' when present in the TME, function to remodel the ECM through contraction, and secretion of numerous ECM components and remodelling enzymes [285, 286]. In turn, this facilitates the activation of TGFβ from the ECM, thereby creating a positive feedback loop. Myofibroblasts are also well-documented as potent promoters of tumour cell invasion [287]. Similarly, in epithelial cells TGFβ induces the expression of ECM proteins including FN and the *de novo* expression of several integrins that are not normally expressed in epithelial cells such integrin αvβ3, αvβ5 and αvβ6, which are implicated in the activation of TGFβ, therefore tumour cells are well equipped to activate TGFβ [225]. These changes promote the invasive capabilities of tumour cells. Indeed, blocking TGFβ pathways inhibits integrin expression, ECM deposition and protease activity, as well as TGFβ-mediated invasion [225]. This suggests inhibiting these changes are sufficient to block invasion. TGFβ may also functions to repress the expression of LN and/or LN-binding integrins α3β1 and α6β4 to inhibit cell adhesion [141]. Together, these changes create a TME that promotes progression into invasion.

1.6 EXTRACELLULAR MATRIX

The ECM is a complex and dynamic network of secreted proteins, glycoproteins and proteoglycans which assemble into diverse forms; the interstitial form within organs, and as specialised forms such as; the BM underlying epithelia, vascular endothelium, and surrounding other cell and tissue types [288, 289]. These provide structural support and anchorage for individual cells, tissues and organs. Cells adhere to the ECM via cell-surface receptors, among which integrins are the most prominent [116]. These cell-ECM interactions allow for the transduction of signals between cells and their microenvironment. In this manner, the biochemical and biophysical properties of the ECM can modulate cell behaviour. In turn, cells can modulate these properties of the ECM through synthesis, assembly and degradation. In addition, the ECM also serves as a reservoir for growth factors, cytokines, and ECM-remodelling enzymes. These interactions must be tightly regulated to maintain tissue development and homeostasis [288, 289], and alterations to these interactions have been associated with various pathological conditions such as fibrosis and cancer [238, 288-290].

Both long-standing, as well as more recent data, has implicated the ECM as a significant contributor to cancer progression [75]. Excessive deposition of ECM proteins is a common feature of cancers with poor prognosis [291]. Moreover, multiple studies have demonstrated that both ECM proteins and ECM receptors are dysregulated in cancer progression [290, 292-295]. Such that the composition of the ECM is a significant predictor of clinical prognosis. Breast cancers can be stratified into four subclasses based solely on ECM composition, and these subclasses are predictive of patient outcome [296]. Unsurprisingly, those with high expression of protease inhibitors in their ECM are associated with a good prognosis, while those with high expression of integrins and proteases are associated with poor prognosis [296]. The different cell types which form the TME, produce distinct ECM profiles, which have been termed the ‘matrisome’ as they were identified through proteomic technologies [297]. Such studies identified that primary tumours of differing metastatic potential differ in the composition of both neoplastic and stromal cell-derived ECM components [297].

More recent attention to the role of the ECM in cancer progression has focused on modification to the mechanical properties [298]. Current clinical techniques utilise tissue stiffness as a feature to detect cancer however, the function of such alterations in promoting progression is poorly understood. Imaging elastography and unconfined compression analyses have consistently revealed that the tumour tissue is stiffer than the surrounding uninvolved tissue. For instance, breast cancer tissue (4kPa) is stiffer than normal breast tissue (0.16kPa) [299, 300]. Moreover, atomic force microscopy (AFM) indentation analysis identified heterogeneity of ECM stiffness within an individual's cancer [301-304]. Such that, AFM indentation revealed that the invasive front of human breast tissue is stiffer [305], and the vasculature within the centre of the cancer is softer than the vasculature at the periphery [306]. Regardless of this heterogeneity, overall, those harbouring the stiffest regions were the most aggressive. In breast cancer, those with the highest number of stiff regions within the stroma were of the basal-like subtype. Considering these basal-like breast cancers also have a poor prognosis, these findings imply ECM stiffness may be linked to cancer aggression. Accumulating experimental evidence demonstrates that this reduction in breast tissue compliance may be attributed to changes in the deposition, composition and organisation of the ECM [307]. More specifically, COL is known to be upregulated within the stroma of breast cancer compared to the stroma of normal breast; as demonstrated by the elevated quantity, reorganisation, crosslinking and stiffness of COL [292, 294, 300, 308]. These alterations promote progression in an integrin-dependent manner [299, 300] and likely occur through modulating both neoplastic and stromal cell behavior in the TME [309]. In addition to COL, the cancer-associated ECM is composed of other fibrillar components whose roles in promoting stiffness are less clear. In particular, FN, which is critical for the deposition of COL in the ECM *in vivo* [310].

1.6.1 FIBRONECTIN

1.6.1.1 Expression of fibronectin

In the normal adult breast, FN is essentially absent from the stroma [311] and the tissue is soft and pliable [312]. In breast cancer, a number of ECM proteins are significantly deregulated [294], and increased FN mRNA and protein levels have been detected in the stroma of breast cancer [311, 313-317]. High levels of FN in breast cancer have been positively associated with an invasive and metastatic breast cancer phenotype and negatively associated with survival of breast cancer patients [314, 318, 319]. Changes in the deposition of FN have been demonstrated to contribute to the 'pre-metastatic niche', which facilitates the adhesion of bone marrow-derived cells to promote breast cancer invasion and metastasis [320, 321]. Like FN, high levels of integrin $\alpha 5\beta 1$ correlate with a decreased survival of breast cancer patients [322]. While evidence provides a role for FN in breast cancer progression, the mechanisms regulating FN expression and function in breast cancer progression are unknown.

1.6.1.2 Structure of fibronectin

FN is composed of two nearly identical ~250 kDa subunits, which are linked by a pair of disulphide bonds near the C-terminus. Each subunit is composed of repeating units of three different homologies; including, 12 type I, 2 type II and 17 type III repeats (Figure 9) [323]. These repeats are classified based on similarities in amino acid sequence, although the sequences of any two repeats of a given type are not always identical. Type I repeats are 40 amino acids in length; type II repeats are 60 amino acids in length, and type III repeats are 90 amino acids in length [324, 325]. Type I and type II repeats are mechanically stable as they are stabilised by disulphide bonds, however, type III repeats lack disulphide bonds and are sensitive to mechanical forces. It has been proposed that the type III repeats unfold to provide the elasticity of FN fibrils. The majority of these domains are constitutively included in mature FN, however, in some cases, their presence and affinity for ligands can be regulated by alternative splicing [326].

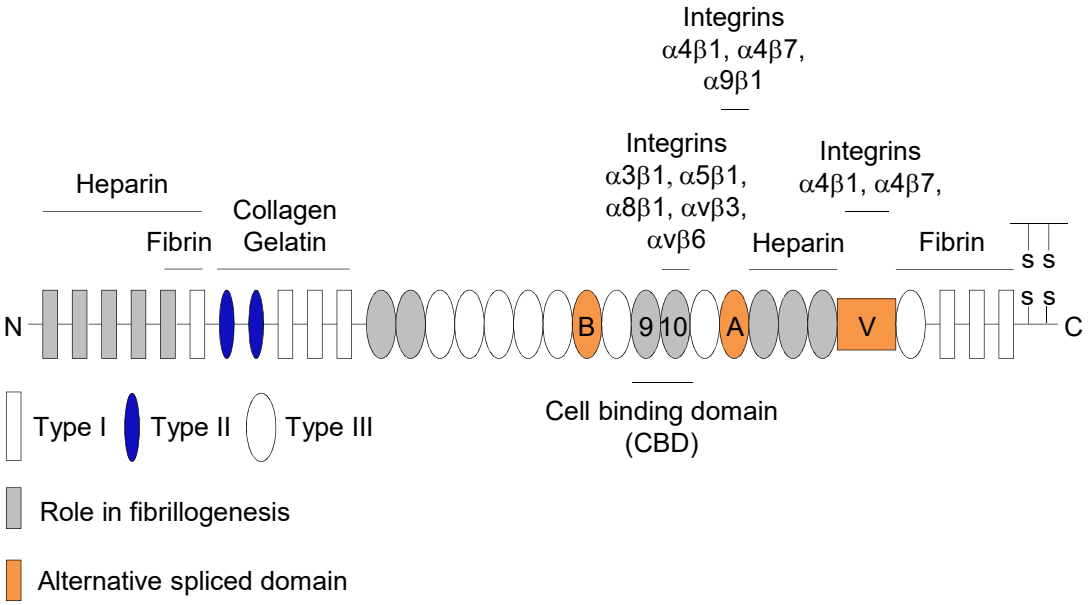

Figure 9. Structure of fibronectin. Fibronectin (FN) is composed of a series of FN type I repeats (white boxes), type II repeats (blue ovals) and type III repeats (white ovals). These repeats are involved in various functions, including binding to integrins or other matrix-associated proteins (denoted), or in the formation of a FN matrix (grey).Two of the type III repeats, as well as a type III connecting segment undergo alternative splicing (orange). Figure adapted from [325].

1.6.1.3 Alternative splicing of fibronectin

FN is encoded by a single gene, which undergoes alternative splicing and various post-translational modifications such as cross-linking. Alternative splicing occurs in three regions of the pre-mRNA: exon usage or skipping leads to either the inclusion or exclusion of two type III repeats, extradomain A (EDA), which is inserted between III11 and III12 domains, and/or extradomain B (EDB), inserted between III7 and III8 domains. The third region of splicing is a type III connecting segment (IIICS), also known as the variable (V) region [326]. The splicing pattern at this region is more complex, this domain may be completely included or excluded, as well as partial inclusion or exclusion. This latter type of splicing is known as exon subdivision, and in humans five variants of the V region have been found; V0, V64, V89, V95 and V120, with the number indicating the number of amino acids in each variant [327]. Alternative splicing leads to protein diversification, and as many as twenty different isoforms of FN exist in humans [328]. These FN isoforms are commonly classified into two forms; plasma FN (pFN) - a soluble form produced by hepatocytes which circulates in the blood (approximately 300–400μg/ml) and cellular FN (cFN) - an insoluble form produced by a variety of fibroblast-like cells in tissues. pFN generally lacks EDA and EDB sequences and one subunit of the dimer is V0, while cFN is a more heterogeneous group of splice variants with variable presence of the EDA, EDB and V regions (Figure 10) [323]. Alternative splicing of FN is regulated by cell type, stage of development and age. In cancer, the splicing pattern is altered, and an increase in the expression of FN isoforms containing EDA and EDB is observed [329-331].

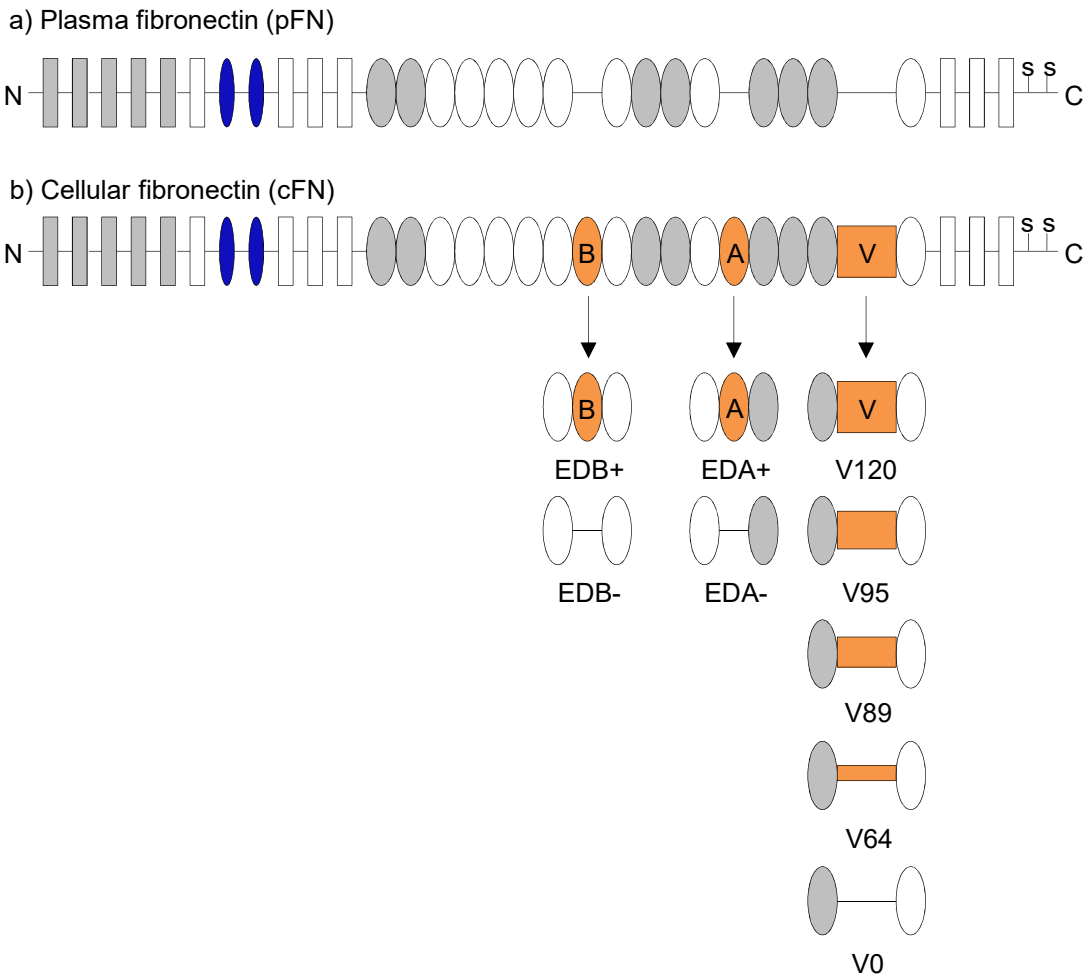

Figure 10. Alternative splicing of fibronectin. FN is encoded by a single gene which undergoes alternative splicing in three regions, including; two type III repeats, extradomain A (EDA) and extradomain B (EDB), and a type III connectin segment (IIICS), known as the variable (V) region. EDA and EDB undergo exon usage or skipping which leads to their inclusion or exclusion, while the V region may be completely or partially included or excluded, known as exon subdivision. This latter splicing pattern of the V region results in five variants in humans (V0, V64, V89, V95 and V120, in which the number indicates the length in amino acids). These FN isoforms are classified as plasma (pFN) or cellular (cFN). pFN lacks EDA and EDB, while one subunit is V0. cFN is more heterogeneous, with variations in the presence of the EDA, EDB and V regions. Figure adapted from [325, 327].

1.6.1.4 Functional domains of fibronectin

Through all of the various domains that compose FN, it is able to bind to other FN molecules, an essential step in the formation of a FN matrix [332, 333]. FN is also able to bind to a variety of other ECM components such as fibrin, COL and heparin, and contributes to their initial and continual assembly and stability [334]. Like other matrix components, FN provides structural support for adhesion interactions between cell-matrix and cell-cell, while at the same time the adhesion receptors, namely integrins, transduce signals that promote actin cytoskeletal reorganisation and alter cellular behaviour [335]. These domains therefore allow for the formation of a FN matrix, which can bind simultaneously to cells and to molecules within the surrounding matrix. Finally, FN controls the bioavailability of growth factors by regulating their activation from the ECM, such as TGFβ [208].

Fibronectin matrix assembly domains

The domains involved in matrix assembly include; the dimerisation domain, which includes the C-terminal pair of cysteines. The covalent linkage between FN subunits is essential to the multimerisation of dimers into fibrils. The cell-binding domain (CBD), which includes RGD cell-binding sequence (III10) and PHSRN (Pro-His-Ser-Arg-Asn) synergy sequence (III9). This domain localises FN to the cell surface. The FN self-association domain, which includes; the N-terminal assembly domain (I1-5), as well as III1-2 and III12-14 domains, which allow matrix assembly [332, 333, 336]. Notably, these sites are located in type III repeats, and the stretching of these repeats exposes these domains for the assembly of FN into fibrils, and are therefore termed cryptic sites [337].

Integrin interaction domains

Two major regions of FN: the CBD and V region, mediate cell adhesion through interaction with multiple integrins. For example, integrins α3β1, α5β1, α8β1, αvβ1, αvβ3 and αvβ6 are able to recognise the RGD sequence in the CBD of FN, while α4β1 and α4β7 recognise the LDV (Leu-Asp-Val) and REDV (Arg-Glu-Asp-Val) sequence in the V region [325]. Specific recognition by the classic FN receptor - α5β1 requires the simultaneous engagement of both the RGD cell binding sequence (III10) and PHSRN synergy sequence (III9) in the CBD of FN, resulting in binding that is highly sensitive to the conformation of FN [116]. In contrast, the binding of other integrins requires only the engagement of the RGD sequence, resulting in binding that is less sensitive to the conformation of FN. In brief, the RGD sequence is separated from the PHSRN synergy sequence by 30-40 Å, and a small rotation between III9 and III10 results in the orientation of these two binding sites onto the same side [338, 339]. Therefore, changes to the conformation of FN alters the type of integrins used by cells to bind to FN, and subsequent downstream signalling. In this manner, FN conformation is able to regulate cell activity via the specificity of integrin binding [340]. In addition, cFN isoforms containing EDA and EDB domains are capable of directing phenotypic behaviours that differ from pFN lacking these domains, it is not surprising that these isoforms bind and signal via different integrins [325]. EDA may bind to α4 (α4β1 and α4β7) and α9β1 through the EDGIHEL (Glu-Asp-Gly-Ile-His-Glu-Leu) sequence [324]. However, these integrins are not specific for EDA, as α4 also binds to the V region. No specific receptors for the EDB domain have been identified [325].

Alternatively spliced domains

All three alternatively spliced domains are positioned to affect cell adhesion: EDA and EDB reside on either side of the RGD and PHSRN synergy sequence in the CBD, whereas the EDA and V region reside on either side of the heparin binding domain [325]. Structural studies have suggested that the insertion of an alternatively spliced domain may induce a conformational change in FN that affects the exposure of the RGD site [338] or other epitopes [341], thereby altering the adhesive properties of FN. Moreover, as mentioned previously, both EDA and the V region have been shown to have a direct role in cell adhesion by binding to integrins, while cell binding to EDB has not been reported [324, 325]. The V region has functions other than adhesion and controls FN dimer secretion. Such that any V0-V0 dimers are retained in the endoplasmic reticulum and degraded intracellularly [342]. FN containing the V region is widely expressed and deposited into the ECM in essentially all tissues [343, 344]. In contrast to the prevalence of the V region in FN, isoforms containing the EDA and EDB domains are most abundant in embryogenesis [344]. These isoforms demonstrate tissue-specific regulation and expression, and their inclusion decreases with age, with adult tissues usually devoid of these domains [344]. However, these isoforms are upregulated in specific conditions such as tissue repair and fibrosis, and angiogenesis in cancer [325]. They have been well-documented as vascular markers of solid cancers, and are often referred to as oncofetal variants [345]. Specific functional roles for EDA and EDB have not been clearly defined from cell culture experiments, and so the generation of null mutations in mice provides insight into their function. Homozygous mutant mice lacking EDA or EDB, EDA-/- and EDB-/- respectively, do not show any degree of embryonic lethality, they grow up without any obvious defects and reproduce normally [346]. Therefore, the single deletion of EDA or EDB suggests these domains may compensate for one another. Moreover, simultaneous deletion of both EDA and EDB results in embryonic lethality with multiple embryonic vascular defects [347]. These domains are therefore essential to embryogenic vasculogenesis. Although the defects seen in these mice lacking both domains are severe, mechanistic insights into specific functions for each individual domain *in vivo* remain to be elucidated.

1.6.1.5 Matrix assembly of fibronectin

Assembly of a FN matrix is the same for both pFN and cFN. FN is synthesised as a monomer, which rapidly undergoes dimerisation in the rough endoplasmic reticulum. FN forms a soluble, compact disulphide-bonded dimer via C-terminal cysteines. This conformation prevents fibril formation. Fibrillogenesis is dependent on the binding of FN to cells. Integrin $\alpha5\beta1$ is the primary receptor for binding to FN, and it binds through the RGD and PSHRN synergy sequence in the CBD. Function-blocking antibodies against either the CBD or $\alpha5\beta1$ inhibit fibrillogenesis [348, 349]. Although integrin $\alpha5\beta1$ is primarily responsible for FN matrix assembly, other integrins can perform this function under appropriate conditions, such as stimulation with manganese ions (Mn^{2+}) or activating anti-integrin antibodies *in vitro*. These integrins include; $\alpha3\beta1$ [350], $\alpha4\beta1$ [351], $\alpha v\beta1$ [352], $\alpha v\beta3$ [353], $\alpha v\beta6$ [354] and $\alpha IIb\beta3$ [355]. Some of these integrins bind to regions in FN other than the CBD, suggesting FN matrix assembly may require more than a single integrin or region within FN [337]. Integrin binding to FN promotes the formation of FAs through the recruitment of cytoplasmic molecules including FAK, which is rapidly phosphorylated in response to integrin binding. Phospho-FAK recruits Src kinase, and together activate intracellular signalling cascades; Ras/MAPK, Rho-GTPase and PKC which stimulate actomyosin-driven contractility [356]. This tension induces a conformational change in FN leading to the exposure of cryptic self-association sites, allowing for FN-FN interactions, which induce fibril formation and elongation (Figure 11) [337, 357, 358]. Formation of a mature FN matrix is monitored by the irreversible conversion of deoxycholate (DOC)-soluble FN fibrils, into a DOC-insoluble matrix [359].

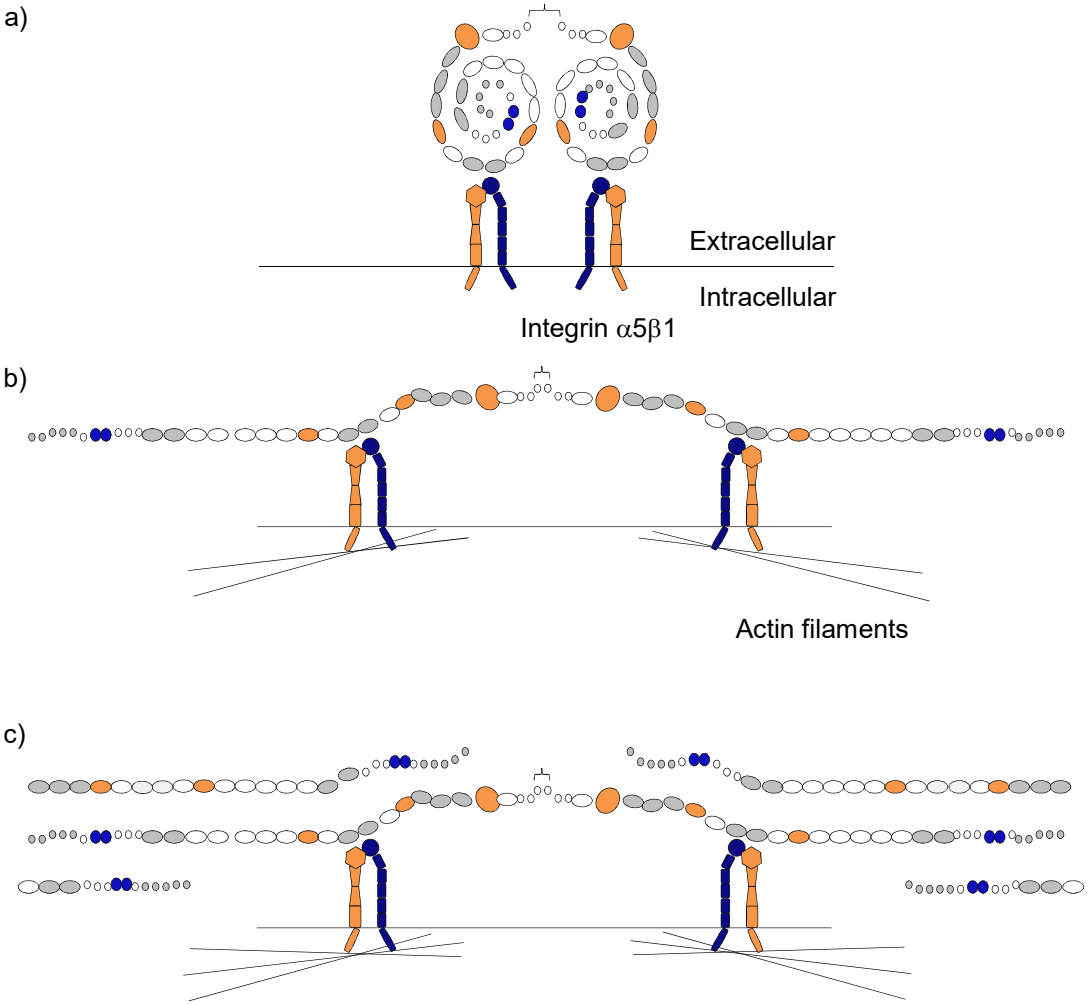

Figure 11. Matrix assembly of fibronectin. a) FN is synthesised as a soluble, compact disulphide-bonded dimer via its C-terminal cysteine residues. FN matrix assembly is initiated by binding to cell-surface receptors, namely integrin α5β1, via its CBD. b) Binding to integrins connects FN to the actin cytoskeleton. These interactions activate intracellular signaling complexes and induce the reorganisation of the actin cytoskeleton.Tension generated by actin reorganization induces conformational changes in FN, thus exposing sequestered FN self-association domains in the bound molecule. c) Fibrils form through FN–FN interactions. Alignment of FN molecules within fibrils might vary depending on which domains interact, such as I1–5 binding to III1–2 versus with III12–14. Overall, an insoluble fibrillar network forms. Figure adapted from [358].

1.6.1.6 Degradation of fibronectin

The ECM undergoes dynamic changes in its organisation and composition as part of tissue homeostasis and repair. ECM remodelling involves alterations in the synthesis, assembly and degradation of ECM components. ECM remodelling is a complex and highly regulated process. Continuous polymerisation of FN is essential for the stabilisation of the FN matrix at the cell surface [360]. Such that in the absence of FN polymerisation, existing FN matrixes are lost, and increased levels of FN degradation are seen [360]. This suggests a steady state between FN polymerisation and turnover exists. The mechanisms for the degradation and removal of ECM proteins includes extracellular proteolysis and endocytosis followed by intracellular degradation. Indeed, FN is a substrate for many extracellular proteases including MMPs [289]. As FN is assembled into cross-linked high-molecular-weight multimers, it is unsurprisingly some proteolytic activity must occur to allow FN endocytosis. It has been demonstrated that MMP14 promotes the turnover of FN by regulating the cleavage of large FN fibrils [211]. Cleaved FN which is bound to $\alpha 5\beta 1$, may then be endocytosed in a caveolin-dependent process [361]. FN is then targeted to the lysosomes and degraded intracellularly [362].

1.6.1.7 Function of fibronectin

Assembly of other matrix proteins

The assembly of FN into the ECM controls the deposition and stability of other ECM proteins including; COL [360, 363], FBN [364], fibulin [365], LTBP [366], and TNC [367]. Some of these proteins associate directly with the FN matrix, whereas others appear to use the FN matrix as a scaffold for deposition of independently structured fibers.

Growth factor reserve

The FN matrix can also sequester growth factors and associated proteins, including BMP1 [368], VEGF [369] and LTBPs [370] to regulate cell signalling events. Moreover, FN has been implicated in the activation of growth factors, including TGFβ, and this function may reflect the localisation of latent TGFβ complexes to the ECM.

Activation of TGFβ

FN localises latent TGFβ complexes to the ECM through interactions with LTBP1, this is an essential step for integrin αvβ6-dependent TGFβ activation [207, 208]. In addition to facilitating the localisation of latent TGFβ to the ECM, FN also facilitates TGFβ activation. A study by Hinz and colleagues proposed that although integrin-mediated force is essential, this force alone may be insufficient for latent TGFβ activation. They demonstrated that in addition to cell contractility, a stiffer FN matrix exerts a stronger force to liberate higher levels of mature TGFβ (Figure 12) [212]. Therefore, enhanced matrix stiffness as seen in solid cancers such as breast cancer, may promote the activation of TGFβ. Furthermore, studies have demonstrated that TGFβ is capable of driving FN expression [371]. Therefore, this may provide a positive feedback loop, in which integrin αvβ6 and FN activate TGFβ, which in turn stimulates expression of both.

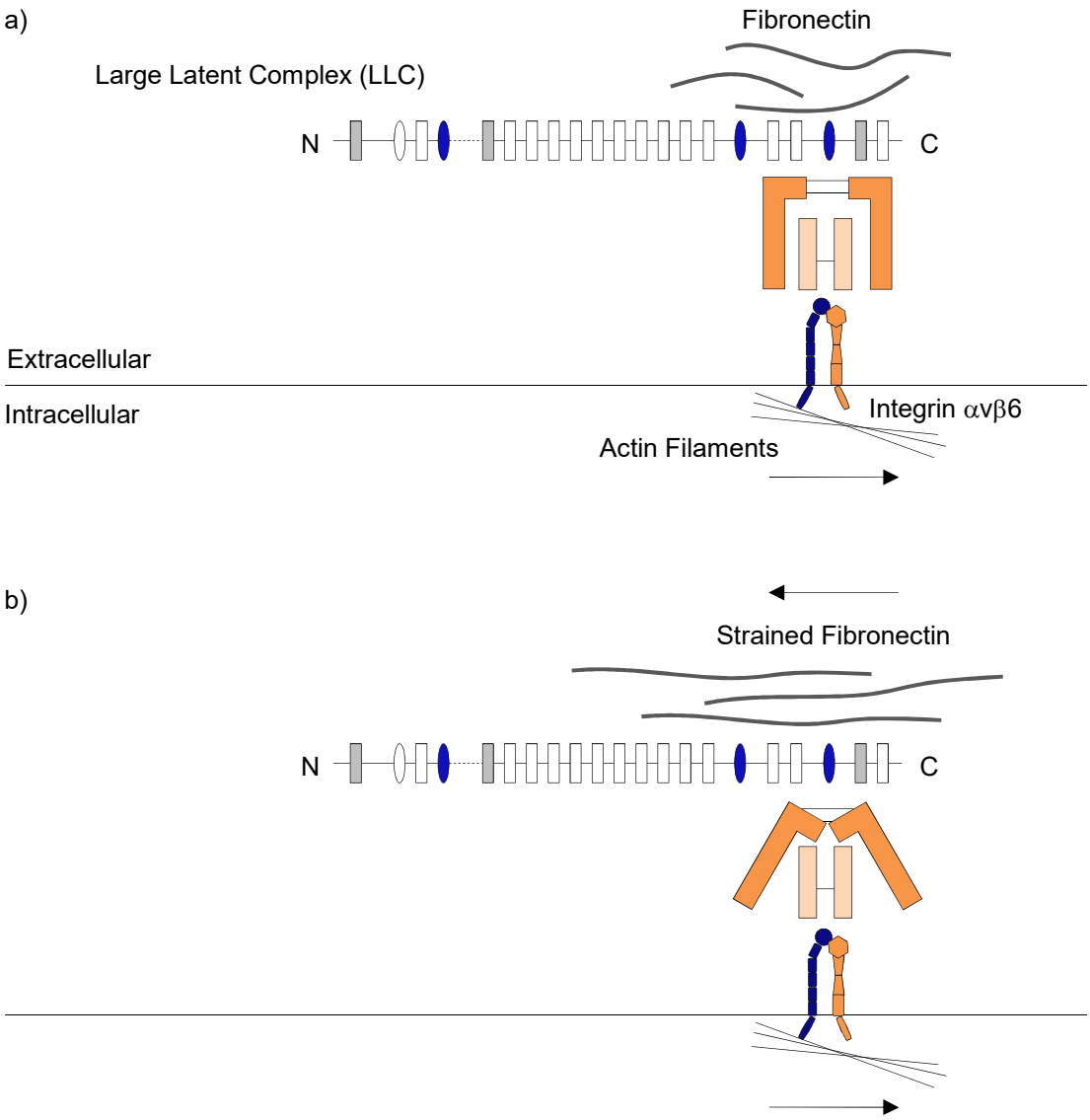

Figure 12. Activation of TGFβ by fibronectin. a) Following the secretion of the LLC, latent TGFβ is then localised to the ECM through interactions between LTBP1 and FN. This localisation step is a prerequisite for the conformational release of active TGFβ from LAP by integrin αvβ6. This mechanism of activation depends on cell contraction to deform LAP however, this force alone may be insufficient in liberating mature TGFβ. b) Straining of ECM fibrils, containing FN and LTBP1, primes latent TGFβ for subsequent activation by integrins. At sufficient prestrain, minimal additional length changes in the ECM fibrils mediated by cell-contaction will be sufficient to release active TGFβ by inducing a conformational change in LAP. Figure adapted from [212].

1.6.2 LATENT TGFβ BINDING PROTEIN

1.6.2.1 Structure of LTBP

LTBPs are extracellular glycoproteins which comprise a family of four proteins; LTBP1, LTBP2, LTBP3 and LTBP4, which are structurally similar to FBNs. LTBP1 and LTBP4 exist in two isoforms, short (S) and long (L), transcribed from different promoters [200]. The long isoforms contain N-terminal amino acid extensions. LTBPs are multidomain proteins; composed primarily of EGF-like domains, the majority of which contain calcium binding sequences, in addition there are domains containing eight cysteine residues, known as 8-Cys or TGFβ-binding protein-like (TB) domains. These 8-Cys domains are unique to the LTBP-FBN superfamily. The first 8-Cys domain, located at the N-terminal, is known as the hybrid domain, since it shares similarities with both 8-Cys and EGF-like domains. Between the second 8-Cys domain (8-Cys-2) and the stretch of repeating EGF-like motifs, there is an unstructured proline-rich region called the hinge domain, which shows the highest degree of sequence diversity amongst the four LTBPs [200, 370]. The third 8-Cys domain forms disulphide linkages with the N-terminal cysteines in LAP, this domain is present in LTBP1, LTBP3 and LTBP4. LTBP1 and LTBP3 covalently bind to all TGFβ-LAP isoforms, while LTBP4 binds poorly and only to TGFβ1-LAP, whereas LTBP2 does not (Figure 13) [200, 372].

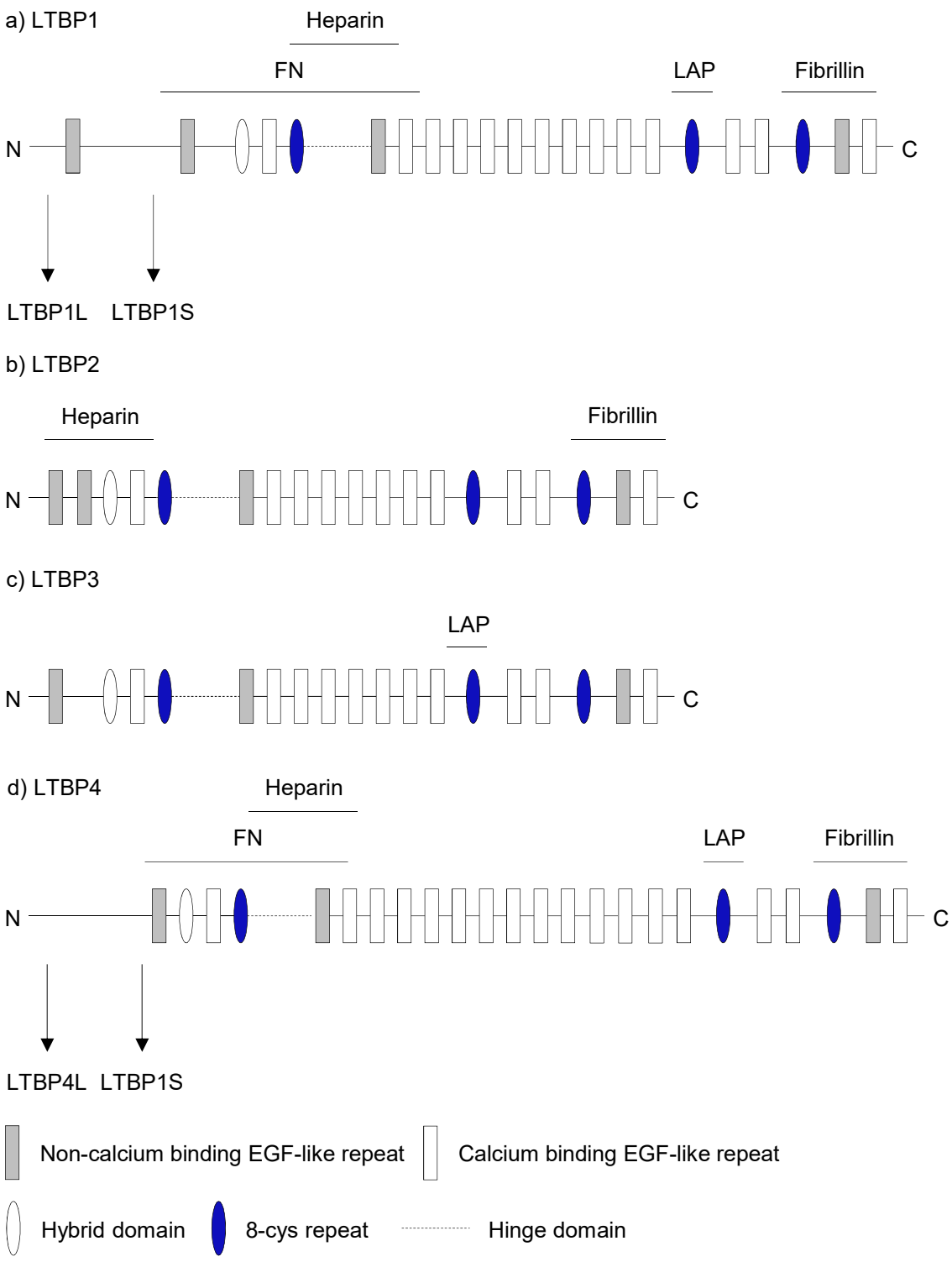

Figure 13. Structure of latent TGFβ binding protein. LTBPs comprise a family of four proteins; LTBP1, LTBP2, LTBP3 and LTBP4. LTBP1 and LTBP4 exist in two isoforms; short (S) and long (L), transcribed by two different promoters. The long isofroms contain N-terminal amino acid extensions. LTBPs are multi domain proteins, composed of EGF-like domains (grey boxes), many of which contain calcium binding sequences (white boxes), and hybrid domains (white ovals), of which the majority contain eight cysteine residues (8-Cys) (blue ovals). There is also is an unstructured proline-rich region known as the hinge domain (dashed line). Figure adapted from [201].

1.6.2.2 Function of LTBP

As discussed previously, TGFβ is secreted as part of a latent complex composed of LAP-LTBP. LTBPs regulate TGFβ activity by facilitating secretion, localisation to the ECM and activation from the latent complex [200, 370]. The localisation of the latent TGFβ in the ECM is a key function of LTBPs, and this step is essential in the process of TGFβ activation [366]. LTBP1, LTBP2 and LTBP4 have been shown to bind to FBN1 and FBN2 by non-covalent interactions through their C-terminus. In addition, the N-terminal regions of LTBP1 and LTBP4 interact with FN, providing a second site for LTBPs to interact with the ECM. The significance of the interaction between LTBP1 and LTBP4 with FN is difficult to assess, as FBN1 assembly also requires FN. However, a later study demonstrated that FBN1 is required for the incorporation of LTBP3 and LTBP4, but not LTBP1, whereas FN is essential for the incorporation of LTBP1 [202]. During ECM maturation, LTBP1 then shifts its association from FN to FBN [366]. FN binds to the hinge region in LTBP1 (amino acids 414-437), and this interaction is essential for the activation of TGFβ1 by integrin αvβ6 [207, 208]. It has been shown that the N-terminal residues (amino acids 291-441) in LTBP1 are essential for the crosslinking of LTBP1 to the matrix by transglutaminases [373]. Interestingly, these residues overlap with the domain that interacts with FN [208]. This suggests that transglutaminases may function to crosslink LTBP1 and FN. These interactions with FBN and FN are essential for the proper localisation of LTBPs.

1.7 MATRIX METALLOPROTEINASES

1.7.1 Classification of MMPs

Proteolytic enzymes are classified as exopeptidases or endopeptidases based on their ability to cleave terminal or non-terminal peptide bonds, respectively [374]. Endopeptidases are classified as serine, cysteine, aspartic and metalloproteinases based on their catalytic mechanism [374]. Metalloproteinases are divalent cation-dependent enzymes which are further subdivided into families, including the metzincins, which comprise: MMPs, a disintegrin and metalloproteinases (ADAM) and ADAMs with thrombospondin domains (ADAMTS), with MMPs being the most studied [374]. MMPs are able to cleave multiple ECM components, as well as non-matrix component [288]. MMP degradation is essential in normal physiological processes, by; degrading ECM components to allow cellular migration, altering ECM composition to alter cellular behaviour, as well as modulating growth factor and cytokine activity by direct cleavage or release from bound storage [374]. MMP activity is regulated at the transcriptional level, and at the protein level through regulation of activation, localisation and inhibition [374]. Altered expression and/or dysregulation of MMPs has been associated with cancer development and progression [288]. In humans, 23 MMPs are known [375]. MMPs were originally classified as collagenases, gelatinases, stromelysins and matrilysins based on their specificity for these ECM components. However, as more MMPs have been identified, a sequential numbering system has been adopted, and MMPs are now classified according to their structure (Table 2) [374, 376].

Enzyme	MMP	Substrates
Secreted MMPs		
Minimal-domain MMP		
Matrilysin 1	MMP7	Aggrecan, COL (I and IV), decorin, elastin, FN, fibulin, gelatin, LN, osteonectin, tenascin, vitronectin, casein, E-cadherin, fibrinogen, integrin β4, pro-MMP1, 2 and 9, pro-TNFα, plasminogen
Matrilysin 2	MMP26	COL4, FN, gelatin, casein, fibrinogen, pro-MMP9
Simple hemopexin-domain-containing MMPs		
Collagenase 1	MMP1	Aggrecan, COL (I, II, III, VII, VIII, X and XI), FN, gelatin, IGFBPs, LN, TN, vitronectin, casein, fibrin, pro-TNFα
Stromelysin 1	MMP3	Aggrecan, COL (III, IV, V, VII, IX, X and XI), decorin, elastin, FBN, FN, gelatin, IGFBPs, LN, osteonectin, tenascin, vitronectin, casein, E-cadherin, fibrin, fibrinogen, pro-MMP1, 7, 8, 9 and 13, pro-TNFα, plasminogen
Collagenase 2	MMP8	Aggrecan, COL (I, II and III), fibrinogen, pro-TNFα, plasminogen
Stromelysin 2	MMP10	Aggrecan, COL (III, IV and V), elastin, FN, gelatin, casein, fibrinogen, pro-MMP1, 7, 8 and 9
Metalloelastase	MMP12	Aggrecan, COL (I and IV), elastin, FBN, FN, gelatin, LN, vitronectin, fibrinogen, pro-TNFα, plasminogen
Collagenase 3	MMP13	Aggrecan, COL (I, II, III, VI, IX, X and XIV), FBN, FN, gelatin, osteonectin, casein, fibrinogen
Collagenase 4	MMP19	COL (I and IV), FN, gelatin, tenascin, casein

Enamelysin	MMP20	Aggrecan, fragments of COL XVIII
	MMP27	No substrates reported
Gelatin-binding MMPs		
Gelatinase A	MMP2	Aggrecan, COL (I, III, IV, V, VII, X and XI), decorin, elastin, FBN, FN, fibulin, gelatin, IFGBPs, LN, oesteonectin, tenascin, vitronectin, FGFR1, fibrin, fibrinogen, pro-MMP9 and 13, latent TGFβ, pro-TNFα, plasminogen
Gelatinase B	MMP9	Aggrecan, COL (IV, V, XI and XIV), decorin, elastin, FBN, gelatin, LN, osteonectin, vitronectin, casein, fibrin, fibrinogen, latent TGFβ, pro-TNFα
Furin-activated secreted MMPs		
Stromelysin 3	MMP11	IGFBPs
Epilysin	MMP28	Casein
Vitronectin-like insert MMPs		
	MMP21	No substrates reported
Membrane type-MMPs (MT-MMPs)		
Transmembrane MMPs		
MT1-MMP	MMP14	COL (I, II and II), FBN, FN, gelatin, LN, vitronectin, fibrin, fibrinogen, integrin αv, pro-MMP2 and 13, pro-TNFα
MT2-MMP	MMP15	Aggrecan, FN, LN, tenascin, pro-MMP2

MT3-MMP	MMP16	COL3, FN, pro-MMP2
MT5-MMP	MMP24	Gelatin, FN, pro-MMP2
Glycosylphosphatidylinositol (GPI)-anchored MMPs		
MT4-MMP	MMP17	Gelatin, fibrin, fibrinogen, pro-MMP2
MT6-MMP	MMP25	COL4, gelatin, FN, fibrinogen, fibrin, pro-MMP2
Type II transmembrane MMPs		
Cysteine Array MMP	MMP23A	No substrates reported
Cysteine Array MMP	MMP23B	No substrates reported

Table 2. Classification of matrix metalloproteinases. Table adapted from [374, 376].

1.7.2 Structure of MMPs

MMPs share a conserved domain structure and activation mechanism (Figure 14) [374]. They are synthesised as inactive zymogens, also known as pro-MMPs, which are composed of a signal peptide, prodomain and catalytic domain [377]. The signal peptide facilitates their secretion to the endoplasmic reticulum. The prodomain contains a zinc-interacting Cys thiol group that maintains MMPs inactive. The catalytic domain contains the catalytic machinery including the zinc-binding site. With the exception of minimal domain MMPs and type II transmembrane MMPs, MMPs contain an additional hemopexin domain, which links to the catalytic domain through a hinge region [374]. The hemopexin domain mediates interactions with TIMPs, cell-surface molecules and proteolytic substrates, and therefore substrate specificity [378]. Additionally, the hinge region is suggested to influence specificity for proteolytic substrates [379]. Gelatin-binding MMPs also contain inserts that resemble the type II repeats in FN, which are required to bind and cleave COL [380, 381]. Furin-activated secreted MMPs contain a recognition motif for intracellular furin-like serine proteinases between their prodomain and catalytic domain. This motif is also found in vitronectin-like insert MMPs and MT-MMPs. Transmembrane MMPs have a C-terminal domain composed of a single-span transmembrane domain and a short cytoplasmic domain. Glycosylphosphatidylinositol (GPI)-anchored MMPs share a similar domain structure however, the C-terminal domain contains a hydrophobic domain that acts as a GPI anchoring signal [382], while type II transmembrane MMPs contain an N-terminal signal anchor that targets it to the cell surface [383].

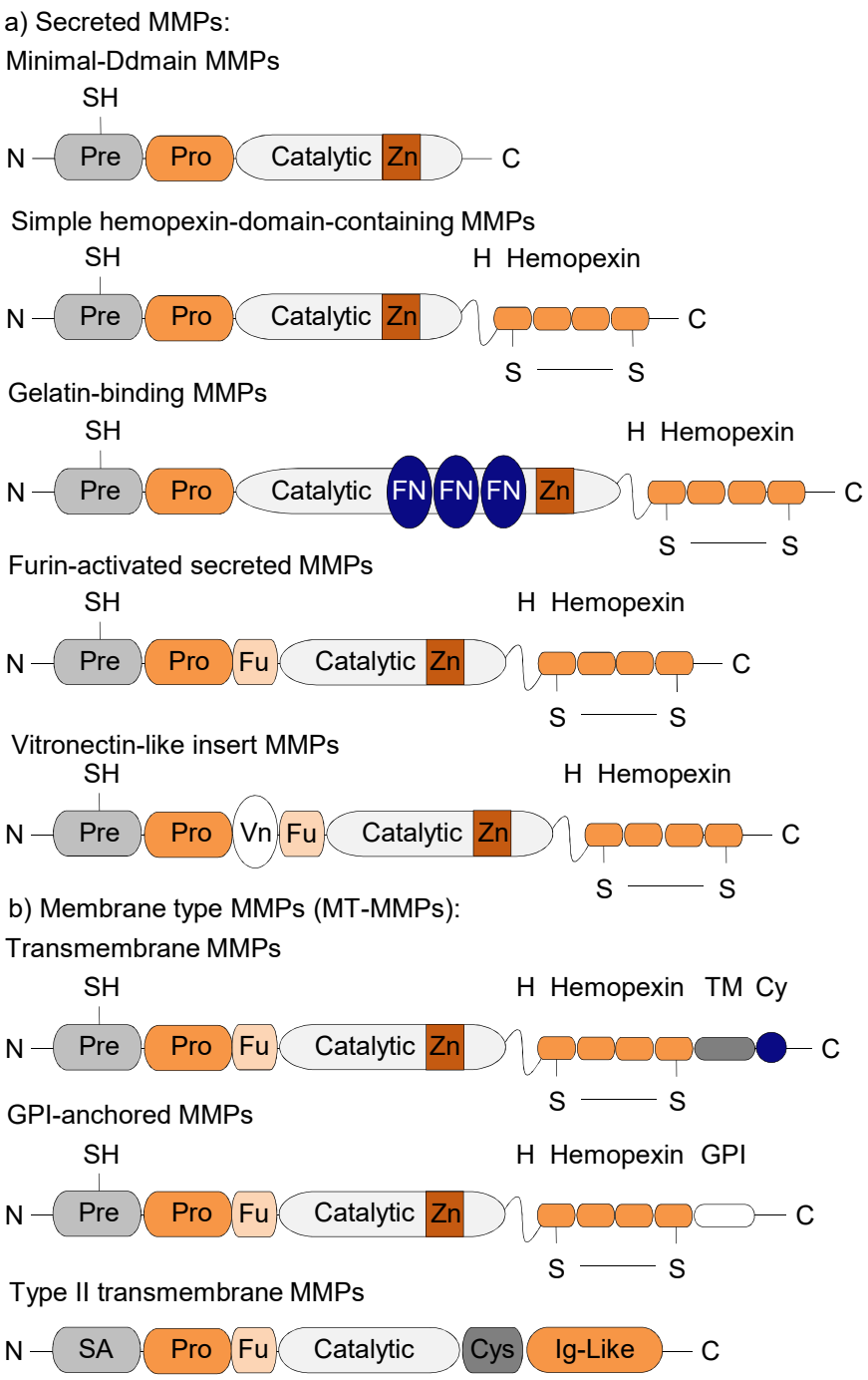

Figure 14. Structure of matrix metalloproteinases. MMPs are classified into eight structural classes, five of which are secreted and three of which are membrane-type MMPs (MT-MMPs). a) Secreted MMPs: Minimal-domain MMPs contain a signal peptide (Pre), a prodomain (Pro) with a thiol (SH) group, and a catalytic domain with a zinc-binding site (Zn). In addition to these domains, the simple hemopexin-domain-containing MMPs have a hemopexin domain that is linked to the catalytic domain by a hinge (H). The first and the last of the four repeats in the hemopexin domain are linked by a disulphide bond (S–S). The gelatin-binding MMPs contain inserts that resemble type II repeats of FN. The furin-activated secreted MMPs contain a recognition motif for intracellular furin-like serine proteinases (Fu). This motif is also found in vitronectin-like insert (Vn) MMPs and the MT-MMPs. b) MT-MMPs: Transmembrane MMPs have a single-span transmembrane domain (TM) and a very short cytoplasmic domain (Cy), while the glycosylphosphatidylinositol (GPI)-anchored MMPs have a GPI anchor domain. The type II transmembrane MMPs contain a signal anchor (SA), and are also characterised by cysteine-rich (Cys) and immunoglobulin (Ig)-like domains. Figure adapted from [374].

1.7.3 Regulation of MMPs

Activation

MMP expression is primarily regulated at the transcriptional level, such that most cells synthesise and immediately secrete MMPs into the stroma when required [384]. Secreted MMPs are then localised to the cell surface through interactions with cell-surface receptors, while MT-MMPs are covalently linked to the cell membrane. The interaction between the thiol group in the prodomain and a zinc ion (Zn^{2+}) bound to the catalytic domain maintains MMPs inactive. The activation of MMPs requires the destabilisation of the interaction or the removal of the prodomain [385]. Most MMPs are activated extracellularly by other activated MMPs or several serine proteinases. However, some MMPs can be activated prior to reaching the cell surface by intracellular furin-like serine proteinases due to their shared presence of a furin proteinase recognition motif [386]. The notable exception to these mechanisms of activation is MMP2, which is often constitutively expressed and controlled through a unique mechanism of activation at the cell surface involving MMP14 and TIMP2. In this way, the N-terminal domain of TIMP2 binds to MMP14 and the C-terminal domain of TIMP2 binds to the hemopexin domain of pro-MMP2 [387]. This allows an adjacent, uninhibited MMP14 to cleave the bound pro-MMP2. MMP14 does not fully activate MMP2, and another, already activated MMP2 is required to remove a residual portion of the prodomain of MMP2 [388]. Data indicate that the basal expression of MMP2, MMP14, and TIMP2 is coregulated, which is consistent with their cooperation during MMP2 activation [389]. Pro-MMP2 may also be activated by MMP15 in a mechanism that does not require the TIMP2/MMP14 complex [390].

Localisation

In addition to anchorage of MMPs to the cell surface, such as the case for MT-MMPs, secreted MMPs may also be localised to cell surface, thereby targeting their catalytic activity to specific substrates within the pericellular space. The mechanisms for localising secreted MMPs to the cell surface include; interaction with cell surface receptors, such as the interaction between MMP2 and integrin $\alpha v\beta 3$ [190] or MMP9 and CD44 [391], and interaction with pericellular ECM components, such as the interaction between MMP7 and heparin sulphate [392]. These mechanisms often promote MMP activation, concentrate active MMPs local to their substrate and modulate the access of MMP inhibitors.

Catabolism and clearance

MMPs are able to regulate their proteolytic inactivation and clearance. Some cleavages result in complete inactivation, whereas other cleavages generate truncated MMPs, which lose their ability to cleave some substrates whilst retaining their ability to cleave other substrates [384]. This processing can also diminish the affinity and ability of MMPs to be inhibited by TIMPs, such as the C-terminal truncation of MMP2 [382]. Moreover, truncation can also prevent the localisation of MMPs to the cell surface. In addition, MT-MMPs may be secreted if they are cleaved at a juxtamembrane site before or after they reach the cell surface [393]. In this fashion, proteolysis of MMPs can alter their substrate specificity, localisation, as well as their activity.

Inhibition

MMPs are inhibited by proteinases inhibitors; TIMPs and inhibitors of metalloproteinases (IMPs) to prevent excessive proteolysis. All active forms of MMPs are inhibited by TIMPs. However, TIMPs differ in tissue-specific expression and ability to inhibit the various MMPs [384]. Such as TIMP2 and TIMP3 both inhibit MT1-MMP, whereas TIMP1 does not, and TIMP3 is most potent at inhibiting MMP9. TIMPs function by forming irreversible complexes with MMPs through interaction with their catalytic sites, and bind in a 1:1 stoichiometric manner [394]. Other types of MMP inhibitors include; the smaller IMPs (SIMPs) and larger IMPs (LIMPs). LIMP is a complex composed of TIMP2 and pro-MMP2 [395], which inhibits gelatinases, collagenases and stromeolysins.

1.7.4 Function of MMPs

Extracellular matrix remodelling

Simply, MMPs degrade structural components of the ECM, and thereby facilitate cell migration. However, the ECM is not a passive scaffold; as well as sequestering growth factors and cytokines, the ECM provides contextual signals to cells through interactions with cell adhesion receptors [116]. By extension, MMPs also influence these processes by altering the organisation and composition of the ECM. Cleavage of ECM components by MMPs can facilitate their removal by endocytosis and degradation. For example, MMP14 cleaves FN prior to caveolin 1-dependent endocytosis and subsequent lysosomal degradation [211, 361, 362]. Moreover, cleavage of ECM components by MMPs can generate fragments with new functions; such as cleavage of LN5 by MMP2 results in the exposure of cryptic sites that promote cellular migration [396]. MMPs also participate in the release and subsequent activation of growth factors that are sequestered in the ECM, including TGFβ. In turn, a function of TGFβ is to regulate MMP expression, such that activated TGFβ can both promote and suppress MMP gene transcription [397]. A similar mechanism of regulating MMP activity is seen in the interplay between COL and MMP1. COL1 acts as a ligand for the discoidin domain receptors (DDR1 and DDR2) which induces MMP1 expression following receptor activation, which occurs following the binding of intact COL1. The DDR is then inactivated following binding of MMP1-cleaved COL1 [398, 399]. In this manner, MMP expression is induced by its own substrate, and may then be repressed once it cleaves that substrate and is no longer required.

Cell surface proteolysis

MMPs can also modulate cell behaviour through cleaving; cell-cell interactions, cell-matrix interactions or cell surface molecules. Cleavage of the adheren junction component E-cadherin by MMP3 and MMP7 results in the release of ectodomain fragments which promotes cell migration due to the loss of cell-cell interactions [400]. It is suggested that the cleaved E-cadherin may interfere with the function of full length, uncleaved E-cadherin molecules. Similarly, cleavage of the hyaluronan receptor CD44 by MMP14 promotes cell migration due to loss of cell-cell and cell-ECM interactions. When the cleavage site is mutated, cell migration is inhibited [401]. In addition to binding to the ECM, CD44 also binds MMP9 localising it to the cell surface. This localisation is essential for MMP9 to promote cancer cell invasion and angiogenesis [391]. MMPs can also release cell surface molecules. Cell surface localised MMPs can activate latent TGFβ, and pro-TNFα. Moreover, cleavage of insulin-like growth factor-binding protein (IGFBP) and perlecan by MMPs releases soluble IGFs [402] and fibroblast growth factors (FGFs) [403], respectively. In addition to releasing and activating growth factors and cytokines, MMPs can also cleave their cell surface receptors. MMP2 is able to cleave FGF receptor 1 (FGFR1) [404]. Moreover, two members of the epidermal growth factor receptor (EGFR) family – HER2 [405] and HER4 [406], as well as the hepatocyte growth factor receptor c-MET [407], are also substrates for MMPs, although specific MMPs involved in the cleavage of these receptors have not yet been identified. In all these cases, receptor cleavage releases a soluble receptor fragment that retains its ability to bind to the respective ligand. Together, these data support the role of MMPs in promoting cancer progression.

Cancer development and progression

MMPs have long been associated with cancer invasion and metastasis due to their ability to degrade the BM to allow invasion into the surrounding environment [408]. A positive correlation between the progression of multiple cancer types and MMP expression has been demonstrated in numerous studies (Table 3) [376]. Such that increased MMP levels represent an independent predictor of reduced survival. These tissue studies have been supported by cancer mouse models, which either transgenically overexpress MMPs or MMP-knockout mice [376, 409]. Together with clinical data [410, 411], these studies support a role for MMPs in cancer invasion and metastasis. On the basis of such studies, it was proposed that the pharmalogical inhibition of MMP activity may provide a mechanism to prevent cancer progression. However, the results from clinical trials with these drugs proved disappointing. Universally, the trials failed to reach their end points of increased survival in patients with advanced stage cancer [412-414]. These clinical trials were designed based on the data that supported these essential roles of MMPs in late stages of cancer progression; invasion and metastasis. However, it is now recognised that the tumour-promoting activity of MMPs may be important in early stages of cancer development. Conversely, studies have shown that several MMPs function as anti-tumourigenic proteases [415]. Furthermore, other MMPs which were originally identified as pro-tumourigenic proteases may also function as anti-tumourigenic proteases [415]. Moreover, other MMPs may play no role in cancer progression, but undoubtedly play normal physiological roles. Therefore, the mechanisms underlying the influence of MMPs in cancer must be fully understood in order to better design therapeutic agents.

It has long been assumed that cancer cells are solely responsible for the production of such proteolytic enzymes however, this concept was disproved following the demonstration that stromal cells surrounding cancer cells, and not the cancer cells alone, were also responsible for producing MMPs. This followed the development of *in situ* hybridisation (ISH) techniques. While some MMPs may be produced by cancer cells; such as MMP7 in breast cancer [416], many MMPs are produced by stromal cells; such as MMP13 by myofibroblasts in breast cancer [417]. MMP secretion from adjacent stromal cells may be induced by cancer cells. Indeed, cancer cells may stimulate cancer-associated stromal cells to synthesise MMPs in a paracrine manner through secretion of growth factors and cytokines, as well as other MMPs [374]. Supporting this notion, MMP expression is not induced by gene amplification or activating mutations, and is likely due to transcriptional changes rather than genetic alterations. This may be the result of activation of oncogenes or loss of tumour suppressors; such as, MMP7 is upregulated through combined activation of the transcription factors PEA3, c-JUN, β-catenin and LEF-1 [418], which are downstream of classical oncogenes, and the transcription of MMP1 and MMP13 is repressed by the tumour suppressor p53 [419, 420]. Moreover, MMPs that are secreted by stromal cells can still be recruited to the cancer-cell surface. For example, MMP2 mRNA is expressed by stromal cells of human breast cancers, whereas MMP2 protein is found on both stromal and cancer-cell surface [421].

MMP	Localisation	Expression and clinical Association
MMP1	*Cancel cells* *Stromal cells*	Positively associated with tumour stage
MMP2	Cancer cells *Stromal cells* at invasive front *Endothelial cells*	Increased expression in tumours Positively associated with tumour stage, lymph-node and distant metastases Negatively associated with survival
MMP3	*Cancer cells* *Stromal cells* *Endothelial cells* ECM surrounding blood vessels	Increased expression in tumours compared to normal tissue and pre-malignant lesions
MMP7	*Cancer cells*	Increased expression in tumours compared to normal tissue
MMP8	MECs	Decreased expression in tumours compared to normal tissue
MMP9	*Cancer cells* MECs Fibroblasts *Macrophages* *Endothelial cells*	Increased expression in tumours compared to normal tissue Positively associated with tumour stage and lymph-node metastases
MMP10	ECM surrounding blood vessels	Positively associated with lymph-node metastases
MMP11	*Cancer cells* *Stromal cells*	Increased expression in tumours Positively associated with lymph-node metastases Negatively associated with survival
MMP12	*Macrophages*	Increased expression in tumours compared to normal tissue
MMP13	*Cancer cells* *Myofibroblasts*	Positively associated with local invasion
MMP19	Cancer cells Endothelial cells	Increased expression in benign lesions compared to invasive disease

Table 3. Matrix metalloproteinases in breast cancer. The localisation of MMPs in breast cancer was determined by *in situ* hybridisation (ISH) is indicated by italics, while localisation that has only been determined by IHC is indicated in roman font. Table adapted from [376].

Anti-tumourigenic proteases. MMP8, also known as a neutrophil collagenase, was the first MMP to be identified as having anti-tumourigenic functions. In these studies, male homozygous mutant mice, MMP8-/- exhibited an increased incidence of skin tumours in a chemically induced cancer model system, compared to wild-type mice. Importantly, female MMP8-/- and wild-type mice demonstrated no difference in the incidence of skin tumours. Female MMP8-/- mice whose ovaries were removed or were treated with tamoxifen also demonstrated an increased incidence of skin tumours compared to wild-type mice, demonstrating a protective role for oestrogen in this model. Conversely, bone-marrow transplantation experiments in these mice showed that MMP8 produced by neutrophils is sufficient to restore the anti-tumour protection mediated by MMP8. Further studies demonstrated that loss of MMP8 leads to inflammatory abnormalities in response to carcinogens, which leads to a sustained inflammatory response that promotes cancer progression [422]. The relevance of MMP8 as an anti-tumourigenic protease has been further shown in human breast cancer cells. The downregulation of MMP8 in non-metastatic breast cancer cells (NM-2C5) increases their metastatic potential, while the upregulation of MMP8 in metastatic breast cancer cells (M-4A4) reduces their metastatic potential [423]. Similarly, manipulation of MMP8 expression in a model of normal and DCIS-MECs, demonstrated a role for MMP8 in negatively regulating breast cancer cell invasion. Moreover, it was found that loss of MMP8 expression was more significantly lost in DCIS/IDC compared to pure DCIS [424]. Together, these data support MMP8 as an anti-tumourigenic protease.

MMP12 has also been implicated as having anti-tumourigenic functions. Studies using MMP12-/- mice revealed a protective role for stromal MMP12 in lung cancer development. Specifically, loss of MMP12 was associated with tumour growth and blood vessel formation [425]. Further studies have shown that these effects seem to be mediated by the ability of MMP12 to generate angiostatin, a potent inhibitor of angiogenesis, formed by cleavage of plasminogen by MMP12, as well as cleavage by MMP2, MMP3, MMP7 and MMP9 *in vitro* [426, 427]. Angiostatin functions by blocking endothelial cell proliferation and migration. Additionally, MMP12 may also inhibit angiogenesis by cleavage and shedding of cell surface-bound urokinase-type plasminogen-activator receptor (uPAR), which is required for endothelial cell invasion into fibrin [428]. Supporting this, MMP12 expression in hepatocellular carcinomas was associated with hypovascularity [425]. MMP26 expression in hormone-regulated cancers is associated with improved clinical outcome. The anti-tumourigenic properties of this MMP may be due to its ability to regulate the expression level of ERβ through its cleavage, and thereby altering oestrogen signalling in hormone-dependent cancers. Moreover, MMP26 expression by macrophages and polymorphonuclear leukocytes has suggested that this protease may have an anti-inflammatory response, similar to MMP8, which contributes to its association with an improved clinical prognosis in patients with breast cancer [429].

Pro-tumourigenic proteases. MMP3, MMP9, MMP11 and MMP19 were first described as pro-tumourigenic proteases, but have now been identified to have dual roles in cancer progression. For instance, MMP3 was initially described as a potent pro-tumourigenic protease [430] however, studies have demonstrated a protective role in skin cancer. Such that, MMP3 overexpression in a chemically induced skin cancer model system reduced tumour growth compared to control [431]. However, gene overexpression studies can be misleading, and MMP3 overexpression may not represent the function of MMP3 when it is expressed at basal concentrations. MMP3-/- mice develop less carcinogen-induced papillomas than control mice [431]. However, the tumours that do form on MMP3-/- mice grow faster and have an increased metastatic potential [431], and therefore MMP3 has a complex role in tumourigenesis. It may be possible however, that MMP3 is pro-tumourigenic during early stages of cancer progression. Similar to MMP3, MMP9 has both pro-tumourigenic and anti-tumourigenic effects depending on stage of progression [376]. In a human papilloma virus (HPV) 16-induced skin cancer model system, MMP9-/- (HPV/MMP9-/-) mice developed less tumours and exhibited delayed progression to invasion compared to wild-type (HPV/MMP9). However, the MMP9-/- cancers that developed were higher grade than wild-type mice, suggesting an increased aggressive nature [432]. In this way, MMP9 may promote progression, whilst limiting development. MMP11 also has paradoxical roles during progression, as identified in MMP11-/- mouse models. Such that MMP11-/- mice have fewer and smaller primary tumours however, more frequently display metastases in comparison to wild-type mice [433]. On one hand, MMP11 promotes the development of primary tumours by inhibiting cancer cell apoptosis [434, 435]. It is suggested that MMP11 may function to in this manner by releasing IGFs [402] which can act as survival factors [436]. On the other hand, MMP11 functions to repress the development of metastases [433]. A final MMP with dual roles in cancer progression is MMP19. The decreased susceptibility of Mmp19-/- mice to develop chemically induced skin tumours suggests that MMP19 may promote tumour growth [437]. However, it also functions to negatively regulate early stages of tumour angiogenesis and invasion [438]

2. AIMS

The aim of this project is to investigate phenotypic and functional differences between normal and DCIS-MECs, with a particular focus on the function and regulation of FN expression by tumour-promoting integrin αvβ6-positive DCIS-MECs. The purpose of this work is to better understand the mechanisms underlying the transition of DCIS to invasion, and by doing so, generate a biomarker signature with which DCIS patients can be better stratified. The objectives specifically include, to;

1) Investigate the phenotypic characteristics of MECs in normal and DCIS tissue, with and without co-existent invasive disease

2) Compare the tissue phenotype to characteristics in primary and cell line models of normal and DCIS MECs

3) Determine the functional relevance of the phenotypic characteristics in primary and cell line models of normal and DCIS MECs

4) Investigate the mechanisms regulating the phenotypic characteristics in normal and DCIS MECs

3. MATERIALS AND METHODS

3.1 IMMUNOHISTOCHEMICAL ANALYSIS

3.1.1 Human breast tumour samples

Human breast tumour samples were obtained from surgical specimens from patients undergoing breast surgery between 2000 and 2015 at Barts Health NHS Trust London. Tissue that was deemed by a pathologist to be surplus to diagnostic and therapeutic requirement were collected together with associated clinical data under the terms of the Breast Cancer Now Tissue Bank (BCN, NRES Cambridgeshire 2 REC number 10/H0308/48), and Barts Cancer Institute Breast Tissue Bank (BCI, NRES East of England REC number 15/EE/0192), with ethical approval. All tissues were obtained from patients with full written informed consent. Samples of DCIS with (n=20; DCIS/IDC) and without (n=20; DCIS) invasion were selected for immunohistochemical analyses. Samples were matched on tumour grade (non-high-grade and high-grade) and patient age. Clinicopathologic details are provided in Table 4.

Type	DCIS		DCIS/IDC
Grade	Non-high-grade	High-grade	High-grade
Cohort	10	10	20
Subtype			
Luminal A	2	1	7
Luminal B	5	2	7
HER2	2	5	4
TN	1	2	2
DCIS size in mm	21.4 (12-30)	37.6 (15-50)	13.4 (4.4-40)
Diagnosis			
Symptomatic	1	1	11
Screen-detected	9	9	9
Age at diagnosis	56 (50-65)	54 (43-58)	56 (51-60)
Follow-up			
Years follow-up	5.5 (3-18)	5 (3-10)	6 (3-12)
Recurrence (years)	0	1 (2)	3 (1)

Surgery			
Wide Local Excision	5	2	6
Mastectomy	5	8	14
Adjuvant Treatment			
None	3	2	1
Radiotherapy	5	5	11
Hormone Therapy	3	2	12
Both	1	0	8
Unknown	0	1	4

Table 4. Clinical annotation of human breast tumour samples analysed

3.1.2 Immunohistochemical staining

Immunohistochemical staining was performed on serial sections of formalin-fixed paraffin-embedded (FFPE) tissues. Sections were dewaxed in xylene (Fisher Scientific, X/2050) and rehydrated through graded alcohols (Fisher Scientific, E/0665DF) to distilled water (dH_2O). Endogenous peroxidases were blocked with 3% (v/v) hydrogen peroxide (H_2O_2, Fisher Scientific, H/1750) in methanol (Fisher Scientific, M/4056) for 10 minutes, followed by antigen retrieval. Antigen retrieval methods used are listed in Table 5. Sections were incubated with a blocking buffer of 5% (w/v) bovine serum albumin (BSA, Sigma, A8022) in phosphate buffered saline (PBS) for 10 minutes. Sections were then incubated with primary antibody diluted in blocking buffer for 1 hour at room temperature (rt). Excess antibody was removed by washing with PBS in triplicate for 5 minutes each. Sections were then incubated with horse anti-mouse biotinylated secondary antibody (Vector laboratories, PK-6102), diluted 1:200 in blocking buffer for 30 minutes at rt. Primary antibodies used as listed in Table 6. Excess antibody was removed by washing with PBS in triplicate for 5 minutes each. Sections were then incubated in avidin-biotin complex (ABC, Vector Laboratories, PK-6100) for 30 minutes at rt. Sections were then washed in PBS in triplicate for 5 minutes each before incubating with diaminobenzidine (DAB, Vector Laboratories, SK-4100). Mayers haematoxylin (Sigma, MHS16) was then used for counterstaining. Sections were then dehydrated through graded alcohols to xylene and mounted in distyrene-tricresyl phosphate-xylene (DPX, Sigma, 06522).

Antigen retrieval	Company	Product code
Pepsin	Life technologies	00-3009
0.1M Citrate (pH 6)	Fisher scientific	S/3280
10mM Tris (pH 9)	Sigma	T1503

Table 5. Antigen retrieval methods for immunohistochemical staining

Antibody	Dilution	Company	Product code	Antigen retrieval
SMA	1:500	Dako	M0851	Tris (pH 9)
Integrin αvβ6	1:800	Calbiochem	407317	Pepsin
TFN	1:500	Sigma	F0916	Pepsin
p63	1:50	Abcam	ab735	Citrate (pH 6)

Table 6. Primary antibodies for immunohistochemical staining

3.1.3 Immunohistochemical analysis

Samples were scanned using a 3DHISTECH Panoramic digital slide scanner (3DHISTECH, Hungary), and analysed using the VisoPharm software (VisioPharm A/S, Hoersholm, Denmark). Disease scores were determined firstly by manually defining normal and tumour areas within H&E stained tissue samples and identifying regions that represented epithelium, stroma or adipose tissue and then training the software to recognise these defined regions. These data were then expressed as a percentage of the whole tissue area. All immunohistochemical analysis was performed on a duct-by-duct basis. Ducts were numbered and identified as either; normal, benign or DCIS within each case. Each duct was then scored as negative or positive for the expression of integrin $\alpha v\beta 6$ and TFN. For samples stained with TFN, periductal staining was measured. Duct size was measured using the equation; $\pi\ x\ r1\ x\ r2$, where '$r1$' is the minor axis length and '$r2$' is the major axis length. MEC size and shape were quantified on SMA stained sections by measuring the minor axis length of at least 3 MECs per duct. MEC nuclei were quantified on p63 stained sections by counting all positive-nuclei within a duct and measuring the minor and major axis length of at least 3 positive-nuclei per duct.

3.2 CELL LINE AND PRIMARY CELL CULTURE

3.2.1 Myoepithelial cell lines

MEC lines with (β6-1089) and without (N-1089) integrin αvβ6 expression recapitulating DCIS and normal MECs respectively, were provided by Dr M. Allen [114]. The parental MEC line 1089 (Myo-1089) was obtained from Prof M. O'Hare and Prof P. Jat, Institute of Neurology, UCL, London. Myo-1089 were isolated from reduction mammoplasty tissue as described by Gomm and colleagues [439], and immortalised as described by O'Hare and colleagues [440]. Dr M. Allen sorted the immortalised Myo-1089 cells by using integrin β4 antibody-coated magnetic beads to purify the MEC population, and cells were designated β4-1089. To generate a cell line overexpressing integrin αvβ6, cells were transfected with CM containing retrovirus from AM12/pBABE-β6 or AM12/pBABE-Puro cells. Cells were then selected using 1μg/mL puromycin. Control 1089 cells were designated normal (N-) 1089; β6-transduced cells were further enriched by positive selection using integrin β6 antibody-coated magnetic beads and designated β6-1089.

These cell lines were shown to phenotypically drift overtime in culture; most notably they demonstrate a gradual downregulation of integrin α6β4 expression. To maintain the expression of integrin α6β4, cells were enriched by positive selection using β4–labelled magnetic beads every 10-12 weeks. Along with the downregulation of integrin α6β4, N-1089 demonstrate a gradual increase in integrin αvβ6 expression, induced by culturing cells on plastic, possibly as a wound healing response [183]. The cell lines then underwent re-selection using β6–labelled magnetic beads, in which β6-1089 are resorted by positive selection, while N-1089 are negatively selected.

N-1089 and β6-1089 cells were cultured in Nutrient Mixture Ham's F-12 (F-12, Sigma, N6658) supplemented with 10% foetal bovine serum (v/v) (FBS, HyClone, SH30071), 1μg/mL hydrocortisone (Sigma, H0888), 10ng/mL epidermal growth factor (EGF, Sigma, 9644), and 10μg/mL insulin (Sigma, I9278).

3.2.2 Breast cancer cell lines

ER-negative, MDA-MB-231 and ER-positive, MCF-7 breast cancer cell lines were obtained from American Type Culture Collection (ATCC) and verified with STR profiling (LGC Standards, Teddington, UK, tracking number 710081047). MDA-MB-231 and MCF-7 cells were cultured in Dulbecco's modified eagle medium (DMEM, Sigma, D6429) supplemented with 10% FBS.

3.2.3 Primary breast cells

Primary normal and DCIS breast cells were isolated from ductal organoids from reduction mammoplasty and DCIS tissues, respectively, obtained from the BCN and BCI breast tissue bank. Samples of reduction mammoplasty were matched on patient age (20-24 years) and menopausal status (premenopausal). Samples of DCIS/IDC were matched on tumour grade (high-grade). Clinicopathologic details are provided in Table 7. Ductal organoids were digested to a single-cell suspension through digestion with 0.05%/0.02% (w/v) trypsin/EDTA solution (Hyclone, SV30031.01) containing 0.4mg/mL DNase (10104159001, Roche Life Science) for 15 minutes at 37^{o}C. The cell suspension was filtered through a cell strainer with 40μM pore size filter (Fisher Scientific, 352340). Pure populations of MECs and LECs were then isolated through either magnetic bead separation or FACS separation. For magnetic bead separation of primary normal breast cells, a single-cell suspension was incubated at 4^{o}C for 20 minutes with CD10-labelled magnetic beads to isolate MECs, followed by incubation at 4^{o}C for 20 minutes with EpCAM-labelled magnetic beads to isolate LECs. For FACS isolation of DCIS breast cells, a single-cell suspension of 20x10^{6} cells in 1mL serum and growth factor-free (SGF) Roswell Park Memorial Institute medium (RPMI, Sigma, R5886) was incubated with 0.25μg/mL allophycocyanin (APC)-conjugated mouse anti-human integrin $\alpha v\beta 6$ (R&D Systems, FAB4155A), 0.03μg/mL phycoerythrin (PE)-conjugated mouse anti-EpCAM (BD Biosciences, 347198) and 10μL Alexa-Fluor 488 anti-human integrin $\alpha 6\beta 4$ (Invitrogen, MA5-23641) for 45 minutes at 4^{o}C. Cells were then incubated with 0.1μg/mL 4′, 6-diamidino-2-phenylindole (DAPI, D9542) at 4^{o}C for 10 minutes prior to separation of MECs and LECs based on expression of integrin $\alpha 6\beta 4$ and EpCAM, respectively. FACS separation was performed on BD FACSAria II cell sorter (BD Biosciences).

Primary normal MECs were cultured on plates precoated with 10μg/cm^2 COL1 and cultured in HuMEC Ready Medium (Life Technologies, 12753-018) supplemented with 50μg/mL bovine pituitary extract (BPE, Invitrogen, 13028-014), 0.5μg/mL hydrocortisone, 10ng/mL EGF, 5μg/mL insulin, 0.5μg/mL fungizone (Invitrogen, 15290-026) and 10μg/mL gentamicin (Sigma, G1397).

Primary normal LECs were cultured in Dulbecco's Modified Eagle's Medium/Nutrient Mixture Hams F-12 (DMEM/F-12, Sigma, D8437) supplemented with 10% FBS (v/v), 0.5μg/mL hydrocortisone, 10ng/mL EGF, 5μg/mL insulin and 10μg/mL apo-Transferrin (Sigma, T1147).

For passaging or harvesting, cells were detached with a 0.5%/0.2% (w/v) trypsin/ethylenediaminetetraacetic acid solution (EDTA, Sigma, 59418C). For long-term preservation, pelleted cells were resuspended in 40% complete-media (v/v), 50% FBS and 10% dimethyl sulphoxide (DMSO, Sigma, D2650) and frozen in a step-wise manner, first at -80^{o}C overnight and then placed in -196^{o}C (liquid nitrogen). For experimental consistency, fresh cells were routinely thawed. All cells were confirmed *Mycoplasma*-free before experiments and were maintained at 37°C in a humidified 5% CO_2 atmosphere.

Type	DCIS/IDC	
Grade	High-grade	
Integrin αvβ6	Positive	Negative
Cohort	2	2
DCIS size in mm	18 (14-22)	14 (12-16)
Age at diagnosis	62 (42-72)	43 (42-43)

Table 7. Clinical annotation of DCIS organoid samples analysed

3.3 TRANSFECTIONS

3.3.1 DNA transfection

Cells at a density of $1x10^6$ in 10mL SGF media were reverse transfected with 10μg integrin β6 pcDNA1 neo (Addgene, plasmid 13580) or pcDNA1 empty vector (Invitrogen, V790-20) using the jetPRIME transfection reagent (PolyPlus, 114). Transfections were carried out by mixing DNA, 1mL JetPRIME buffer and 20μl jetPRIME reagent by vortexing for 10 seconds and incubating at rt for 10 minutes to allow complex formation. After that the DNA-buffer-reagent complex was added to the dish in a drop wise manner and the plate swirled to ensure homogenous distribution. The media was then changed to fresh SGF media after 24 hours. Both cells and CM were harvested for subsequent experiments 48 hours after transfection.

3.3.2 siRNA transfection

Cells at a density of $1x10^6$ in 8mL SGF media were reverse transfected with 9nM integrin β6 (Dharmacon, M-008012-01-0005), total fibronectin (TFN, Dharmacon, M-009853-01-0005), MMP13 (MMP13, Dharmacon, M-005955-01-0005) or non-targeting control (NTC, Dharmacon, D-001206-14-20) small interfering RNA (siRNA) by using the interferin transfection reagent (PolyPlus, 409). Transfections were carried out by mixing siRNA and 31μL interferin in 1.6mL SGF media by vortexing for 10 seconds and incubating at rt for 15 minutes to allow complex formation. After that the siRNA-interferin complex was added to the dish in a drop wise manner and the plate swirled to ensure homogenous distribution. The media was then changed to fresh SGF media after 24 hours. Both cells and CM were harvested for subsequent experiments 48 hours after transfection.

3.4 TGFβ STIMULATION

Immediately prior to stimulation, media was removed and cells were washed in PBS to remove residual media. Cells were then stimulated with 5ng/mL recombinant human active TGFβ1 (PeproTech, 100-21) in SGF media for 5, 15 and 30 minutes, or for 72 hours, in which fresh TGFβ1 in SGF media was replaced daily. To stop stimulation, cells were washed with ice cold PBS and kept on ice, and harvested for subsequent experiments.

3.5 TGFβRII INHIBITION

Cells at a density of $2x10^6$ were incubated with 10μg/mL IgG isotype control antibody (Merckmillipore, MABC004) or TGFβRII-blocking antibody (R&D Systems, AF-241-NA) in SGF media for 20 minutes at 4°C on a rotating-wheel before plating. The media was then changed to the respective SGF media after 24 hours. Both cells and CM were harvested for subsequent experiments 48 hours after antibody treatment.

3.6 CONDITIONED MEDIA

In the preparation of concentrated CM (cCM) from cell culture, CM was centrifuged at 1,200rcf for 3 minutes. The supernatant was transferred to a new tube and the pellet discarded. CM was then concentrated 24-fold with centrifugal filters (Fisher, 10403892) with 3K molecular weight cut off (MWCO) at 4000g for 45 minutes at 4°C. The cCM was frozen at -80°C for later use.

3.7 IMMUNOBLOTTING

3.7.1 Isolation of proteins

In the isolation of protein from cells, excess media was removed and cells were washed in ice cold PBS. Total cellular protein was isolated by the addition of radio-immunoprecipitation assay (RIPA) buffer (50mM Tris-hydrochloride (Tris-HCl, Sigma, T3253) pH 7.4, 150mM sodium chloride (NaCl, Fisher, 358-1), 1% IGEPAL CA-630 (Calbiochem, 490216), 0.1% sodium deoxycholate (Na-DOC, Sigma, D6750), 1mM EDTA (Fisher, BP 118-500), supplemented with 1:100 protease inhibitor cocktail set (Calbiochem, 539131), 1mM activated sodium orthovanadate (Na_3VO_4, Sigma, S6508) and 1mM sodium fluoride (NaF, Sigma, S7920) when required). Cells were scraped and the suspension was placed in an Eppendorf tube, and incubated on ice for 15 minutes. The tube was then centrifuged at 10,000rpm at 4^{o}C for 5 minutes. The supernatant was transferred to a new tube and the pellet discarded. DOC-soluble material was isolated by the addition of Na-DOC buffer (2% Na-DOC, 20mM Tris-HCl pH 8.8, 2mM EDTA, supplemented with 1:100 protease inhibitor cocktail set when required). Cells were scraped and the suspension was placed in an Eppendorf tube. The tube was then centrifuged at 16,000rpm at 4^{o}C for 15 minutes. The supernatant was transferred to a new tube and the DOC-insoluble material was solubilised in sodium dodecyl sulphate (SDS) buffer (1% SDS (National Diagnostics, EC 874), 20mM Tris-HCl pH 8.8, 2mM EDTA, supplemented with 1:100 protease inhibitor cocktail set when required). Samples were frozen at -20^{o}C until required.

3.7.2 Quantification of proteins

Protein concentrations for both cell lysates and cCM were quantified using the Bio-Rad DC Protein Assay Kit (Bio-Rad Laboratories, Reagent A 500-0113, Reagent B -114, Reagent S -115), according to the manufacturer's instructions. Absorbance was measured at 595nm using a microplate reader (Tecan, Infinite F50). Concentrations of samples were calculated from a standard curve generated from increasing concentrations of BSA, ranging from 0.1 to 5mg/mL versus their respective absorbance values.

3.7.3 Electrophoresis of proteins

Subsequently, 30μg of protein were mixed with reducing 4x laemmli buffer (0.25M Tris-HCl pH 6.8, 8% SDS, 40% glycerol (Fisher, G/0600/17), 0.04% bromophenol blue (Sigma, B8026) and 2.5% β-mercaptoethanol (βME, Sigma, M7522)) to give a final concentration of 1x laemmli buffer. Samples were then denatured further by heating at 95°C for 5 minutes prior to loading onto 6-15% polyacrylamide gels. To prepare polyacrylamide gels, a resolving gel solution of varying volumes of 30% acrylamide mix (National Diagnostics, EC 890), 1.5M Tris-Base (Fisher, BP152) pH 8.8, 10% SDS, 10% ammonia persulphate (APS, National Diagnostics, EC 504) and tetramethylethylenediamine (TEMED, Flowgen, H17459) was dispensed into a gel cassette (Invitrogen, NC2010). After the resolving gel was set, a 5% stacking gel solution of varying volumes of 30% acrylamide mix, 1M Tris-Base pH 6.8, 10% SDS, 10% APS and TEMED was overlaid the resolving gel in the cassette, and a comb was inserted. After the stacking gel was set, the comb was removed and the cassette inserted into a gel tank containing running buffer (25mM Tris-Base, 192mM Glycine and 0.1% SDS). Samples were then loaded into wells and electrophoresed at 150V for 90 minutes.

3.7.4 Electroblotting of proteins

Following protein separation, the gel was removed from the cassette and placed in a transfer assembly where the gel faces towards a 0.45μM pore size nitrocellulose membrane (Whatman). The inner chamber was filled with transfer buffer (25mM Tris-HCl, 192mM Glycine and 20% (v/v) Methanol), while the outer chamber was filled with H_2O. Proteins were transferred at 30V for 90 minutes at 4°C. Protein sizes were determined by comparison to a protein ladder of defined molecular weights (Generon, SM0671). Transfer verification was confirmed with Ponceau S stain (Sigma, P7170).

3.7.5 Immunoblotting of proteins

Membranes were incubated with a blocking buffer of 5% (w/v) milk (Sigma, 70166), 0.1% (v/v) Tween-20 (Applichem, A4974) in Tris Buffered Saline (TBS-T) for 1 hour at rt. Membranes were then blotted with primary antibody diluted in blocking buffer overnight at 4^{o}C. Excess antibody was removed by washing with TBS-T in triplicate for 5 minutes each. Depending on the species in which the primary antibody was raised, membranes were then incubated with horseradish peroxidase (HRP)-conjugated secondary antibodies, diluted in blocking buffer for 1 hour at rt. Primary and secondary antibodies used as listed in Table 8 and Table 9, respectively. Membranes were washed with TBS-T in triplicate for 5 minutes each before incubating with Enhanced Chemiluminescence (ECL) reagents (Amersham, RPN 2106) and exposure to film. Films were developed in a Konica Film Processor (SRX-101A).

Antibody	Host	Dilution	Company	Product code
Integrin αvβ6	Goat	1:1,000	Santa cruz	SC-6632
TFN	Mouse	1:2,000	Sigma	F0916
FN-EDA	Mouse	1:1,000	Abcam	ab6328
p-SMAD2	Rabbit	1:1,000	Cell signalling	3101
SMAD2	Rabbit	1:1,000	Cell signalling	8657
p-ERK1/2	Rabbit	1:1,000	Cell signalling	9101
ERK1/2	Rabbit	1:1,000	Cell signalling	9102
HSC70	Mouse	1:10,000	Santa cruz	SC-7298

Table 8. Primary antibodies for immunoblotting

Antibody	Host	Dilution	Company	Product Code
Anti-Goat	Rabbit	1:1,000	Dako	P0449
Anti-Mouse	Rabbit	1:1,000	Dako	P0260
Anti-Rabbit	Goat	1:1,000	Dako	P0448

Table 9. Secondary antibodies for immunoblotting

3.7.6 Densitometric analysis

To compare protein signal intensities, density measurements of non-signal-saturated bands were determined using ImageJ software (National Institutes of Health, Bethesda, MD, USA). Relative protein phosphorylation levels were obtained by normalising the level of protein phosphorylation to total protein level, while all signals were normalised to HSC70 on the same membrane. These arbitrary values were then converted into ratios by normalising to the control of that replicate to avoid varying intensities of each replicate. The total density of each replicate was then determined, and each individual band was normalised to the total density of that repeat. The average density of 3 replicate controls was then calculated. This value was then used to find the relative density of the normalised values of each individual band. This allows for the presentation of the data normalised to the control, with the control demonstrating variation also.

3.8 IMMUNOFLUORESCENT STAINING

Cells were seeded onto 13mm^2 glass coverslips at a density of 5x10^4 per well in 1mL SGF media. At the desired time point, cells were fixed in 4% formaldehyde in PBS (Cell Path, BAF-0010-01A) for 10 minutes. Cells were then permeabilised with 0.1% Triton X-100 in PBS for 5 minutes before staining for intracellular proteins only. Subsequently, cells were incubated with a blocking buffer of 5% BSA in PBS, with the exception of staining for integrin $\alpha v\beta 6$, in which cells were incubated with a blocking buffer of 5% BSA in DMEM, both for 10 minutes at rt. Cells were then incubated in primary antibody diluted in the respective blocking buffer for 1 hour at rt. Excess antibody was removed by washing with PBS in triplicate. Cells were then incubated with goat anti-mouse Alexa-Fluor 488 secondary antibody (Invitrogen, A11029), diluted 1:200 in the respective blocking buffer for 1 hour at rt. Primary antibodies used as listed in Table 10. Cells were washed with PBS in triplicate and once in dH_2O before mounting and counterstaining with ProLong Gold Antifade reagent containing DAPI (Invitrogen, P36931). Images were viewed on a Zeiss LSM 710 Meta microscope, and captured at x63 objective magnification. Fluorescence analysis was determined using the ZEN 2009 image analysis software. Relative fluorescence intensity was calculated by normalising to the control. Average fibril length was calculated by measuring the length of fibrils extending from at least 5 different cells within a minimum of 3 fields of view. The percentage of cells with FN fibrils was determined by counting the number of nuclei with adjacent FN fibrils compared to the total number of nuclei within a minimum of 3 fields of view.

Antibody	Dilution	Company	Product Code
Integrin αvβ6	1:100	Merck	MAB2077Z
TFN	1:100	Sigma	F0916
FN-EDA	1:100	Abcam	ab6328

Table 10. Primary antibodies for immunofluorescent staining

3.9 QUANTITATIVE REAL-TIME POLYMERASE CHAIN REACTION

3.9.1 Isolation of RNA

In the isolation of RNA from cells, cells were detached using 0.5%/0.2% (w/v) trypsin/EDTA and centrifuged at 1,200rcf for 3 minutes. Cell pellets were then washed in ice cold PBS. RNA was then extracted from the cell pellets using the Quick-RNA MiniPrep Kit (Zymo Research, R1065) according to the manufacturer's instructions. Following elution, RNA quantity was estimated using the Nanodrop system (Thermo Scientific).

3.9.2 Synthesis of cDNA

Using isolated RNA as a template, cDNA was obtained by reverse transcription (RT). To initiate RT, 1μL of 50ng/μL hexanucleotide primers (Sigma, H0268) and 1μL of 10 mM deoxynucleotide (dNTPs, Sigma, GE28-4065-57) are added to 1μL of 50ng mRNA with 7μL of nuclease-free dH_2O (HyClone, SH30538.02) to give a total volume of 10μL per reaction. The reaction was performed with the following conditions: 70°C for 10 minutes, followed by 4°C for 5 minutes in a Mastercycler Polymerase Chain Reaction (PCR) system (Eppendorf). To synthesise cDNA from the RNA-DNA hybrid by polymerisation, 1μL of Moloney-murine leukaemia virus (M-MLV) reverse transcriptase enzyme and 2μL of M-MLV buffer (Sigma, M1302) are added to the initial reaction mix with 7μL of nuclease-free deionised water to give a final volume of 20μL per reaction. The reaction is performed with the following conditions: 22°C for 10 minutes, 37°C for 50 minutes and 90°C for 10 min. cDNA was kept at 4°C until required.

3.9.3 qRT-PCR

Primer sequences are shown in Table 11. All primers were kept at 100μM stock concentration and used at 0.3μM final concentration. qRT-PCR was carried out using KiCqStart SYBR Green qPCR ReadyMix (Sigma, KCQS02-250RXN) according to the manufacturer's instructions. Each reaction was prepared as: 1μL of 3μM forward primer, 1μL of 3μM reverse primer, 2μL SYBR Green and 5μL of nuclease-free deionised water to give a total volume of 9μL. This reaction mix was added to the plate with 1μL cDNA to give a final volume of 10μL. Each reaction was performed in triplicate within the same plate for each all genes. Reactions were run using a StepOnePlus PCR system (Applied Biosystems) using the following conditions: for one cycle 95^{o}C for 10 minutes, followed by 95^{o}C for 15 seconds and 60^{o}C for 1 minute for 40 cycles. The change in gene expression is then determined by the equation 2-(ddCT) The change in cycle threshold (dCT) is calculated by subtracting the average CT for the reference gene (18S) from the average CT of the target gene. The change in CT of the control is then subtracted from the change in CT of the sample (ddCT).

Primer	Forward 5’ – 3’	Reverse 5’ – 3’
Integrin αvβ6	GAAGGAATGATCACGTACAAG	AGCAGGGAGTCTTCACAGGT
TFN	AACAAACACTAATGTTAATTGCC	TCGGGAATCTTCTCTGTCAGC
FN-EDA	CGAGCCCTGAGGATGGAATC	TGTGTACTGAGAACCCGGTC
FN-EDB	CCTCACCAACCTCACTCCAG	GGGACTTTCCTCTCTGCCATT
MMP2	GCCCATCATCAAGTTCCCCG	AAGGTGTTCAGGTATTGCACTG
MMP3	GGGATTAATGGAGATGCCCAC	GTGGCCAATTTCATGAGCAGC
MMP7	GAACGCTGGACGGATGGTAG	CAGAGGAATGTCCCATACCCA
MMP9	GAACCAATCTCACCGACAGG	GCCACCCGAGTGTAACCATA
MMP10	TAACAGCAGGGACACCGTTT	CAGGGTATGGATGCCTCTTGG
MMP13	TCTACACCTACACCGGCAAA	GGTTGGGGTCTTCATCTCCT
18S	CACGGGAAACCTCACCCGGC	AACGGCCATGCACCACCACC

Table 11. Primer sequences for qRT-PCR

3.10 ADHESION ASSAY

Non-tissue culture treated 96-well plates were coated with 100μL of 0.5μg/mL recombinant human LAP (246-LP-025, R&D Systems) or 0.1% BSA, in triplicate. Coated plates were then incubated for 1 hour at 37°C, and wells were then washed with PBS twice. Cells were seeded at a density of $2x10^4$ per well in 100μL of SGF media and allowed to adhere for 1 hour at 37°C. Media was then removed, and cells were fixed in 100% methanol for 10 mins at rt. Methanol was removed, and the cells were stained with 0.1% crystal violet for 1 hour at rt. Excess crystal violet was removed, and cells were washed with dH_2O in triplicate. Cells were then solubilised with 0.2% Triton X-100 in PBS on shaker for 10 mins. Absorbance was measured at 550nm using a microplate reader. The background binding to BSA was subtracted from LAP, and relative adhesion was calculated by normalising to the control.

3.11 MIGRATION ASSAY

The underside of 8μM Transwell inserts (Fisher, 734-1574) were coated with 100μL of 0.5μg/mL recombinant human LAP or 0.1% BSA, in triplicate. Coated inserts were then incubated for 1 hour at rt, and were then washed with PBS twice. Inserts were then placed into 500μL of SGF media in the outer chamber. Cells were then seeded into the inner chamber of the insert at a density of $2x10^4$ per well in 200μL of SGF media and allowed to migrate for 8 hrs at 37°C. Media was then removed from both the inner and outer chamber, and migrating cells were then quantified by adding 200μL and 500μL of 0.5%/0.2% (w/v) trypsin/EDTA solution to the inner and outer chamber of the Transwell insert, respectively and incubating for 1 hour at 37°C. This was then added to 9.8mL and 9.5mL of isoton solution (BD Biosciences, 342003), respectively, and counted with a CASY counter (Schärfe System). Total cell count for each sample was calculated by adding the inner and outer chamber counts. Relative cell migration was then calculated by using the outer chamber count versus total cell count.

3.12 TRANSWELL INVASION ASSAY

The upper insert of 8μM Transwell inserts were coated with 70μL of Matrigel (Corning, 354234) diluted 1:3 in ice cold SGF DMEM. Coated inserts were then incubated for 40 minutes at 37°C. 500μL of CM was then added to the outer chamber, in triplicate. MDA-MB-231 and MCF-7 were then seeded into the inner chamber of the insert at a density of $3x10^4$ per well in 200μL of media and allowed to migrate for 24 and 48 hours at 37°C, respectively. Media was then removed from the outer chamber, and invading cells were then quantified by adding 500μL of 0.5%/0.2% (w/v) trypsin/EDTA solution to the outer chamber of the Transwell insert and incubating for 1 hour at 37°C. This solution was then added to 9.5mL of isoton solution and counted with a CASY counter. Relative breast cancer cell invasion was calculated by normalising to the control.

3.13 PROLIFERATION ASSAY

MDA-MB-231 and MCF-7 were seeded at a density of $3x10^4$ per well of a 96-well plate in 200μL of CM, in triplicate and incubated for 24 and 48 hours at 37°C, respectively. 40μL of Cell Titer-Blue Reagent (Promega, G8081) was then added to each well and incubated for 2 hours at 37°C. Absorbance was then measured at 550nm and 600nm using a microplate reader. Relative breast cancer cell proliferation was calculated by normalising to the control.

3.14 PROTEOME PROFILER HUMAN PROTEASE ARRAY

3.14.1 Sample Preparation

250μg of cCM was prepared to a total volume of 1.5mL with blocking buffer (buffer 6), and incubated with 15μL of antibody cocktail for 1 hour at rt. These reagents were provided in the Protease Array Kit.

3.14.2 Protease array

Simultaneously, membranes were incubated with blocking buffer for 1 hour at rt. Membranes were then incubated with the sample-antibody mixture overnight at 4°C. Excess antibody was removed by washing with a wash buffer in triplicate for 10 minutes each. Membranes were then incubated with streptavidin-HRP-conjugated secondary antibody, diluted in blocking buffer for 30 minutes at rt. Membranes were washed with wash buffer in triplicate for 10 minutes each before incubating with ECL and exposing to film.

3.14.3 Densitometric analysis

To compare analyte signal intensities, density measurements of individual dots were determined using ImageJ software. These arbitrary values obtained were then expressed as ratios by normalising to the appropriate control as indicated on the y-axis of the respective graphs.

3.15 GELATIN ZYMOGRAPHY

3.15.1 Sample preparation

100μg of cCM was mixed with non-reducing 4x laemmli buffer (0.25M Tris-HCl pH 6.8, 8% SDS, 40% glycerol, 0.04% bromophenol blue) to give a final concentration of 1x laemmli buffer.

3.15.2 Electrophoresis of proteins

Precast 10% Tris-Glycine gels supplemented with 0.1% gelatin (Invitrogen, EC6175BOX) were inserted into a gel tank containing running buffer (25mM Tris-Base, 192mM Glycine and 0.1% SDS). Samples were then loaded into wells and electrophoresed at 150V for 90 minutes.

3.15.3 Detecting proteolytic expression

The gel was then placed into a renaturing buffer of 2.5% (v/v) Triton X-100 in dH_2O, for 30 minutes at rt with gentle agitation. Gels were then equilibrated by transferring them into a developing buffer of 5mM Tris-Base, 4mM HCl, 20mM NaCl, 0.5mM calcium chloride ($CaCl_2$, Sigma, C7902) in dH_2O and incubated overnight at 37°C. Gels were then stained with a staining solution of 0.1% (w/v) Coomassie R-250 (Thermo Scientific, 20278), 40% (v/v) ethanol and 10% (v/v) acetic acid (Sigma, A6283) in dH_2O, for 15 minutes at rt with gentle agitation. To visualise protease expression, gels were destained by washing with 10% (v/v) ethanol and 7.5% (v/v) acetic acid in dH_2O, in triplicate for 15 minutes each.

3.15.4 Densitometric analysis

To compare proteolytic expression, density measurements of bands were determined using ImageJ software. These arbitrary values were then converted into ratios by normalising to the control of that replicate to avoid varying intensities of each replicate. The total density of each replicate was then determined, and each individual band was normalised to the total density of that repeat. The average density of 3 replicate controls was then calculated. This value was then used to find the relative density of the normalised values of each individual band. This allows for the presentation of the data normalised to the control, with the control demonstrating variation also.

3.16 MECHANICAL STRAIN

Cells were seeded at a density of $7x10^4$ per well in 2mL of media into 6-well flexible-bottomed BioFlex culture plates coated with COL4 (Dunn Lab, BF-3001C/IV). Immediately prior to stretching, cells were removed from the periphery of the well, and the media was replaced for fresh SGF media. Cells were then exposed to a static stretch using a computerised vacuum-operated instrument (Flexcell strain unit FX-5000 Tension Plus, Flexcell International). The vacuum-induced constant stretch with 10% elongation of the flexible surface. The Bioflex loading station is designed to provide equibiaxial strain (uniform radial and circumferential strain) across a membrane surface by using cylindrical loading posts. The cells were exposed to stretch for 48 hours. Controls cells were plated on BioFlex culture plates for an equivalent time but were not subjected to stretch.

3.17 STATISTICAL ANALYSIS

Experiments were performed at least three times and statistical significance was determined by using two-tailed Students t-test or one-way ANOVA using Prism (Graphpad Software). The association between tissue composition, and MEC expression of integrin $\alpha v\beta 6$ and periductal FN deposition was analysed using Pearson x^2 test using Prism. Results were considered as significant with a p-value equal to or less than 0.05 ('*' in figures), equal to or less than 0.01 ('**' in figures), and equal to or less than 0.001 ('***' in figures). Results with a p-value more than 0.05 were considered as non-significant ('ns' in figures). Quantitative data of at least 3 independent experiments are expressed as ± standard error of the mean (SEM).

4. RESULTS

4.1 PHENOTYPIC CHARACTERISTICS OF MYOEPITHELIAL CELLS IN NORMAL AND DCIS TISSUE

4.1.1 Breast tissue composition in DCIS progression

A cohort of DCIS tissues with (DCIS/IDC; n=20) and without (n=20) invasive disease (Table 4), and adjacent normal tissue were selected and analysed by H&E staining. The presence or absence of invasion was confirmed with H&E staining (Figure 15a; panel 2-3), and the presence of invasion is used as a marker of DCIS progression. The extent of breast tissue components; epithelium, stroma and adipose, in each sample were measured by digital histopathology on H&E stained sections and calculated as the percentage tissue area occupied. Breast tissues were remodelled in the progression of DCIS, such that adipose tissue was replaced with an increase in both epithelial and stromal components ($p<0.05$) (Table 12). To identify any significant changes in tissue architecture through the tissue block that might impact on subsequent immunohistochemical analyses, H&E staining was carried out on the first (panel 2) and last (panel 3) sections cut. No major changes in tissue composition were observed between the different sections analysed (Supplementary Table S1). These findings demonstrate alterations in the composition of human breast cancer as a function of malignant progression from normal through DCIS to invasive IDC.

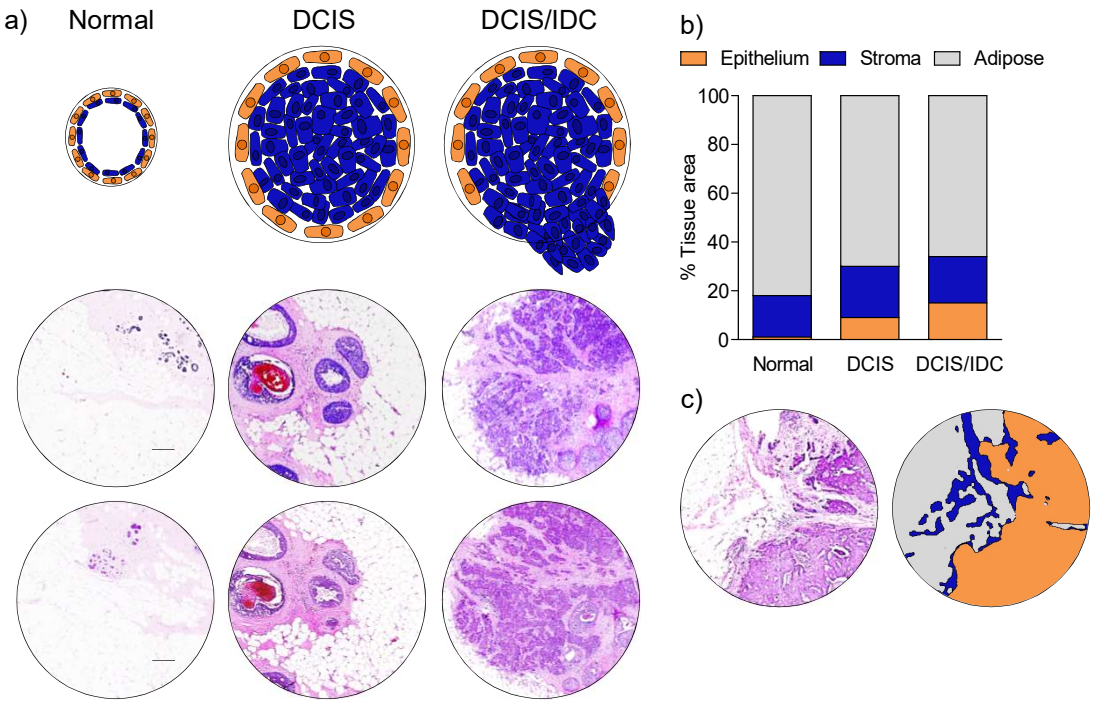

Figure 15. Breast tissue composition in DCIS progression. a) Haematoxylin and eosin (H&E) staining of the first (panel 2) and last (panel 3) serial sections of human breast tumour samples featuring areas of DCIS (n=20), DCIS with associated invasion (DCIS/IDC) (n=20) and adjacent normal. Magnification x2. Scale bar, 200μm. b) Digital analysis of architecture of H&E images. Bars represent the average percentage of epithelium, stroma and adipose tissue coloured orange, blue and grey, respectively in normal (1%, 10% and 83%, respectively), DCIS (9%, 21% and 70%) and DCIS/IDC (16%, 21% and 68%) patient samples. c) H&E stained images of a sample and the same sample pseudo-coloured as orange for epithelium, blue for stroma and grey for adipose. Representative images are shown.

	Tissue area % (range)		
	Epithelium	Stroma	Adipose
Normal	1% (1-5%)	10% (2-17%)	83 (78-93%)
DCIS			
Non-high-grade	5% (2-9%)	17% (8-31%)	78% (67-93%)
High-grade	13% (4-50%)	25% (8-61%)	63% (13-88%)
DCIS/IDC	16% (3-48%)	21% (5-33%)	68% (37-88%)

Table 12. Tissue composition of DCIS and DCIS with associated invasion

4.1.2 DCIS progression is accompanied by integrin αvβ6 upregulation by myoepithelial cells and increased periductal fibronectin deposition

We conducted an analysis of MEC expression of integrin αvβ6 and periductal deposition of TFN by immunohistochemical staining on a duct-by-duct basis in serial sections of DCIS tissues to assess their predictive value. Normal breast ducts, benign and DCIS lesions show an intact MEC layer as shown by SMA immunoreactivity (Figure 16a; panel 1-2 and Supplementary Figure S1). No staining for integrin αvβ6 was seen in normal ducts or benign lesions, whereas 70% of non-high-grade pure DCIS cases exhibited staining for integrin αvβ6, compared to 90% of high-grade pure DCIS and DCIS/IDC cases. In these cases, 45% (256/569) of high-grade and 27% (165/621) of non-high-grade pure DCIS ducts showed MEC staining for integrin αvβ6, with a significantly higher frequency of positivity in high-grade DCIS ($p<0.05$). The frequency of integrin αvβ6 expression by MECs in high-grade DCIS/IDC ducts is significantly higher than in pure DCIS, with 68% (473/697) of ducts showing positivity ($p<0.05$) (Figure 16a; panel 3-4; quantified in Figure 16b; top bar graph) (Table 13). In contrast, all DCIS cases, with and without invasion, exhibited staining for total FN (TFN). Quantification of the amount of TFN surrounding each duct demonstrated that the stromal region bordering DCIS ducts contained more TFN than normal ducts (68%; 796/1170), and this significantly increased further in DCIS/IDC (87%; 556/638) ($p<0.05$) (Figure 16a; panel 5-6; quantified in Figure 16b; bottom bar graph) (Table 14). These findings support previous work in our laboratory, with the *de novo* expression of integrin αvβ6 by MECs and increased deposition of FN in DCIS, and these alterations are associated with progression to invasion. These data suggest integrin αvβ6 and FN may be used as a marker of DCIS more likely to progress to invasive disease.

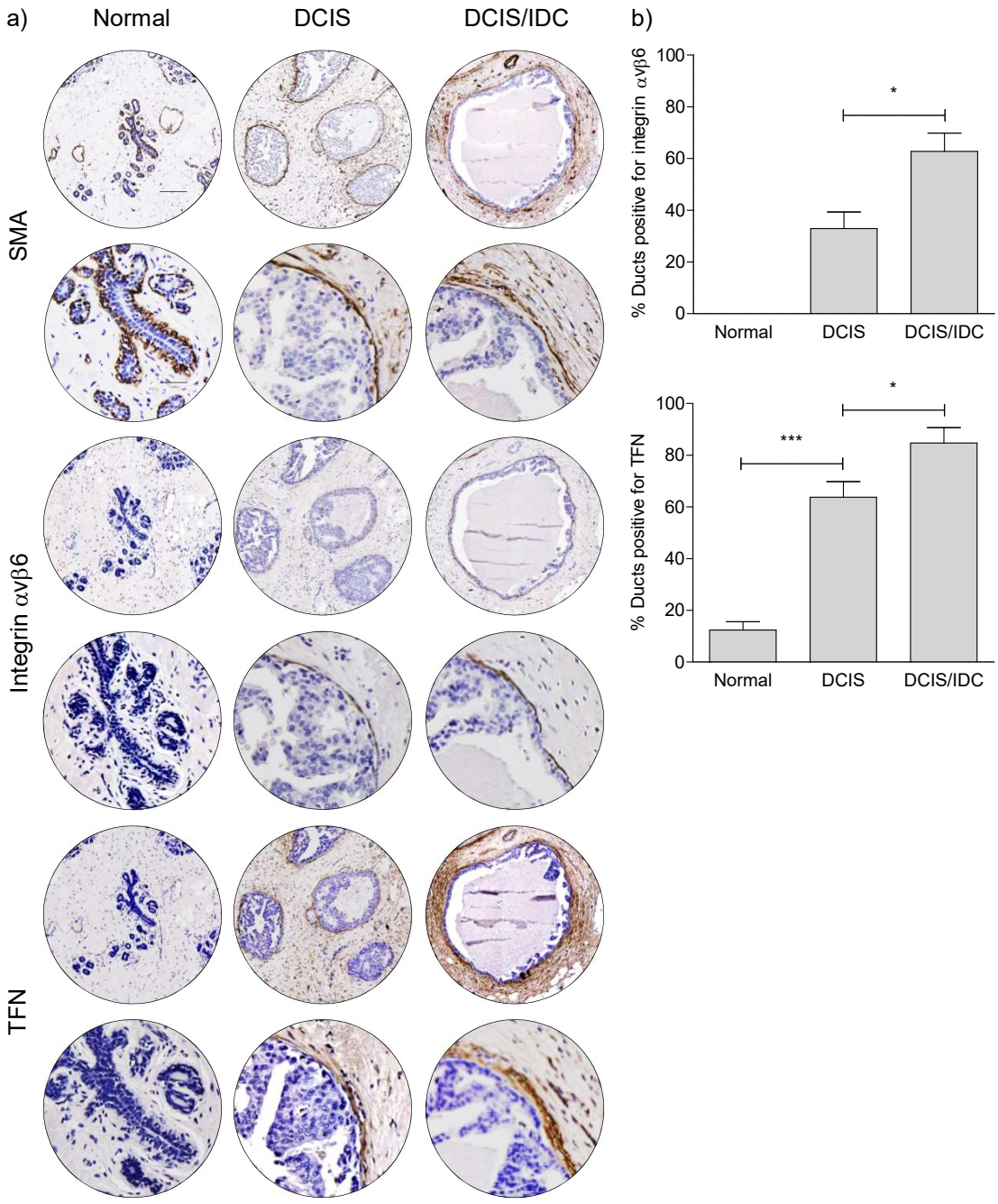

Figure 16. DCIS progression is accompanied by upregulation of integrin αvβ6 by myoepithelial cells and increased periductal fibronectin deposition. a) Immunohistological staining of human breast tumour samples (staining for SMA; panel 1-2, integrin αvβ6; panel 3-4, and TFN; panel 5-6) featuring areas of normal, DCIS and DCIS/IDC. Magnification x5 and x20. Scale bar, 200μm and 100μm, respectively. b) Quantitative analysis of duct-by-duct staining (integrin αvβ6; top bar graph, and TFN; second bar graph). Bars represent the average percentage of ducts positive for integrin αvβ6 or TFN in normal (0/944 and 57/921 ducts, respectively), DCIS (421/1190 and 796/1170 ducts) and DCIS/IDC (473/697 and 556/638 ducts) patient samples and errors bars represent ±SEM. Representative images are shown. p-value ≤0.001 ('***'), ≤0.01 ('**') and ≤0.05 ('*') considered significant.

	Number of ducts (%)		
	αvβ6-positive	αvβ6-negative	Total
Normal	0 (0%)	944 (100%)	944
Benign	0 (0%)	38 (100%)	38
DCIS			
Non-high-grade	165 (27%)	456 (74%)	621
High-grade	256 (45%)	313 (55%)	569
DCIS/IDC	473 (68%)	224 (32%)	697
			2869

Table 13. Myoepithelial cell expression of integrin αvβ6 in DCIS and DCIS with associated invasion

	Number of ducts (%)		
	TFN-positive	TFN-negative	Total
Normal	57 (6%)	864 (94%)	921
Benign	8 (21%)	30 (79%)	38
DCIS			
Non-high-grade	432 (70%)	188 (30%)	620
High-grade	364 (66%)	186 (34%)	550
DCIS/IDC	556 (87%)	82 (13%)	638
			2767

Table 14. Periductal fibronectin expression in DCIS and DCIS with associated invasion

4.1.3 Breast tissue composition correlates with integrin αvβ6 upregulation by myoepithelial cells and increased periductal fibronectin deposition in DCIS progression

The number of positive DCIS ducts for both integrin αvβ6 and TFN were correlated to tissue composition within each case using Pearsons x^2 test. This identified the progressive increase in the epithelial component in DCIS progression correlated with the upregulation of integrin αvβ6 by MECs ($p<0.05$) (Figure 17a; quantified in left bar graph). In contrast, the progressive increase in the stromal component correlated with the increased deposition of TFN into the periductal microenvironment with DCIS progression ($p<0.05$) (Figure 17b; quantified in right bar graph). These data suggest that breast tissue remodelling in the progression of DCIS to invasive disease, associates with specific cellular and matrix changes.

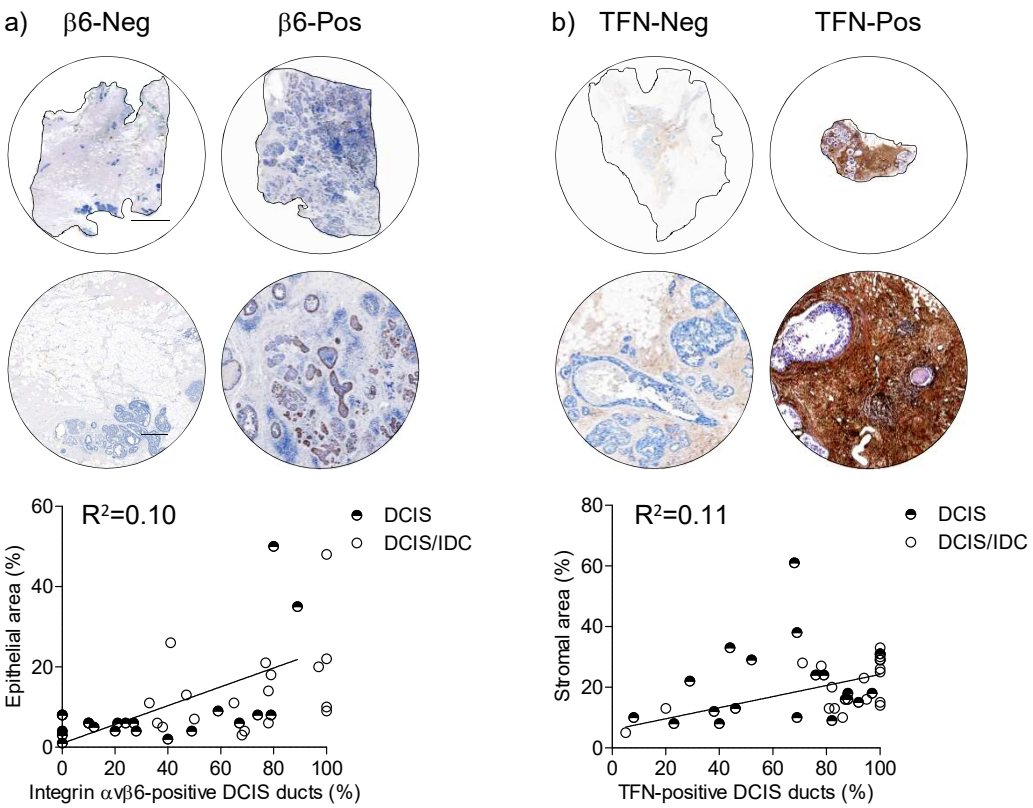

Figure 17. Breast tissue composition correlates with integrin αvβ6 upregulation by myoepithelial cells and increased periductal fibronectin deposition in DCIS progression. a) Immunohistochemical images of an integrin αvβ6-negative and integrin αvβ6-positive case with low and high epithelial content (panel 1-2; left and right, respectively). Correlation of percentage epithelial area and the percentage of integrin αvβ6-positive ducts within each DCIS case (scatter plot; left). Magnification x0.2 and x2. Scale bar 5000μm and 500μm respectively. b) Immunohistochemical images of a TFN-negative and TFN-positive case with low and high stromal content (panel 1-2; left and right, respectively). Correlation of percentage stromal area and the percentage of TFN-positive ducts within each DCIS case (scatter plot; right). Representative images are shown.

4.1.4 Integrin αvβ6 expression by myoepithelial cells and periductal fibronectin deposition are correlated in DCIS ducts

To investigate a relationship between integrin αvβ6 and TFN, we examined on a matched duct-by-duct basis the dual expression of integrin αvβ6 by MECs and TFN deposition surrounding the duct in serial sections of DCIS tissues. A significant association between their expression was identified using Pearsons x^2 test ($p<0.001$) (Figure 18a; quantified in Figure 18b) (Table 15). These data support a relationship between integrin αvβ6 and FN expression in DCIS ducts. Together, the data presented here suggest evolving tissue mechanics during DCIS progression associate with the upregulation of integrin αvβ6 expression by MECs and increased periductal FN deposition, and their expression is associated in DCIS. However, it is unclear here whether integrin αvβ6-positive MECs are a contributing source of FN deposition in DCIS.

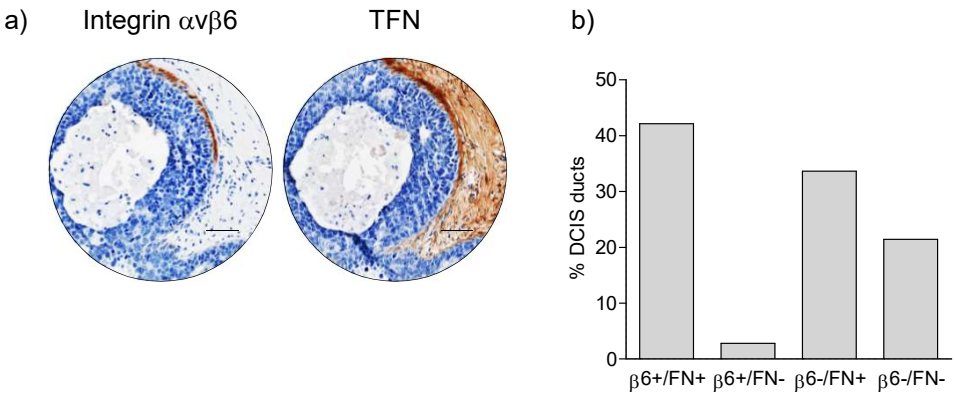

Figure 18. Integrin αvβ6 expression by myoepithelial cells and periductal fibronectin deposition are correlated in DCIS ducts. a) Colocalisation of integrin αvβ6 and TFN in serial sections of human breast tumour samples. Magnification x10. Scale bar, 100μm. b) Quantification of the percentage of DCIS ducts (total of 1685 matched ducts) stained negative or positive for integrin αvβ6 and TFN on serial tissue sections. Representative images are shown.

	Number of ducts (%)		
	αvβ6-positive	αvβ6-negative	Total
TFN-positive	710 (42%)	567 (34%)	1277
TFN-negative	47 (3%)	361 (21%)	408
Total	757	928	1685

Table 15. Myoepithelial cell expression of integrin αvβ6 and periductal fibronectin expression in DCIS and DCIS with associated invasion

4.2 PHENOTYPIC CHARACTERISTICS IN PRIMARY AND CELL LINE MODELS OF NORMAL AND DCIS MYOEPITHELIAL CELLS

4.2.1 Integrin αvβ6-positive primary DCIS-myoepithelial cells upregulate fibronectin expression

To investigate MEC expression of integrin αvβ6 in promoting the expression and deposition of FN, we used isolated primary DCIS-associated and normal MECs and established MEC lines with and without the expression of integrin αvβ6. Integrin αvβ6 expression by MECs in DCIS cases with organoid samples available was first assessed using immunohistochemical analyses. Two integrin αvβ6-negative (D1632 and D1730) and two integrin αvβ6-positive (β6-D2168 and β6-D2089) DCIS tissue samples with organoid preparations (Figure 19a; panel 1-2 and Supplementary Figure S2) (tumour grade matched; Table 7) were then selected to establish whether alterations in FN expression were associated with integrin αvβ6 in DCIS-MECs. DCIS organoids were depleted of mature LECs ($EpCAM^+$) and fractionated into MECs ($ITGB4^+/ITGB6^{-/+}$) and stromal cells ($ITGB4^-/ITGB6^-$) (Figure 19b-c; Supplementary Figure S2). Significantly more FN mRNA was detected in primary DCIS-MECs isolated from integrin αvβ6-positive than integrin αvβ6-negative DCIS cases (Figure 19d; Supplementary Figure S2). No integrin αvβ6 expression was seen in normal primary MECs isolated by FACS from reduction mammoplasty organoid samples (Supplementary Figure S3). These findings support the *de novo* expression of integrin αvβ6 by DCIS-MECs, and suggest the increased deposition of FN in DCIS is contributed by integrin αvβ6-positive MECs.

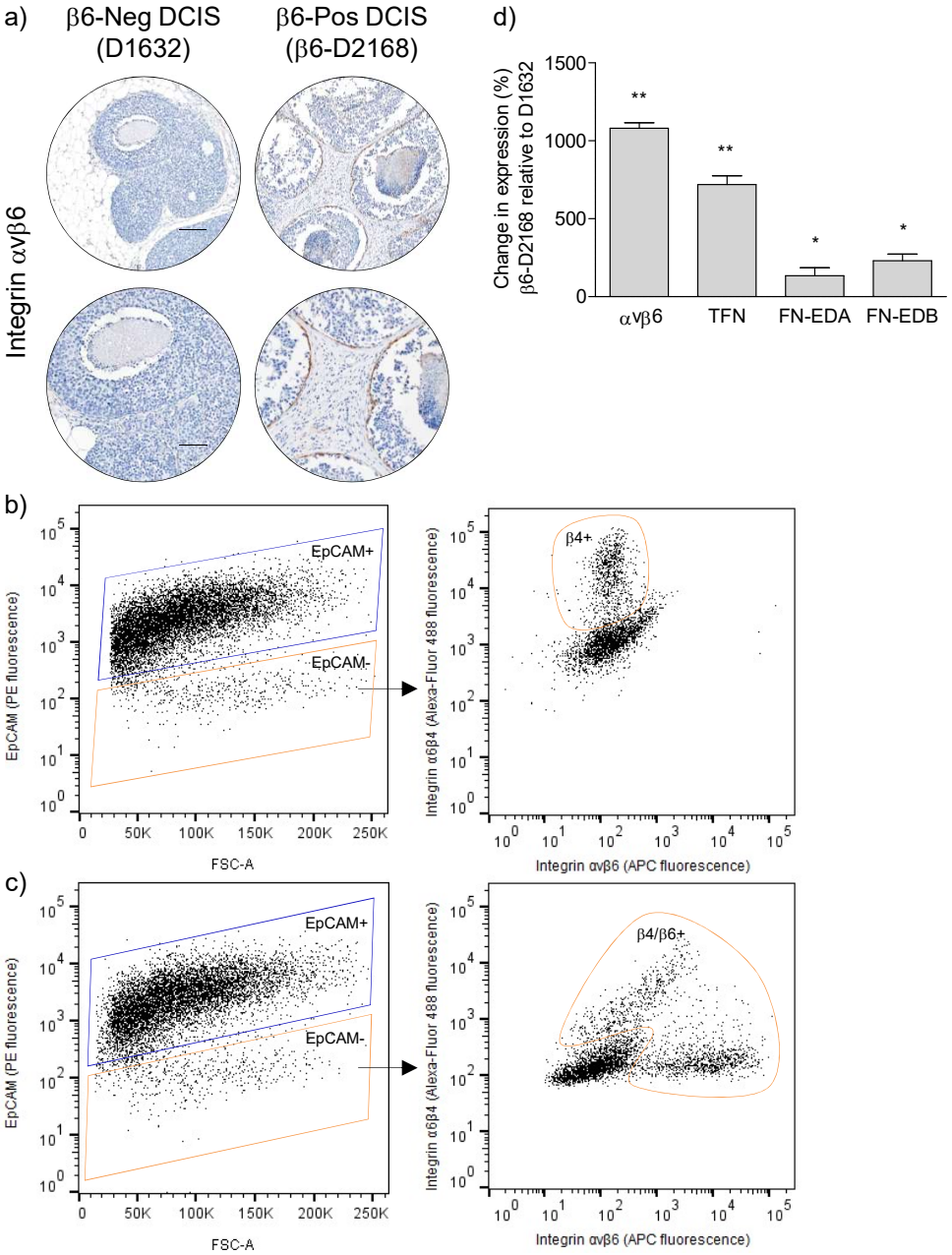

Figure 19. Integrin αvβ6-positive primary DCIS-myoepithelial cells upregulate fibronectin expression. a) Immunohistochemical images of an integrin αvβ6-negative and integrin αvβ6-positive DCIS case is shown (additional patients in Supplementary Figure S2). Magnification x5 and x10. Scale bar, 200μm and 100μm, respectively. b, c) FACS plots of DCIS organoid samples; D1632 (b) and β6-D2168 (c) separated by the expression of EpCAM (phycoerythrin (PE) fluorescence; blue gate), integrin α6β4 and αvβ6 (Alexa-Fluor 488 and allophycocyanin (APC) fluorescence, respectively; orange gate). d) qRT-PCR analysis of integrin αvβ6, TFN, FN-EDA and FN-EDB mRNA levels in D1632 and β6-D2168. The values are presented as the mean percentage change in expression relative to D1632. Representative images are shown, and analyses is shown as a mean of 3 independent experiments ±SEM. p-value ≤0.01 ('**') and ≤0.05 ('*') considered significant.

4.2.2 Integrin αvβ6 overexpression in primary normal myoepithelial cells upregulates fibronectin expression

Primary normal MECs which lack integrin αvβ6 expression (N-127, N-1492 and N-1989), were isolated by magnetic bead separation from reduction mammoplasty organoid samples (patient age and menopausal status matched) based on their expression of CD10 [439]. To further support the findings observed in isolated DCIS-MECs, transient overexpression of integrin αvβ6 was induced in primary normal MECs to model DCIS-MECs (β6-127, β6-1492 and β6-1989, respectively). Overexpression of integrin αvβ6 was confirmed using immunoblotting ($p<0.01$, $p<0.01$, and $p<0.001$, respectively) (Figure 20ai-iii; quantified in Figure 20bi-iii, respectively). A concomitant increase in TFN and FN-EDA expression in integrin αvβ6-overexpressing primary normal MECs was identified by immunoblotting ($p<0.05$) (Figure 20ai-iii; quantified in Figure 20bi-iii, respectively). These findings further support a relationship between integrin αvβ6 expression and FN deposition by DCIS-MECs.

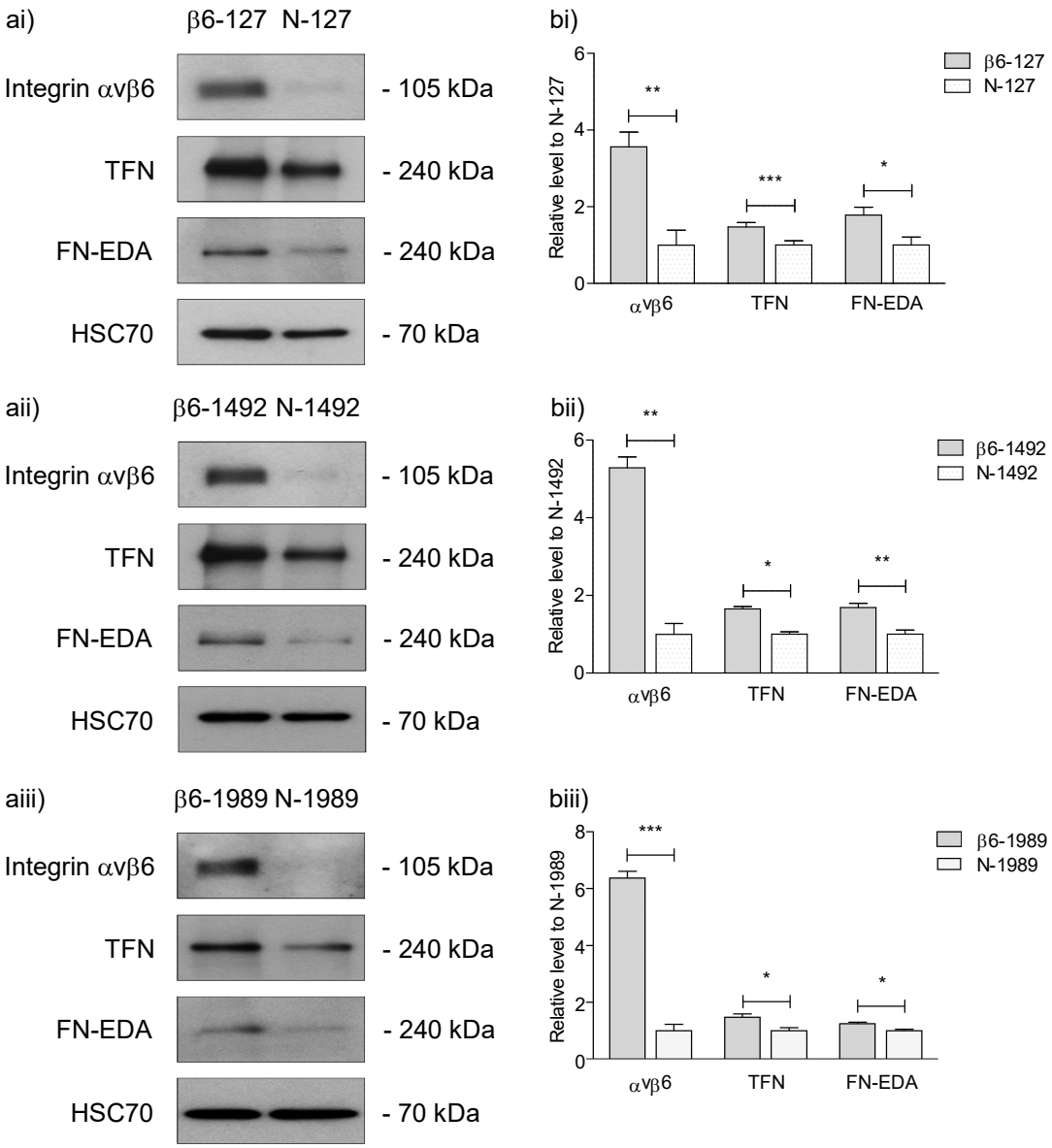

Figure 20. Integrin αvβ6 overexpression in primary normal myoepithelial cells upregulates fibronectin expression. a) Immunoblotting for integrin αvβ6, TFN, FN-EDA and HSC70 in primary normal MECs with and without integrin αvβ6 expression ((i) β6-127 and N-127; (ii) β6-1492 and N-1492; (iii) β6-1989 and N-1989, respectively). b) Densitometric analysis of integrin αvβ6, TFN, FN-EDA and HSC70 signal intensities were determined using ImageJ. The relative protein levels of integrin αvβ6, TFN and FN-EDA were normalised to HSC70 on the same membrane. The values are presented as the relative level in integrin αvβ6-positive MECs normalised to integrin αvβ6-negative MECs. Representative immunoblots of at least 3 independent experiments are shown, and analyses is shown as a mean of 3 independent experiments ±SEM. p-value ≤0.001 ('***'), ≤0.01 ('**') and ≤0.05 ('*') considered significant.

4.2.3 Integrin αvβ6-positive myoepithelial cell line upregulates deposition of a fibronectin matrix

A MEC line with and without stable expression of integrin αvβ6 (β6-1089 and N-1089, respectively) were used to further model DCIS and normal MECs, respectively. Integrin αvβ6 was confirmed to be upregulated by β6-1089 using immunofluorescent staining ($p<0.05$) and immunoblotting ($p<0.05$), with low levels of integrin αvβ6 detected in N-1089 (Figure 21a and 21c; quantified in Figure 21b and 21d, respectively). A concomitant increase in TFN and FN-EDA expression in β6-1089 was identified by immunoblotting ($p<0.05$ and $p<0.01$, respectively) (Figure 21c; quantified in Figure 21d). TFN and FN-EDA expression were also significantly upregulated in cCM obtained from β6-1089 ($p<0.01$) (Figure 21e; quantified in Figure 21f). These findings were supported at the mRNA level (Figure 21g). Additionally, higher levels of TFN and FN-EDA were detected in both DOC-soluble and DOC-insoluble material isolated from β6-1089 compared to N-1089 ($p<0.01$) (Figure 22a; quantified in Figure 22b). Furthermore, significantly more TFN and FN-EDA was detected in DOC-insoluble material compared to DOC-soluble material in β6-1089 ($p<0.01$ and $p<0.001$, respectively). Integrin αvβ6 was only detectable in DOC-soluble material, and higher levels of integrin αvβ6 were confirmed in β6-1089 compared to N-1089 ($p<0.01$) (Figure 22a; quantified in Figure 22b). Consistently, immunofluorescent staining revealed a progressive and significant increase in the incorporation of FN; both TFN and FN-EDA, into a fibrillar matrix surrounding β6-1089, as compared to N-1089 ($p<0.01$) (Figure 23a; quantified in Figure 23b), and these FN fibrils surrounding β6-1089 progressively increased in number and length ($p<0.01$) (Table 16). These data support our immunohistochemical analysis, which identified an association between MEC expression of integrin αvβ6 and periductal FN deposition. Together, these data support the use of both primary and MEC lines with and without integrin αvβ6 expression as a model of DCIS and normal MECs to investigate the tumour-promoting function of such alterations.

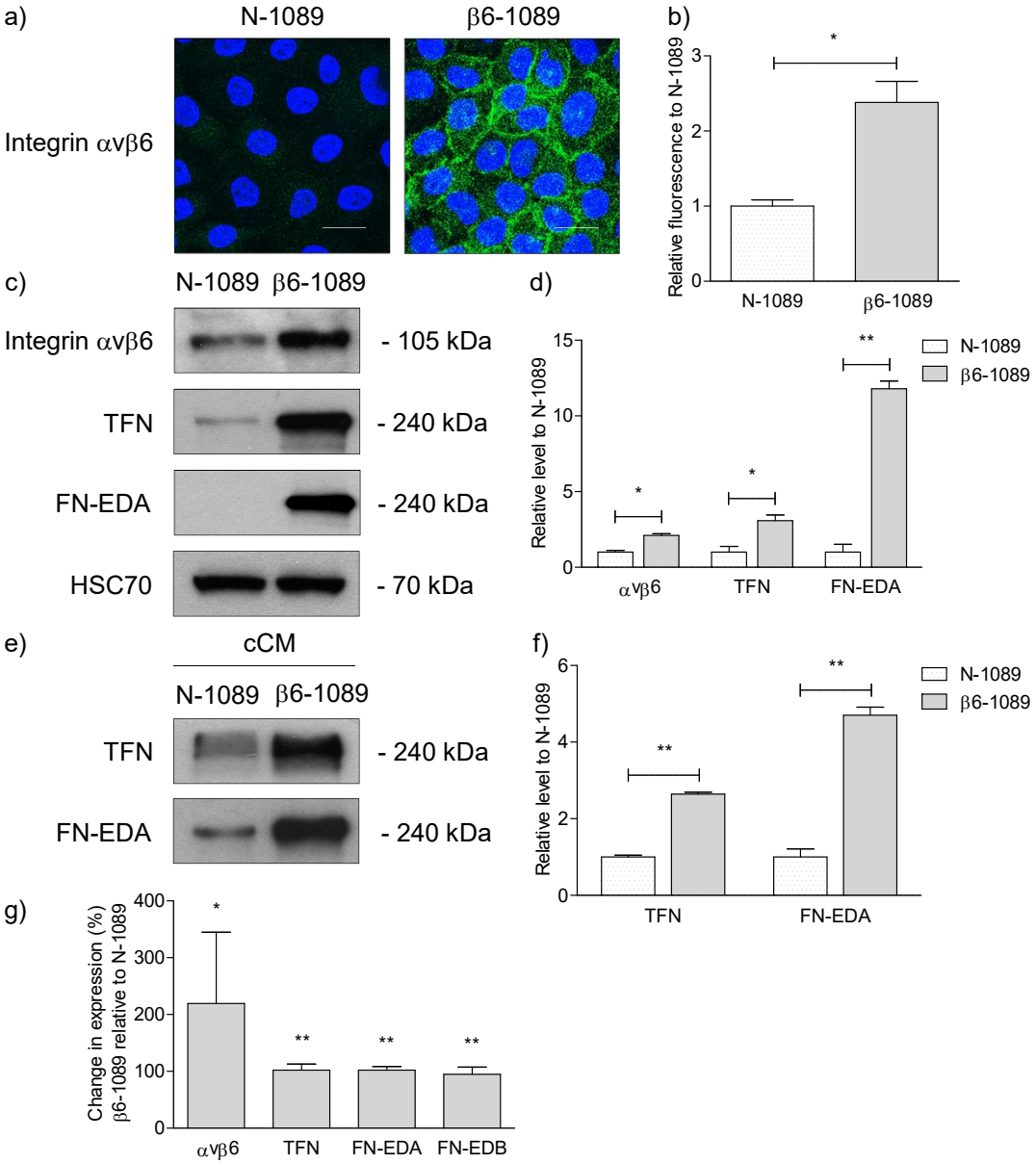

Figure 21. Integrin αvβ6-positive myoepithelial cell line upregulates fibronectin expression. a) Immunofluorescent staining for integrin αvβ6 in N-1089 and β6-1089. Magnification ×63. Scale bar, 20μm. b) Fluorescent analysis of integrin αvβ6 signal intensities were determined using the ZEN 2009 image analysis software. The values are presented as the relative fluorescence in β6-1089 normalised to N-1089. c) Immunoblotting for integrin αvβ6, TFN, FN-EDA and HSC70 in N-1089 and β6-1089. d) Densitometric analysis of integrin αvβ6, TFN, FN-EDA and HSC70 signal intensities were determined using ImageJ. The relative protein levels of integrin αvβ6, TFN and FN-EDA were normalised to HSC70 on the same membrane. The values are presented as the relative level in β6-1089 normalised to N-1089. e) Immunoblotting for TFN and FN-EDA in concentrated conditioned media (cCM) from N-1089 and β6-1089. f) Densitometric analysis of TFN and FN-EDA signal intensities were determined using ImageJ and are presented as the relative level in β6-1089 normalised to N-1089. g) qRT-PCR analysis of integrin αvβ6, TFN, FN-EDA and FN-EDB mRNA levels in N-1089 and β6-1089. The values are presented as the mean percentage change in expression relative to N-1089. Representative fluorescent images and immunoblots of at least 3 independent experiments are shown, and analyses is shown as a mean of 3 independent experiments ±SEM. p-value ≤0.01 ('**') and ≤0.05 ('*') considered significant.

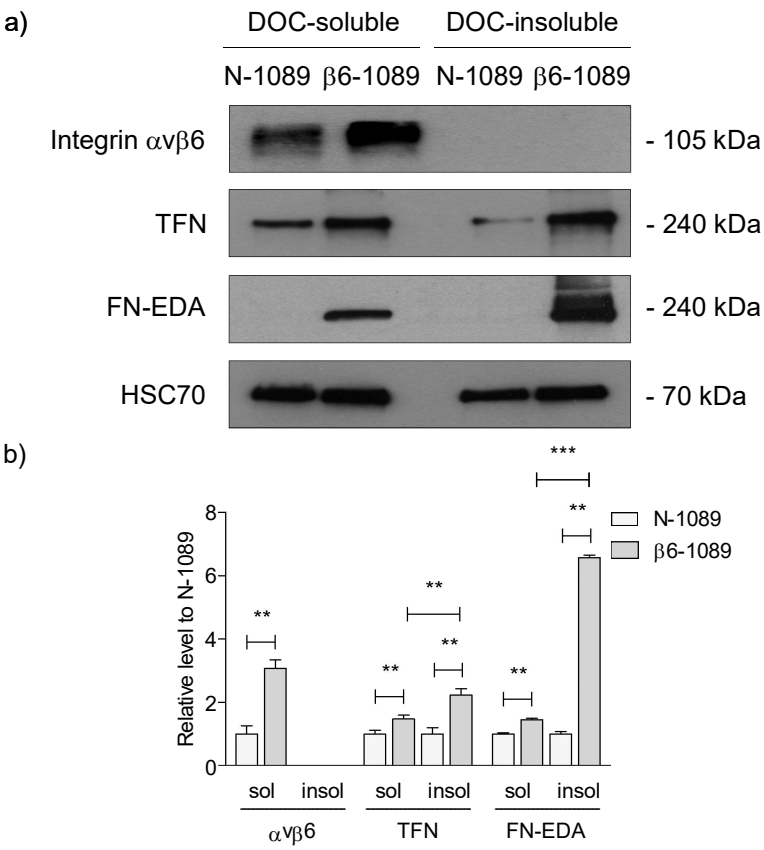

Figure 22. Integrin αvβ6-positive myoepithelial cell line upregulates DOC-soluble and DOC-insoluble fibronectin expression. a) Immunoblotting for integrin αvβ6, TFN, FN-EDA and HSC70 in DOC-soluble and DOC-insoluble material from N-1089 and β6-1089. b) Densitometric analysis of integrin αvβ6, TFN, FN-EDA and HSC70 signal intensities in DOC-soluble (sol) and DOC-insoluble (insol) material were determined using ImageJ. The relative protein levels of integrin αvβ6, TFN and FN-EDA were normalised to HSC70 on the same membrane. The values are presented as the relative level in β6-1089 normalised to N-1089. Representative immunoblots of 3 independent experiments are shown, and densitometric analysis is shown as a mean of 3 independent experiments ±SEM. p-value ≤0.001 ('***') and ≤0.01 ('**') considered significant.

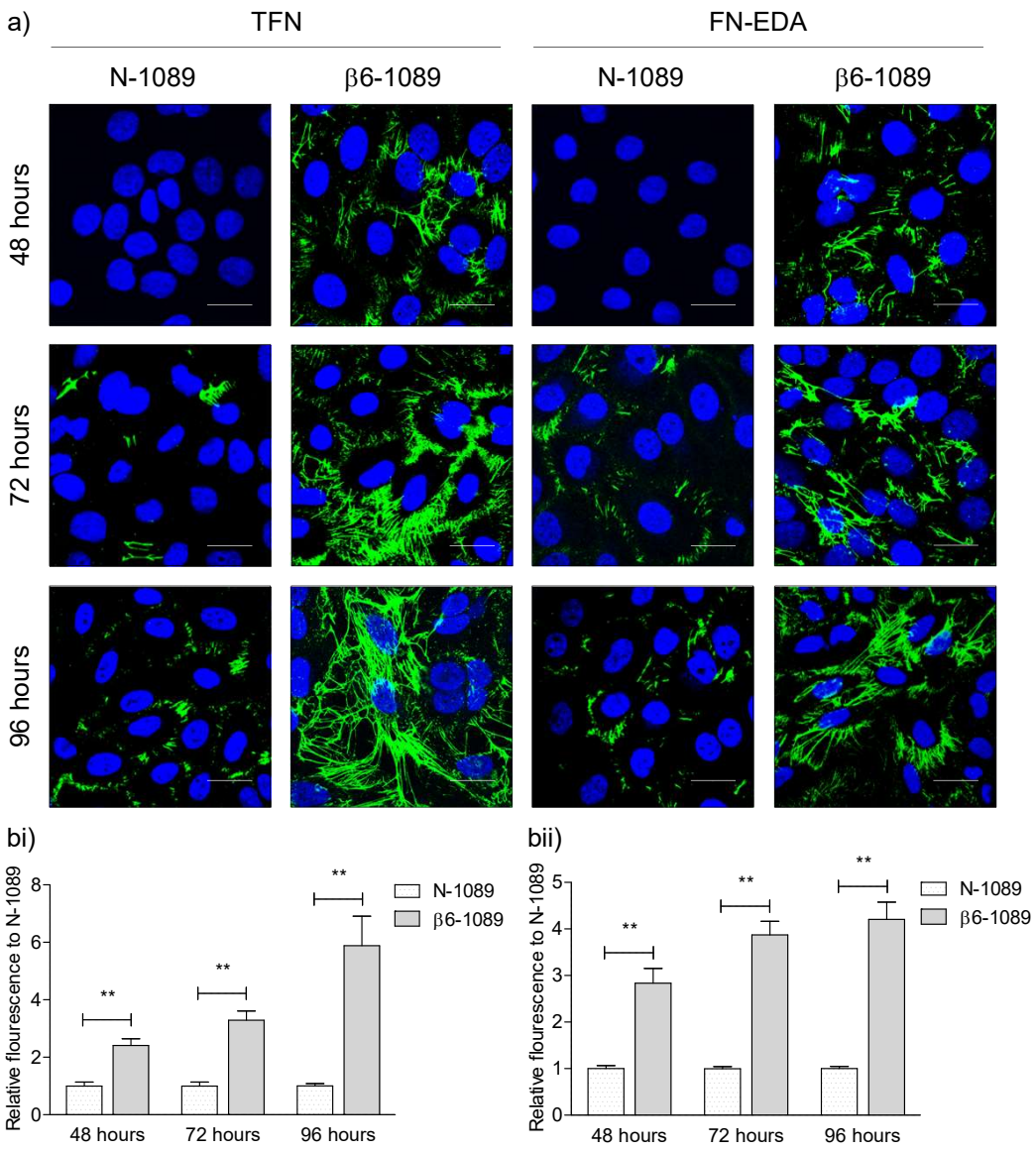

Figure 23. Integrin αvβ6-positive myoepithelial cell line upregulates deposition of a fibronectin matrix. a) Immunofluorescent staining for TFN and FN-EDA in N-1089 and β6-1089 cultured for 48, 72 and 96 hours. Substantially higher levels of TFN and FN-EDA were detected in β6-1089 compared to N-1089, and FN produced by β6-1089 assembled into a fibrillar matrix. Magnification ×63. Scale bar, 20μm. b) Fluorescence analysis of (i) TFN and (ii) FN-EDA signal intensities were determined using the ZEN 2009 image analysis software. The values are presented as the relative fluorescence in β6-1089 normalised to N-1089 of the same time point. Representative fluorescent images of 3 independent experiments are shown, and analyses is shown as a mean of 3 independent experiments ±SEM. p-value ≤0.01 ('**') considered significant.

	Fibril length in μm (% of cells with fibrils)			
	N-1089		β6-1089	
	TFN	FN-EDA	TFN	FN-EDA
48 hours	0 (0)	0 (0)	6.2 (40)	5.4 (55)
72 hours	4.8 (32)	4.1 (30)	11.8 (66)	11.6 (74)
96 hours	6.1 (48)	5.8 (41)	17.2 (91)	15.5 (92)

Table 16. Integrin αvβ6-positive myoepithelial cell line upregulates deposition of a fibronectin matrix

4.3 FUNCTION OF PHENOTYPIC CHARACTERISTICS IN PRIMARY AND CELL LINE MODELS OF NORMAL AND DCIS MYOEPITHELIAL CELLS

4.3.1 Integrin αvβ6-overexpressing primary normal myoepithelial cells activate TGFβ signalling in a fibronectin-dependent manner

Previous studies have demonstrated a role for a mechanically resistant FN matrix in liberating active TGFβ by integrin αvβ6 [212]. Allen and colleagues demonstrated the ability of β6-1089 to preferentially migrate and bind to LAP, and activate TGFβ compared to N-1089, and these functions are mediated exclusively by integrin αvβ6 [114]. We next assessed the expression of phospho-SMAD2 as a marker of activate TGFβ signalling to analyse the role of FN in integrin αvβ6-mediated TGFβ activation by MECs. We have then shown that overexpression of integrin αvβ6 in all primary normal MECs (β6-127, β6-1492 and β6-1989), led to the upregulation of phospho-SMAD2 under basal conditions ($p<0.01$, $p<0.05$ and $p<0.01$, respectively) (Figure 24-26a; quantified in Figure 24-26b, respectively) and following stimulation with exogenous TGFβ1 at all time points ($p<0.05$) (Figure 24-26c, quantified in Figure 24-26d, respectively) compared to their integrin αvβ6-negative counterpart (N-127, N-1492 and N-1989). The contribution of FN expression by integrin αvβ6-overexpressing primary MECs to activate TGFβ signalling was next analysed. Knockdown of TFN expression using siRNA targeting TFN in integrin αvβ6-overexpressing primary MECs ($p<0.01$) (Figure 27ai-iii; quantified in Figure 27bi-iii) reduced the level of phospho-SMAD2 under basal conditions ($p<0.01$, $p<0.01$ and $p<0.05$, respectively) (Figure 28-30a; quantified in Figure 28-30b, respectively) and following stimulation with exogenous TGFβ1 at all time points ($p<0.05$) (Figure 28-30c, quantified in Figure 28-30d, respectively). These data support the function of FN in integrin αvβ6-mediated activation of TGFβ signaling.

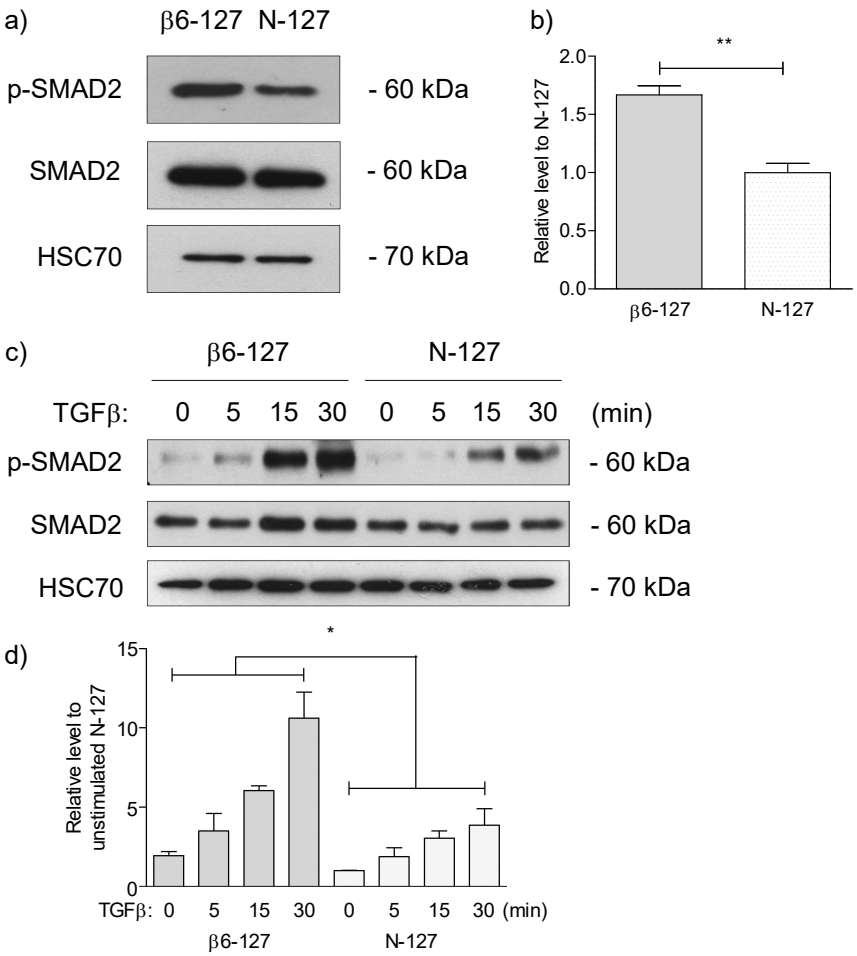

Figure 24. Integrin αvβ6-overexpressing primary normal myoepithelial cells promote canonical TGFβ signalling. a, c) Immunoblotting for phospho-SMAD2 (p-SMAD2), SMAD2 and HSC70 in β6-127 and N-127 in (a) basal conditions and (c) stimulation with exogenous TGFβ1. b, d) Densitometric analysis of p-SMAD2, SMAD2 and HSC70 signal intensities were determined using ImageJ. The relative protein levels of p-SMAD2 and SMAD2 were normalised to HSC70 on the same membrane. The expression of p-SMAD2 is normalised to SMAD2 expression under the same conditions. These data are then presented as the relative level by normalising to the control as depicted on the y-axis. Representative images of 3 independent immunoblots are shown, and densitometric analysis is shown as a mean of 3 experiments ±SEM. p-value ≤0.01 ('**') and ≤0.05 ('*') considered significant.

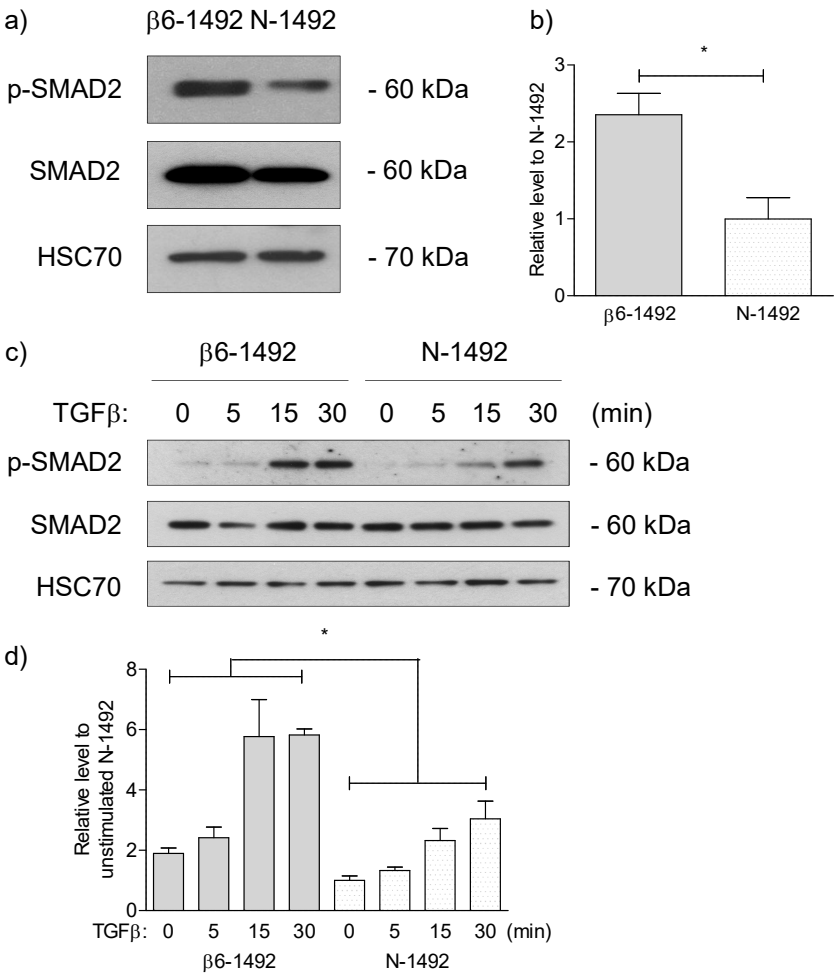

Figure 25. Integrin αvβ6-overexpressing primary normal myoepithelial cells promote canonical TGFβ signalling. a, c) Immunoblotting for p-SMAD2, SMAD2 and HSC70 in β6-1492 and N-1492 in (a) basal conditions and (c) stimulation with exogenous TGFβ1. b, d) Densitometric analysis of p-SMAD2, SMAD2 and HSC70 signal intensities were determined using ImageJ. The relative protein levels of p-SMAD2 and SMAD2 were normalised to HSC70 on the same membrane. The expression of p-SMAD2 is normalised to SMAD2 expression under the same conditions. These data are then presented as the relative level by normalising to the control as depicted on the y-axis. Representative images of 3 independent immunoblots are shown, and densitometric analysis is shown as a mean of 3 experiments ±SEM. p-value ≤0.05 ('*') considered significant.

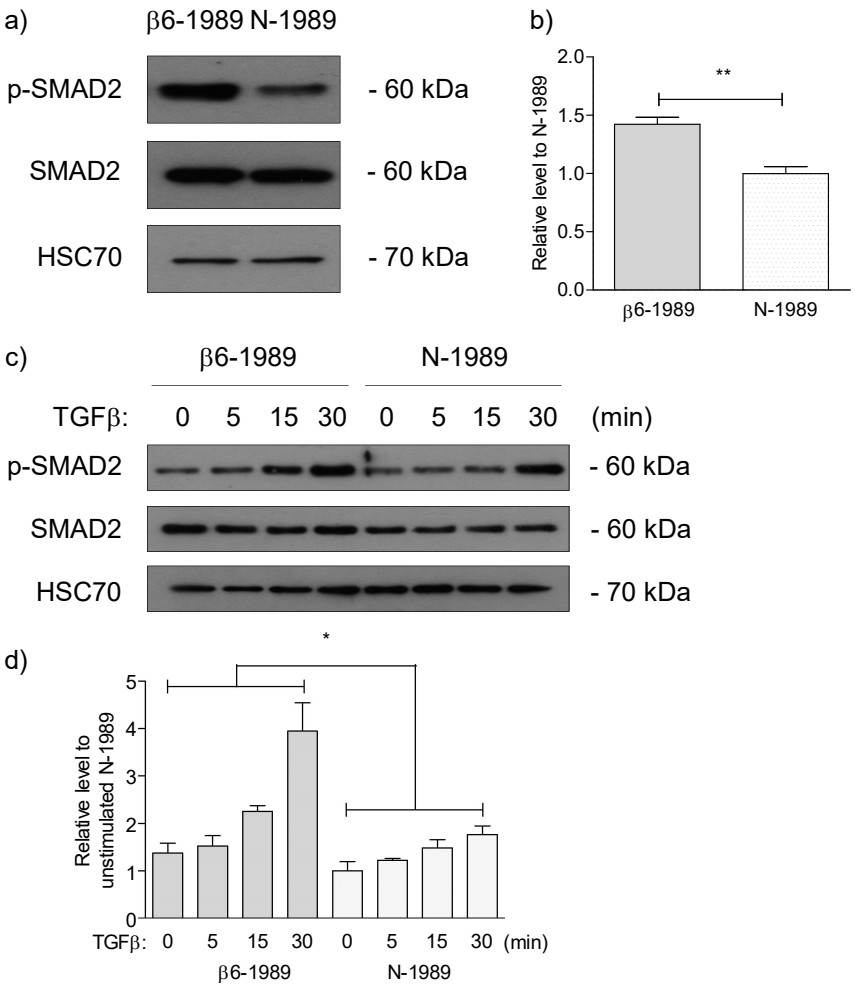

Figure 26. Integrin αvβ6-overexpressing primary normal myoepithelial cells promote canonical TGFβ signalling. a, c) Immunoblotting for p-SMAD2, SMAD2 and HSC70 in β6-1989 and N-1989 in (a) basal conditions and (c) stimulation with exogenous TGFβ1. b, d) Densitometric analysis of p-SMAD2, SMAD2 and HSC70 signal intensities were determined using ImageJ. The relative protein levels of p-SMAD2 and SMAD2 were normalised to HSC70 on the same membrane. The expression of p-SMAD2 is normalised to SMAD2 expression under the same conditions. These data are then presented as the relative level by normalising to the control as depicted on the y-axis. Representative images of 3 independent immunoblots are shown, and densitometric analysis is shown as a mean of 3 experiments ±SEM. p-value ≤0.01 ('**') and ≤0.05 ('*') considered significant.

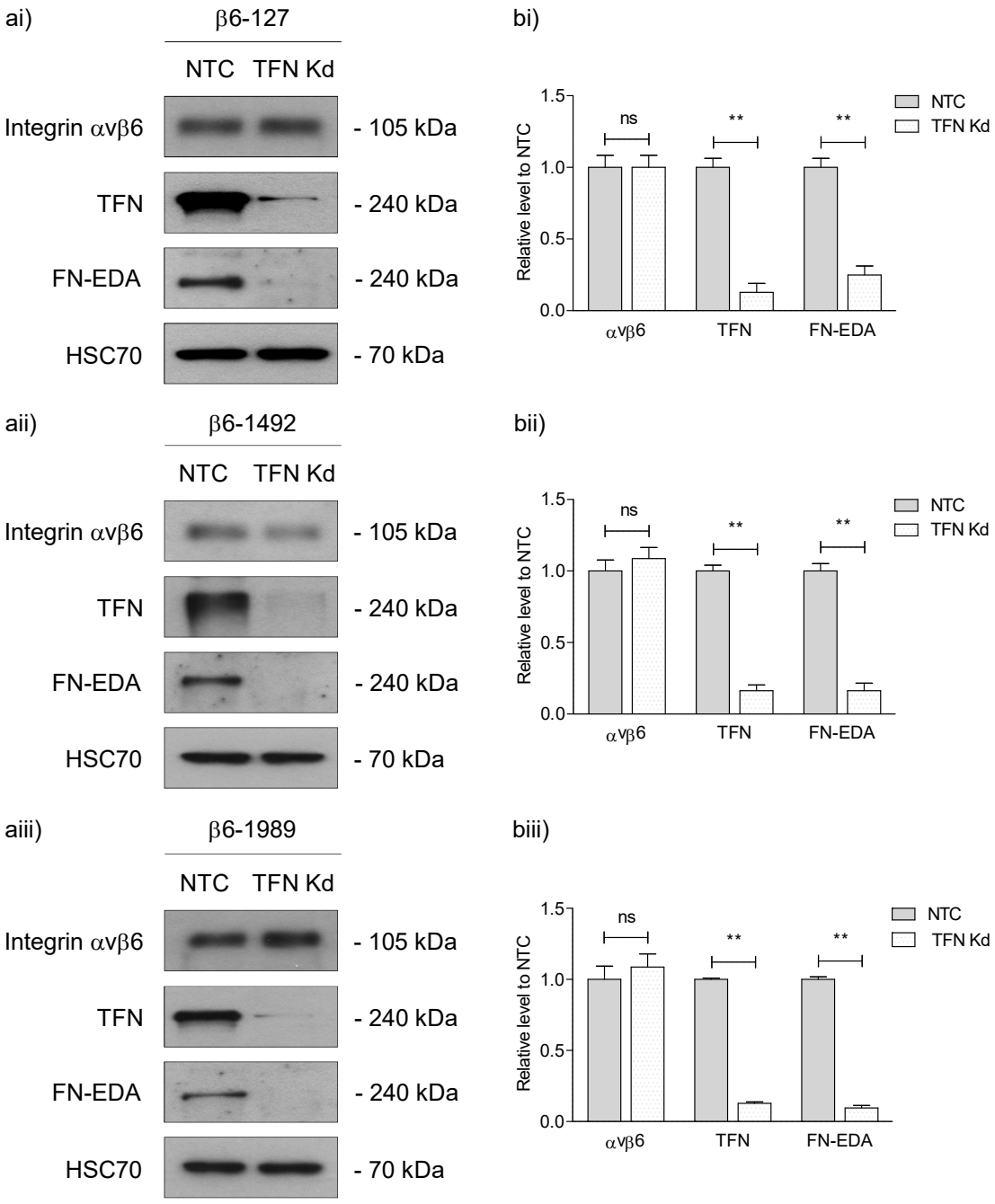

Figure 27. Knockdown of fibronectin expression in integrin αvβ6-overexpressing primary normal myoepithelial cells. a) Immunoblotting for integrin αvβ6, TFN, FN-EDA and HSC70 in integrin αvβ6-positive primary normal MECs ((i) β6-127, (ii) β6-1492 and (iii) β6-1989) with NTC or TFN siRNA (TFN Kd). b) Densitometric analysis of integrin αvβ6, TFN, FN-EDA and HSC70 signal intensities were determined using ImageJ. The relative protein levels of integrin αvβ6, TFN and FN-EDA were normalised to HSC70 on the same membrane. The values are presented as the relative level in TFN Kd normalised to NTC. Representative immunoblots of at least 3 independent experiments are shown, and analyses is shown as a mean of 3 independent experiments ±SEM. p-value ≤0.01 ('**') considered significant, 'ns' indicates not significant.

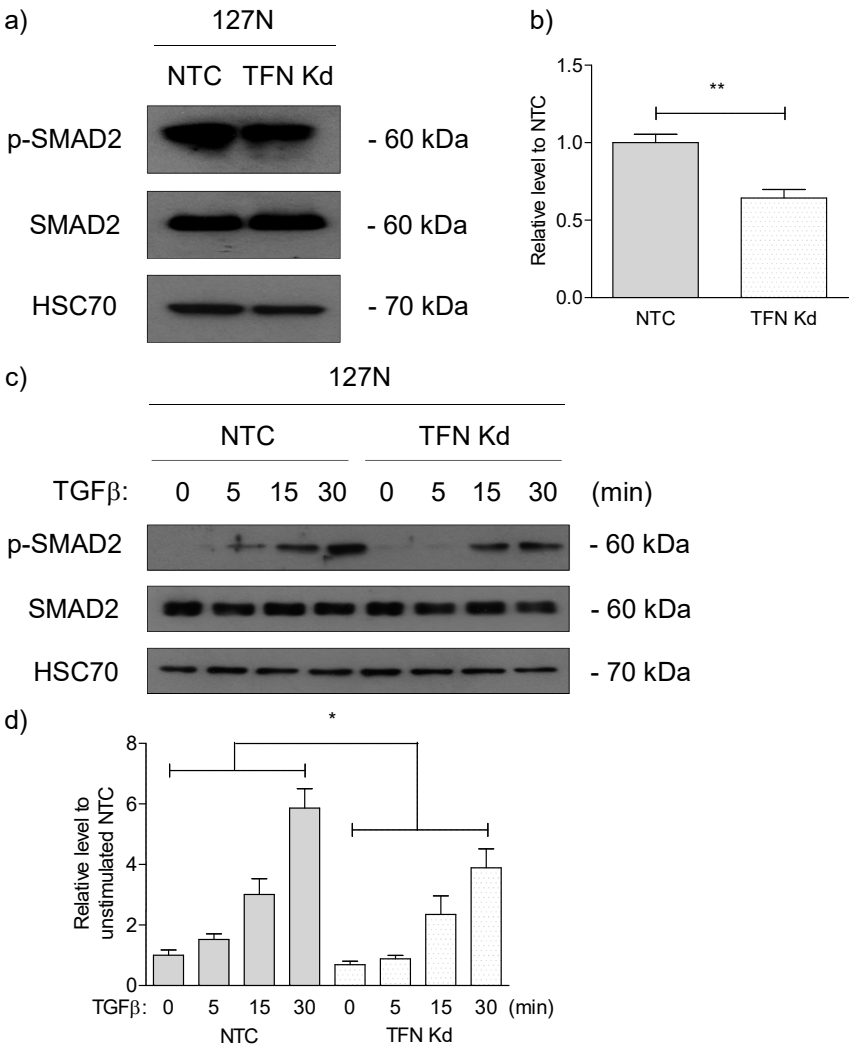

Figure 28. Integrin αvβ6-overexpressing primary normal myoepithelial cells promote canonical TGFβ signalling in a fibronectin-dependent manner. a, c) Immunoblotting for p-SMAD2, SMAD2 and HSC70 in β6-127 with NTC or TFN siRNA (TFN Kd) in (a) basal conditions and (c) stimulation with exogenous TGFβ1. b, d) Densitometric analysis of p-SMAD2, SMAD2 and HSC70 signal intensities were determined using ImageJ. The relative protein levels of p-SMAD2 and SMAD2 were normalised to HSC70 on the same membrane. The expression of p-SMAD2 is normalised to SMAD2 expression under the same conditions. These data are then presented as the relative level by normalising to the control as depicted on the y-axis. Representative images of 3 independent immunoblots are shown, and densitometric analysis is shown as a mean of 3 experiments ±SEM. p-value ≤0.01 ('**') and ≤0.05 ('*') considered significant.

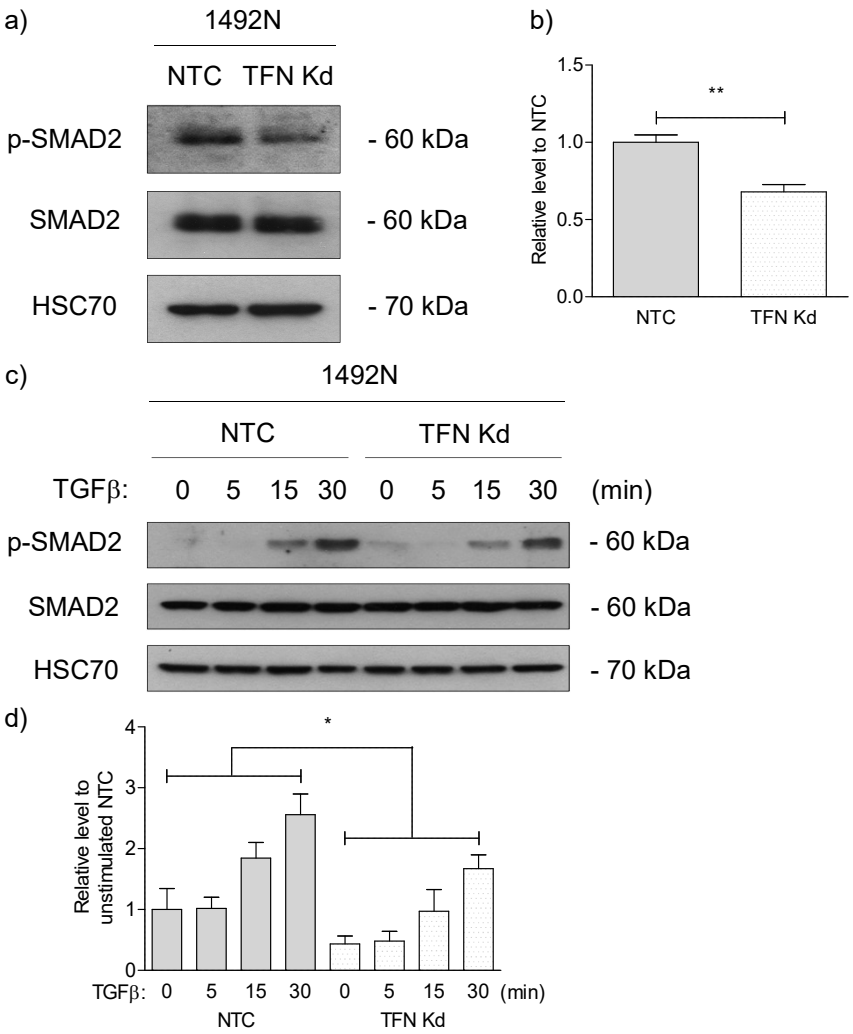

Figure 29. Integrin αvβ6-overexpressing primary normal myoepithelial cells promote canonical TGFβ signalling in a fibronectin-dependent manner. a, c) Immunoblotting for p-SMAD2, SMAD2 and HSC70 in β6-1492 with NTC or TFN siRNA (TFN Kd) in (a) basal conditions and (c) stimulation with exogenous TGFβ1. b, d) Densitometric analysis of p-SMAD2, SMAD2 and HSC70 signal intensities were determined using ImageJ. The relative protein levels of p-SMAD2 and SMAD2 were normalised to HSC70 on the same membrane. The expression of p-SMAD2 is normalised to SMAD2 expression under the same conditions. These data are then presented as the relative level by normalising to the control as depicted on the y-axis. Representative images of 3 independent immunoblots are shown, and densitometric analysis is shown as a mean of 3 experiments ±SEM. p-value ≤0.01 ('**') and ≤0.05 ('*') considered significant.

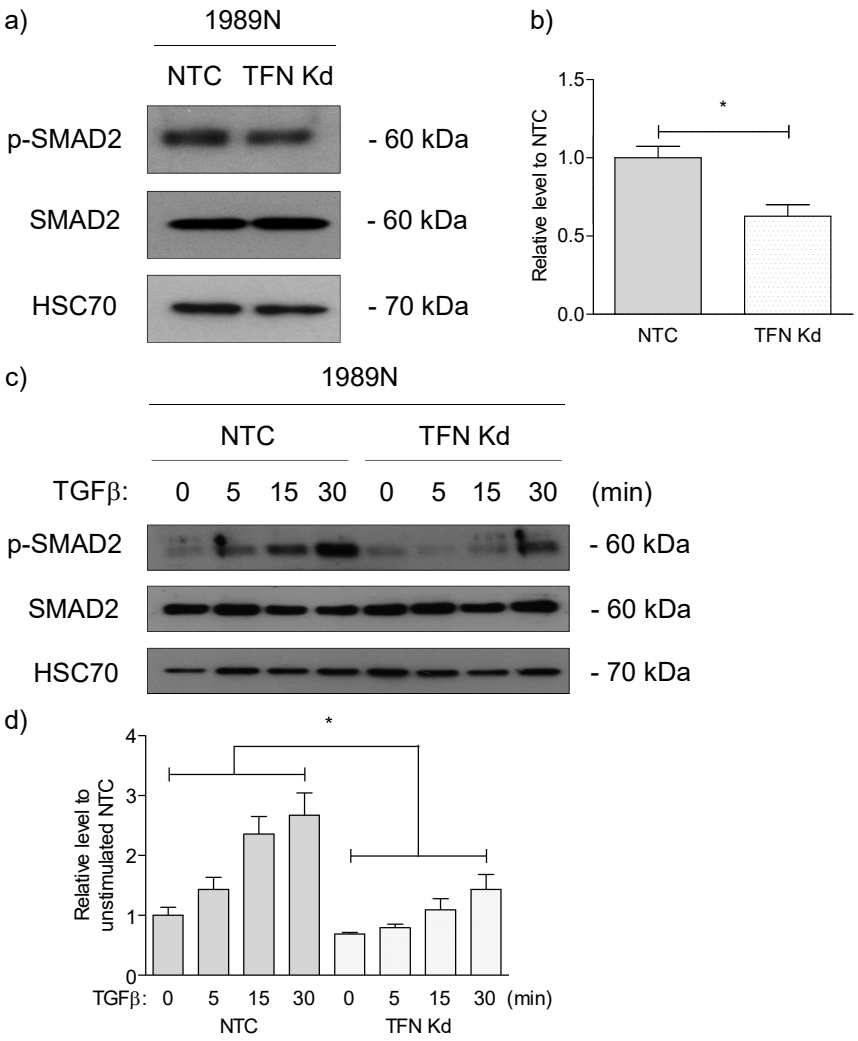

Figure 30. Integrin αvβ6-overexpressing primary normal myoepithelial cells promote canonical TGFβ signalling in a fibronectin-dependent manner. a, c) Immunoblotting for p-SMAD2, SMAD2 and HSC70 in β6-1989 with NTC or TFN siRNA (TFN Kd) in (a) basal conditions and (c) stimulation with exogenous TGFβ1. b, d) Densitometric analysis of p-SMAD2, SMAD2 and HSC70 signal intensities were determined using ImageJ. The relative protein levels of p-SMAD2 and SMAD2 were normalised to HSC70 on the same membrane. The expression of p-SMAD2 is normalised to SMAD2 expression under the same conditions. These data are then presented as the relative level by normalising to the control as depicted on the y-axis. Representative images of 3 independent immunoblots are shown, and densitometric analysis is shown as a mean of 3 experiments ±SEM. p-value ≤0.05 ('*') considered significant.

4.3.2 Integrin αvβ6-positive myoepithelial cell line activates TGFβ signalling in a fibronectin-dependent manner

Consistent with the overexpression of integrin αvβ6 in primary MECs, significantly more phospho-SMAD2 was detected in β6-1089 compared to N-1089 using immunoblotting, both under basal conditions ($p<0.05$) (Figure 31a; quantified in Figure 31bi) and following stimulation with exogenous TGFβ1 ($p<0.05$) (Figure 31c; quantified in Figure 31di). Additionally, phospho-ERK1/2 was upregulated in β6-1089 under basal conditions ($p<0.05$) (Figure 32a; quantified in Figure 32bi, respectively) and following stimulation with exogenous TGFβ1 at all time points ($p<0.05$) (Figure 32c, quantified in Figure 32di), compared to N-1089. This effect was reduced by knockdown of integrin αvβ6 expression in β6-1089 using siRNA targeting integrin β6 (Figure 33), both at the basal level ($p<0.01$) (Figure 31a and 32a; quantified in Figure 31bii and 32bii, respectively) and in response to exogenous TGFβ1 ($p<0.05$) (Figure 31c and 32c; quantified in Figure 31dii and 32dii, respectively). Moreover, knockdown of TFN expression in β6-1089 using siRNA targeting TFN (Figure 34), reduced the level of phospho-SMAD2 both at the basal level ($p<0.05$) (Figure 35a; quantified in Figure 35b) and in response to exogenous TGFβ1 ($p<0.05$) (Figure 35c; quantified in Figure 35d). The role of FN expression by integrin αvβ6-positive MECs in their ability bind to LAP was analysed. Knockdown of TFN expression in β6-1089 reduced both migration ($p<0.01$) (Figure 36a) and adhesion ($p<0.01$) (Figure 36b) to LAP. These data further support FN in integrin αvβ6-mediated activation of TGFβ signalling.

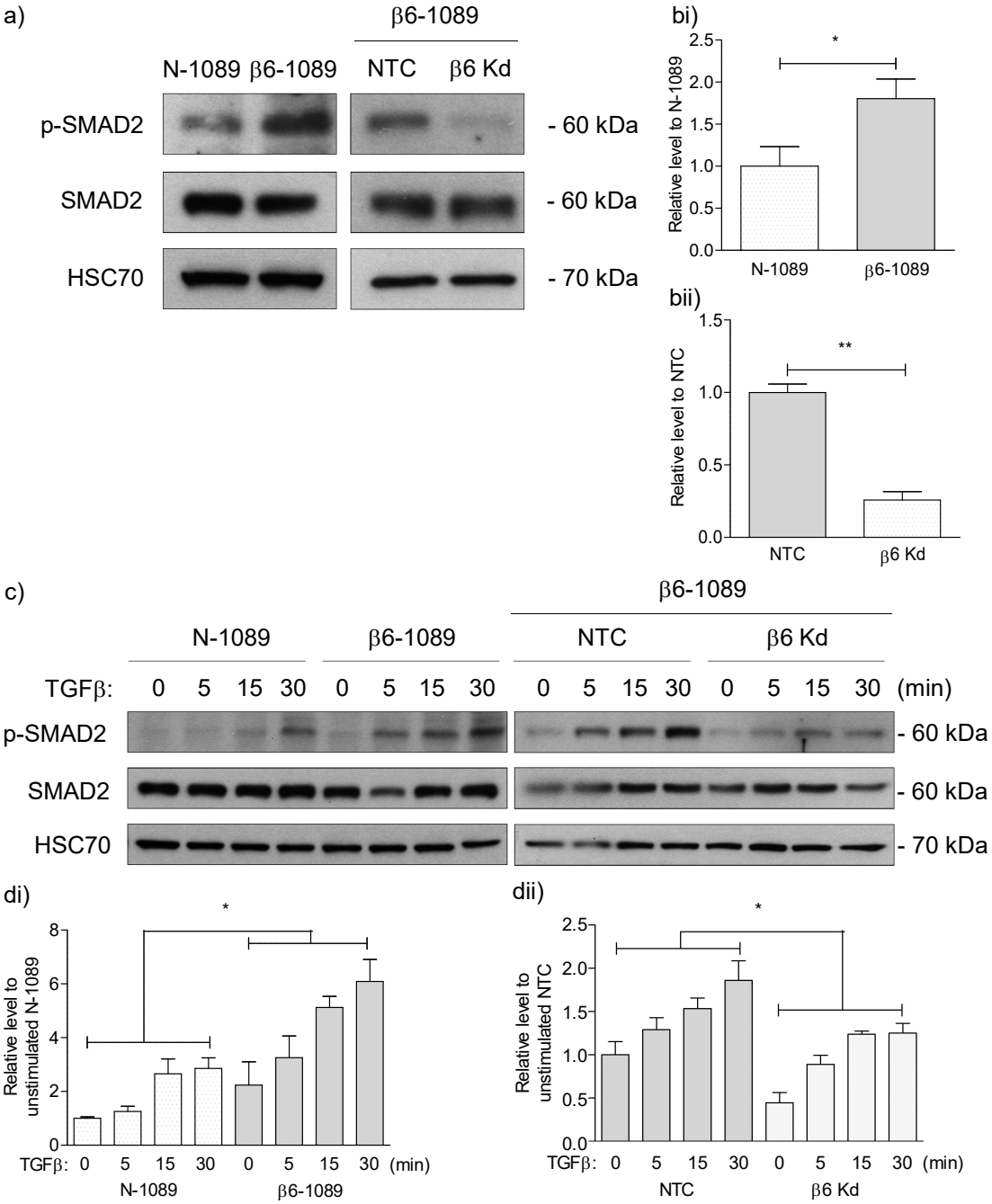

Figure 31. Integrin αvβ6-positive myoepithelial cell line promotes canonical TGFβ signalling. a, c) Immunoblotting for p-SMAD2, SMAD2 and HSC70 in (i) N-1089 and β6-1089, and (ii) β6-1089 with NTC or integrin β6 siRNA (β6 Kd) in (a) basal conditions and (c) stimulation with exogenous TGFβ1. b, d) Densitometric analysis of p-SMAD2, SMAD2 and HSC70 signal intensities were determined using ImageJ. The relative protein levels of p-SMAD2 and SMAD2 were normalised to HSC70 on the same membrane. The expression of p-SMAD2 is normalised to SMAD2 expression under the same conditions. These data are then presented as the relative level by normalising to the control as depicted on the y-axis. Representative images of 3 independent immunoblots are shown, and densitometric analysis is shown as a mean of 3 experiments ±SEM. p-value ≤0.01 ('**') and ≤0.05 ('*') considered significant.

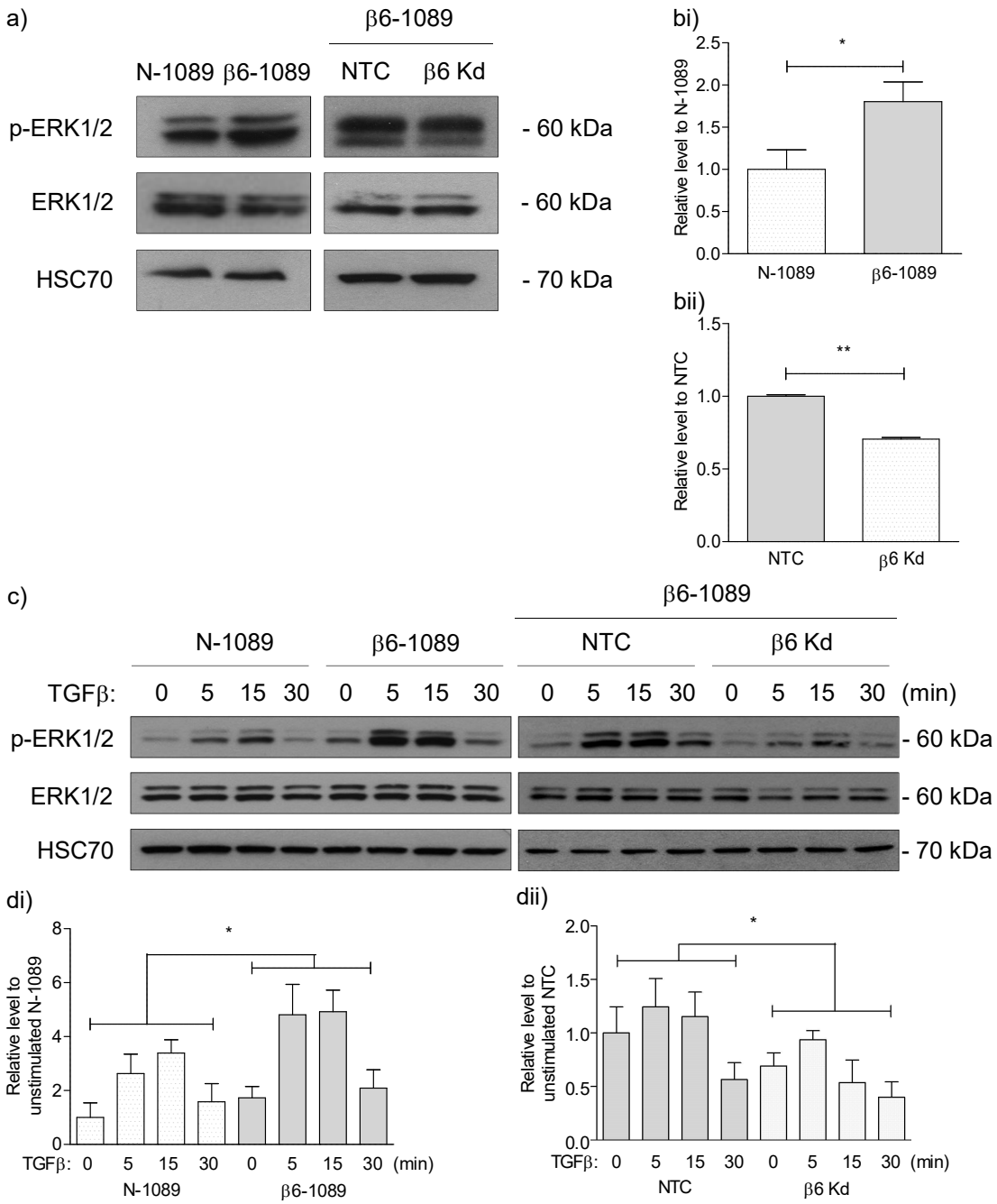

Figure 32. Integrin αvβ6-positive myoepithelial cell line promotes non-canonical TGFβ signalling. a, c) Immunoblotting for p-ERK1/2, ERK1/2 and HSC70 in (i) N-1089 and β6-1089, and (ii) β6-1089 with NTC or integrin β6 siRNA (β6 Kd) in (a) basal conditions and (c) stimulation with exogenous TGFβ1. b, d) Densitometric analysis of p-ERK1/2, ERK1/2 and HSC70 signal intensities were determined using ImageJ. The relative protein levels of p-ERK1/2 and ERK1/2 were normalised to HSC70 on the same membrane. The expression of p-ERK1/2 is normalised to ERK1/2 expression under the same conditions. These data are then presented as the relative level by normalising to the control as depicted on the y-axis. Representative images of 3 independent immunoblots are shown, and densitometric analysis is shown as a mean of 3 experiments ±SEM. p-value ≤0.01 ('**') and ≤0.05 ('*') considered significant.

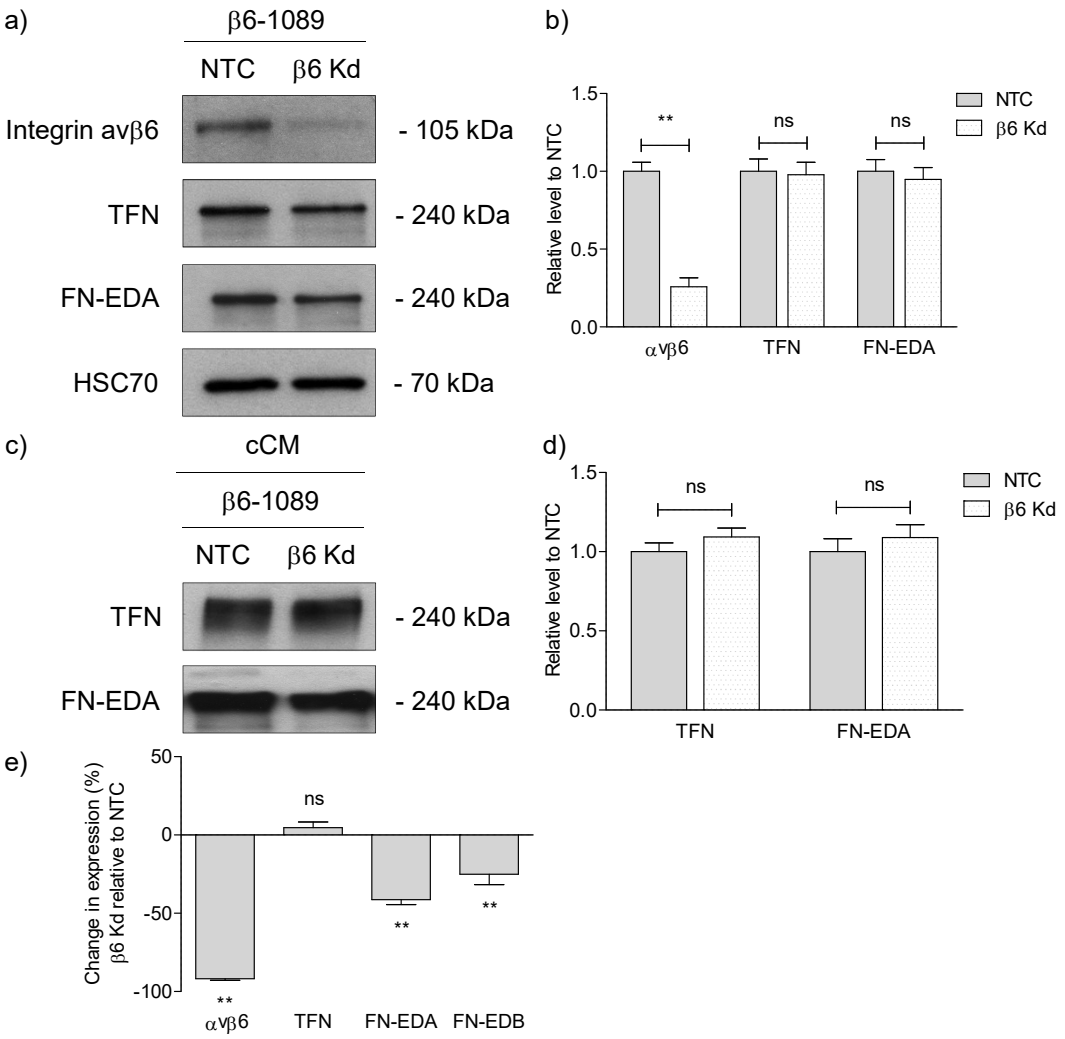

Figure 33. Knockdown of integrin αvβ6 expression in an integrin αvβ6-positive myoepithelial cell line. a) Immunoblotting for integrin αvβ6, TFN, FN-EDA and HSC70 in β6-1089 with NTC or integrin β6 siRNA (β6 Kd). b) Densitometric analysis of integrin αvβ6, TFN, FN-EDA and HSC70 signal intensities were determined using ImageJ. The relative protein levels of integrin αvβ6, TFN and FN-EDA were normalised to HSC70 on the same membrane. The values are presented as the relative level in β6 Kd normalised to NTC. c) Immunoblotting for TFN and FN-EDA in cCM from β6-1089 with NTC or integrin β6 siRNA (β6 Kd). d) Densitometric analysis of TFN and FN-EDA signal intensities were determined using ImageJ and are presented as the relative level in β6 Kd normalised to NTC. e) qRT-PCR analysis of integrin αvβ6, TFN, FN-EDA and FN-EDB mRNA levels in β6-1089 with NTC or integrin β6 siRNA (β6 Kd). The values are presented as the mean percentage change in expression relative to the NTC. Representative immunoblots of at least 3 independent experiments are shown, and analyses is shown as a mean of 3 independent experiments ±SEM. p-value ≤0.01 ('**') considered significant, 'ns' indicates not significant.

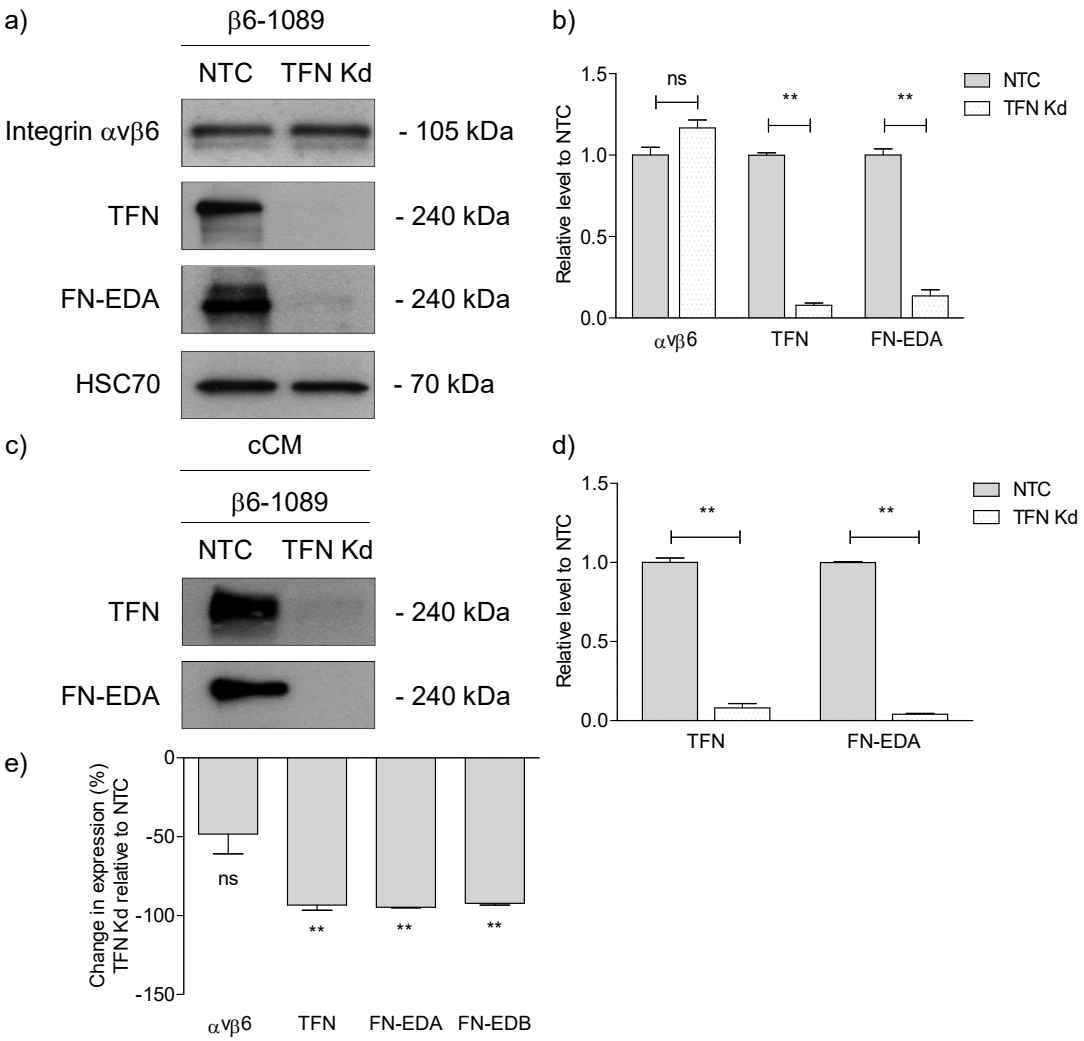

Figure 34. Knockdown of fibronectin expression in an integrin αvβ6-positive myoepithelial cell line. a) Immunoblotting for integrin αvβ6, TFN, FN-EDA and HSC70 in β6-1089 with NTC or TFN siRNA (TFN Kd). b) Densitometric analysis of integrin αvβ6, TFN, FN-EDA and HSC70 signal intensities were determined using ImageJ. The relative protein levels of integrin αvβ6, TFN and FN-EDA were normalised to HSC70 on the same membrane. The values are presented as the relative level in TFN Kd normalised to NTC. c) Immunoblotting for TFN and FN-EDA in cCM from β6-1089 with NTC or TFN siRNA (TFN Kd). d) Densitometric analysis of TFN and FN-EDA signal intensities were determined using ImageJ and are presented as the relative level in TFN Kd normalised to NTC. e) qRT-PCR analysis of integrin αvβ6, TFN, FN-EDA and FN-EDB mRNA levels in β6-1089 with NTC or TFN siRNA (TFN Kd). The values are presented as the mean percentage change in expression relative to the NTC. Representative immunoblots of at least 3 independent experiments are shown, and analyses is shown as a mean of 3 independent experiments ±SEM. p-value ≤0.01 ('**') considered significant, 'ns' indicates not significant.

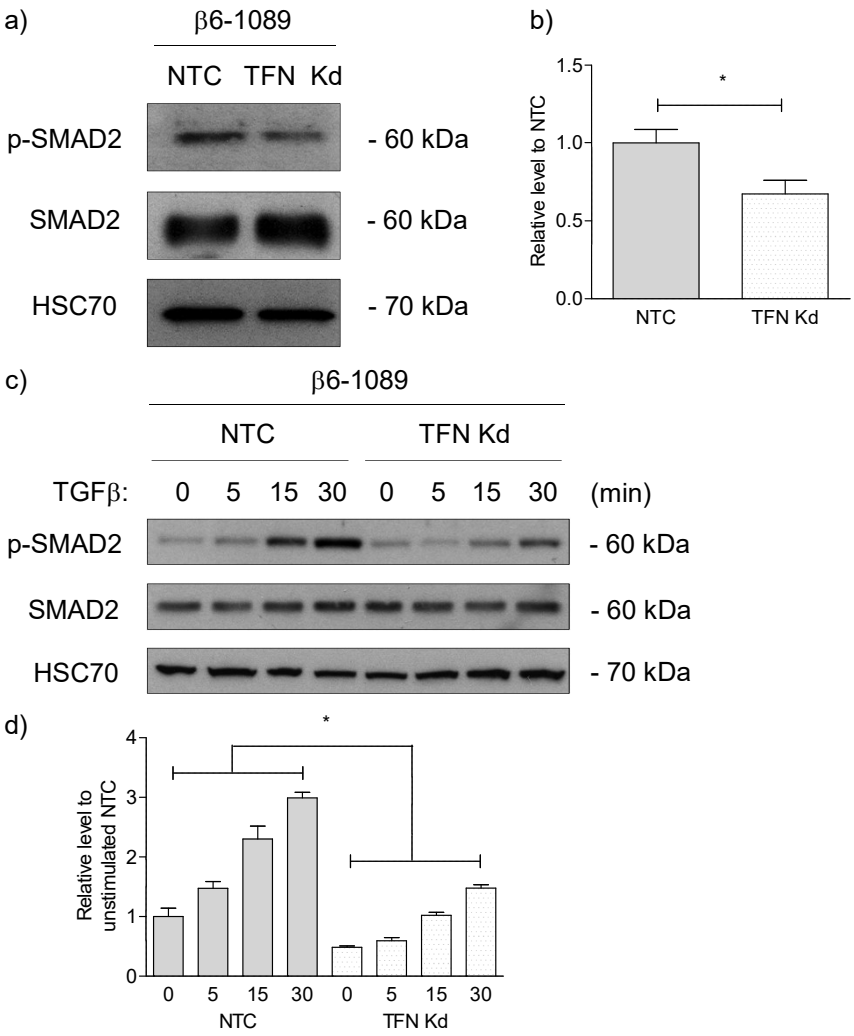

Figure 35. Integrin αvβ6-positive myoepithelial cell line promotes canonical TGFβ signalling in a fibronectin-dependent manner. a, c) Immunoblotting for p-SMAD2, SMAD2 and HSC70 in β6-1089 with NTC or TFN siRNA (TFN Kd) in (a) basal conditions and (c) stimulation with exogenous TGFβ1. b, d) Densitometric analysis of p-SMAD2, SMAD2 and HSC70 signal intensities were determined using ImageJ. The relative protein levels of p-SMAD2 and SMAD2 were normalised to HSC70 on the same membrane. The expression of p-SMAD2 is normalised to SMAD2 expression under the same conditions. These data are then presented as the relative level by normalising to the control as depicted on the y-axis. Representative images of 3 independent immunoblots are shown, and densitometric analysis is shown as a mean of 3 experiments ±SEM. p-value ≤0.05 ('*') were considered significant, 'ns' indicates not significant.

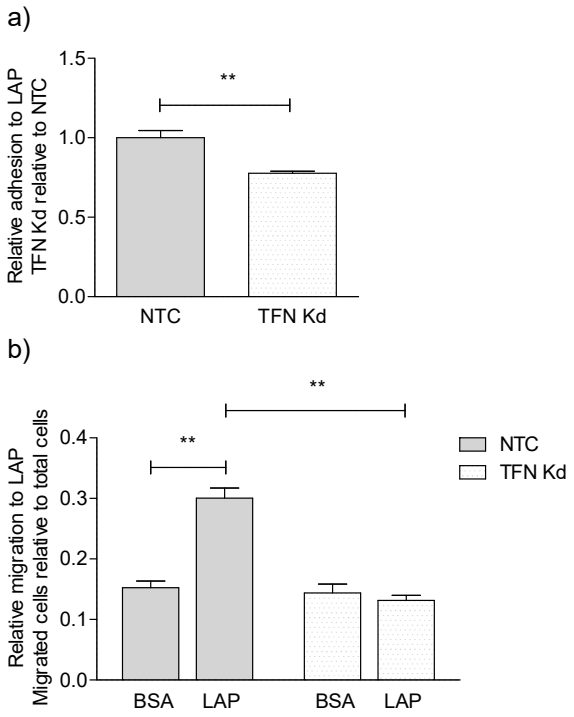

Figure 36. Integrin αvβ6-positive myoepithelial cell line mediates adhesion and migration to LAP in a fibronectin-dependent manner. a) Adhesion of β6-1089 with NTC or TFN siRNA (TFN Kd) to BSA and LAP. Background binding to BSA was subtracted from LAP, and the values are then presented as the relative adhesion to LAP in TFN Kd normalised to NTC. b) Migration of β6-1089 with NTC or TFN siRNA (TFN Kd) to BSA and LAP. The number of migrating cells was quantified by counting the cells within the Transwell insert and on the underside of the Transwell, and the total cell count was calculated by their addition. The values are then presented as the relative migration to LAP by using the outer chamber count versus total cell count. Analyses is shown as a mean of 3 independent experiments ±SEM. p-value ≤0.01 ('**') and ≤0.05 ('*') considered significant.

4.1.1 Integrin αvβ6-positive myoepithelial cell line mediates breast cancer cell invasion by TGFβ-dependent upregulation of MMP13

We next investigated the role of FN in the tumour promoting function of integrin αvβ6-positive MECs. Previous data demonstrated integrin αvβ6-positive MECs promoted breast cancer cell invasion *in vitro* in a TGFβ-dependent upregulation of MMP9 [114]. Interestingly, we identified that CM isolated following knockdown of TFN in β6-1089 reduced both MDA-MB-231 and MCF-7 cell invasion ($p<0.01$) (Figure 37a), with no effect on proliferation (Figure 37b). Proteases were next measured in the CM using a human protease array to identify potential invasive-promoting factors. We identified β6-1089 induce an overall increase in the secretion of MMPs, in particular, those involved in degradation of the BM and surrounding collagenous stroma, including; MMP9 and MMP13 (Figure 38ai). These findings were supported at the mRNA level (Figure 38bi), and increased MMP9 expression by β6-1089 was confirmed using gelatin zymography ($p<0.01$) (Figure 39a; quantified in Figure 39bi, respectively) (Supplementary Figure 4). These effects were reduced following knockdown of integrin αvβ6 in β6-1089 ($p<0.01$) (Figure 38aii; Figure 38bii, Figure 39a; quantified in Figure 39bii, respectively). Moreover, knockdown of TFN in β6-1089 reduced MMP secretion, as identified by human protease array analysis (Figure 40a). These alterations were supported at the mRNA level (Figure 40b) and using gelatin zymography to detect MMP9 expression ($p<0.05$) (Figure 40c; quantified in Figure 40d). MMP expression by β6-1089 was further reduced by a TGFβRII blocking antibody (Figure 41a), in which MMP9 and MMP13 mRNA were significantly reduced ($p<0.01$ and 0.05, respectively) (Figure 41a), as supported by gelatin zymography for MMP9 expression ($p<0.01$) (Figure 41b; quantified in Figure 41c). The function of MMP13 in promoting breast cancer cell invasion *in vitro* by β6-1089 was analysed. CM isolated following the knockdown of MMP13 expression in β6-1089 using siRNA targeting MMP13 ($p<0.001$) (Figure 42a) reduced both MDA-MB-231 and MCF-7 cell invasion ($p<0.01$) (Figure 42b), with no effect on proliferation (Figure 42c). These data suggest that our model of DCIS-myoepithelial cells have a protease signature that is regulated by in a TGFβ-dependent manner. While a functional relationship is demonstrated between integrin αvβ6 and FN here, the mechanism regulating their expression is unclear.

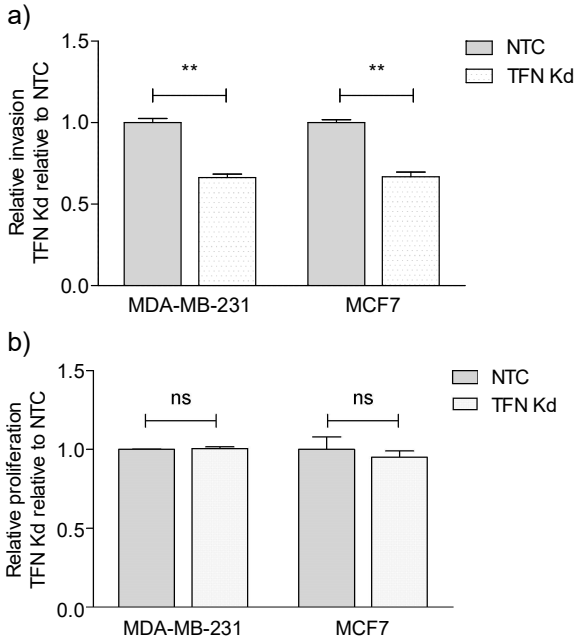

Figure 37. Integrin αvβ6-positive myoepithelial cell line mediates breast cancer cell invasion *in vitro* in a fibronectin-dependent manner. a) Invasion of MDA-MB-231 and MCF-7 in response to CM from β6-1089 with NTC or TFN siRNA (TFN Kd). The number of invading cells was quantified by counting the cells on the underside of the Transwell. The values are presented as the relative invasion of breast cancer cells in the presence of CM from β6-1089 with TFN Kd normalised to NTC. b) Proliferation of MDA-MB-231 and MCF-7 in response to CM from β6-1089 with NTC or TFN siRNA (TFN Kd). The values are presented as the relative proliferation of breast cancer cells in the presence of CM from β6-1089 with TFN Kd normalised to NTC. Analyses is shown as a mean of 3 independent experiments ±SEM. p-value ≤0.01 ('**') considered significant, 'ns' indicates not significant.

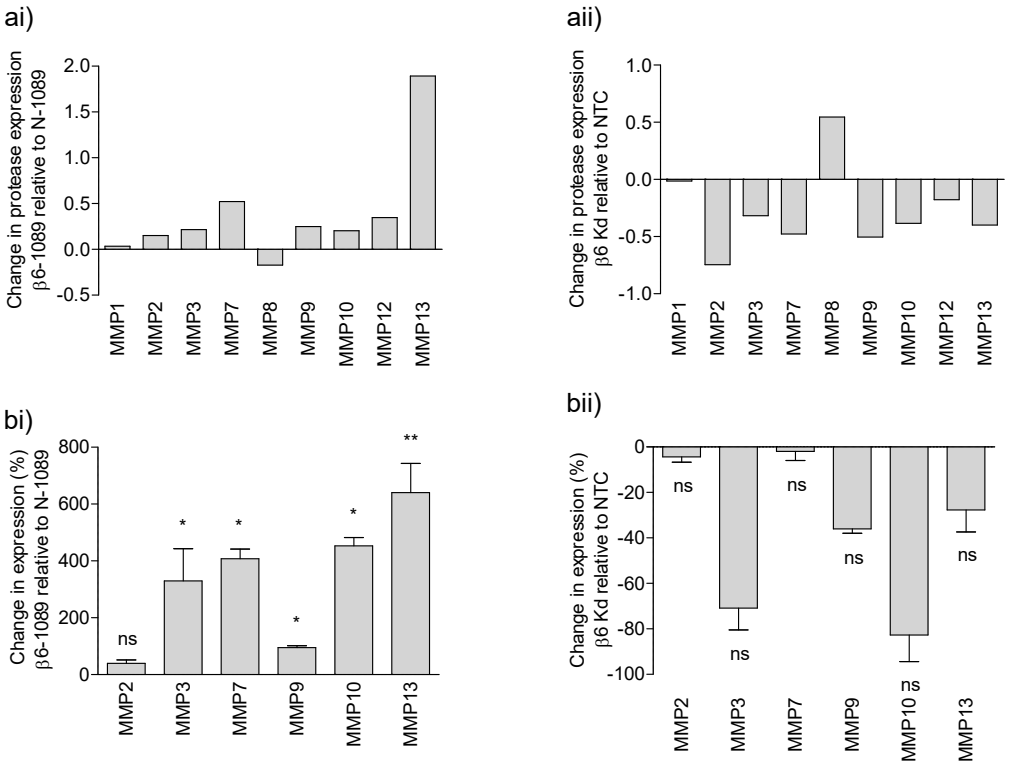

Figure 38. Integrin αvβ6-positive myoepithelial cell line upregulates protease expression. a) Human protease array analysis of cCM from (i) N-1089 and β6-1089, and (ii) β6-1089 with NTC or integrin β6 siRNA (β6 Kd). Signal intensities of analytes were determined using ImageJ and presented the relative level by normalising to the control as depicted on the y-axis. b) qRT-PCR analysis of MMP2, MMP3, MMP7, MMP9, MMP10 and MMP13 mRNA levels in (i) N-1089 and β6-1089, and (ii) β6-1089 with NTC or integrin β6 siRNA (β6 Kd). The values are presented as the mean percentage change in expression relative to the control. Analyses is shown as a mean of 3 independent experiments ±SEM. p-value ≤0.01 ('**') and ≤0.05 ('*') considered significant, 'ns' indicates not significant.

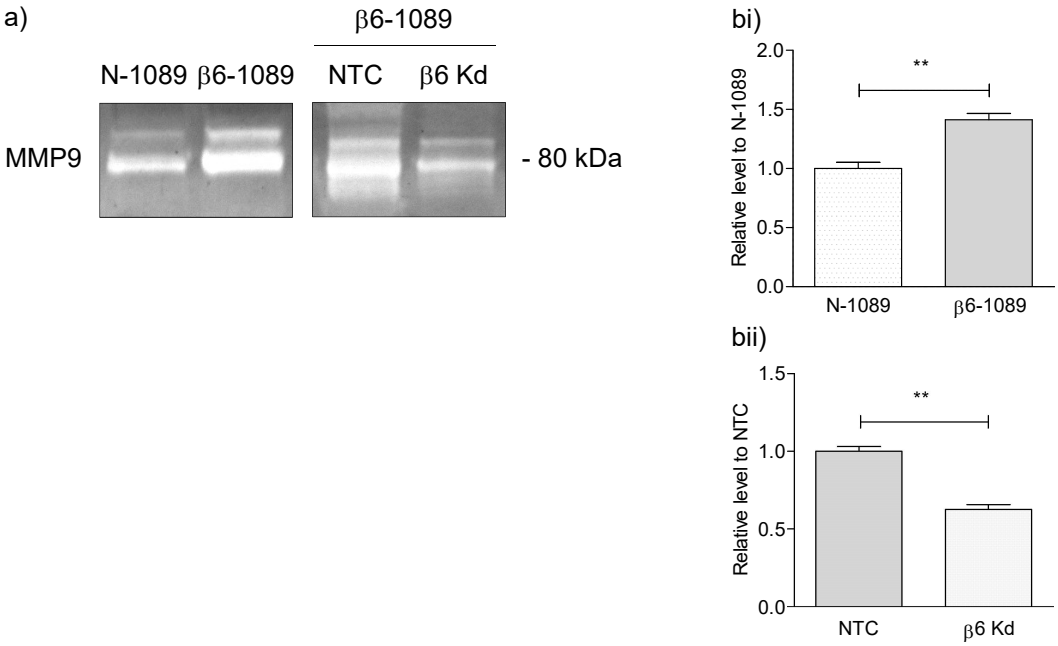

Figure 39. Integrin αvβ6-positive myoepithelial cell line upregulates MMP9 expression. a) Gelatin zymography for MMP9 expression in cCM from (i) N-1089 and β6-1089, and (ii) β6-1089 with NTC or integrin β6 siRNA (β6 Kd). b) Densitometric analysis of MMP9 signal intensities were determined using ImageJ. These data are then presented as the relative level by normalising to the control as depicted on the y-axis. Representative images of 3 independent gelatin zymograms are shown, and densitometric analysis is shown as a mean of 3 experiments ±SEM. p-value ≤0.01 ('**') considered significant.

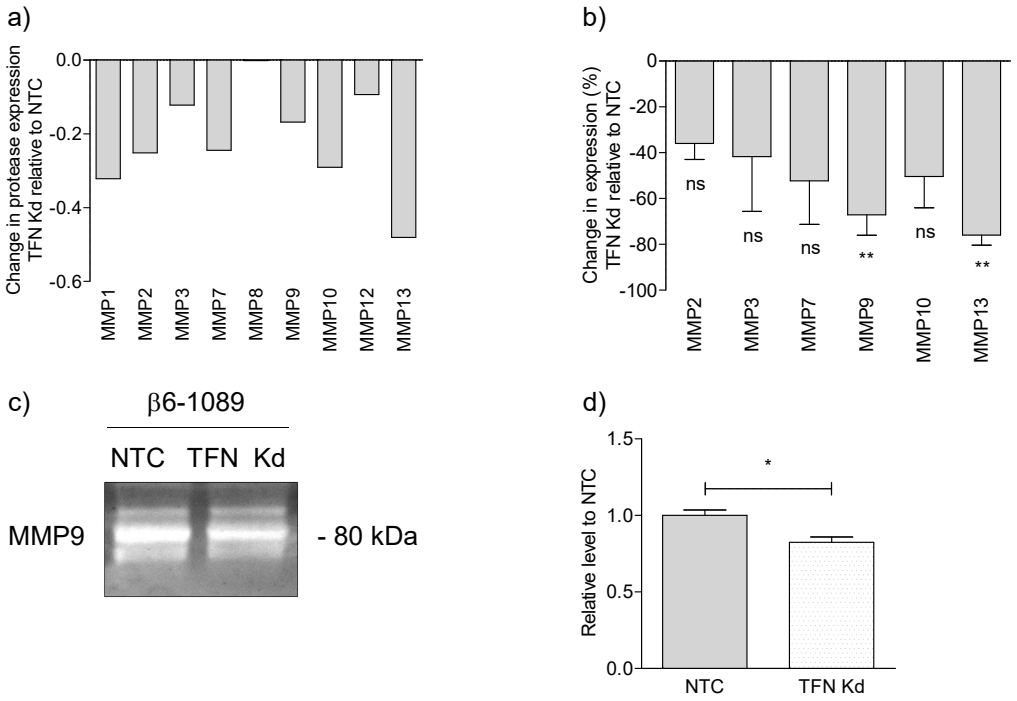

Figure 40. Integrin αvβ6-positive myoepithelial cell line upregulates protease expression in a fibronectin-dependent manner. a) Human protease array analysis of cCM from β6-1089 with NTC or TFN siRNA (TFN Kd). Signal intensities of analytes were determined using ImageJ and presented the relative level by normalising to the NTC. b) qRT-PCR analysis of MMP2, MMP3, MMP7, MMP9, MMP10 and MMP13 mRNA levels in β6-1089 with NTC or TFN siRNA (TFN Kd). The values are presented as the mean percentage change in expression relative to the NTC. c) Gelatin zymography for MMP9 expression in cCM from β6-1089 with NTC or TFN siRNA (TFN Kd). d) Densitometric analysis of MMP9 signal intensities were determined using ImageJ. These data are then presented as the relative level by normalising to the NTC. Representative images of 3 independent gelatin zymograms are shown, and analyses is shown as a mean of 3 experiments ±SEM. p-value ≤0.01 ('**') and ≤0.05 ('*') considered significant, 'ns' indicates not significant.

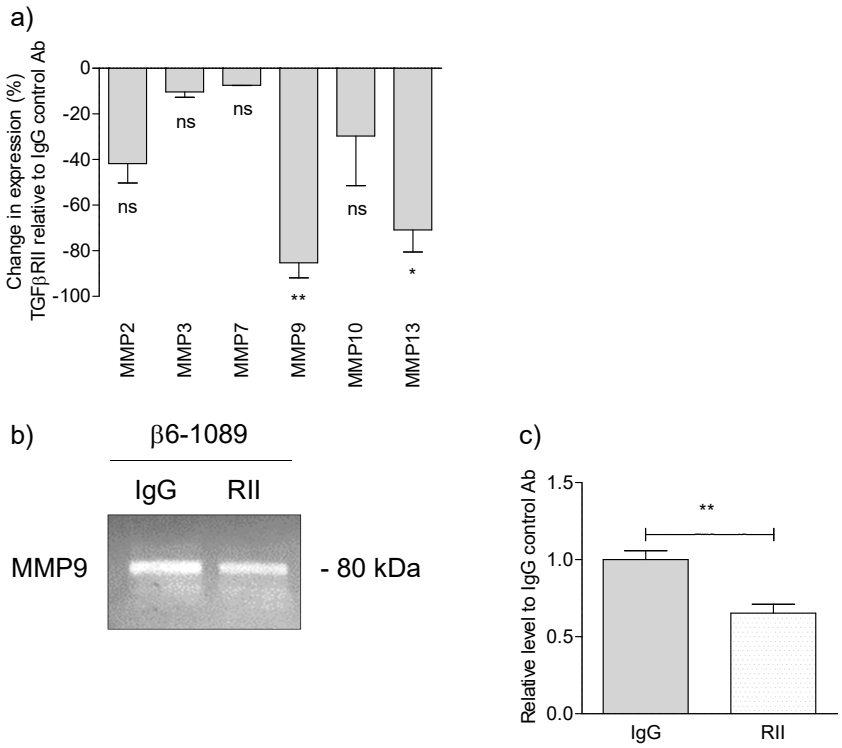

Figure 41. Integrin αvβ6-positive myoepithelial cell line upregulates protease expression in a TGFβ-dependent manner. a) qRT-PCR analysis of MMP2, MMP3, MMP7, MMP9, MMP10 and MMP13 mRNA levels in β6-1089 with IgG control or TGFβRII (RII) blocking antibody. The values are presented as the mean percentage change in expression relative to the IgG control antibody. b) Gelatin zymography for MMP9 expression in cCM from β6-1089 with IgG control or TGFβRII (RII) blocking antibody. c) Densitometric analysis of MMP9 signal intensities were determined using ImageJ. These data are then presented as the relative level by normalising to the IgG control antibody. Representative images of 3 independent gelatin zymograms are shown, and analyses is shown as a mean of 3 experiments ±SEM. p-value ≤0.01 ('**') and ≤0.05 ('*') considered significant, 'ns' indicates not significant.

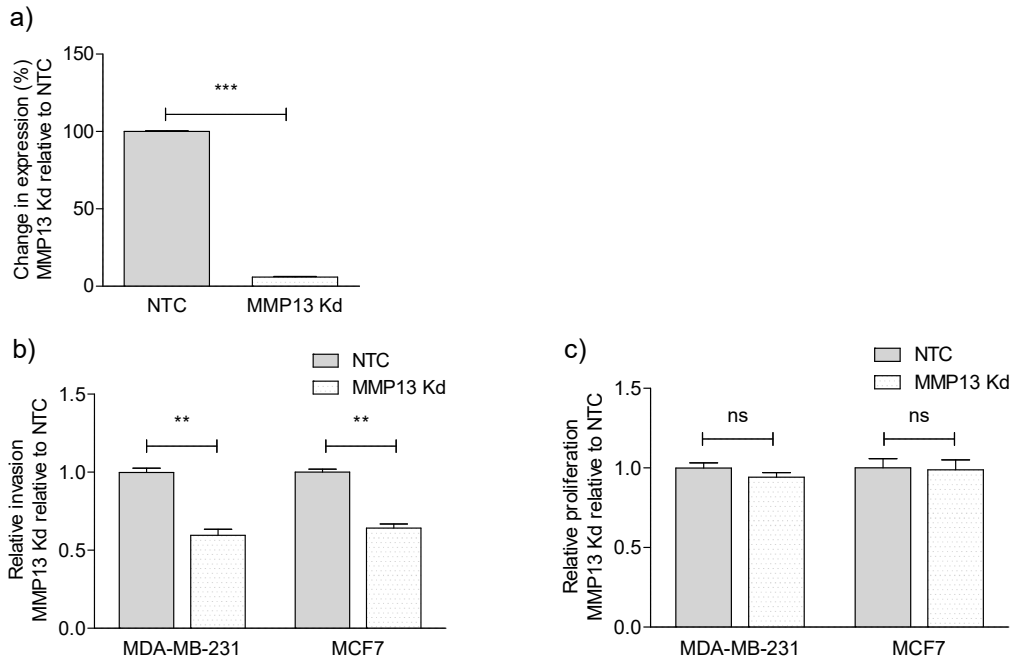

Figure 42. Integrin αvβ6-positive myoepithelial cell line mediates breast cancer cell invasion *in vitro* in a MMP13-dependent manner. a) qRT-PCR analysis of MMP13 mRNA levels in β6-1089 with NTC and MMP13 siRNA (MMP13 Kd). The values are presented as the mean percentage change in expression relative to the NTC, which was set to 100%. b) Invasion of MDA-MB-231 and MCF-7 in response to CM from β6-1089 with NTC or MMP13 siRNA (MMP13 Kd). The number of invading cells was quantified by counting the cells on the underside of the Transwell. The values are presented as the relative invasion of breast cancer cells in the presence of CM from β6-1089 with MMP13 Kd normalised to NTC. c) Proliferation of MDA-MB-231 and MCF-7 in response to CM from β6-1089 with NTC or MMP13 siRNA (MMP13 Kd). The values are presented as the relative proliferation of breast cancer cells in the presence of CM from β6-1089 with MMP13 Kd normalised to NTC. Analyses is shown as a mean of 3 independent experiments ±SEM. p-value ≤0.001 ('***') and ≤0.01 ('**') considered significant, 'ns' indicates not significant.

4.4 REGULATION OF PHENOTYPIC CHARACTERISTICS IN NORMAL AND DCIS MYOEPITHELIAL CELLS

4.4.1 DCIS-myoepithelial cell phenotype is induced in primary normal myoepithelial cells by TGFβ1

TGFβ has been implicated in inducing a tumour-promoting phenotype in stromal cell types which constitute the breast microenvironment, including endothelial, immune cells and fibroblasts [285]. We next investigated the influence of TGFβ1 on primary normal MEC phenotype. Stimulation of integrin αvβ6-negative primary normal MECs (N-127, N-1492 and N-1989) with TGFβ1 led to the induction of integrin αvβ6 expression ($p<0.01$, $p<0.01$ and $p<0.05$ respectively), and a concomitant increase in TFN and FN-EDA expression, as shown by immunoblotting ($p<0.01$, $p<0.01$ and $p<0.05$ respectively) (Figure 43ai-iii; quantified in Figure 43bi-iii, respectively). These findings were supported at the mRNA level (Figure 44ai-iii). Moreover, stimulation with TGFβ1 induced the secretion of MMPs, with the exception of MMP7 and 8, in N-1492 and N-1989, as shown using human protease arrays (Figure 45i-ii). These findings were supported at the mRNA level (Figure 45bi-ii). These data suggest TGFβ may be capable of switching the normal phenotype of MECs to that characteristic of tumour-promoting DCIS-MECs.

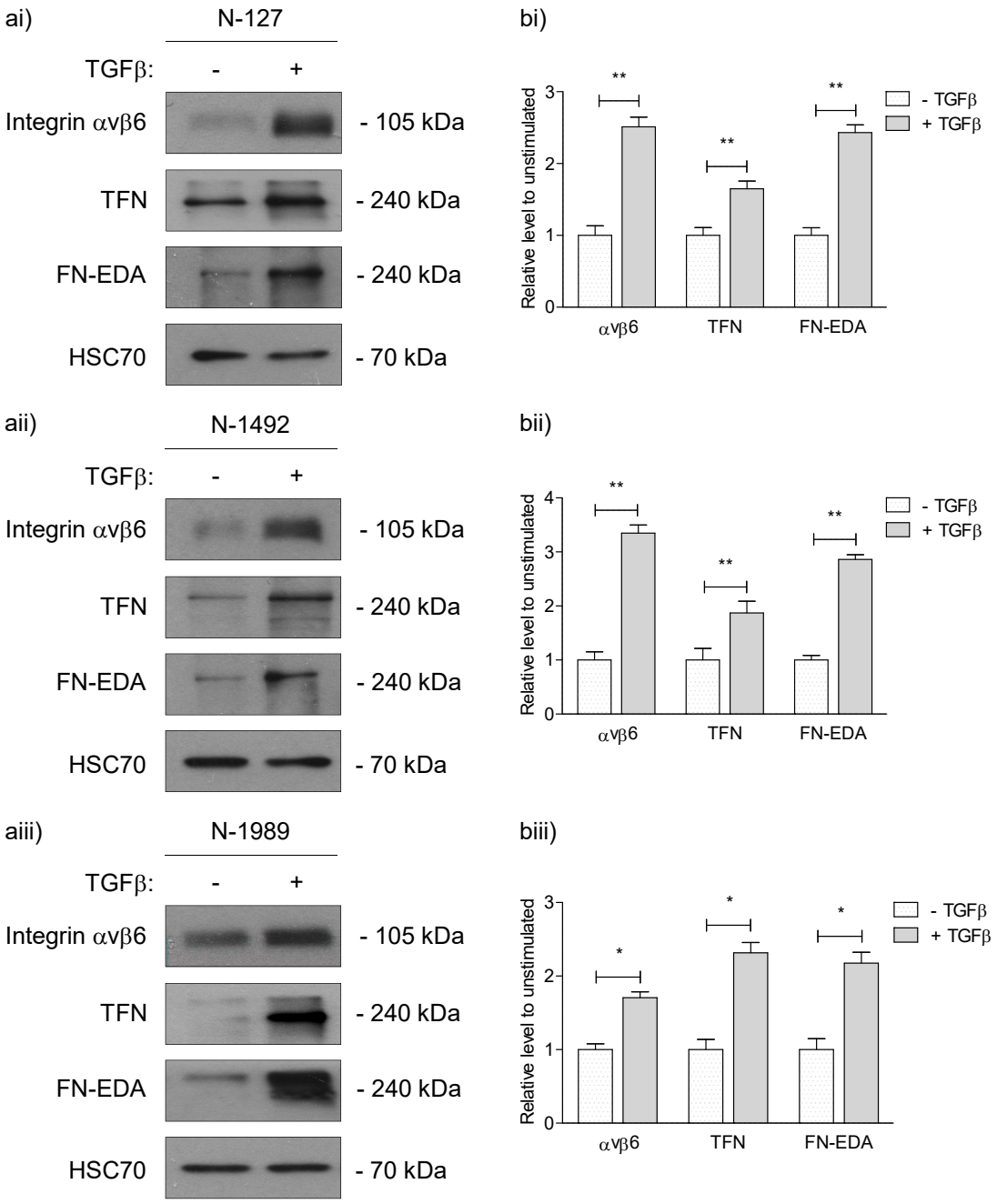

Figure 43. Integrin αvβ6 and fibronectin expression is induced in primary normal myoepithelial cells by TGFβ1. a) Immunoblotting for integrin αvβ6, TFN, FN-EDA and HSC70 in primary normal MECs (N-127, N-1492 and N-1989) with (+) and without (-) TGFβ1 stimulation. b) Densitometric analysis of integrin αvβ6, TFN, FN-EDA and HSC70 signal intensities were determined using ImageJ. The relative protein levels of integrin αvβ6, TFN and FN-EDA were normalised to HSC70 on the same membrane. The values are presented as the relative level in stimulated primary normal MECs normalised to their unstimulated control. Representative immunoblots of at least 3 independent experiments are shown, and analyses is shown as a mean of 3 independent experiments ±SEM. p-value ≤0.01 ('**') and ≤0.05 ('*') considered significant, 'ns' indicates not significant.

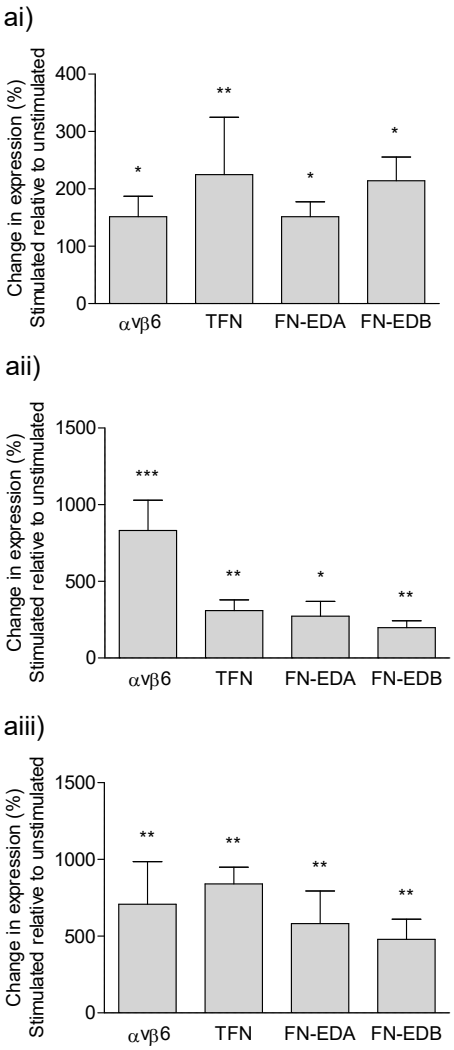

Figure 44. Integrin αvβ6 and fibronectin expression is induced in primary normal myoepithelial cells by TGFβ1. a) qRT-PCR analysis of integrin αvβ6, TFN, FN-EDA and FN-EDB mRNA levels in primary normal MECs ((i) N-127, (ii) N-1492 and (iii) N-1989) with (+) and without (-) TGFβ1 stimulation. The values are presented as the mean percentage change in expression relative to the unstimulated control. Analyses is shown as a mean of 3 independent experiments ±SEM. p-value ≤0.001 ('***'), ≤0.01 ('**') and ≤0.05 ('*') considered significant.

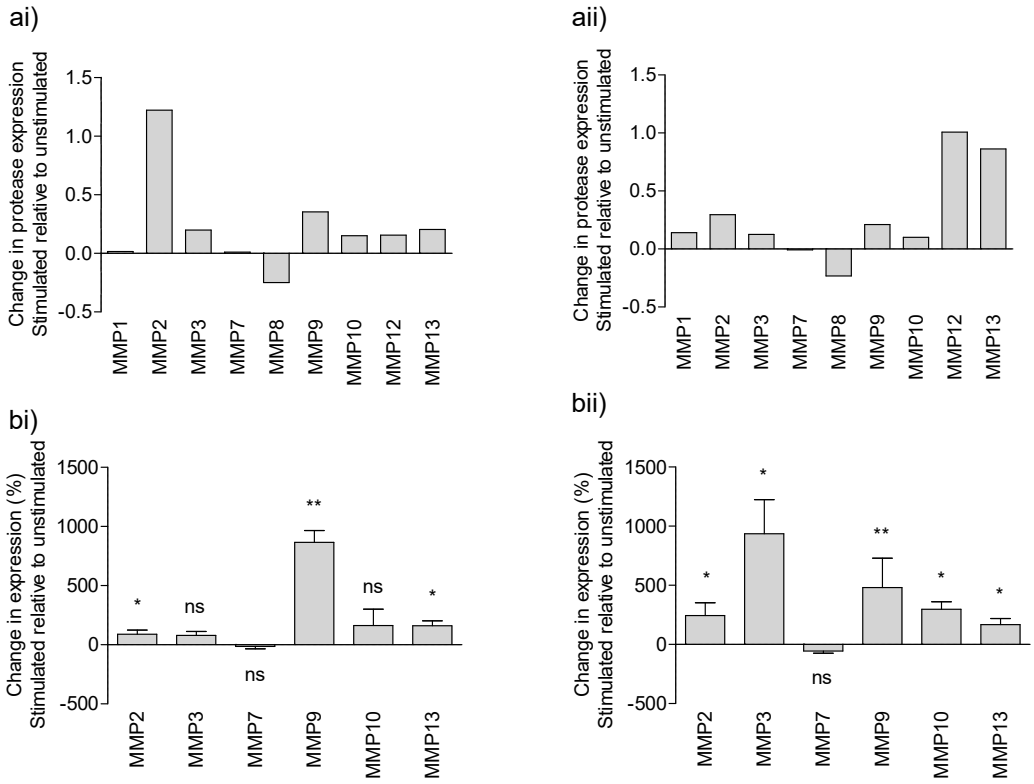

Figure 45. Protease expression is induced in primary normal myoepithelial cells by TGFβ1. a) Human protease array analysis of cCM from primary normal MECs ((i) N-1492 and (ii) N-1989) with (+) and without (-) TGFβ1 stimulation. Signal intensities of analytes were determined using ImageJ and presented the relative level in stimulated primary normal MECs normalised to their unstimulated control. b) qRT-PCR analysis of MMP2, MMP3, MMP7, MMP9, MMP10 and MMP13 mRNA levels in primary normal MECs ((i) N-1492 and (ii) N-1989) with (+) and without (-) TGFβ1 stimulation. The values are presented as the mean percentage change in expression relative to the unstimulated control. Analyses is shown as a mean of 3 independent experiments ±SEM. p-value ≤0.01 ('**') and ≤0.05 ('*') considered significant, 'ns' indicates not significant.

4.4.2 DCIS-myoepithelial cell phenotype is induced in a normal myoepithelial cell line by TGFβ1

Consistent with TGFβ1 stimulation in primary normal MECs, stimulation of N-1089 with TGFβ1 led to the induction of integrin αvβ6 expression ($p<0.01$), and a concomitant increase in TFN and FN-EDA expression ($p<0.01$) (Figure 46a; quantified in Figure 46b, respectively), as shown by immunoblotting. In turn, stimulation of β6-1089 with TGFβ1 led to a further increase in the expression of integrin αvβ6, TFN and FN-EDA ($p<0.01$) (Figure 46a; quantified in Figure 46b, respectively). These findings were supported at the mRNA level (Figure 46c). Moreover, as seen in primary normal MECs, stimulation of N-1089 with TGFβ1 induced the expression of MMPs, with the exception of MMP7, as identified at the mRNA level (Figure 47). These data suggest that the consistent DCIS-MEC phenotype observed, with upregulation of integrin αvβ6, FN and MMP13, may be induced by TGFβ. However, it is unclear whether the increased level of TGFβ activation by integrin αvβ6-positive MECs is capable of inducing this phenotype.

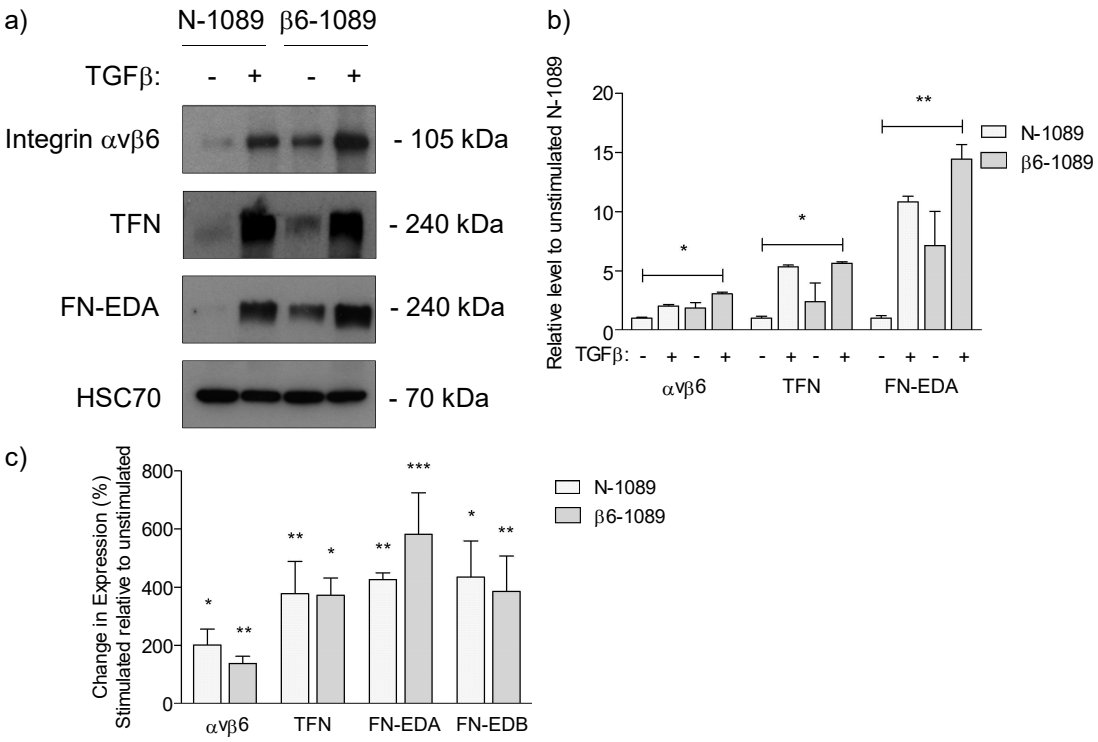

Figure 46. Integrin αvβ6 and fibronectin expression is induced in a normal myoepithelial cell line by TGFβ1. a) Immunoblotting for integrin αvβ6, TFN, FN-EDA and HSC70 in N-1089 and β6-1089 with (+) and without (-) TGFβ1 stimulation. b) Densitometric analysis of integrin αvβ6, TFN, FN-EDA and HSC70 signal intensities were determined using ImageJ. The relative protein levels of integrin αvβ6, TFN and FN-EDA were normalised to HSC70 on the same membrane. The values are presented as the relative level by normalising to unstimulated N-1089. c) qRT-PCR analysis of integrin αvβ6, TFN, FN-EDA and FN-EDB mRNA levels in N-1089 and β6-1089 with (+) and without (-) TGFβ1 stimulation. The values are presented as the mean percentage change in expression relative to the unstimulated control. Representative immunoblots of at least 3 independent experiments are shown, and analyses is shown as a mean of 3 independent experiments ±SEM. p-value ≤ 0.001 ('***'), ≤0.01 ('**') and ≤0.05 ('*') considered significant.

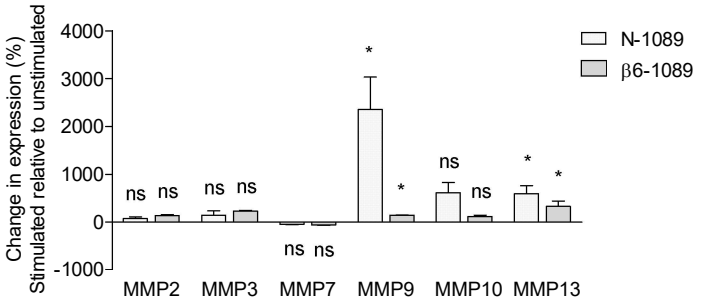

Figure 47. Protease expression is induced in a normal myoepithelial cell line by TGFβ1. qRT-PCR analysis of MMP2, MMP3, MMP7, MMP9, MMP10 and MMP13 mRNA levels in N-1089 and β6-1089 with (+) and without (-) TGFβ1 stimulation. The values are presented as the mean percentage change in expression relative to the unstimulated control. Analyses is shown as a mean of 3 independent experiments ±SEM. p-value ≤0.05 ('*') considered significant, 'ns' indicates not significant.

4.4.3 Deposition of a fibronectin matrix by an integrin αvβ6-positive myoepithelial cell line is TGFβ-dependent

Knockdown of integrin αvβ6 expression by siRNA targeting integrin β6 in β6-1089, was demonstrated using immunoblotting ($p<0.01$) (Figure 33a; quantified in Figure 33b) and immunofluorescence ($p<0.01$) however, TFN and FN-EDA expression were maintained (Figure 33a and 48a; quantified in Figure 33b and 48bi, respectively). These findings were supported at the mRNA level (Figure 33g). However, blockade of TGFβRII with both a blocking antibody in β6-1089 significantly reduced TFN and FN-EDA expression, as shown by immunofluorescent staining ($p<0.001$) (Figure 48a; quantified in Figure 48bii) and immunoblotting ($p<0.001$) (Figure 49a; quantified in Figure 49b). TFN and FN-EDA expression were also significantly reduced in cCM obtained from β6-1089 following blockade of TGFβRII ($p<0.001$) (Figure 49c; quantified in Figure 49d). These findings were supported at the mRNA level (Figure 49e). Successful blockade of TGFβRII was confirmed by the almost complete reduction in phospho-SMAD2 levels, in comparison to the partial reduction seen following the knockdown of integrin αvβ6 expression in β6-1089 (Figure 50a; quantified in Figure 50b). These data suggest the increased deposition of FN in integrin αvβ6-positive MECs is likely to due to the increased TGFβ signalling. However, unanswered in our model of DCIS progression is whether TGFβ initiates the upregulation of integrin αvβ6 to facilitate further TGFβ activation or another mechanism induces the upregulation of integrin αvβ6 to activate TGFβ. Regardless of the initiation event, TGFβ is likely to provide a feed forward mechanism to promote DCIS progression.

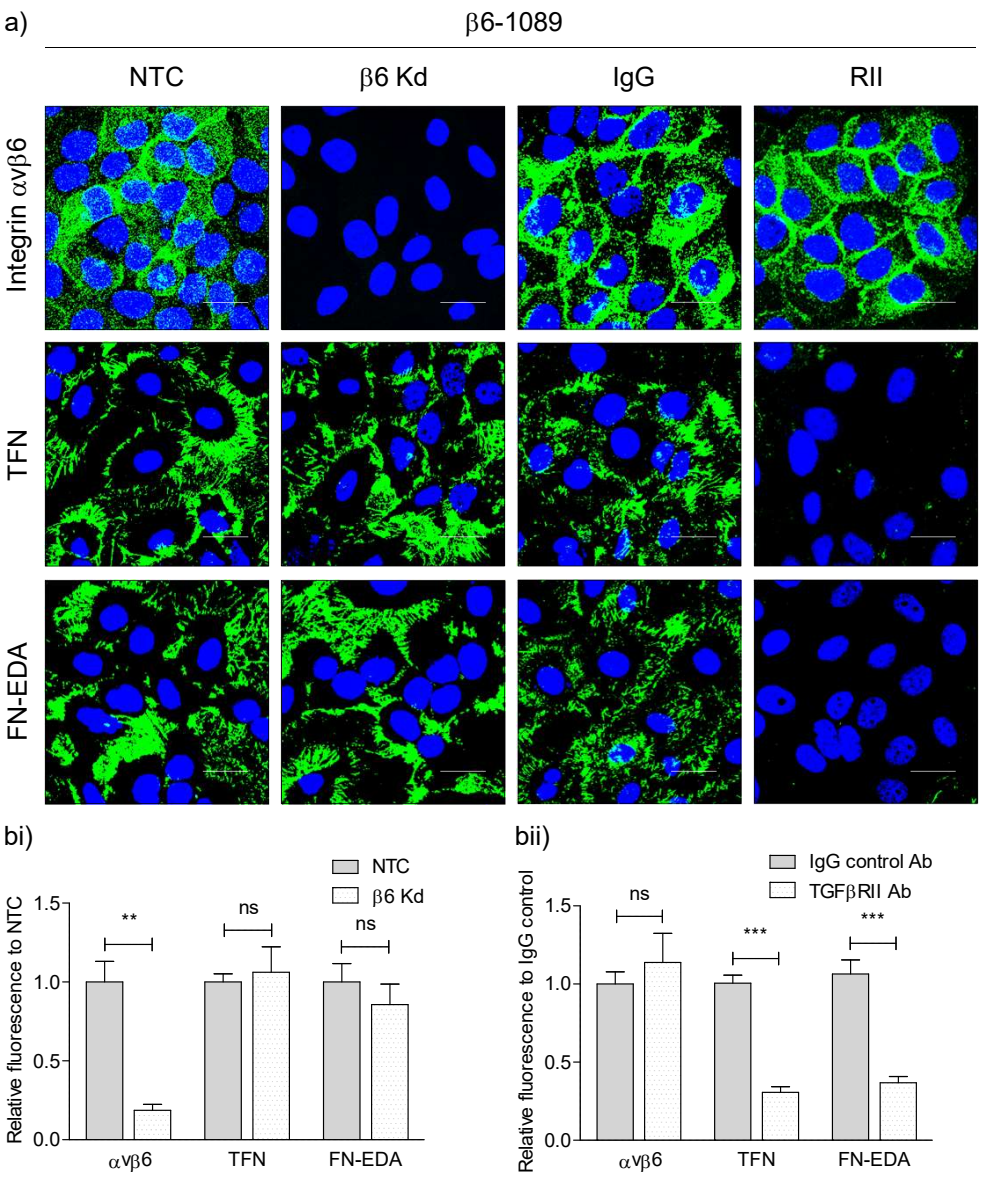

Figure 48. Deposition of a fibronectin matrix by an integrin αvβ6-positive myoepithelial cell line is TGFβ-dependent. a) Immunofluorescent staining for integrin αvβ6, TFN and FN-EDA in β6-1089 with NTC or integrin β6 siRNA (β6 Kd), and β6-1089 with IgG control or TGFβRII (RII) blocking antibody. Magnification ×63. Scale bar, 20μm. b) Fluorescent analysis of integrin αvβ6, TFN and FN-EDA signal intensities were determined using the ZEN 2009 image analysis software. The values are presented as the relative fluorescence in (i) β6 Kd normalised to NTC and (ii) TGFβRII blocking antibody normalised to IgG control antibody. Representative fluorescent images of at least 3 independent experiments are shown, and analyses is shown as a mean of 3 independent experiments ±SEM. p-value ≤0.001 ('***') and ≤0.01 ('**') considered significant, 'ns' indicates not significant.

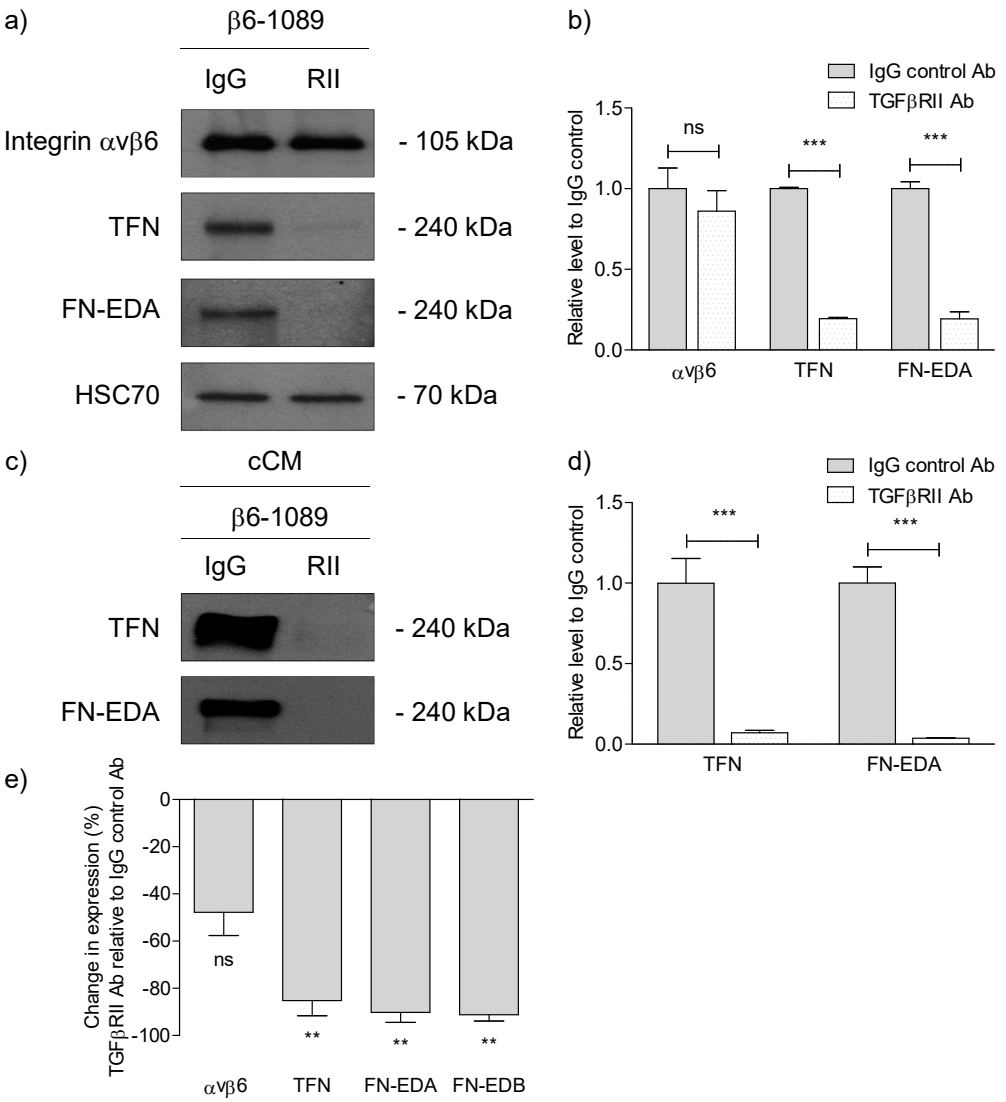

Figure 49. Upregulation of fibronectin expression by an integrin αvβ6-positive myoepithelial cell line is TGFβ-dependent. a) Immunoblotting for integrin αvβ6, TFN, FN-EDA and HSC70 in β6-1089 with IgG control and TGFβRII (RII) blocking antibody. b) Densitometric analysis of integrin αvβ6, TFN, FN-EDA and HSC70 signal intensities were determined using ImageJ. The relative protein levels of integrin αvβ6, TFN and FN-EDA were normalised to HSC70 on the same membrane. The values are presented as the relative level in TGFβRII blocking antibody normalised to IgG control antibody. c) Immunoblotting for TFN and FN-EDA in cCM from β6-1089 with IgG control and TGFβRII (RII) blocking antibody. d) Densitometric analysis of TFN and FN-EDA signal intensities were determined using ImageJ, and are presented as the relative level in TGFβRII blocking antibody normalised to IgG control antibody. e) qRT-PCR analysis of integrin αvβ6, TFN, FN-EDA and FN-EDB mRNA levels in β6-1089 with IgG control and TGFβRII blocking antibody. The values are presented as the mean percentage change in expression relative to the IgG control. Representative immunoblots of at least 3 independent experiments are shown, and analyses is shown as a mean of 3 independent experiments ±SEM. p-value ≤0.001 ('***') and ≤0.01 ('**') considered significant, 'ns' indicates not significant.

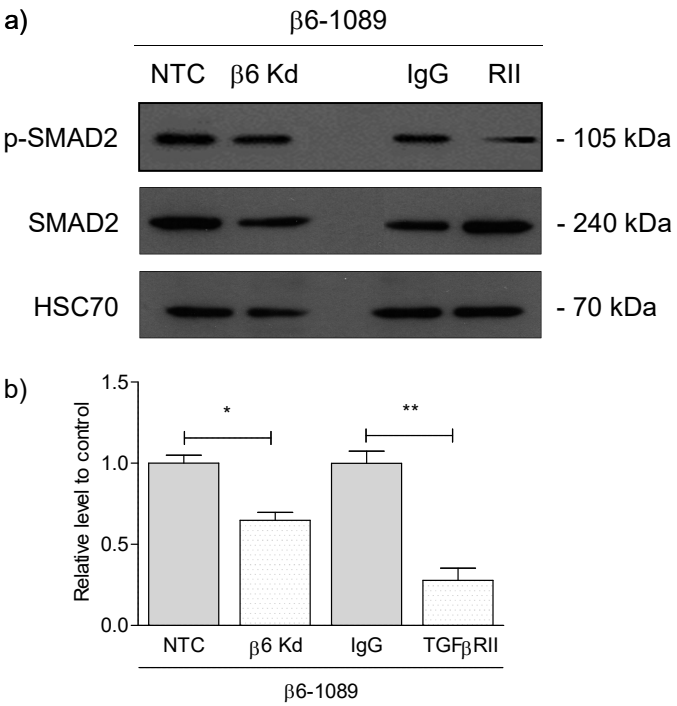

Figure 50. Integrin αvβ6-positive myoepithelial cell line activates TGFβ signalling through TGFβRII. a) Immunoblotting for p-SMAD2, SMAD2 and HSC70 in β6-1089 with (i) NTC or integrin β6 siRNA (β6 Kd) and (ii) IgG control or TGFβRII (RII) antibody. b) Densitometric analysis of p-SMAD2, SMAD2 and HSC70 signal intensities were determined using ImageJ. The relative protein levels of p-SMAD2 and SMAD2 were normalised to HSC70 on the same membrane. The expression of p-SMAD2 is normalised to SMAD2 expression under the same conditions. These data are then presented as the relative level by normalising to the respective control. Representative images of 3 independent immunoblots are shown, and densitometric analysis is shown as a mean of 3 experiments ±SEM. p-value ≤0.01 ('**') and ≤0.05 ('*') considered significant.

4.4.4 DCIS duct expansion correlates with upregulation of integrin αvβ6 by myoepithelial cells

Increased ECM deposition, as demonstrated here, can disrupt normal tissue homeostasis, and thereby the tension breast cells experience. Solid stress due to the expanding tumour volume in DCIS also alters tension. These mechanical stimuli detected by cells, induce gene-expression changes in order to respond to the new tissue tension. To investigate the role of duct expansion in influencing MEC phenotype, normal, benign and DCIS duct sizes (420, 38 and 1369 ducts, respectively) were analysed within our cohort of human breast tumour samples on sections stained immunohistochemically for integrin αvβ6 (Figure 51a; panel 2-3 and Supplementary Figure S5). Only cross-sectional ducts were included in these analyses. Quantification of duct sizes, independent of integrin αvβ6 expression, identified an average normal duct size of 1.3mm^2, compared to an average benign duct size of 90mm^2, and DCIS duct size of 140mm^2. Moreover, DCIS ducts from high-grade pure DCIS were larger than those from non-high-grade pure DCIS ($p<0.0001$) (160mm^2 compared to 81mm^2, respectively), while those from DCIS/IDC were similar in size (163mm^2). Interestingly, integrin αvβ6-positive DCIS ducts on average were larger than integrin αvβ6-negative DCIS ducts ($p<0.0001$) (162mm^2 compared to 117mm^2, respectively) (Figure 51a; panel 2-3; quantified in Figure 51b) (Table 17). These data demonstrate high-grade DCIS ducts are larger than non-high-grade DCIS ducts, perhaps due to differences in proliferation rates or tumour cell size. Moreover, these data suggest the pressure exerted by neoplastic epithelial cells on MECs may be a factor regulating the expression of integrin αvβ6.

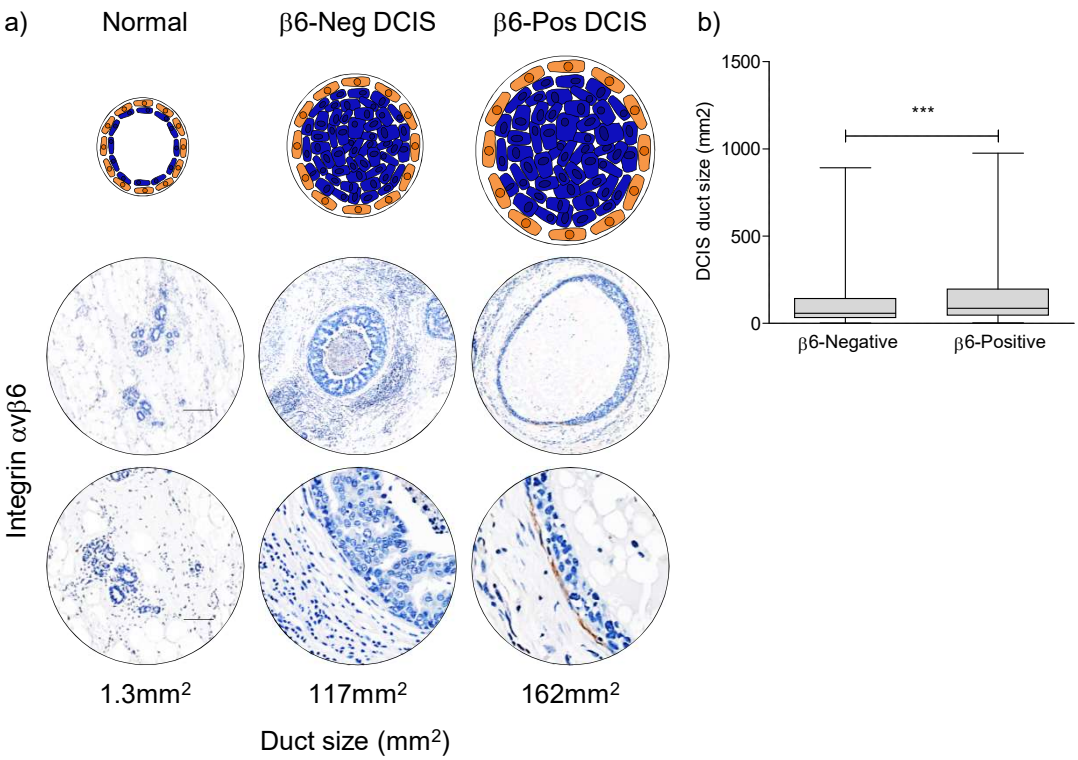

Figure 51. DCIS duct expansion correlates with upregulation of integrin αvβ6 by myoepithelial cells. a) Immunohistological staining of human breast tumour samples (staining for integrin αvβ6; panel 2-3) featuring normal breast ducts, and DCIS ducts with and without the expression of integrin αvβ6. Magnification x5 and x20. Scale bar, 200μm and 100μm, respectively. b) Quantitative analysis of DCIS duct size with and without integrin αvβ6 expression (total of 713 and 656 ducts, respectively) in patient samples. Box represents the third interquartile (IQR3) and first interquartile (IQR1) range and the median is represented by the black line within the box. The whiskers represent the complete data range. p-value ≤0.001 ('***') considered significant.

	Duct size in mm^2 (number of ducts)		
	αvβ6-positive	αvβ6-negative	Total
Normal	-	1.3 (420)	420
Benign	-	90 (38)	38
DCIS			
Non-high-grade	92 (125)	75 (233)	358
High-grade	176 (235)	146 (238)	473
DCIS/IDC	178 (353)	135 (185)	538
			1827

Table 17. Quantification of DCIS duct size in relation to integrin αvβ6 expression

4.4.5 DCIS is associated with morphological changes in myoepithelial cells which correlates with integrin αvβ6 positivity

With duct expansion in DCIS, MECs appear attenuated compared to normal breast ducts. The size, shape and number of 4536 MECs and 2736 MEC nuclei were then analysed in normal and DCIS ducts within our cohort of DCIS samples. The minor axis of individual MECs was determined by SMA immunoreactivity and the minor and major axis of MEC nuclei was determined by p63 immunoreactivity on serial sections to integrin αvβ6 immunohistochemical staining. In normal ducts, MECs appeared rounded (minor axis 6.1μm) (Figure 52a; panel 2-3), while in both DCIS and benign lesions appeared flattened or spindle-shaped ($p<0.001$) (2.7μm and 3.6μm, respectively) (Table 18) (Supplementary Figure S6). However, MEC nuclei appeared flattened in DCIS (minor axis by major axis; 2.2μm by 8.4μm) (Figure 52a; panel 4-5), while in both normal and benign lesions appeared rounded ($p<0.001$) (minor axis by major axis; 4.3μm x 4.7μm, and 4.3μm x 5.1μm, respectively) (Table 19) (Supplementary Figure S6). Interestingly, the minor axis of MECs in integrin αvβ6-positive DCIS ducts was significantly reduced compared to integrin αvβ6-negative DCIS ducts ($p<0.0001$) (2.5μm compared to 3.0μm) (Table 18) (Supplementary Figure S7). Similarly, MEC nuclei were more significantly compressed and elongated in integrin αvβ6-positive DCIS ducts compared to integrin αvβ6-negative DCIS ducts ($p<0.005$) (minor axis by major axis; 2.1μm by 8.6μm compared to 2.4μm by 8.1μm) (Table 19) (Supplementary Figure S7). In normal ducts, an average of 21 MECs were identified per duct using p63 staining, while in both benign lesions and DCIS an average of 20 MECs were identified (Table 20). These data suggest nuclear markers may help identify attenuated MECs in DCIS, and thereby help the distinction between DCIS and IDC. Moreover, these data suggest alteration to duct size in DCIS alters MEC nuclei morphology which may influence the transcriptional activation of integrin αvβ6.

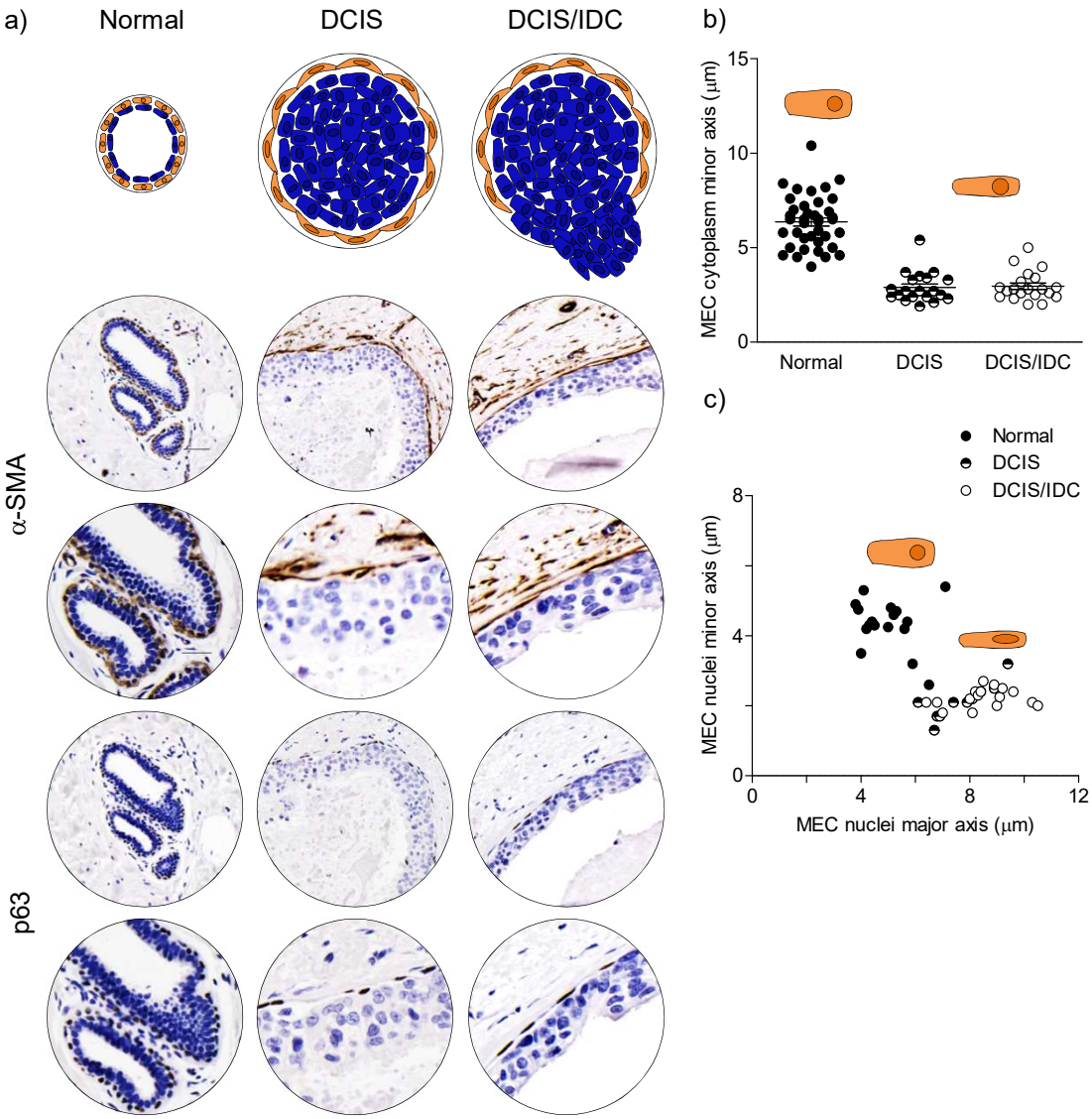

Figure 52. DCIS is associated with morphological changes in myoepithelial cells which correlates with integrin αvβ6 positivity. a) Immunohistological staining of human breast tumour samples (staining for α-SMA; panel 2-3 and p63; panel 4-5) featuring areas of normal, DCIS and DCIS/IDC. Magnification ×20 and x40. Scale bar, 50μm and 25μm, respectively. b) Quantitative analysis of MEC cytoplasm minor axis. Dots represent the average minor axis of MEC cytoplasm in each patient sample and error bars represent standard deviation. c) Quantitative analysis of MEC nuclei minor and major axis. Dots represent the average minor/major axis of MEC nuclei in each patient sample and error bars represent ±SEM.

	Cell size in μm (number of cells)		
	αvβ6-positive	αvβ6-negative	Total
Normal	-	6.0 (1635)	1635
Benign	-	3.6 (108)	108
DCIS			
Non-high-grade	2.6 (261)	2.8 (486)	747
High-grade	2.4 (606)	3.1 (456)	1062
DCIS/IDC	2.6 (663)	3.1 (321)	984
			4536

Table 18. Quantification of myoepithelial cell size and shape in relation to integrin αvβ6 expression

	Nuclei size in μm (number of cells)				
	αvβ6-positive		αvβ6-negative		
	Minor	Major	Minor	Major	Total
Normal	-	-	4.3 (780)	4.7 (780)	780
Benign	-	-	4.3 (108)	5.0 (108)	108
DCIS					
Non-high-grade	2.2 (171)	8.3 (171)	2.4 (258)	7.7 (258)	429
High-grade	2.0 (309)	7.7 (309)	2.5 (285)	8.3 (285)	594
DCIS/IDC	2.1 (549)	9.2 (549)	2.4 (276)	8.4 (276)	825
					2736

Table 19. Quantification of myoepithelial nuclei size and shape in relation to integrin αvβ6 expression

	Number of MECs per duct (number of ducts)		
	αvβ6-positive	αvβ6-negative	Total
Normal	-	21 (260)	260
Benign	-	20 (36)	36
DCIS			
Non-high-grade	19 (57)	20 (86)	143
High-grade	20 (103)	21 (95)	198
DCIS/IDC	20 (183)	21 (92)	275
			912

Table 20. Quantification of myoepithelial cell number in relation to integrin αvβ6 expression

4.4.6 Mechanostimulation of integrin αvβ6 expression and fibronectin deposition in primary normal myoepithelial cells

Primary normal MECs were exposed to mechanical stretch, as seen in the expansion of DCIS lesions, to investigate the mechanoregulation of integrin αvβ6 here. Consistent with our immunohistochemical analyses, mechanical stretching of primary normal MECs (N-1492 and N-1989), revealed an increase in integrin αvβ6 expression using immunofluorescence ($p<0.01$ and $p<0.001$, respectively) (Figure 53-54a; quantified in Figure 53-54b, respectively) and immunoblotting ($p<0.001$) (Figure 53-54d; quantified in Figure 53-54e, respectively). A concomitant increase in TFN and FN-EDA expression in primary normal MECs exposed to mechanical stretching was observed ($p<0.001$) (Figure 53-54a and 53-54d; quantified in Figure 53-54b and 53-54e, respectively). These findings were supported at the mRNA level (Figure 53-54c). These data support our immunohistochemical analysis, such that application of mechanical stretch to MECs, as seen in expansion of DCIS ducts, induces a DCIS-MEC phenotype associated with upregulation of integrin αvβ6 and FN expression.

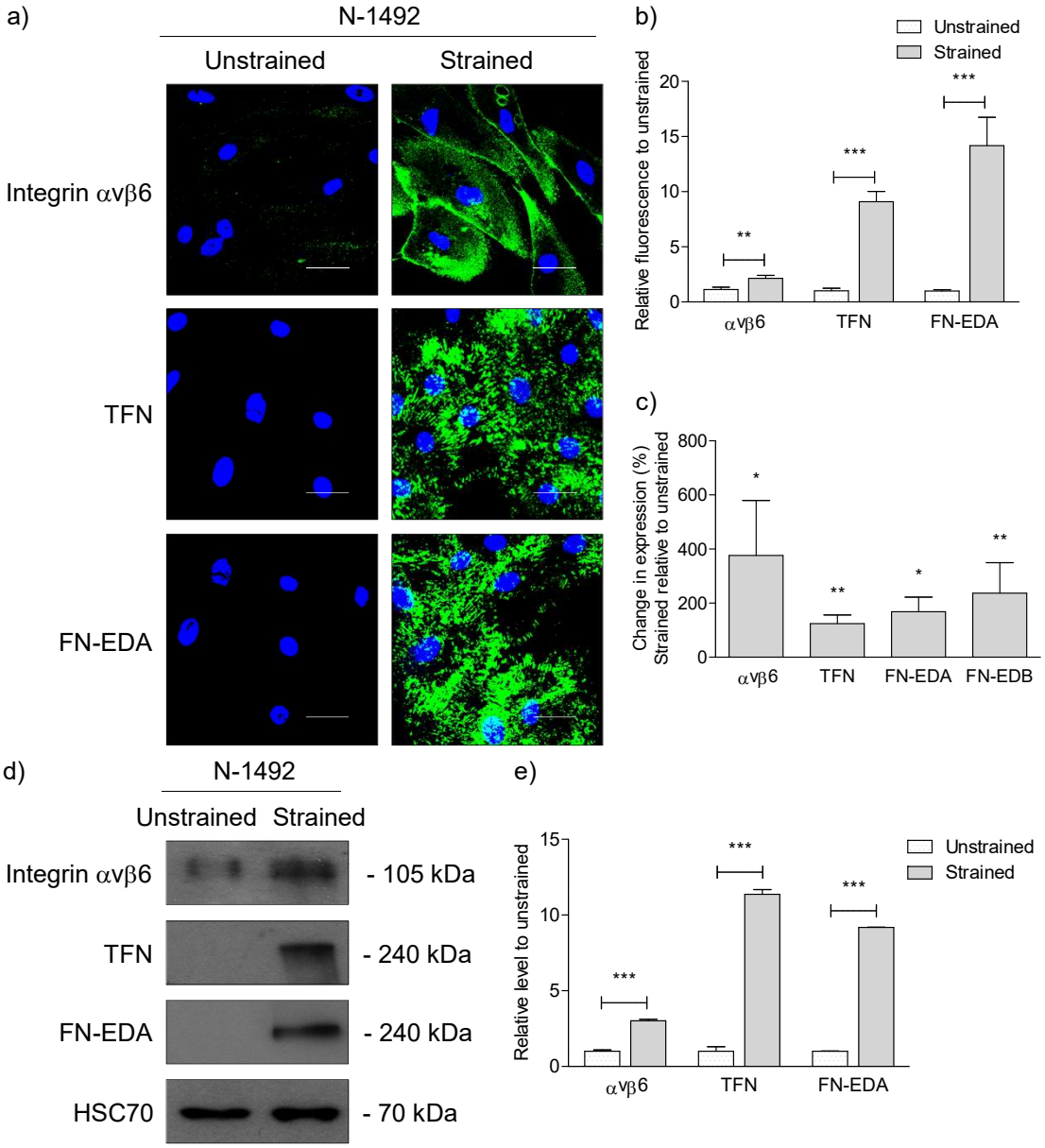

Figure 53. Mechanostimulation of integrin αvβ6 expression and fibronectin deposition in primary normal myoepithelial cells. a) Immunofluorescent staining for integrin αvβ6, TFN and FN-EDA in unstrained or strained N-1492. Magnification ×63. Scale bar, 20μm. b) Fluorescent analysis of integrin αvβ6, TFN and FN-EDA signal intensities were determined using the ZEN 2009 image analysis software. The values are presented as the relative fluorescence in strained normalised to unstrained N-1492. c) qRT-PCR analysis of integrin αvβ6, TFN, FN-EDA and FN-EDB mRNA levels in unstrained or strained N-1492. The values are presented as the mean percentage change in expression relative to unstrained N-1492. d) Immunoblotting for integrin αvβ6, TFN, FN-EDA and HSC70 in unstrained or strained N-1492. e) Densitometric analysis of integrin αvβ6, TFN, FN-EDA and HSC70 signal intensities were determined using ImageJ. The relative protein levels of integrin αvβ6, TFN and FN-EDA were normalised to HSC70 on the same membrane. The values are presented as the relative level in strained normalised to unstrained N-1492. Representative fluorescent images and immunoblots of at least 3 independent experiments are shown, and analyses is shown as a mean of 3 independent experiments ±SEM. p-value ≤0.001 ('***'), ≤0.01 ('**') and ≤0.05 ('*') considered significant.

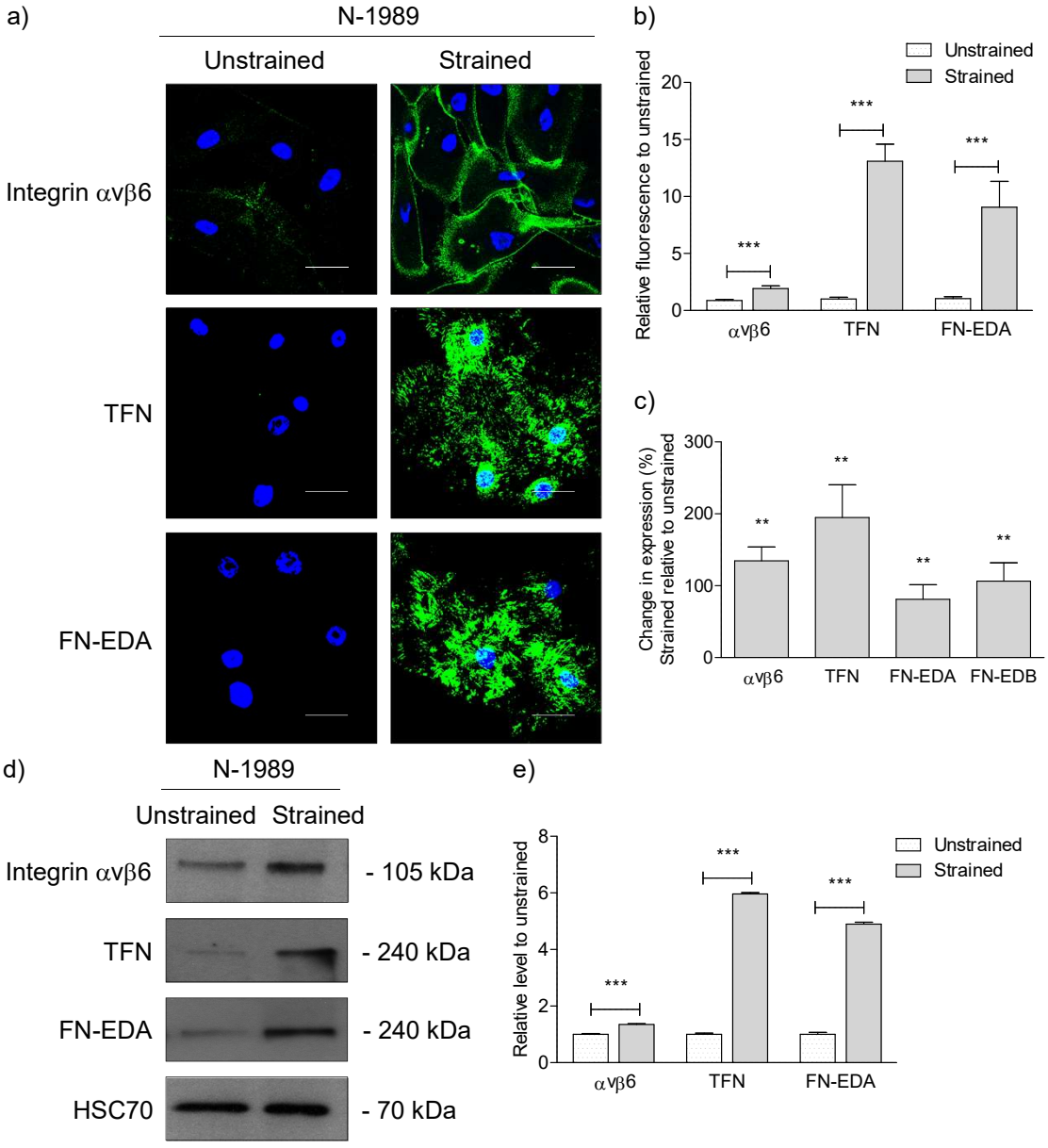

Figure 54. Mechanostimulation of integrin αvβ6 expression and fibronectin deposition in primary normal myoepithelial cells. a) Immunofluorescent staining for integrin αvβ6, TFN and FN-EDA in unstrained or strained N-1989. Magnification ×63. Scale bar, 20μm. b) Fluorescent analysis of integrin αvβ6, TFN and FN-EDA signal intensities were determined using the ZEN 2009 image analysis software. The values are presented as the relative fluorescence in strained normalised to unstrained N-1989. c) qRT-PCR analysis of integrin αvβ6, TFN, FN-EDA and FN-EDB mRNA levels in unstrained or strained N-1989. The values are presented as the mean percentage change in expression relative to unstrained N-1989. d) Immunoblotting for integrin αvβ6, TFN, FN-EDA and HSC70 in unstrained or strained N-1989. e) Densitometric analysis of integrin αvβ6, TFN, FN-EDA and HSC70 signal intensities were determined using ImageJ. The relative protein levels of integrin αvβ6, TFN and FN-EDA were normalised to HSC70 on the same membrane. The values are presented as the relative level in strained normalised to unstrained N-1989. Representative fluorescent images and immunoblots of at least 3 independent experiments are shown, and analyses is shown as a mean of 3 independent experiments ±SEM. p-value ≤0.001 ('***') and ≤0.01 ('**') considered significant.

4.4.7 Mechanostimulation of integrin αvβ6 expression and fibronectin deposition in a normal myoepithelial cell line

Similarly, mechanical stretching of N-1089 revealed an increase in integrin αvβ6 expression using immunofluorescence ($p<0.001$) and immunoblotting ($p<0.01$) (Figure 55a and 55d; quantified in Figure 55b and 55e, respectively). Likewise, we also identified a concomitant increase in TFN and FN-EDA expression in N-1089 exposed to mechanical stretching using immunofluorescence ($p<0.001$) and immunoblotting ($p<0.01$) (Figure 55a and 55d; quantified in Figure 55b and 55e, respectively). These findings were supported at the mRNA level (Figure 55c). These data further support the role of mechanostimulation in inducing integrin αvβ6 expression and FN deposition by MECs.

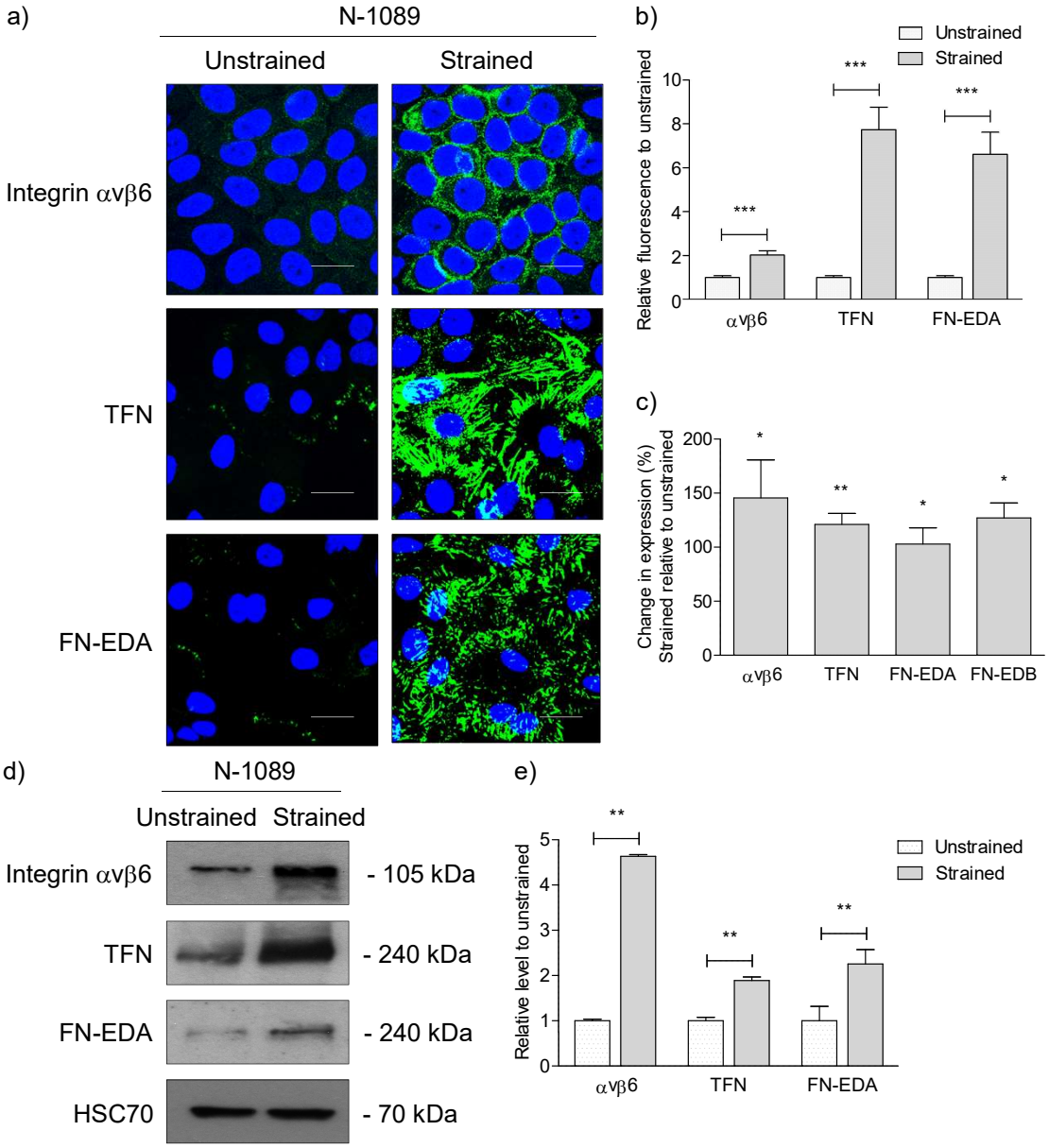

Figure 55. Mechanostimulation of integrin αvβ6 expression and fibronectin deposition in a normal myoepithelial cell line. a) Immunofluorescent staining for integrin αvβ6, TFN and FN-EDA in unstrained or strained N-1089. Magnification ×63. Scale bar, 20μm. b) Fluorescent analysis of integrin αvβ6, TFN and FN-EDA signal intensities were determined using the ZEN 2009 image analysis software. The values are presented as the relative fluorescence in strained normalised to unstrained N-1089. c) qRT-PCR analysis of integrin αvβ6, TFN, FN-EDA and FN-EDB mRNA levels in unstrained or strained N-1089. The values are presented as the mean percentage change in expression relative to unstrained N-1089. d) Immunoblotting for integrin αvβ6, TFN, FN-EDA and HSC70 in unstrained or strained N-1089. e) Densitometric analysis of integrin αvβ6, TFN, FN-EDA and HSC70 signal intensities were determined using ImageJ. The relative protein levels of integrin αvβ6, TFN and FN-EDA were normalised to HSC70 on the same membrane. The values are presented as the relative level in strained normalised to unstrained N-1089. Representative fluorescent images and immunoblots of at least 3 independent experiments are shown, and analyses is shown as a mean of 3 independent experiments ±SEM. p-value ≤0.001 ('***'), ≤0.01 ('**') and ≤0.05 ('*') considered significant.

4.4.8 Mechanostimulation of primary normal myoepithelial cells induces an invasive-promoting phenotype

We next investigated the influence of mechanical stretch on MEC function. Interestingly, CM isolated from primary normal MECs (N-1492 and N-1989) exposed to mechanical stretching increased both MDA-MB-231 ($p<0.01$ and $p<0.05$, respectively) and MCF-7 cell invasion ($p<0.01$) (Figure 56ai-ii, respectively), with no effect on proliferation (Figure 56bi-ii). Moreover, as seen in TGFβ1 stimulated primary normal MECs, application of mechanical stretching to these cells also induced the expression of MMPs, with the exception of MMP8, as identified by human protease array analysis (Figure 57ai-ii). These alterations were confirmed at the mRNA level (Figure 57bi-ii). Specifically, MMP13 mRNA expression was significantly upregulated in comparison to other MMPs analysed following mechanical stimulation ($p<0.05$ and $p<0.01$, respectively). These data demonstrate a common MEC phenotype in DCIS, with an invasive promoting function, which may be mechanically stimulated.

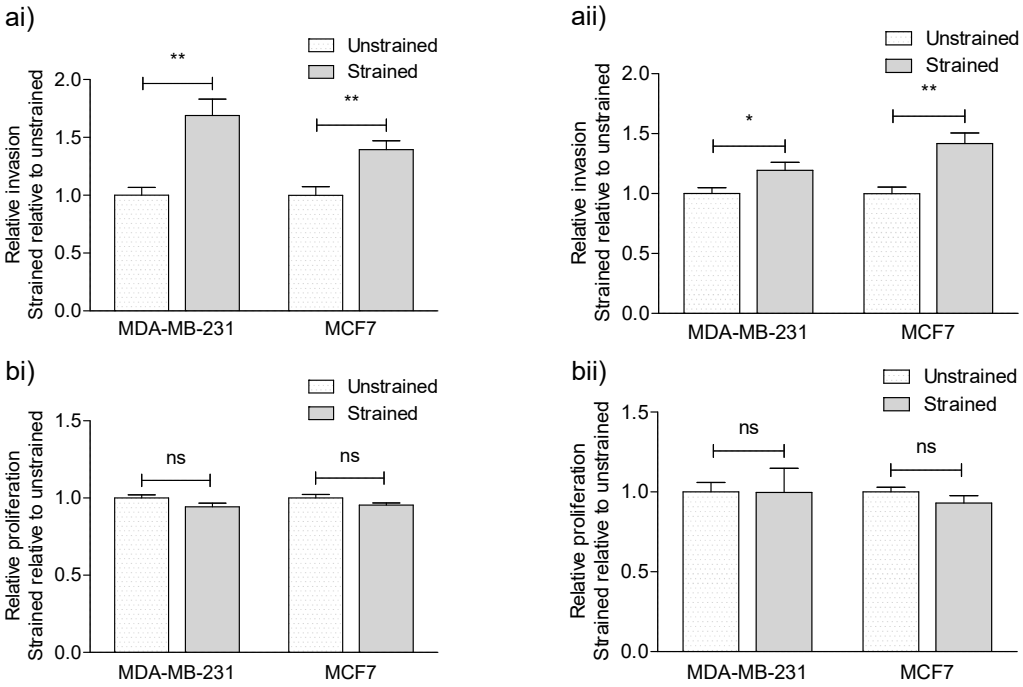

Figure 56. Mechanostimulation of primary normal myoepithelial cells mediates breast cancer cell invasion *in vitro*. a) Invasion of MDA-MB-231 and MCF-7 in response to CM from unstrained or strained (i) N-1492 and (i) N-1989. The number of invading cells was quantified by counting the cells on the underside of the Transwell. The values are presented as the relative invasion of breast cancer cells in the presence of CM from strained normalised to unstrained. b) Proliferation of MDA-MB-231 and MCF-7 in response to CM from unstrained or strained (i) N-1492 and (i) N-1989. The values are presented as the relative proliferation of breast cancer cells in the presence of CM from CM from strained normalised to unstrained. Analyses is shown as a mean of 3 independent experiments ±SEM. p-value ≤0.01 ('**') and ≤0.05 ('*') considered significant, 'ns' indicates not significant.

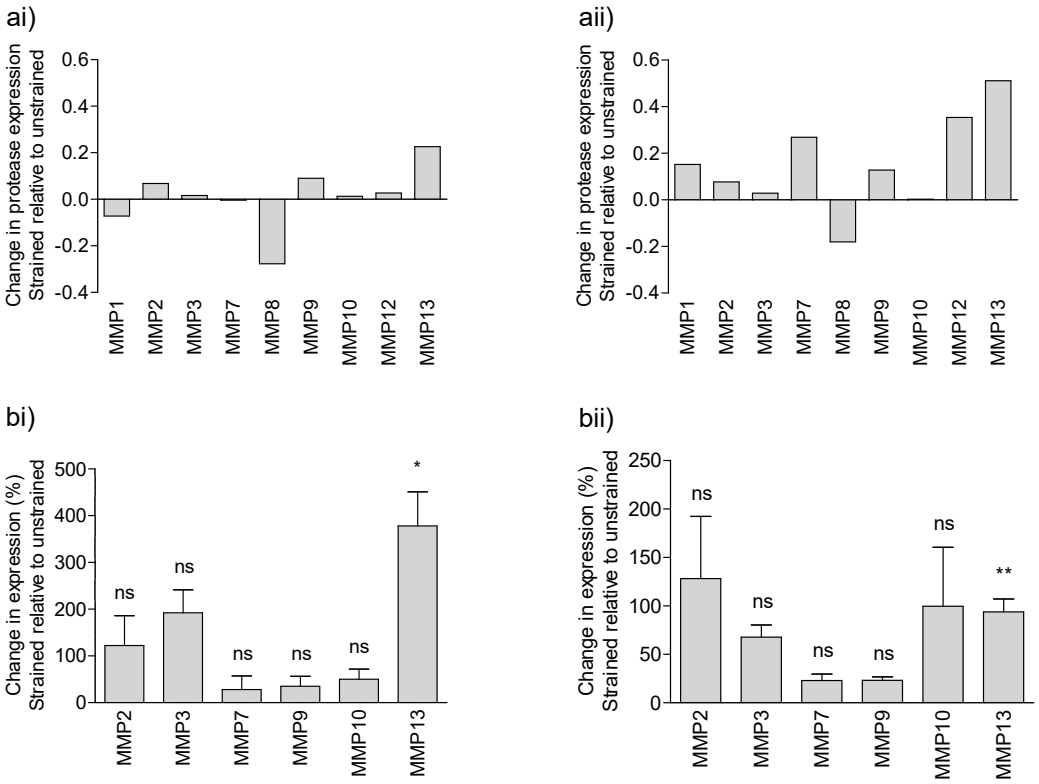

Figure 57. Mechanostimulation of primary normal myoepithelial cells upregulates protease expression. a) Human protease array analysis of cCM from unstrained or strained (i) N-1492 and (ii) N-1989. Signal intensities of analytes were determined using ImageJ and presented the relative level in strained by normalising to unstrained. b)) qRT-PCR analysis of MMP2, MMP3, MMP7, MMP9, MMP10 and MMP13 mRNA levels in unstrained or strained (i) N-1492 and (ii) N-1989. The values are presented as the mean percentage change in expression relative to unstrained. Analyses is shown as a mean of 3 independent experiments ±SEM. p-value ≤0.01 ('**') and ≤0.05 ('*') considered significant, 'ns' indicates not significant.

4.4.9 Mechanostimulation of a normal myoepithelial cell line induces an invasive-promoting phenotype

Similar to that seen in primary normal MECs, CM isolated from N-1089 exposed to mechanical stretching increased both MDA-MB-231 and MCF-7 cell invasion ($p<0.01$) (Figure 58a), with no effect on proliferation (Figure 58b). Moreover, as seen in both β6-1089 and TGFβ1 stimulated N-1089, application of mechanical stretching to N-1089 also induced the expression of MMPs, with the exception of MMP7 and MMP8, as identified by human protease array analysis (Figure 59a). These alterations were supported at the mRNA level (Figure 59b) and using gelatin zymography to detect MMP9 expression ($p<0.01$) (Figure 59c; quantified in Figure 59d). Specifically, MMP13 mRNA expression was significantly upregulated in comparison to other MMPs analysed following mechanical stretching of N-1089 ($p<0.05$) (Figure 59b). Mechanostimulation of integrin avb6 expression was inhibited by siRNA targeting β6 in N-1089, as demonstrated using immunofluorescence ($p<0.001$) and immunoblotting ($p<0.01$) however, TFN and FN-EDA expression were maintained (Figure 60a and 60d; quantified in Figure 60b and 60e, respectively). These findings were supported at the mRNA level (Figure 60c). CM isolated following the knockdown of integrin αvβ6 in mechanostimulated N-1089 resulted in a reduction in MDA-MB-231 and MCF-7 cell invasion *in vitro* ($p<0.001$) (Figure 61a), with no effect on proliferation (Figure 61b). Moreover, this led to the reduction in MMP9 ($p<0.05$) and MMP13 mRNA levels (Figure 62). Together, these further data support the characteristic MEC phenotype in DCIS, which may be activated by mechanical tension.

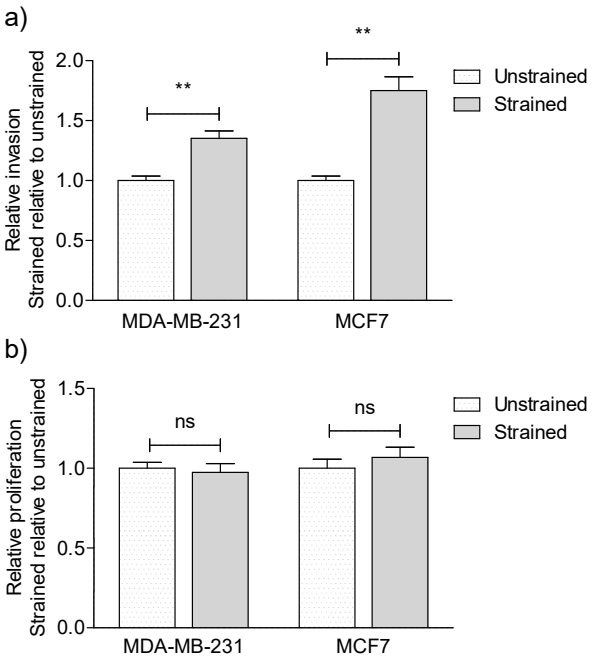

Figure 58. Mechanostimulation of a normal myoepithelial cell line mediates breast cancer cell invasion *in vitro*. a) Invasion of MDA-MB-231 and MCF-7 in response to CM from unstrained or strained N-1089. The number of invading cells was quantified by counting the cells on the underside of the Transwell. The values are presented as the relative invasion of breast cancer cells in the presence of CM from CM from strained normalised to unstrained N-1089. b) Proliferation of MDA-MB-231 and MCF-7 in response to CM from unstrained or strained N-1089. The values are presented as the relative proliferation of breast cancer cells in the presence of CM from strained normalised to unstrained N-1089. Analyses is shown as a mean of 3 independent experiments ±SEM. p-value ≤0.01 ('**') considered significant, 'ns' indicates not significant.

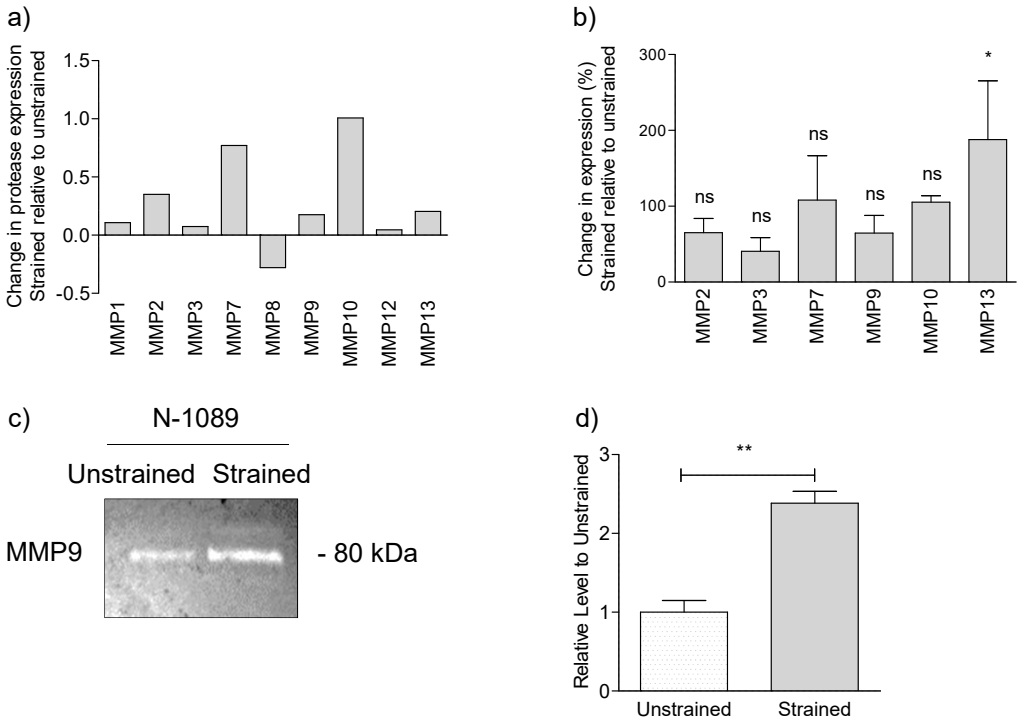

Figure 59. Mechanostimulation of a normal myoepithelial cell line upregulates protease expression. a) Human protease array analysis of cCM from unstrained or strained N-1089. Signal intensities of analytes were determined using ImageJ and presented the relative level in strained by normalising to unstrained. b)) qRT-PCR analysis of MMP2, MMP3, MMP7, MMP9, MMP10 and MMP13 mRNA levels in unstrained or strained N-1089. The values are presented as the mean percentage change in expression relative to unstrained. c) Gelatin zymography for MMP9 expression in cCM from unstrained or strained N-1089. d) Densitometric analysis of MMP9 signal intensities were determined using ImageJ. These data are then presented as the relative level in strained by normalising to unstrained N-1089. Representative images of 3 independent gelatin zymograms are shown, and analyses is shown as a mean of 3 experiments ±SEM. p-value ≤0.01 ('**') and ≤0.05 ('*') considered significant, 'ns' indicates not significant.

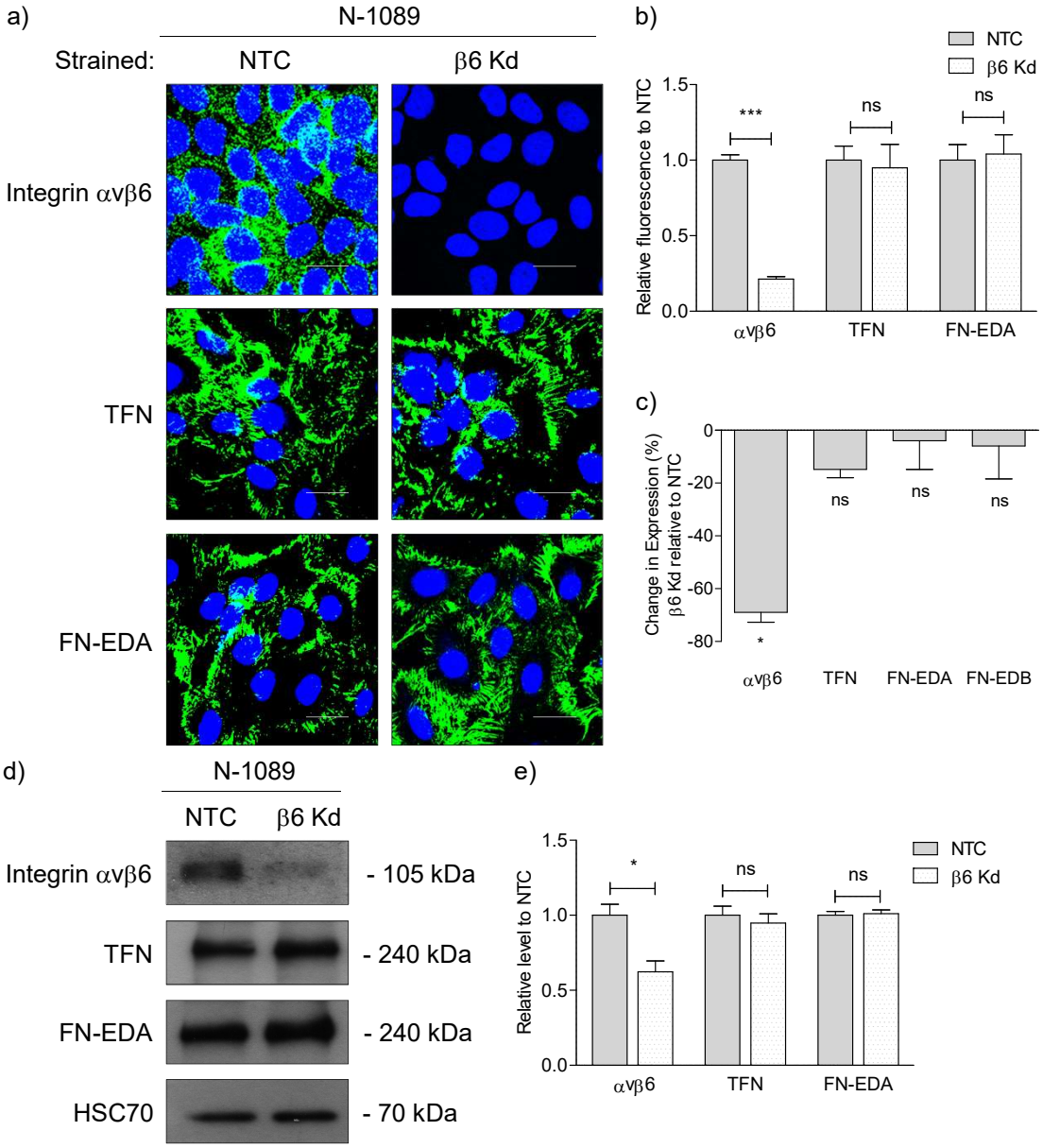

Figure 60. Knockdown of integrin αvβ6 expression in a mechanostimulated normal myoepithelial cell line. a) Immunofluorescent staining for integrin αvβ6, TFN and FN-EDA in strained N-1089 with NTC or integrin β6 siRNA (β6 Kd). Magnification ×63. Scale bar, 20μm. b) Fluorescent analysis of integrin αvβ6, TFN and FN-EDA signal intensities were determined using the ZEN 2009 image analysis software. The values are presented as the relative fluorescence in β6 Kd normalised to NTC. c) qRT-PCR analysis of integrin αvβ6, TFN, FN-EDA and FN-EDB mRNA levels in strained N-1089 with NTC or integrin β6 siRNA (β6 Kd). The values are presented as the mean percentage change in expression relative to NTC. d) Immunoblotting for integrin αvβ6, TFN, FN-EDA and HSC70 in strained N-1089 with NTC or integrin β6 siRNA (β6 Kd). e) Densitometric analysis of integrin αvβ6, TFN, FN-EDA and HSC70 signal intensities were determined using ImageJ. The relative protein levels of integrin αvβ6, TFN and FN-EDA were normalised to HSC70 on the same membrane. The values are presented as the relative level in β6 Kd normalised to NTC. Representative fluorescent images and immunoblots of at least 3 independent experiments are shown, and analyses is shown as a mean of 3 independent experiments ±SEM. p-value ≤0.001 ('***') and ≤0.05 ('*') considered significant, 'ns' indicates not significant.

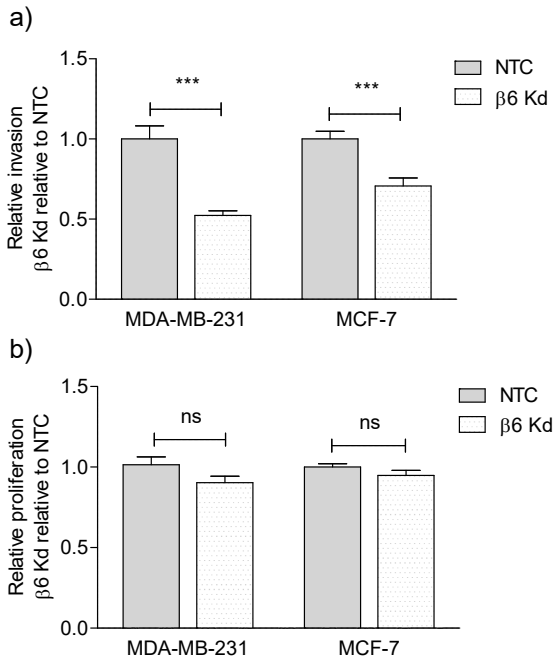

Figure 61. Mechanostimulation of integrin αvβ6 in a normal myoepithelial cell line mediates breast cancer cell invasion *in vitro*. a) Invasion of MDA-MB-231 and MCF-7 in response to CM from strained N-1089 with NTC or integrin β6 siRNA (β6 Kd). The number of invading cells was quantified by counting the cells on the underside of the Transwell. The values are presented as the relative invasion of breast cancer cells in the presence of CM from β6 Kd normalised to NTC. b) Proliferation of MDA-MB-231 and MCF-7 in response to CM from unstrained or strained N-1089. The values are presented as the relative proliferation of breast cancer cells in the presence of CM from β6 Kd normalised to NTC. Analyses is shown as a mean of 3 independent experiments ±SEM. p-value ≤0.001 ('***') considered significant, 'ns' indicates not significant.

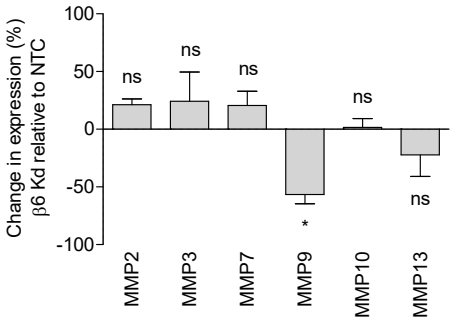

Figure 62. Mechanostimulation of integrin αvβ6 in a normal myoepithelial cell line upregulates protease expression. qRT-PCR analysis of MMP2, MMP3, MMP7, MMP9, MMP10 and MMP13 mRNA levels in strained N-1089 with NTC or integrin β6 siRNA (β6 Kd). The values are presented as the mean percentage change in expression relative to NTC. Analyses is shown as a mean of 3 experiments ±SEM. p-value ≤0.05 ('*') considered significant, 'ns' indicates not significant.

4.4.10 Mechanostimulation of integrin αvβ6 expression and fibronectin deposition by a normal myoepithelial cell line is TGFβ-dependent

Consistent with blockade of TGFβRII in β6-1089, TGFβRII block in N-1089 exposed to mechanical stretching inhibited the upregulation of integrin αvβ6 expression and FN deposition; both TFN and FN-EDA, as identified using immunofluorescence ($p<0.001$) (Figure 63a; quantified in 63b) and immunoblotting ($p<0.05$, $p<0.001$ and $p<0.001$) (Figure 63d; quantified in 63e). These findings were confirmed at the mRNA level (Figure 63c). These data suggest initiation of TGFβ activation may be mediated by mechanical stress, to induce the characteristic DCIS-MEC phenotype with upregulation of integrin αvβ6 and FN deposition. Together, these data suggest that mechanostimulation of MECs may activate TGFβ to induce the switch in MEC phenotype to that of a tumour-promoting phenotype.

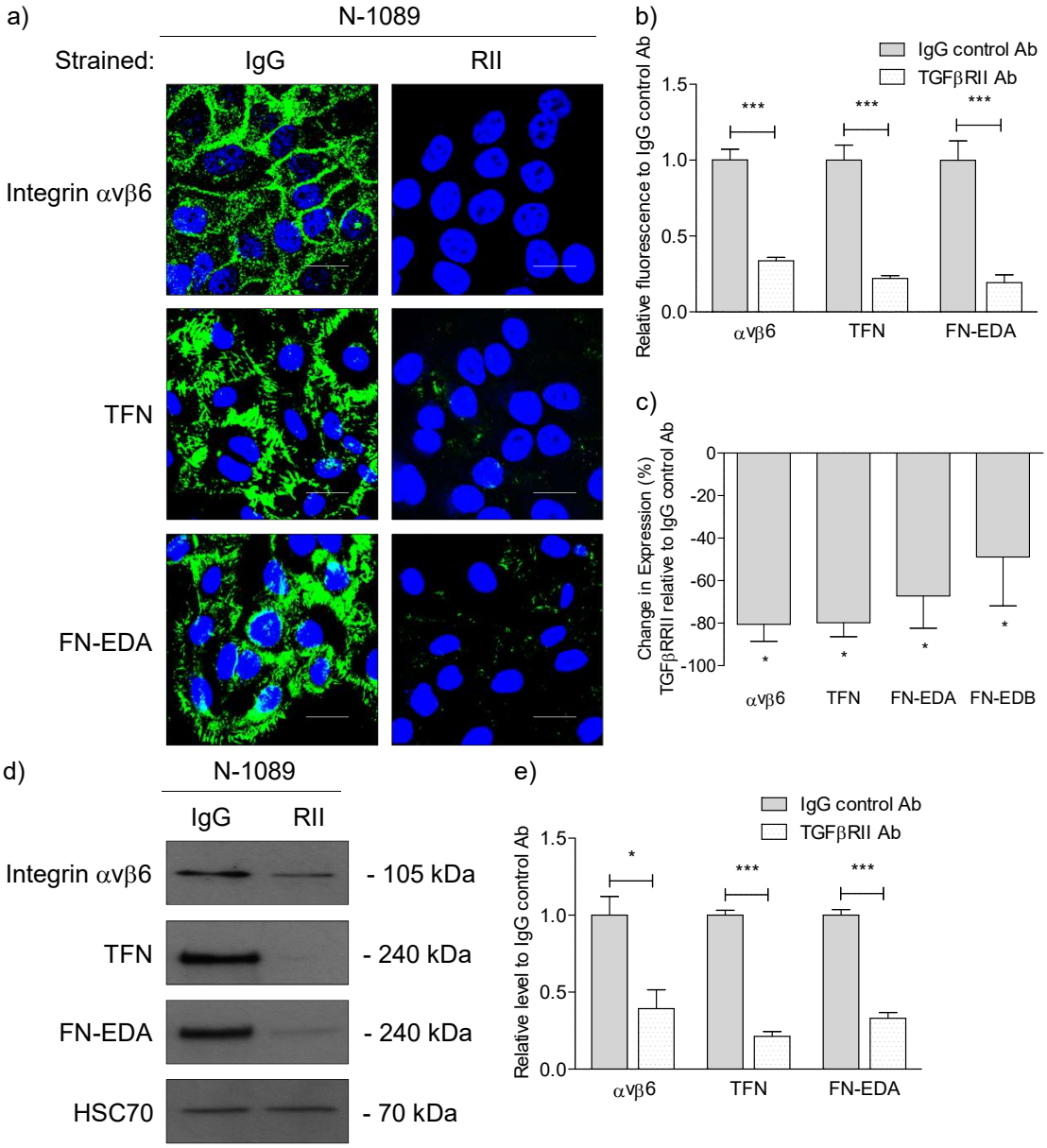

Figure 63. Mechanostimulation of integrin αvβ6 expression and fibronectin deposition in a normal myoepithelial cell line is TGFβ-dependent. a) Immunofluorescent staining for integrin αvβ6, TFN and FN-EDA in strained N-1089 with IgG control or TGFβRII (RII) antibody. Magnification ×63. Scale bar, 20μm. b) Fluorescent analysis of integrin αvβ6, TFN and FN-EDA signal intensities were determined using the ZEN 2009 image analysis software. The values are presented as the relative fluorescence in TGFβRII blocking antibody normalised to IgG control antibody. c) qRT-PCR analysis of integrin αvβ6, TFN, FN-EDA and FN-EDB mRNA levels in strained N-1089 with IgG control or TGFβRII antibody The values are presented as the mean percentage change in expression relative to NTC. d) Immunoblotting for integrin αvβ6, TFN, FN-EDA and HSC70 in strained N-1089 with IgG control or TGFβRII (RII) antibody. e) Densitometric analysis of integrin αvβ6, TFN, FN-EDA and HSC70 signal intensities were determined using ImageJ. The relative protein levels of integrin αvβ6, TFN and FN-EDA were normalised to HSC70 on the same membrane. The values are presented as the relative level TGFβRII blocking antibody normalised to IgG control antibody. Representative fluorescent images and immunoblots of at least 3 independent experiments are shown, and analyses is shown as a mean of 3 independent experiments ±SEM. p-value ≤0.001 (‘***’) and ≤0.05 (‘*’) considered significant.

5. DISCUSSION

For the majority of invasive breast cancers, progression follows transition through a preinvasive stage, DCIS [13]. DCIS is non-lethal however, due to its potential to invade and metastasise, patients are treated with surgery, radiation and/or hormone therapy [35, 36]. However, it is estimated that in fact only half of DCIS cases will progress to invasion within a patient's lifetime, and therefore concerns surround the overdiagnosis and overtreatment of DCIS [37]. Studies aimed at identifying markers to predict DCIS progression to better direct therapeutic intervention have demonstrated that neoplastic epithelial cells from DCIS and invasive breast cancer are genetically identical, and so currently there are no markers to robustly predict which cases will and will not progress [55, 66-70]. However, these studies failed to incorporate the microenvironment of DCIS, which comprises the MEC population and stromal compartment. In this study, we show that the breast microenvironment is altered, with upregulation of integrin $\alpha v\beta 6$ by MECs and increased periductal FN deposition, and these alterations are associated with DCIS progression to invasion. We identified a correlation between integrin $\alpha v\beta 6$ and FN in DCIS ducts, and demonstrated integrin $\alpha v\beta 6$-positive MECs upregulate the expression of FN. Subsequently, these alterations parallel enhanced activation of TGFβ signalling. Accompanying the activation of TGFβ, our model of DCIS-MECs upregulate the expression of MMPs associated with invasive-promoting functions, in particular MMP13. We found the expression of MMP13 promoted breast cancer cell invasion *in vitro*, consistent with prior reports that MMP13 associates with DCIS progression to invasive disease [417]. Interestingly, we identify that integrin $\alpha v\beta 6$ expression associates with increased DCIS duct size, and suggest a role for altered tissue mechanics in altering MEC phenotype. Moreover, we demonstrate integrin $\alpha v\beta 6$ and FN expression by MECs is mechanically regulated in a TGFβ-dependent manner. We suggest that *in vivo*, DCIS duct expansion induces TGFβ activation, to drive the expression of integrin $\alpha v\beta 6$ and FN, which provide a feedforward mechanism driving TGFβ signalling and MMP activation to promote invasion. Together, this work suggests that integrin $\alpha v\beta 6$ and FN may be used as markers to identify DCIS more likely to progress into invasive disease, in order to stratify patients with DCIS.

5.1 PHENOTYPIC CHARACTERISTICS OF MYOEPITHELIAL CELLS IN NORMAL AND DCIS TISSUE

Normal breast tissue is comprised of epithelium, stroma and adipose tissue, each of which is heterogeneous and complex in composition, and alters with development, menstrual cycle, pregnancy and ageing within an individual (intra-variability), as well as between individuals (inter-variability) [6, 8]. In breast cancer, the composition of breast tissue is altered however, studies depicting the proportion of these components has not been previously documented. The functional relevance of breast tissue composition is supported by direct association between mammographic density (proportion of radiodense glandular and fibrous tissue) and breast cancer risk [441], and growing experimental evidence that the ECM may influence breast cancer development, prognosis and treatment response [442, 443]. A digital histopathology analysis of our DCIS cohort demonstrated as DCIS develops there is a consequent increase in the relative proportion of epithelium and stroma, with a reduction in adipose tissue, and this is further enhanced with progression to invasion. This transition towards a less fatty, more fibrous microenvironment may itself alter both tumour and stromal cell behaviour. Studies have shown that increasing stiffness, accompanied by the reduction in adipose tissue and increased stroma – provided by the elevated quantify, reorganisation and crosslinking of ECM proteins [292, 294, 300, 308], can promote invasion and metastasis in *in vivo* models of mammary cancer [238, 300, 306]. Therefore, we suggest such alterations in breast tissue composition may promote DCIS progression.

Previous studies in our laboratory identified the *de novo* expression of integrin αvβ6 by DCIS-MECs, with 52% of non–high-grade and 69% of high-grade pure DCIS cases showing MEC staining for integrin αvβ6. The frequency of MEC staining for integrin αvβ6 in DCIS/IDC is significantly higher than in pure DCIS, with 87% of non-high-grade and 96% of high-grade DCIS/IDC cases exhibiting staining [114]. It already has been established that high-grade DCIS progresses to invasion and recurrence more quickly than low-grade [444, 445]. In this previous study, it was shown that the upregulation of integrin αvβ6 by DCIS-MECs was associated with recurrence of breast cancer either as *in situ* or invasive disease, independent of tumour grade, with integrin αvβ6-positive DCIS cases developing recurrence more quickly than integrin αvβ6-negative DCIS cases, with a median time to recurrence of 2.3 versus 11.4 years, respectively [114]. In work presented here, consistently no staining for integrin αvβ6 in normal tissue or benign lesions was detected, whereas 70% of non-high-grade pure DCIS, and 90% of high-grade pure DCIS and DCIS/IDC cases exhibited MEC staining for integrin αvβ6. One element not taken into consideration in the previous studies from our laboratory was the level of intratumour heterogeneity in DCIS. In work presented here, DCIS ducts were analysed on a duct-by-duct basis to address this. Analysis of integrin αvβ6 on a duct-by-duct basis in DCIS cases identified; 27% (10-59%) of non-high-grade and 45% (24-89%) of high-grade pure DCIS ducts showed MEC staining for integrin αvβ6. The frequency of MEC staining for integrin αvβ6 in DCIS/IDC is significantly higher than in pure DCIS, with 68% (33-100%) of DCIS/IDC ducts exhibiting staining. Together, this suggests integrin αvβ6 positivity in DCIS-MECs is a marker of DCIS cases more likely to progress to invasion and recurrence.

Further preliminary studies in our laboratory identified the upregulation of TFN by DCIS-MECs compared to normal MECs (29-fold), using Affymetrix cDNA microarray analysis of MECs isolated by LCM from normal (n=4) and DCIS tissue samples with (n=4) and without (n=1) invasion. The purity of MECs was confirmed by comparing MECs isolated from normal breast and DCIS tissue, for MEC and LEC-specific differentiation makers using qRT-PCR. The upregulation of TFN in DCIS-MECs was reflected at the mRNA level. Here, analysis of TFN on a duct-by-duct basis in DCIS cases supported these preliminary results; with all DCIS cases exhibiting periductal staining for TFN. Low levels of staining for TFN were detected in normal ducts or benign lesions, 6% (1-13%) and 21% (7-28%), respectively, whereas 70% (8-88%) of non-high-grade and 66% (23-97%) of high-grade pure DCIS ducts showed periductal FN expression. The frequency of periductal FN expression in DCIS/IDC is significantly higher than in pure DCIS, such that it is almost universally expressed, with 87% (20-100%) of DCIS/IDC ducts exhibiting staining. The increased deposition of FN in the periductal microenvironment was independent of tumour grade and is related to DCIS progression to invasion. The excessive deposition of ECM proteins is common in cancers with poor prognosis [291], and the increased deposition of FN has previously been documented in the stroma surrounding DCIS, and this increases in DCIS/IDC [69]. While such studies support our data, these studies analyse FN expression in the whole tumour stroma and do not accurately account for intratumour heterogeneity within the periductal microenvironment as addressed here. Moreover, a study by Hattar and colleagues demonstrated mammary ECM isolated from tamoxifen-treated rats has decreased FN levels, and suppressed breast tumour cell invasion *in vitro*. This effect could be reversed by the addition of exogenous FN [446], suggesting the tumour-promoting potential of the ECM is FN-dependent. Together, these data suggest periductal FN expression is a marker of DCIS cases more likely to progress to invasion, and indicate that the altered periductal microenvironment is regulated by DCIS-MECs.

Furthermore, there was a significant association between the upregulation of integrin αvβ6 expression by MECs and the deposition of FN into the periductal microenvironment. These alterations correlate with the altered composition of DCIS tissues. As such, the increased expression of integrin αvβ6 correlated with the increased proportion of epithelium, reflecting the expansion of DCIS ducts by neoplastic epithelial cells, whilst the increased deposition of FN correlates with the increased proportion of stroma. Recently, it has been demonstrated that the expression of integrin αvβ6 by MECs alters their response to changes in the properties of the stroma. It has been shown that normal MECs are able to sense and respond to increased matrix stiffness via integrin α5β1 binding to FN, thereby restoring tensional homeostasis and reducing the forces MECs experience to normal. This response is eventually overcome as the stiffness continues to increase; however, when MECs express integrin αvβ6, their ability to respond to a stiffening microenvironment is lost and consequently MECs experience the increase in stiffness more quickly [447]. These changes may be generated through alterations to the stroma, including the increased deposition of FN. These data suggest another mechanism by which integrin αvβ6 alters the normal phenotype of MECs, and may promote progression into invasion. Together, our immunohistochemical analyses confirm an alteration to MEC phenotype in DCIS, and suggests this alteration is associated with disease progression, since the altered phenotype is more frequent in DCIS/IDC. Next, we investigated the expression of FN by integrin αvβ6-positive primary DCIS-associated and normal MECs, along with MEC lines to further establish the relationship between, and function of these molecules in DCIS ducts.

5.2 PHENOTYPIC CHARACTERISTICS IN PRIMARY AND CELL LINE MODELS OF NORMAL AND DCIS MYOEPITHELIAL CELLS

Our laboratory regularly isolates different cell populations from normal and tumour breast tissue through enzymatic digestion and cell purification. In this study, primary MECs from normal breast and DCIS tissue were used, alongside established MEC lines. Consistent with immunohistochemical analyses of DCIS tissues, primary DCIS-MECs isolated from an integrin αvβ6-positive DCIS case demonstrated a significant increase in FN mRNA expression compared to DCIS-MECs isolated from an integrin αvβ6-negative case. Similarly, overexpression of integrin αvβ6 in primary normal MECs, which normally lack integrin αvβ6, demonstrated a concomitant increase in FN protein expression. Moreover, using a MEC line with (β6-1089) and without (N-1089) stable expression of integrin αvβ6 identified a significant increase in FN protein and mRNA expression in β6-108 compared to N-1089. All models of integrin αvβ6-positive MECs which expressed FN, expressed EDA and/or EDB sequences, which are markers of cFN [323]. No significant differences between cFN and TFN levels were detected throughout, demonstrating integrin αvβ6-positive MECs dominantly express cFN compared to pFN. The assembly of FN into a mature fibrillar matrix is essential for the function of FN. Assembly of a FN matrix is the same for both pFN and cFN. It has previously been shown that the development of a FN matrix can be monitored by the irreversible conversion of DOC-soluble, cell-associated FN, into a DOC-insoluble FN matrix. DOC-soluble, cell-associated FN is thought to represent FN bound to cell surface receptors which has not yet been assembled into DOC-insoluble FN fibrils [359]. Both DOC-soluble and DOC-insoluble FN were upregulated in β6-1089, compared to N-1089, with significantly more DOC-insoluble FN identified in β6-1089, suggesting β6-1089 convert most FN into a mature fibrillar matrix. The FN matrix produced by β6-1089 demonstrated an increase in FN fibril length and number with time, indicative of a more mature FN matrix. These data suggest that integrin αvβ6-positive MECs upregulate FN expression, and assembly into a fibrillar matrix. Together with our immunhistochemical analyses, these data further support a potential relationship between integrin αvβ6 and FN expression by DCIS-MECs, however, the mechanism regulating their expression is unclear.

5.3 FUNCTION OF PHENOTYPIC CHARACTERISTICS IN PRIMARY AND CELL LINE MODELS OF NORMAL AND DCIS MYOEPITHELIAL CELLS

A primary function of integrin αvβ6 is the activation of TGFβ [207]. This mechanism depends on binding to LAP, where LAP is bound to a LTBP. Previous work in our laboratory has demonstrated that integrin αvβ6 expressed by β6-1089 is functional, such that it is able to bind to LAP and activate latent TGFβ1 [114]. Following activation, TGFβ may then bind to its receptors to activate TGFβ signalling pathways. Canonical TGFβ signalling involves the phosphorylation of TGFβRI by TGFβRII following ligand binding. TGFβRI then induces the phosphorylation of R-SMADs, which transmit TGFβ signals to the nucleus through association with Co-SMAD [238]. Non-canonical signalling pathways activated by TGFβ bypass SMAD signalling and involve phosphorylation events that activate Ras-ERK signalling pathways, among others [223]. Overexpression of integrin αvβ6 in primary normal MECs, led to an increase in p-SMAD2 under basal conditions and following stimulation with exogenous TGFβ1. Similarly, β6-1089 demonstrated increased levels of both p-SMAD2 and p-ERK1/2 under both basal conditions and following stimulation with exogenous TGFβ1. This effect was reversed by knockdown of integrin αvβ6 expression in β6-1089 using siRNA targeting integrin β6. These data support the role of integrin αvβ6 expressed by MECs in the activation of TGFβ signalling pathways. Moreover, it has been shown that LTBP1 of the LLC must interact with FN as a structural precondition to integrin αvβ6-mediated TGFβ1 activation [208]. Data presented here identified the knockdown of TFN expression using siRNA targeting TFN in integrin αvβ6-overexpressing primary MECs and β6-1089, led to a reduction in p-SMAD2 under basal conditions and following exogenous TGFβ1. Moreover, knockdown of TFN by β6-1089 led to a reduction in both migration and adhesion to LAP. These data suggest that both integrin αvβ6 and FN in MECs must be present for the activation of TGFβ signalling pathways. Together, these data suggest that DCIS-MECs are equipped to activate TGFβ. Integrin αvβ6-mediated activation of TGFβ functions to promote invasion in cancer cells through an autocrine manner [448].

Previous work in our laboratory demonstrated that integrin αvβ6 expressed by MECs is able to promote breast cancer cell invasion *in vitro*, through paracrine mechanisms generated by TGFβ-dependent upregulation of MMP9 [114]. Here, we demonstrate the upregulation of FN by integrin αvβ6-positive MECs is required to facilitate TGFβ activation, and the knockdown of TFN expression in β6-1089 reduced breast cancer cell invasion *in vitro*. To investigate the mechanism by which these alterations in MEC phenotype might contribute to DCIS progression, MMP secretion was analysed. MMPs have long been associated with cancer invasion and metastasis due to their direct function in remodelling the surrounding ECM [288] however, they have been shown to have paradoxical roles in cancer progression [415]. Previous work in our laboratory has shown that MMP8 is a tumour-suppressive MMP expressed by normal MECs however, MMP8 expression is lost in DCIS-MECs [424]. Data presented here support these data. We confirm our model of DCIS-MECs, β6-1089 downregulate MMP8 compared to normal MECs, N-1089, and this effect is reversed by knockdown of integrin αvβ6. In addition to the known upregulation of MMP9, β6-1089 also upregulate MMP13, and these effects are reversed by knockdown of either integrin αvβ6 or TFN expression. Moreover, both MMP9 and MMP13 expression can be blocked by inhibiting TGFβRII with a blocking antibody. Whilst previous studies from our laboratory have focused on the tumour-promoting function of MMP9 [114], less is known about MMP13 in DCIS progression. MMP13 functions to degrade collagen structures [449], and has previously been shown to be upregulated in the progression of DCIS to invasive breast cancer by subjacent myofibroblasts in the surrounding stroma [417], which are often indistinguishable from DCIS-MECs [450]. Here we demonstrate the knockdown of MMP13 expression in β6-1089 reduces breast cancer cell invasion *in vitro*. Together, these data support the paracrine tumour-promoting function of integrin αvβ6-positive MECs on breast cancer cell invasion, and this effect is dependent on TGFβ-dependent activation of MMP13, in addition to its known effects on MMP9 activation.

5.4 REGULATION OF PHENOTYPIC CHARACTERISTICS IN NORMAL AND DCIS MYOEPITHELIAL CELLS

TGFβ regulates integrin expression, ECM deposition and protease activity [193]. This is shown by fibroblast-to-myofibroblast transition induced by TGFβ, which is characterised by stronger actomyosin contractility than resident fibroblast precursors and exacerbated ECM remodelling through the production of ECM proteins, ECM-modifying enzymes and cross-linking enzymes [300, 451-453]. Here we show that stimulation of primary normal MECs and a normal MEC line with TGFβ1, upregulated integrin αvβ6 and FN expression. Furthermore, TGFβ1 stimulation upregulated MMP expression, in particular MMP9 and MMP13 were consistently upregulated. These results are consistent with the identification of a TGFβ regulatory domain in both MMP9 and MMP13 [454]. These data also support previous publications in which exogenous TGFβ stimulation *in vitro* induced the expression of MMP9 [283] and MMP13 [397]. Furthermore, the effect of TGFβ in altering MEC gene-expression was shown by inhibition of TGFβRII in β6-1089 with a blocking antibody, which resulted in the downregulation of FN mRNA and protein expression. Integrin αvβ6 was unchanged, likely due to its constitutive expression in β6-1089. The effect of TGFβRII inhibition was attributed to the almost complete reduction in TGFβ signalling, compared to the partial reduction seen following the knockdown of integrin β6 expression. We postulate a positive feedback loop in which active TGFβ upregulates MEC expression of integrin αvβ6 and FN. This, in turn, increases TGFβ activation to upregulate MMP expression, specifically MMP9 and MMP13. However, the initial production of TGFβ and/or its activation is unclear.

Breast cancers are stiffer than the surrounding uninvolved tissue. The nature of the mechanical perturbations in a solid tumour includes solid stress and compression forces resulting from the expanding tumour cells. DCIS and benign proliferative lesions are characterised by the proliferation of neoplastic and hyperproliferative epithelial cells confined within the ductal-lobular network [16], which results in duct expansion from an average normal duct size of 1.3mm^2 to 140mm^2 and 90mm^2, respectively. Interestingly, DCIS ducts from high-grade pure DCIS were larger than those from non-high-grade pure DCIS, with an average duct size of 160mm^2 compared to 81mm^2, while those from high-grade DCIS/IDC were similar in size, with an average duct size of 163mm^2. These data support the histological grading of breast cancers, as low-grade DCIS consists of small, cohesive, polarised, uniform cells of low proliferative capacity, while high-grade DCIS consists of large, pleomorphic cells of high proliferative capacity, accounting for the increased duct size seen in high-grade DCIS ducts. Moreover, it was shown that integrin $\alpha v\beta 6$-positive DCIS ducts on average were larger than integrin $\alpha v\beta 6$-negative DCIS ducts, independent of tumour grade, with an average duct size of 162mm^2 compared to 117mm^2. These findings demonstrate an association between expansion of DCIS ducts and expression of integrin $\alpha v\beta 6$ expression by DCIS-MECs.

MECs undergo morphological changes as a consequence of the pressure exerted by neoplastic and hyperproliferative epithelial cells in DCIS and benign proliferative lesions, respectively [455]. Such that with duct expansion, MECs become attenuated and are not easily identifiable in H&E stained breast tissue sections, as they are often indistinguishable from subjacent myofibroblasts in the surrounding stroma, immunohistochemical staining for SMA is routinely used to assist in the identification of MECs [450]. In SMA immunohistochemistry images, MECs in normal ducts appeared rounded, while in both DCIS and benign lesions appeared flattened or spindle-shaped, with an average minor axis of 6.1μm, compared to 2.7μm and 3.6μm, respectively. However, in p63 immunohistochemistry images, MEC nuclei appeared flattened in DCIS, while in both normal and benign lesions appeared rounded, with an average minor axis by major axis of 2.2μm by 8.4μm, compared to 4.3μm by 4.7μm and 4.3μm by 5.1μm, respectively. Interestingly, MECs in integrin αvβ6-positive DCIS ducts appeared more significantly flattened or spindle-shaped than in integrin αvβ6-negative DCIS ducts, with an average minor axis of 2.5μm compared to 3.0μm. MEC nuclei were also more significantly compressed and elongated in integrin αvβ6-positive DCIS ducts compared to integrin αvβ6-negative DCIS ducts, with an average minor axis by major axis of 2.1μm by 8.6μm compared to 2.4μm by 8.1μm. The change in MEC nuclei is not explained only by physical pressure and is also likely due to altered crosstalk in tumours [456]. Breast tumour cells under high tension demonstrate elevated integrins and increased integrin signalling, suggesting tissue mechanics regulate malignancy by enhancing integrin-dependent mechanotransduction [299]. This is the first study to suggest that MECs under high tension may increase expression of integrin αvβ6 as an adaptive response. Together, these results suggest that the morphology of MEC nuclei could be helpful in distinguishing between benign proliferative lesions and DCIS, and such morphological changes to DCIS-MECs may influence integrin αvβ6 expression, though this would need to be investigated directly through cell compression analyses.

These data indicate MECs in DCIS are subject to significant mechanical stress. As with exposure to TGFβ, cells subject to mechanical stress generate sustained responses by altering their gene-expression of ECM proteins, ECM receptors and ECM-remodelling enzymes to allow modification of the composition, organisation and elasticity of their microenvironment [452]. Such modifications to the ECM can in turn, activate TGFβ [451]. This mechanism of mechanoreciprocity equips cells with the ability to alter their behaviour to correspond with the biophysical properties of the surrounding ECM [452]. Mechanical stimulation of primary normal MECs and a normal MEC line lead to an increase in integrin αvβ6 and FN mRNA and protein expression. With this, CM isolated from all mechanically stimulated MECs promoted breast cancer cell invasion *in vitro*, and this effect was not attributed to increased breast cancer cell proliferation. In turn, mechanical stimulation of MECs upregulated MMP expression, specifically MMP13. The mechanical stimulation of integrin αvβ6 was inhibited by knockdown of integrin αvβ6 expression using siRNA however, FN expression was maintained. This effect reduced breast cancer cell invasion *in vitro*, which is likely due to the reduction seen in MMP9 and MMP13 expression. Furthermore, inhibition of TGFβRII with a blocking antibody, prevented the mechanostimulation of both integrin αvβ6 and FN expression. We postulate a positive feedback loop in which mechanical tension, provided by duct expansion and increased ECM stiffness, facilitates initial TGFβ production and/or activation, which upregulates integrin αvβ6 expression and FN deposition. This, in turn, increases force production and tension development, to activate TGFβ further. Together these changes form a DCIS-MEC phenotype, with the ability to promote breast cancer cell invasion through consequent activation of MMP9 and MMP13.

The data presented here suggest evolving tissue mechanics during DCIS development activate TGFβ to induce an alteration in MEC phenotype from tumour-suppressive to tumour-promoting, with upregulation of integrin αvβ6 and FN expression. Indeed, we identified DCIS progression is associated with the upregulation of integrin αvβ6 expression by MECs and periductal FN deposition, and show their expression is associated in DCIS ducts. We also found that the transition of a normal breast duct to DCIS is accompanied with a dramatic increase in duct size, and demonstrated an association with duct expansion and integrin αvβ6 expression. Subsequently, mechanical stretching of MECs induces the expression of integrin αvβ6 and deposition of FN in a TGFβ-dependent manner. In this way, integrin αvβ6-FN-positive MECs are equipped to further mediate TGFβ-dependent activation of MMP9 and MMP13 expression to promote breast cancer cell invasion *in vitro*. Further investigation into the mechanism by which mechanical stretching of MECs in DCIS ducts translates into altered gene-expression would provide a unique understanding of the alteration in MEC phenotype in DCIS. Together, these data support the role for DCIS-MECs in altering the TME to facilitate DCIS progression to invasion, and suggest integrin αvβ6 and FN may be used as markers to identify DCIS cases more likely to progress into invasive disease.

6. REFERENCES

1. Rønnov-Jessen, L., O.W. Petersen, and M.J. Bissell, *Cellular changes involved in conversion of normal to malignant breast: importance of the stromal reaction.* Physiol Rev, 1996. **76**(1): p. 69-125.
2. Gusterson, B.A., et al., *Distribution of myoepithelial cells and basement membrane proteins in the normal breast and in benign and malignant breast diseases.* Cancer Res, 1982. **42**(11): p. 4763-70.
3. Emerman, J.T. and A.W. Vogl, *Cell size and shape changes in the myoepithelium of the mammary gland during differentiation.* Anat Rec, 1986. **216**(3): p. 405-15.
4. Sopel, M., *The myoepithelial cell: its role in normal mammary glands and breast cancer.* Folia Morphol (Warsz), 2010. **69**(1): p. 1-14.
5. Sternlicht, M.D., *Key stages in mammary gland development: the cues that regulate ductal branching morphogenesis.* Breast Cancer Res, 2006. **8**(1): p. 201.
6. Javed, A. and A. Lteif, *Development of the human breast.* Semin Plast Surg, 2013. **27**(1): p. 5-12.
7. Fata, J.E., Z. Werb, and M.J. Bissell, *Regulation of mammary gland branching morphogenesis by the extracellular matrix and its remodeling enzymes.* Breast Cancer Res, 2004. **6**(1): p. 1-11.
8. Macias, H. and L. Hinck, *Mammary gland development.* Wiley Interdiscip Rev Dev Biol, 2012. **1**(4): p. 533-57.
9. McCready, J., et al., *The contribution of dynamic stromal remodeling during mammary development to breast carcinogenesis.* Breast Cancer Res, 2010. **12**(3): p. 205.
10. Haaksma, C.J., R.J. Schwartz, and J.J. Tomasek, *Myoepithelial cell contraction and milk ejection are impaired in mammary glands of mice lacking smooth muscle alpha-actin.* Biol Reprod, 2011. **85**(1): p. 13-21.
11. Milanese, T.R., et al., *Age-related lobular involution and risk of breast cancer.* J Natl Cancer Inst, 2006. **98**(22): p. 1600-7.
12. Ghosh, K., et al., *Association Between Mammographic Density and Age-Related Lobular Involution of the Breast.* Journal of Clinical Oncology, 2010. **28**(13): p. 2207-2212.
13. Sgroi, D.C., *Preinvasive breast cancer.* Annu Rev Pathol, 2010. **5**: p. 193-221.
14. Wellings, S.R. and H.M. Jensen, *On the origin and progression of ductal carcinoma in human breast.* J Natl Cancer Inst, 1973. **50**(5): p. 1111-8.
15. Wellings, S.R., H.M. Jensen, and R.G. Marcum, *An atlas of subgross pathology of the human breast with special reference to possible precancerous lesions.* J Natl Cancer Inst, 1975. **55**(2): p. 231-73.
16. Cichon, M.A., et al., *Microenvironmental influences that drive progression from benign breast disease to invasive breast cancer.* J Mammary Gland Biol Neoplasia, 2010. **15**(4): p. 389-97.
17. Silverstein, M.J., et al., *Prognostic classification of breast ductal carcinoma-in-situ.* Lancet, 1995. **345**(8958): p. 1154-7.

18. Ellis, I.O., et al., *Guidelines for breast needle core biopsy handling and reporting in breast screening assessment.* Journal of Clinical Pathology, 2004. **57**(9): p. 897-902.
19. Silverstein, M.J., et al., *A prognostic index for ductal carcinoma in situ of the breast.* Cancer, 1996. **77**(11): p. 2267-74.
20. Badve, S., et al., *Prediction of local recurrence of ductal carcinoma in situ of the breast using five histological classifications: a comparative study with long follow-up.* Hum Pathol, 1998. **29**(9): p. 915-23.
21. Pinder, S.E., *Ductal carcinoma in situ (DCIS): pathological features, differential diagnosis, prognostic factors and specimen evaluation.* Mod Pathol, 2010. **23** Suppl 2: p. S8-13.
22. Allred, D.C., et al., *Ductal carcinoma in situ and the emergence of diversity during breast cancer evolution.* Clin Cancer Res, 2008. **14**(2): p. 370-8.
23. Silverstein, M.J., *Ductal Carcinoma In Situ of the Breast: Controversial Issues.* Oncologist, 1998. **3**(2): p. 94-103.
24. Allegra, C.J., et al., *NIH state-of-the-science conference statement: diagnosis and management of ductal carcinoma in situ (DCIS).* NIH Consens State Sci Statements, 2009. **26**(2): p. 1-27.
25. Allred, D.C., S.K. Mohsin, and S.A. Fuqua, *Histological and biological evolution of human premalignant breast disease.* Endocr Relat Cancer, 2001. **8**(1): p. 47-61.
26. Simpson, P.T., et al., *Columnar cell lesions of the breast: the missing link in breast cancer progression? A morphological and molecular analysis.* Am J Surg Pathol, 2005. **29**(6): p. 734-46.
27. Foote, F.W. and F.W. Stewart, *Comparative Studies of Cancerous Versus Noncancerous Breasts.* Ann Surg, 1945. **121**(2): p. 197-222.
28. Dupont, W.D. and D.L. Page, *Risk factors for breast cancer in women with proliferative breast disease.* N Engl J Med, 1985. **312**(3): p. 146-51.
29. Page, D.L., et al., *Atypical hyperplastic lesions of the female breast. A long-term follow-up study.* Cancer, 1985. **55**(11): p. 2698-708.
30. London, S.J., et al., *A prospective study of benign breast disease and the risk of breast cancer.* JAMA, 1992. **267**(7): p. 941-4.
31. Dupont, W.D., et al., *Breast cancer risk associated with proliferative breast disease and atypical hyperplasia.* Cancer, 1993. **71**(4): p. 1258-65.
32. Ernster, V.L., et al., *Mortality among women with ductal carcinoma in situ of the breast in the population-based surveillance, epidemiology and end results program.* Arch Intern Med, 2000. **160**(7): p. 953-8.
33. van Dongen, J.A., et al., *In-situ breast cancer: the EORTC consensus meeting.* Lancet, 1989. **2**(8653): p. 25-7.
34. Jones, J.L., *Overdiagnosis and overtreatment of breast cancer: progression of ductal carcinoma in situ: the pathological perspective.* Breast Cancer Res, 2006. **8**(2): p. 204.
35. Nelson, N.J., *DCIS prognostic markers: a few new candidates emerge.* J Natl Cancer Inst, 2010. **102**(9): p. 588-90.

36. Lari, S.A. and H.M. Kuerer, *Biological markers in DCIS and risk of breast recurrence: a systematic review.* J Cancer, 2011. **2**: p. 232-61.
37. Sanders, M.E., et al., *The natural history of low-grade ductal carcinoma in situ of the breast in women treated by biopsy only revealed over 30 years of long-term follow-up.* Cancer, 2005. **103**(12): p. 2481-4.
38. Collins, L.C., et al., *Outcome of patients with ductal carcinoma in situ untreated after diagnostic biopsy: results from the Nurses' Health Study.* Cancer, 2005. **103**(9): p. 1778-84.
39. Leeper, A.D. and J.M. Dixon, *DCIS of the breast: Are we over-diagnosing it? Are we over-treating it?* Maturitas, 2011. **68**(4): p. 295-6.
40. Screening, I.U.P.o.B.C., *The benefits and harms of breast cancer screening: an independent review.* Lancet, 2012. **380**(9855): p. 1778-86.
41. Marmot, M.G., et al., *The benefits and harms of breast cancer screening: an independent review.* Br J Cancer, 2013. **108**(11): p. 2205-40.
42. Esserman, L.J., et al., *Addressing overdiagnosis and overtreatment in cancer: a prescription for change.* Lancet Oncol, 2014. **15**(6): p. e234-42.
43. Roylance, R., et al., *Comparative genomic hybridization of breast tumors stratified by histological grade reveals new insights into the biological progression of breast cancer.* Cancer Res, 1999. **59**(7): p. 1433-6.
44. Buerger, H., et al., *Different genetic pathways in the evolution of invasive breast cancer are associated with distinct morphological subtypes.* J Pathol, 1999. **189**(4): p. 521-6.
45. Buerger, H., et al., *Comparative genomic hybridization of ductal carcinoma in situ of the breast-evidence of multiple genetic pathways.* J Pathol, 1999. **187**(4): p. 396-402.
46. Buerger, H., et al., *Ductal invasive G2 and G3 carcinomas of the breast are the end stages of at least two different lines of genetic evolution.* J Pathol, 2001. **194**(2): p. 165-70.
47. Simpson, P.T., et al., *Molecular evolution of breast cancer.* J Pathol, 2005. **205**(2): p. 248-54.
48. Sotiriou, C., et al., *Gene expression profiling in breast cancer: understanding the molecular basis of histologic grade to improve prognosis.* J Natl Cancer Inst, 2006. **98**(4): p. 262-72.
49. Perou, C.M., et al., *Molecular portraits of human breast tumours.* Nature, 2000. **406**(6797): p. 747-52.
50. Peppercorn, J., C.M. Perou, and L.A. Carey, *Molecular subtypes in breast cancer evaluation and management: divide and conquer.* Cancer Invest, 2008. **26**(1): p. 1-10.
51. Sørlie, T., et al., *Gene expression patterns of breast carcinomas distinguish tumor subclasses with clinical implications.* Proc Natl Acad Sci U S A, 2001. **98**(19): p. 10869-74.
52. Ho-Yen, C., R.L. Bowen, and J. Jones, *Characterization of basal-like breast cancer.* Diagnostic Histopathology, 2012. **18**(3): p. 104–111.

53. Sorlie, T., et al., *Repeated observation of breast tumor subtypes in independent gene expression data sets.* Proc Natl Acad Sci U S A, 2003. **100**(14): p. 8418-23.
54. Dai, X., et al., *Breast cancer intrinsic subtype classification, clinical use and future trends.* Am J Cancer Res, 2015. **5**(10): p. 2929-43.
55. Yao, J., et al., *Combined cDNA array comparative genomic hybridization and serial analysis of gene expression analysis of breast tumor progression.* Cancer Res, 2006. **66**(8): p. 4065-78.
56. Lakhani, S.R., et al., *Atypical ductal hyperplasia of the breast: clonal proliferation with loss of heterozygosity on chromosomes 16q and 17p.* J Clin Pathol, 1995. **48**(7): p. 611-5.
57. O'Connell, P., et al., *Analysis of LOH in premalignant breast lesions at 15 genetic loci.* J Natl Cancer Inst, 1998. **90**(9): p. 697-703.
58. Amari, M., et al., *LOH analyses of premalignant and malignant lesions of human breast: frequent LOH in 8p, 16q, and 17q in atypical ductal hyperplasia.* Oncol Rep, 1999. **6**(6): p. 1277-80.
59. Moinfar, F., et al., *Genetic abnormalities in mammary ductal intraepithelial neoplasia-flat type ("clinging ductal carcinoma in situ"): a simulator of normal mammary epithelium.* Cancer, 2000. **88**(9): p. 2072-81.
60. Hannemann, J., et al., *Classification of ductal carcinoma in situ by gene expression profiling.* Breast Cancer Res, 2006. **8**(5): p. R61.
61. Clark, S.E., et al., *Molecular subtyping of DCIS: heterogeneity of breast cancer.* Br J Cancer, 2011. **104**(1): p. 120-7.
62. Carey, L.A., et al., *Race, breast cancer subtypes, and survival in the Carolina Breast Cancer Study.* JAMA, 2006. **295**(21): p. 2492-502.
63. Park, K., et al., *HER2 status in pure ductal carcinoma in situ and in the intraductal and invasive components of invasive ductal carcinoma determined by fluorescence in situ hybridization and immunohistochemistry.* Histopathology, 2006. **48**(6): p. 702-7.
64. Garnis, C., et al, *Genetic alteration and gene expression modulation during cancer progression.* Mol Cancer, 2004. **3**: p. 9.
65. Adeyinka, A., et al., *Analysis of gene expression in ductal carcinoma in situ of the breast.* Clin Cancer Res, 2002. **8**(12): p. 3788-95.
66. Ma, X.J., et al., *Gene expression profiles of human breast cancer progression.* Proc Natl Acad Sci U S A, 2003. **100**(10): p. 5974-9.
67. Porter, D., et al., *Molecular markers in ductal carcinoma in situ of the breast.* Mol Cancer Res, 2003. **1**(5): p. 362-75.
68. Chin, K., et al., *In situ analyses of genome instability in breast cancer.* Nat Genet, 2004. **36**(9): p. 984-8.
69. Ma, X.J., et al., *Gene expression profiling of the tumor microenvironment during breast cancer progression.* Breast Cancer Res, 2009. **11**(1): p. R7.
70. Castro, N.P., et al., *Evidence that molecular changes in cells occur before morphological alterations during the progression of breast ductal carcinoma.* Breast Cancer Res, 2008. **10**(5): p. R87.

71. Bell, R., R. Barraclough, and O. Vasieva, *Gene Expression Meta-Analysis of Potential Metastatic Breast Cancer Markers.* Curr Mol Med, 2017. **17**(3): p. 200-210.
72. Schuetz, C.S., et al., *Progression-specific genes identified by expression profiling of matched ductal carcinomas in situ and invasive breast tumors, combining laser capture microdissection and oligonucleotide microarray analysis.* Cancer Res, 2006. **66**(10): p. 5278-86.
73. DeCosse, J.J., et al., *Embryonic inductive tissues that cause histologic differentiation of murine mammary carcinoma in vitro.* J Natl Cancer Inst, 1975. **54**(4): p. 913-22.
74. DeCosse, J.J., et al., *Breast cancer: induction of differentiation by embryonic tissue.* Science, 1973. **181**(4104): p. 1057-8.
75. Bissell, M.J. and D. Radisky, *Putting tumours in context.* Nat Rev Cancer, 2001. **1**(1): p. 46-54.
76. Radisky, D., C. Hagios, and M.J. Bissell, *Tumors are unique organs defined by abnormal signaling and context.* Semin Cancer Biol, 2001. **11**(2): p. 87-95.
77. Tlsty, T.D., *Stromal cells can contribute oncogenic signals.* Semin Cancer Biol, 2001. **11**(2): p. 97-104.
78. Jones, J.L., et al., *Primary breast myoepithelial cells exert an invasion-suppressor effect on breast cancer cells via paracrine down-regulation of MMP expression in fibroblasts and tumour cells.* J Pathol, 2003. **201**(4): p. 562-72.
79. Maffini, M.V., et al., *The stroma as a crucial target in rat mammary gland carcinogenesis.* J Cell Sci, 2004. **117**(Pt 8): p. 1495-502.
80. Allinen, M., et al., *Molecular characterization of the tumor microenvironment in breast cancer.* Cancer Cell, 2004. **6**(1): p. 17-32.
81. Zhang, R.R., et al., *A subset of morphologically distinct mammary myoepithelial cells lacks corresponding immunophenotypic markers.* Breast Cancer Res, 2003. **5**(5): p. R151-6.
82. Hilson, J.B., S.J. Schnitt, and L.C. Collins, *Phenotypic alterations in myoepithelial cells associated with benign sclerosing lesions of the breast.* Am J Surg Pathol, 2010. **34**(6): p. 896-900.
83. Toussaint, J., et al., *Low CD10 mRNA expression identifies high-risk ductal carcinoma in situ (DCIS).* PLoS One, 2010. **5**(8).
84. Deugnier, M.A., et al., *The importance of being a myoepithelial cell.* Breast Cancer Res, 2002. **4**(6): p. 224-30.
85. Orimo, A., et al., *Stromal fibroblasts present in invasive human breast carcinomas promote tumor growth and angiogenesis through elevated SDF-1/CXCL12 secretion.* Cell, 2005. **121**(3): p. 335-48.
86. Man, Y.G., et al., *Cell clusters overlying focally disrupted mammary myoepithelial cell layers and adjacent cells within the same duct display different immunohistochemical and genetic features: implications for tumor progression and invasion.* Breast Cancer Res, 2003. **5**(6): p. R231-41.

87. Zhu, G., et al., *Combination of microdissection and microarray analysis to identify gene expression changes between differentially located tumour cells in breast cancer.* Oncogene, 2003. **22**(24): p. 3742-8.
88. Waldman, F.M., et al., *Chromosomal alterations in DCIS and their in situ recurrences.* J Natl Cancer Inst, 2000. **92**(4): p. 313-20.
89. Lazard, D., et al., *Expression of smooth muscle-specific proteins in myoepithelium and stromal myofibroblasts of normal and malignant human breast tissue.* Proc Natl Acad Sci U S A, 1993. **90**(3): p. 999-1003.
90. Dairkee, S. and H.W. Heid, *Cytokeratin profile of immunomagnetically separated epithelial subsets of the human mammary gland.* In Vitro Cell Dev Biol Anim, 1993. **29A**(5): p. 427-32.
91. Runswick, S.K., et al., *Desmosomal adhesion regulates epithelial morphogenesis and cell positioning.* Nat Cell Biol, 2001. **3**(9): p. 823-30.
92. Glukhova, M., et al., *Adhesion systems in normal breast and in invasive breast carcinoma.* Am J Pathol, 1995. **146**(3): p. 706-16.
93. Sonnenberg, A., et al., *Integrin alpha 6 beta 4 complex is located in hemidesmosomes, suggesting a major role in epidermal cell-basement membrane adhesion.* J Cell Biol, 1991. **113**(4): p. 907-17.
94. Shaw, L.M., *Integrin function in breast carcinoma progression.* J Mammary Gland Biol Neoplasia, 1999. **4**(4): p. 367-76.
95. Adriance, M.C., et al., *Myoepithelial cells: good fences make good neighbors.* Breast Cancer Res, 2005. **7**(5): p. 190-7.
96. Warburton, M.J., et al., *Distribution of myoepithelial cells and basement membrane proteins in the resting, pregnant, lactating, and involuting rat mammary gland.* J Histochem Cytochem, 1982. **30**(7): p. 667-76.
97. Rudolph-Owen, L.A. and L.M. Matrisian, *Matrix metalloproteinases in remodeling of the normal and neoplastic mammary gland.* J Mammary Gland Biol Neoplasia, 1998. **3**(2): p. 177-89.
98. Gudjonsson, T., et al., *Normal and tumor-derived myoepithelial cells differ in their ability to interact with luminal breast epithelial cells for polarity and basement membrane deposition.* J Cell Sci, 2002. **115**(Pt 1): p. 39-50.
99. Sternlicht, M.D., et al., *The human myoepithelial cell is a natural tumor suppressor.* Clin Cancer Res, 1997. **3**(11): p. 1949-58.
100. Shao, Z.M., et al., *The human MECI exerts antiproliferative effects on breast carcinoma cells characterized by p21WAF1/CIP1 induction, G2/M arrest, and apoptosis.* Exp Cell Res, 1998. **241**(2): p. 394-403.
101. Nguyen, M., et al., *The human myoepithelial cell displays a multifaceted anti-angiogenic phenotype.* Oncogene, 2000. **19**(31): p. 3449-59.
102. Barsky, S.H. and N.J. Karlin, *Myoepithelial cells: autocrine and paracrine suppressors of breast cancer progression.* J Mammary Gland Biol Neoplasia, 2005. **10**(3): p. 249-60.
103. Sternlicht, M.D., et al., *Establishment and characterization of a novel human myoepithelial cell line and matrix-producing xenograft from a parotid basal cell adenocarcinoma.* In Vitro Cell Dev Biol Anim, 1996. **32**(9): p. 550-63.

104. Zou, Z., et al., *Maspin, a serpin with tumor-suppressing activity in human mammary epithelial cells.* Science, 1994. **263**(5146): p. 526-9.
105. Miller, F.R., et al., *MCF10DCIS.com xenograft model of human comedo ductal carcinoma in situ.* J Natl Cancer Inst, 2000. **92**(14): p. 1185-6.
106. Hu, M., et al., *Regulation of in situ to invasive breast carcinoma transition.* Cancer Cell, 2008. **13**(5): p. 394-406.
107. Foschini, M.P. and V. Eusebi, *Carcinomas of the breast showing myoepithelial cell differentiation. A review of the literature.* Virchows Arch, 1998. **432**(4): p. 303-10.
108. Angèle, S., et al., *Expression of ATM, p53, and the MRE11-Rad50-NBS1 complex in myoepithelial cells from benign and malignant proliferations of the breast.* J Clin Pathol, 2004. **57**(11): p. 1179-84.
109. Sternlicht, M.D., et al., *Characterizations of the extracellular matrix and proteinase inhibitor content of human myoepithelial tumors.* Lab Invest, 1996. **74**(4): p. 781-96.
110. Barsky, S.H., *Myoepithelial mRNA expression profiling reveals a common tumor-suppressor phenotype.* Exp Mol Pathol, 2003. **74**(2): p. 113-22.
111. Reis-Filho, J.S., et al., *Maspin expression in myoepithelial tumors of the breast.* Pathol Res Pract, 2001. **197**(12): p. 817-21.
112. Bergstraesser, L.M., et al., *Expression of hemidesmosomes and component proteins is lost by invasive breast cancer cells.* Am J Pathol, 1995. **147**(6): p. 1823-39.
113. Adams, M., et al., *Changes in tenascin-C isoform expression in invasive and preinvasive breast disease.* Cancer Res, 2002. **62**(11): p. 3289-97.
114. Allen, M.D., et al., *Altered microenvironment promotes progression of preinvasive breast cancer: myoepithelial expression of $\alpha v\beta 6$ integrin in DCIS identifies high-risk patients and predicts recurrence.* Clin Cancer Res, 2014. **20**(2): p. 344-57.
115. Tamkun, J.W., et al., *Structure of integrin, a glycoprotein involved in the transmembrane linkage between fibronectin and actin.* Cell, 1986. **46**(2): p. 271-282.
116. Hynes, R.O., *Integrins: bidirectional, allosteric signaling machines.* Cell, 2002. **110**(6): p. 673-87.
117. Takada, Y., X. Ye, and S. Simon, *The integrins.* Genome Biol, 2007. **8**(5): p. 215.
118. Barczyk, M., S. Carracedo, and D. Gullberg, *Integrins.* Cell Tissue Res, 2010. **339**(1): p. 269-80.
119. Nermut, M.V., et al., *Electron-microscopy and structural model of human fibronectin receptor.* Embo Journal, 1988. **7**(13): p. 4093-4099.
120. Springer, T.A., *Folding of the N-terminal, ligand-binding region of integrin alpha-subunits into a beta-propeller domain.* Proceedings of the National Academy of Sciences of the USA, 1997. **94**(1): p. 65-72.
121. Xiong, J.P., et al., *Crystal structure of the extracellular segment of integrin alpha v beta 3.* Science, 2001. **294**(5541): p. 339-45.

122. Luo, B.H., C.V. Carman, and T.A. Springer, *Structural basis of integrin regulation and signaling.* Annual Review of Immunol, 2007. **25**: p. 619-647.
123. Lee, J.O., et al., *Two conformations of the integrin A-domain (I-domain): a pathway for activation?* Structure, 1995. **3**(12): p. 1333-40.
124. Campbell, I.D. and M.J. Humphries, *Integrin structure, activation, and interactions.* Cold Spring Harbor Perspectives in Biology, 2011. **3**(3).
125. Liddington, R.C. and M.H. Ginsberg, *Integrin activation takes shape.* Journal of Cell Biology, 2002. **158**(5): p. 833-839.
126. Gottschalk, K.E., *A coiled-coil structure of the alpha IIb beta 3 integrin transmembrane and cytoplasmic domains in its resting state.* Structure, 2005. **13**(5): p. 703-712.
127. Adair, B.D. and M. Yeager, *Three-dimensional model of the human platelet integrin alpha IIb beta 3 based on electron cryomicroscopy and x-ray crystallography.* Proceedings of the National Academy of Sciences of the United States of America, 2002. **99**(22): p. 14059-14064.
128. Vinogradova, O., et al., *A structural basis for integrin activation by the cytoplasmic tail of the alpha IIb-subunit.* Proceedings of the National Academy of Sciences of the United States of America, 2000. **97**(4): p. 1450-1455.
129. Calderwood, D.A., et al., *Integrin beta cytoplasmic domain interactions with phosphotyrosine-binding domains: A structural prototype for diversity in integrin signaling.* Proceedings of the National Academy of Sciences of the United States of America, 2003. **100**(5): p. 2272-2277.
130. Yue, J., K. Zhang, and J. Chen, *Role of integrins in regulating proteases to mediate extracellular matrix remodeling.* Cancer Microenviron, 2012. **5**(3): p. 275-83.
131. Xiong, J.P., et al., *New insights into the structural basis of integrin activation.* Blood, 2003. **102**(4): p. 1155-1159.
132. Arnaout, M.A., S.L. Goodman, and J.P. Xiong, *Structure and mechanics of integrin-based cell adhesion.* Current Opinion in Cell Biology, 2007. **19**(5): p. 495-507.
133. Kim, C. et al., *Basic amino-acid side chains regulate transmembrane integrin signalling*. Nature, 2011. **481**(7380):209-213.
134. Lau, T.L., et al., *The structure of the integrin alpha IIb beta 3 transmembrane complex explains integrin transmembrane signalling.* Embo Journal, 2009. **28**(9): p. 1351-1361.
135. Montanez, E., et al., *Kindlin-2 controls bidirectional signaling of integrins.* Genes & Development, 2008. **22**(10): p. 1325-1330.
136. Ma, Y.Q., et al., *Kindlin-2 (Mig-2): a co-activator of beta 3 integrins.* Journal of Cell Biology, 2008. **181**(3): p. 439-446.
137. Giancotti, F.G. and E. Ruoslahti, *Transduction - Integrin signaling.* Science, 1999. **285**(5430): p. 1028-1032.
138. Kim, L.T. and K.M. Yamada, *The regulation of expression of integrin receptors.* Proceedings of the Society for Experimental Biology and Medicine, 1997. **214**(2): p. 123-131.

139. Anderson, L.R., T.W. Owens, and M.J. Naylor, *Structural and mechanical functions of integrins.* Biophys Rev, 2014. **6**(2): p. 203-213.
140. Johnson, M.S., et al., *Integrins during evolution: Evolutionary trees and model organisms.* Biochimica Et Biophysica Acta-Biomembranes, 2009. **1788**(4): p. 779-789.
141. Heino, J., et al., *Regulation of cell adhesion receptors by transforming growth factor-beta - concomitant regulation of integrins that share a common beta 1 subunit.* Journal of Biological Chemistry, 1989. **264**(1): p. 380-388.
142. Sheppard, D., et al., *Transforming growth factor beta differentially regulates expression of integrin subunits in guinea-pig airway epithelial-cells.* Journal of Biological Chemistry, 1992. **267**(24): p. 17409-17414.
143. Lambert, A.W., S. Ozturk, and S. Thiagalingam, *Integrin signaling in mammary epithelial cells and breast cancer.* ISRN Oncol, 2012. **2012**: p. 493283.
144. Taddei, I., et al., *Integrins in mammary gland development and differentiation of mammary epithelium.* J Mammary Gland Biol Neoplasia, 2003. **8**(4): p. 383-94.
145. Allen, M.D., et al., *Clinical and functional significance of $\alpha 9\beta 1$ integrin expression in breast cancer: a novel cell-surface marker of the basal phenotype that promotes tumour cell invasion.* J Pathol, 2011. **223**(5): p. 646-58.
146. Asselin-Labat, M.L., et al., *Gata-3 is an essential regulator of mammary-gland morphogenesis and luminal-cell differentiation.* Nat Cell Biol, 2007. **9**(2): p. 201-9.
147. Hall, P.A., et al., *Characterization of integrin chains in normal and neoplastic human pancreas.* J Pathol, 1991. **165**(1): p. 33-41.
148. Damjanovich, L., et al., *Distribution of integrin cell adhesion receptors in normal and malignant lung tissue.* Am J Respir Cell Mol Biol, 1992. **6**(2): p. 197-206.
149. Jones, J.L., D.R. Critchley, and R.A. Walker, *Alteration of stromal protein and integrin expression in breast--a marker of premalignant change?* J Pathol, 1992. **167**(4): p. 399-406.
150. van Duinen, C.M., et al., *The distribution of cellular adhesion molecules in pigmented skin lesions.* Cancer, 1994. **73**(8): p. 2131-9.
151. Guo, W. and F.G. Giancotti, *Integrin signalling during tumour progression.* Nat Rev Mol Cell Biol, 2004. **5**(10): p. 816-26.
152. Friedrichs, K., et al., *High expression level of alpha 6 integrin in human breast carcinoma is correlated with reduced survival.* Cancer Res, 1995. **55**(4): p. 901-6.
153. Diaz, L.K., et al., *Beta 4 integrin subunit gene expression correlates with tumor size and nuclear grade in early breast cancer.* Mod Pathol, 2005. **18**(9): p. 1165-75.

154. Meyer, T., J.F. Marshall, and I.R. Hart, *Expression of alpha v integrins and vitronectin receptor identity in breast cancer cells.* Br J Cancer, 1998. **77**(4): p. 530-6.
155. Zutter, M.M., H. Sun, and S.A. Santoro, *Altered integrin expression and the malignant phenotype: the contribution of multiple integrated integrin receptors.* J Mammary Gland Biol Neoplasia, 1998. **3**(2): p. 191-200.
156. Zutter, M.M., et al., *Re-expression of the alpha 2 beta 1 integrin abrogates the malignant phenotype of breast carcinoma cells.* Proc Natl Acad Sci U S A, 1995. **92**(16): p. 7411-5.
157. Sun, H., S.A. Santoro, and M.M. Zutter, *Downstream events in mammary gland morphogenesis mediated by reexpression of the alpha 2 beta 1 integrin: the role of the alpha 6 and beta 4 integrin subunits.* Cancer Res, 1998. **58**(10): p. 2224-33.
158. Horton, E.R., et al., *Definition of a consensus integrin adhesome and its dynamics during adhesion complex assembly and disassembly.* Nature Cell Biology, 2015. **17**(12): p. 1577-1587.
159. Huttenlocher, A. and A.R. Horwitz, *Integrins in Cell Migration.* Cold Spring Harbor Perspectives in Biology, 2011. **3**(9).
160. Zaidel-Bar, R., et al., *Early molecular events in the assembly of matrix adhesions at the leading edge of migrating cells.* Journal of Cell Science, 2003. **116**(22): p. 4605-4613.
161. Yoshigi, M., et al., *Mechanical force mobilizes zyxin from focal adhesions to actin filaments and regulates cytoskeletal reinforcement.* Journal of Cell Biology, 2005. **171**(2): p. 209-215.
162. Kaverina, I., O. Krylyshkina, and J.V. Small, *Microtubule targeting of substrate contacts promotes their relaxation and dissociation.* Journal of Cell Biology, 1999. **146**(5): p. 1033-1043.
163. Pankov, R., et al., *Integrin dynamics and matrix assembly: Tensin-dependent translocation of alpha 5 beta 1 integrins promotes fibronectin fibrillogenesis.* Journal of Cell Biology, 2000. **148**(5): p. 1075-1090.
164. Zamir, E., et al., *Molecular diversity of cell-matrix adhesions.* Journal of Cell Science, 1999. **112**(11): p. 1655-1669.
165. Linder, S., *The matrix corroded: podosomes and invadopodia in ECM degradation.* Trends in Cell Biology, 2007. **17**(3): p. 107-117.
166. Linder, S. and M. Aepfelbacher, *Podosomes: adhesion hot-spots of invasive cells.* Trends in Cell Biology, 2003. **13**(7): p. 376-385.
167. Nievers, M.G., R.Q.J. Schaapveld, and A. Sonnenberg, *Biology and function of hemidesmosomes.* Matrix Biology, 1999. **18**(1): p. 5-17.
168. Nievers, M.G., et al., *Formation of hemidesmosome-like structures in the absence of ligand binding by the alpha 6 beta 4 integrin requires binding of HD1/plectin to the cytoplasmic domain of the beta 4 integrin subunit.* Journal of Cell Science, 2000. **113**(6): p. 963-973.
169. Lee, J.L. and C.H. Streuli, *Integrins and epithelial cell polarity.* Journal of Cell Science, 2014. **127**(15): p. 3217-3225.

170. Ferrari, A., et al., *ROCK-mediated contractility, tight junctions and channels contribute to the conversion of a preapical patch into apical surface during isochoric lumen initiation.* Journal of Cell Science, 2008. **121**(21): p. 3649-3663.
171. Yu, W., et al., *Beta 1 integrin orients epithelial polarity via Rac1 and laminin.* Mol Biol Cell, 2005. **16**(2): p. 433-45.
172. Apodaca, G., L.I. Gallo, and D.M. Bryant, *Role of membrane traffic in the generation of epithelial cell asymmetry.* Nature Cell Biology, 2012. **14**(12): p. 1235-1243.
173. Macara, I.G., *Parsing the polarity code.* Nature Reviews Molecular Cell Biology, 2004. **5**(3): p. 220-231.
174. Cohen, D., et al., *Mammalian PAR-1 determines epithelial lumen polarity by organizing the microtubule cytoskeleton.* Journal of Cell Biology, 2004. **164**(5): p. 717-727.
175. Lauffenburger, D.A. and A.F. Horwitz, *Cell migration: A physically integrated molecular process.* Cell, 1996. **84**(3): p. 359-369.
176. Ridley, A.J., et al., *Cell migration: Integrating signals from front to back.* Science, 2003. **302**(5651): p. 1704-1709.
177. Vicente-Manzanares, M., D.J. Webb, and A.R. Horwitz, *Cell migration at a glance.* Journal of Cell Science, 2005. **118**(21).
178. Vicente-Manzanares, M., C.K. Choi, and A.R. Horwitz, *Integrins in cell migration - the actin connection.* Journal of Cell Science, 2009. **122**(2): p. 199-206.
179. Ballestrem, C., et al., *Marching at the front and dragging behind: differential alpha v beta 3 integrin turnover regulates focal adhesion behavior.* Journal of Cell Biology, 2001. **155**(7): p. 1319-1332.
180. Li, S.H., et al., *The role of laminin in embryonic cell polarization and tissue organization.* Developmental Cell, 2003. **4**(5): p. 613-624.
181. Schwarzbauer, J.E. and J.L. Sechler, *Fibronectin fibrillogenesis: a paradigm for extracellular matrix assembly.* Current Opinion in Cell Biology, 1999. **11**(5): p. 622-627.
182. Kessenbrock, K., V. Plaks, and Z. Werb, *Matrix metalloproteinases: regulators of the tumor microenvironment.* Cell, 2010. **141**(1): p. 52-67.
183. Thomas, G.J., et al., *alpha v beta 6 Integrin upregulates matrix metalloproteinase 9 and promotes migration of normal oral keratinocytes.* J Invest Dermatol, 2001. **116**(6): p. 898-904.
184. Li, X., et al., *Alpha v beta 6-Fyn signaling promotes oral cancer progression.* J Biol Chem, 2003. **278**(43): p. 41646-53.
185. Gu, X., et al., *Integrin alpha v beta 6-associated ERK2 mediates MMP9 secretion in colon cancer cells.* Br J Cancer, 2002. **87**(3): p. 348-51.
186. Ahmed, N., et al., *Overexpression of alpha v beta 6 integrin in serous epithelial ovarian cancer regulates extracellular matrix degradation via the plasminogen activation cascade.* Carcinogenesis, 2002. **23**(2): p. 237-44.

187. Baum, O., et al., *Increased invasive potential and up-regulation of MMP2 in MDA-MB-231 breast cancer cells expressing the beta 3 integrin subunit.* Int J Oncol, 2007. **30**(2): p. 325-32.
188. Iyer, V., K. Pumiglia, and C.M. DiPersio, *Alpha 3 beta 1 integrin regulates MMP9 mRNA stability in immortalized keratinocytes: a novel mechanism of integrin-mediated MMP gene expression.* J Cell Sci, 2005. **118**(Pt 6): p. 1185-95.
189. Lamar, J.M., V. Iyer, and C.M. DiPersio, *Integrin alpha 3 beta 1 potentiates TGFbeta-mediated induction of MMP9 in immortalized keratinocytes.* J Invest Dermatol, 2008. **128**(3): p. 575-86.
190. Brooks, P.C., et al., *Localization of matrix metalloproteinase MMP2 to the surface of invasive cells by interaction with integrin alpha v beta 3.* Cell, 1996. **85**(5): p. 683-93.
191. Rolli, M., et al., *Activated integrin alpha v beta 3 cooperates with metalloproteinase MMP9 in regulating migration of metastatic breast cancer cells.* Proc Natl Acad Sci U S A, 2003. **100**(16): p. 9482-7.
192. Brooks, P.C., et al., *Disruption of angiogenesis by PEX, a noncatalytic metalloproteinase fragment with integrin binding activity.* Cell, 1998. **92**(3): p. 391-400.
193. Massagué, J., *TGFβ signalling in context.* Nat Rev Mol Cell Biol, 2012. **13**(10): p. 616-30.
194. Wakefield, L.M. and C.S. Hill, *Beyond TGFβ: roles of other TGFβ superfamily members in cancer.* Nat Rev Cancer, 2013. **13**(5): p. 328-41.
195. Horiguchi, M., M. Ota, and D.B. Rifkin, *Matrix control of transforming growth factor-β function.* J Biochem, 2012. **152**(4): p. 321-9.
196. Dubois, C.M., et al., *Processing of Transforming growth factor beta-1 precursor by human furin convertase.* Journal of Biological Chemistry, 1995. **270**(18): p. 10618-10624.
197. Lawrence, D.A., et al., *Normal embryo fibroblasts release transforming growth-factors in a latent form.* Journal of Cellular Physiology, 1984. **121**(1): p. 184-188.
198. Miyazono, K., et al., *Latent high molecular-weight complex of transforming growth factor beta-1: purification and structural characterization.* Journal of Biological Chemistry, 1988. **263**(13): p. 6407-6415.
199. Dallas, S.L., et al., *Characterization and autoregulation of latent transforming growth-factor-beta (TGFβ) omplexes in osteoblast-like cell-lines - production of a latent complex lacking the latent TGF-beta-binding protein.* Journal of Biological Chemistry, 1994. **269**(9): p. 6815-6822.
200. Todorovic, V. and D.B. Rifkin, *LTBPs, more than just an escort service.* J Cell Biochem, 2012. **113**(2): p. 410-8.
201. Rifkin, D.B., *Latent transforming growth factor-β binding proteins: orchestrators of TGF-β availability.* J Biol Chem, 2005. **280**(9): p. 7409-12.

202. Zilberberg, L., et al., *Specificity of latent TGF-β binding protein (LTBP) incorporation into matrix: role of fibrillins and fibronectin.* J Cell Physiol, 2012. **227**(12): p. 3828-36.
203. Chaudhry, S.S., et al., *Fibrillin-1 regulates the bioavailability of TGFbeta1.* J Cell Biol, 2007. **176**(3): p. 355-67.
204. Annes, J.P., J.S. Munger, and D.B. Rifkin, *Making sense of latent TGFbeta activation.* J Cell Sci, 2003. **116**(Pt 2): p. 217-24.
205. Ge, G. and D.S. Greenspan, *BMP1 controls TGFβ1 activation via cleavage of latent TGFbeta-binding protein.* J Cell Biol, 2006. **175**(1): p. 111-20.
206. Munger, J.S. and D. Sheppard, *Cross talk among TGF-β signaling pathways, integrins, and the extracellular matrix.* Cold Spring Harb Perspect Biol, 2011. **3**(11): p. a005017.
207. Annes, J.P., et al., *Integrin alphaVbeta6-mediated activation of latent TGF-beta requires the latent TGF-beta binding protein-1.* J Cell Biol, 2004. **165**(5): p. 723-34.
208. Fontana, L., et al., *Fibronectin is required for integrin alpha v beta 6-mediated activation of latent TGF-beta complexes containing LTBP-1.* FASEB J, 2005. **19**(13): p. 1798-808.
209. Wipff, P.J., et al., *Myofibroblast contraction activates latent TGF-beta1 from the extracellular matrix.* J Cell Biol, 2007. **179**(6): p. 1311-23.
210. Munger, J.S., et al., *The integrin alpha v beta 6 binds and activates latent TGF beta 1: a mechanism for regulating pulmonary inflammation and fibrosis.* Cell, 1999. **96**(3): p. 319-28.
211. Shi, F. and J. Sottile, *MT1-MMP regulates the turnover and endocytosis of ECM fibronectin.* Journal of Cell Science, 2011. **124**(23): p. 4039-4050.
212. Klingberg, F., et al., *Prestress in the extracellular matrix sensitizes latent TGF-β1 for activation.* J Cell Biol, 2014. **207**(2): p. 283-97.
213. Mu, D., et al., *The integrin alpha v beta 8 mediates epithelial homeostasis through MT1-MMP-dependent activation of TGF-beta1.* J Cell Biol, 2002. **157**(3): p. 493-507.
214. Shi, Y. and J. Massagué, *Mechanisms of TGF-beta signaling from cell membrane to the nucleus.* Cell, 2003. **113**(6): p. 685-700.
215. Massagué, J., *TGF-beta signal transduction.* Annu Rev Biochem, 1998. **67**: p. 753-91.
216. Moustakas, A., et al., *The transforming growth factor beta receptors types I, II, and III form hetero-oligomeric complexes in the presence of ligand.* J Biol Chem, 1993. **268**(30): p. 22215-8.
217. Wrana, J.L., et al., *Mechanism of activation of the TGF-beta receptor.* Nature, 1994. **370**(6488): p. 341-7.
218. Xu, L. and J. Massagué, *Nucleocytoplasmic shuttling of signal transducers.* Nat Rev Mol Cell Biol, 2004. **5**(3): p. 209-19.
219. Massagué, J. and Y.G. Chen, *Controlling TGF-beta signaling.* Genes Dev, 2000. **14**(6): p. 627-44.

220. Derynck, R., Y. Zhang, and X.H. Feng, *Smads: transcriptional activators of TGF-beta responses.* Cell, 1998. **95**(6): p. 737-40.
221. Feng, X.H. and R. Derynck, *Specificity and versatility in TGF-beta signaling through Smads.* Annual Review of Cell and Developmental Biology, 2005. **21**: p. 659-693.
222. Derynck, R. and Y.E. Zhang, *Smad-dependent and -independent pathways in TGFβ family signalling.* Nature, 2003. **425**(6958): p. 577-84.
223. Moustakas, A. and C.H. Heldin, *Non-Smad TGF-beta signals.* J Cell Sci, 2005. **118**(Pt 16): p. 3573-84.
224. Zhang, Y.E., *Non-Smad pathways in TGF-beta signaling.* Cell Research, 2009. **19**(1): p. 128-139.
225. Margadant, C. and A. Sonnenberg, *Integrin-TGF-beta crosstalk in fibrosis, cancer and wound healing.* EMBO Rep, 2010. **11**(2): p. 97-105.
226. Tsukazaki, T., et al., *SARA, a FYVE domain protein that recruits Smad2 to the TGF beta receptor.* Cell, 1998. **95**(6): p. 779-791.
227. Watanabe, Y., et al., *TMEPAI, a Transmembrane TGF-beta-Inducible Protein, Sequesters Smad Proteins from Active Participation in TGF-beta Signaling.* Molecular Cell, 2010. **37**(1): p. 123-134.
228. Liu, T. and X.H. Feng, *Regulation of TGF-beta signalling by protein phosphatases.* Biochemical Journal, 2010. **430**: p. 191-198.
229. Lo, R.S. and J. Massague, *Ubiquitin-dependent degradation of TGF-beta-activated Smad2.* Nature Cell Biology, 1999. **1**(8): p. 472-478.
230. Gao, S., et al., *Ubiquitin Ligase Nedd4L Targets Activated Smad2/3 to Limit TGF-beta Signaling.* Molecular Cell, 2009. **36**(3): p. 457-468.
231. Afrakhte, M., et al., *Induction of inhibitory Smad6 and Smad7 mRNA by TGF-beta family members.* Biochemical and Biophysical Research Communications, 1998. **249**(2): p. 505-511.
232. Imamura, T., et al., *Smad6 inhibits signalling by the TGF-beta superfamily.* Nature, 1997. **389**(6651): p. 622-626.
233. Hayashi, H., et al., *The MAD-related protein Smad7 associates with the TGFbeta receptor and functions as an antagonist of TGFbeta signaling.* Cell, 1997. **89**(7): p. 1165-73.
234. Kavsak, P., et al., *Smad7 binds to Smurf2 to form an E3 ubiquitin ligase that targets the TGF beta receptor for degradation.* Molecular Cell, 2000. **6**(6): p. 1365-1375.
235. Di Guglielmo, G.M., et al., *Distinct endocytic pathways regulate TGFβR signalling and turnover.* Nature Cell Biology, 2003. **5**(5): p. 410-421.
236. Hayes, S., A. Chawla, and S. Corvera, *TGF beta receptor internalization into EEA1-enriched early endosomes: role in signaling to Smad2.* Journal of Cell Biology, 2002. **158**(7): p. 1239-1249.
237. Penheiter, S.G., et al., *Internalization-dependent and -independent requirements for TGFβ receptor signaling via the Smad pathway.* Molecular and Cellular Biology, 2002. **22**(13): p. 4750-4759.

238. Pickup, M., S. Novitskiy, and H.L. Moses, *The roles of TGFβ in the tumour microenvironment.* Nat Rev Cancer, 2013. **13**(11): p. 788-99.
239. Markowitz, S., et al., *Inactivation of the Type-II TGF-beta receptor in colon-cancer cells with microsatellite instability.* Science, 1995. **268**(5215): p. 1336-1338.
240. Wang, D., et al., *Analysis of specific gene mutations in the transforming growth factor-beta signal transduction pathway in human ovarian cancer.* Cancer Research, 2000. **60**(16): p. 4507-4512.
241. Goggins, M., et al., *Genetic alterations of the transforming growth factor beta receptor genes in pancreatic and biliary adenocarcinomas.* Cancer Research, 1998. **58**(23): p. 5329-5332.
242. Chen, T.P., et al., *Transforming growth factor beta type I receptor kinase mutant associated with metastatic breast cancer.* Cancer Research, 1998. **58**(21): p. 4805-4810.
243. Bornstein, S., et al., *Smad4 loss in mice causes spontaneous head and neck cancer with increased genomic instability and inflammation.* Journal of Clinical Investigation, 2009. **119**(11): p. 3408-3419.
244. Derynck, R., R.J. Akhurst, and A. Balmain, *TGF-beta signaling in tumor suppression and cancer progression.* Nature Genetics, 2001. **29**(2): p. 117-129.
245. Feng, X.H., X. Lin, and R. Derynck, *Smad2, Smad3 and Smad4 cooperate with Sp1 to induce p15(Ink4B) transcription in response to TGF-beta.* EMBO J, 2000. **19**(19): p. 5178-93.
246. Gomis, R.R., et al., *A FoxO-Smad synexpression group in human keratinocytes.* Proceedings of the National Academy of Sciences of the United States of America, 2006. **103**(34): p. 12747-12752.
247. Pardali, K., et al., *Role of smad proteins and transcription factor Sp1 in p21(Wafl/Cip1) regulation by transforming growth factor-beta.* Journal of Biological Chemistry, 2000. **275**(38): p. 29244-29256.
248. Siegel, P.M. and J. Massague, *Cytostatic and apoptotic actions of TGF-beta in homeostasis and cancer.* Nature Reviews Cancer, 2003. **3**(11): p. 807-820.
249. Scandura, J.M., et al., *Transforming growth factor beta-induced cell cycle arrest of human hematopoietic cells requires p57KIP2 up-regulation.* Proceedings of the National Academy of Sciences of the United States of America, 2004. **101**(42): p. 15231-15236.
250. Staller, P., et al., *Repression of p15(INK4b) expression by Myc through association with Miz-1.* Nature Cell Biology, 2001. **3**(4): p. 392-399.
251. Seoane, J., et al., *TGF beta influences Myc, Miz-1 and Smad to control the CDK inhibitor p15(INK4b).* Nature Cell Biology, 2001. **3**(4): p. 400-408.
252. Seoane, J., H.V. Le, and J. Massague, *Myc suppression of the p21(Cip1) Cdk inhibitor influences the outcome of the p53 response to DNA damage.* Nature, 2002. **419**(6908): p. 729-734.
253. Lebrun, J.J., *The dual role of TGFbeta in human cancer: from tumor suppression to cancer metastasis.* ISRN Mol Biol, 2012. **2012**: p. 381428.

254. Kim, S.G., et al., *Transforming growth factor-beta 1 induces apoptosis through Fas ligand-independent activation of the Fas death pathway in human gastric SNU-620 carcinoma cells.* Molecular Biology of the Cell, 2004. **15**(2): p. 420-434.
255. Yoo, J.Y., et al., *Transforming growth factor-beta-induced apoptosis is mediated by SMad-dependent expression of GADD45b through p38 activation.* Journal of Biological Chemistry, 2003. **278**(44): p. 43001-43007.
256. Ohgushi, M., et al., *Transforming growth factor beta-dependent sequential activation of Smad, Bim, and caspase-9 mediates physiological apoptosis in gastric epithelial cells.* Molecular and Cellular Biology, 2005. **25**(22): p. 10017-10028.
257. Jang, C.W., et al., *TGF-beta induces apoptosis through Smad-mediated expression of DAP-kinase.* Nature Cell Biology, 2002. **4**(1): p. 51-58.
258. Katz, L.H., et al., *Targeting TGF-beta signaling in cancer.* Expert Opinion on Therapeutic Targets, 2013. **17**(7): p. 743-760.
259. Tsushima, H., et al., *High levels of transforming growth factor beta 1 in patients with colorectal cancer: Association with disease progression.* Gastroenterology, 1996. **110**(2): p. 375-382.
260. Wikstrom, P., et al., *Transforming growth factor beta 1 is associated with angiogenesis, metastasis, and poor clinical outcome in prostate cancer.* Prostate, 1998. **37**(1): p. 19-29.
261. Friedman, E., et al., *High-levels of transforming growth-factor-beta-1 correlate with disease progression in human colon-cancer.* Cancer Epidemiology Biomarkers & Prevention, 1995. **4**(5): p. 549-554.
262. Walker, R.A. and S.J. Dearing, *Transforming growth factor beta 1 in ductal carcinoma in situ and invasive carcinomas of the breast.* Eur J Cancer, 1992. **28**(2-3): p. 641-4.
263. Picon, A., et al., *A subset of metastatic human colon cancers expresses elevated levels of transforming growth factor beta1.* Cancer Epidemiol Biomarkers Prev, 1998. **7**(6): p. 497-504.
264. Dalal, B.I., P.A. Keown, and A.H. Greenberg, *Immunocytochemical localization of secreted transforming growth factor-beta 1 to the advancing edges of primary tumors and to lymph node metastases of human mammary carcinoma.* Am J Pathol, 1993. **143**(2): p. 381-9.
265. Lamouille, S., J. Xu, and R. Derynck, *Molecular mechanisms of epithelial-mesenchymal transition.* Nat Rev Mol Cell Biol, 2014. **15**(3): p. 178-96.
266. Moustakas, A. and C.H. Heldin, *Signaling networks guiding epithelial-mesenchymal transitions during embryogenesis and cancer progression.* Cancer Science, 2007. **98**(10): p. 1512-1520.
267. Xu, J., S. Lamouille, and R. Derynck, *TGF-beta-induced epithelial to mesenchymal transition.* Cell Research, 2009. **19**(2): p. 156-172.
268. Huber, M.A., N. Kraut, and H. Beug, *Molecular requirements for epithelial-mesenchymal transition during tumor progression.* Current Opinion in Cell Biology, 2005. **17**(5): p. 548-558.

269. Yin, J.J., et al., *TGF-beta signaling blockade inhibits PTHrP secretion by breast cancer cells and bone metastases development.* Journal of Clinical Investigation, 1999. **103**(2): p. 197-206.
270. Guise, T.A., et al., *Evidence for a causal role of parathyroid hormone-related protein in the pathogenesis of human breast cancer-mediated osteolysis.* Journal of Clinical Investigation, 1996. **98**(7): p. 1544-1549.
271. Kondo, H., J. Guo, and F.R. Bringhurst, *Cyclic adenosine monophosphate/protein kinase A mediates parathyroid hormone/parathyroid hormone-related protein receptor regulation of osteoclastogenesis and expression of RANKL and osteoprotegerin mRNAs by marrow stromal cells.* Journal of Bone and Mineral Research, 2002. **17**(9): p. 1667-1679.
272. Kakonen, S.M., et al., *Transforming growth factor-beta stimulates parathyroid hormone-related protein and osteolytic metastases via Smad and mitogen-activated protein kinase signaling pathways.* Journal of Biological Chemistry, 2002. **277**(27): p. 24571-24578.
273. Xu, C., et al., *Co-expression of parathyroid hormone related protein and TGF-beta in breast cancer predicts poor survival outcome.* Bmc Cancer, 2015. **15**.
274. De Jong, J.S., et al., *Expression of growth factors, growth-inhibiting factors, and their receptors in invasive breast cancer: Correlations with proliferation and angiogenesis.* Journal of Pathology, 1998. **184**(1): p. 53-57.
275. Hasegawa, Y., et al., *Transforming growth factor-beta 1 level correlates with angiogenesis, tumor progression, and prognosis in patients with nonsmall cell lung carcinoma.* Cancer, 2001. **91**(5): p. 964-971.
276. Ito, N., et al., *Positive Correlation of Plasma Transforming Growth-Factor-Beta-1 Levels with Tumor Vascularity in Hepatocellular-Carcinoma.* Cancer Letters, 1995. **89**(1): p. 45-48.
277. Pertovaara, L., et al., *Vascular Endothelial Growth-Factor Is Induced in Response to TGFβ in Fibroblastic and Epithelial-Cells.* Journal of Biological Chemistry, 1994. **269**(9): p. 6271-6274.
278. Kang, Y.B., et al., *A multigenic program mediating breast cancer metastasis to bone.* Cancer Cell, 2003. **3**(6): p. 537-549.
279. Sanchez-Elsner, T., et al., *Synergistic cooperation between hypoxia and transforming growth factor-beta pathways on human vascular endothelial growth factor gene expression.* Journal of Biological Chemistry, 2001. **276**(42): p. 38527-38535.
280. Shimo, T., et al., *Involvement of CTGF, a hypertrophic chondrocyte-specific gene product, in angiogenesis.* Oncology, 2001. **61**(4): p. 315-322.
281. Madri, J.A., B.M. Pratt, and A.M. Tucker, *Phenotypic modulation of endothelial-cells by transforming growth factor-beta depends upon the composition and organization of the extracellular-matrix.* Journal of Cell Biology, 1988. **106**(4): p. 1375-1384.

282. Sunderkotter, C., et al., *Macrophage-derived angiogenesis factors.* Pharmacology & Therapeutics, 1991. **51**(2): p. 195-216.
283. Hagedorn, H.G., B.E. Bachmeier, and A.G. Nerlich, *Synthesis and degradation of basement membranes and extracellular matrix and their regulation by TGF-beta in invasive carcinomas (Review).* International Journal of Oncology, 2001. **18**(4): p. 669-681.
284. Enholm, B., et al., *Comparison of VEGF, VEGF-B, VEGF-C and Ang-1 mRNA regulation by serum, growth factors, oncoproteins and hypoxia.* Oncogene, 1997. **14**(20): p. 2475-2483.
285. De Wever, O., et al., *Stromal myofibroblasts are drivers of invasive cancer growth.* International Journal of Cancer, 2008. **123**(10): p. 2229-2238.
286. Desmouliere, A., C. Guyot, and C. Gabbiani, *The stroma reaction myofibroblast: a key player in the control of tumor cell behavior.* International Journal of Developmental Biology, 2004. **48**(5-6): p. 509-517.
287. Kalluri, R. and M. Zeisberg, *Fibroblasts in cancer.* Nature Reviews Cancer, 2006. **6**(5): p. 392-401.
288. Lu, P., et al., *Extracellular matrix degradation and remodeling in development and disease.* Cold Spring Harb Perspect Biol, 2011. **3**(12).
289. Bonnans, C., J. Chou, and Z. Werb, *Remodelling the ECM in development and disease.* Nat Rev Mol Cell Biol, 2014. **15**(12): p. 786-801.
290. Cox, T.R. and J.T. Erler, *Remodeling and homeostasis of the extracellular matrix: implications for fibrotic diseases and cancer.* Dis Model Mech, 2011. **4**(2): p. 165-78.
291. Butcher, D.T., T. Alliston, and V.M. Weaver, *A tense situation: forcing tumour progression.* Nature Reviews Cancer, 2009. **9**(2): p. 108-122.
292. Provenzano, P.P., et al., *Collagen density promotes mammary tumor initiation and progression.* Bmc Medicine, 2008. **6**.
293. Frantz, C., K.M. Stewart, and V.M. Weaver, *The extracellular matrix at a glance.* Journal of Cell Science, 2010. **123**(24): p. 4195-4200.
294. Lu, P.F., V.M. Weaver, and Z. Werb, *The extracellular matrix: A dynamic niche in cancer progression.* Journal of Cell Biology, 2012. **196**(4): p. 395-406.
295. Insua-Rodriguez, J. and T. Oskarsson, *The extracellular matrix in breast cancer.* Advanced Drug Delivery Reviews, 2016. **97**: p. 41-55.
296. Bergamaschi, A., et al., *Extracellular matrix signature identifies breast cancer subgroups with different clinical outcome.* Journal of Pathology, 2008. **214**(3): p. 357-367.
297. Naba, A., et al., *The matrisome: in silico definition and in vivo characterization by proteomics of normal and tumor extracellular matrices.* Molecular & Cellular Proteomics, 2012. **11**(4).
298. Pickup, M.W., J.K. Mouw, and V.M. Weaver, *The extracellular matrix modulates the hallmarks of cancer.* Embo Reports, 2014. **15**(12): p. 1243-1253.
299. Paszek, M.J., et al., *Tensional homeostasis and the malignant phenotype.* Cancer Cell, 2005. **8**(3): p. 241-54.

300. Levental, K.R., et al., *Matrix crosslinking forces tumor progression by enhancing integrin signaling.* Cell, 2009. **139**(5): p. 891-906.
301. Evans, A., et al., *Invasive breast cancer: relationship between shear-wave elastographic findings and histologic prognostic factors.* Radiology, 2012. **263**(3): p. 673-677.
302. Plodinec, M., et al., *The nanomechanical signature of breast cancer.* Nature Nanotechnology, 2012. **7**(11): p. 757-765.
303. Yi, A., et al., *Association of tumour stiffness on sonoelastography with axillary nodal status in T1 breast carcinoma patients.* European Radiology, 2013. **23**(11): p. 2979-2987.
304. Fenner, J., et al., *Macroscopic stiffness of breast tumors predicts metastasis.* Scientific Reports, 2014. **4**.
305. Acerbi, I., et al., *Human breast cancer invasion and aggression correlates with ECM stiffening and immune cell infiltration.* Integrative Biology, 2015. **7**(10): p. 1120-1134.
306. Lopez, J.I., et al., *In situ force mapping of mammary gland transformation.* Integrative Biology, 2011. **3**(9): p. 910-921.
307. Schedin, P. and P.J. Keely, *Mammary gland ECM remodeling, stiffness, and mechanosignaling in normal development and tumor progression.* Cold Spring Harb Perspect Biol, 2011. **3**(1): p. a003228.
308. Provenzano, P.P., et al., *Collagen reorganization at the tumor-stromal interface facilitates local invasion.* Bmc Medicine, 2006. **4**.
309. Hinz, B., *The myofibroblast: Paradigm for a mechanically active cell.* Journal of Biomechanics, 2010. **43**(1): p. 146-155.
310. Shi, F., et al., *Collagen I matrix turnover is regulated by fibronectin polymerization.* American Journal of Physiology-Cell Physiology, 2010. **298**(5): p. C1265-C1275.
311. Koukoulis, G.K., et al., *Distribution of tenascin, cellular fibronectins and integrins in the normal, hyperplastic and neoplastic breast.* J Submicrosc Cytol Pathol, 1993. **25**(2): p. 285-95.
312. Paszek, M.J. and V.M. Weaver, *The tension mounts: mechanics meets morphogenesis and malignancy.* J Mammary Gland Biol Neoplasia, 2004. **9**(4): p. 325-42.
313. Christensen, L., *The distribution of fibronectin, laminin and tetranectin in human breast cancer with special attention to the extracellular matrix.* APMIS Suppl, 1992. **26**: p. 1-39.
314. Ioachim, E., et al., *Immunohistochemical expression of extracellular matrix components tenascin, fibronectin, collagen type IV and laminin in breast cancer: their prognostic value and role in tumour invasion and progression.* European Journal of Cancer, 2002. **38**(18): p. 2362-2370.
315. Kadar, A., et al., *Extracellular matrix components in breast carcinomas.* Seminars in Cancer Biology, 2002. **12**(3): p. 243-257.
316. Vasaturo, F., et al., *Comparison of extracellular matrix and apoptotic markers between benign lesions and carcinomas in human breast.* International Journal of Oncology, 2005. **27**(4): p. 1005-1011.

317. Hao, X., et al., *Differential gene and protein expression in primary breast malignancies and their lymph node metastases as revealed by combined cDNA microarray and tissue microarray analysis.* Cancer, 2004. **100**(6): p. 1110-22.
318. Helleman, J., et al., *Association of an extracellular matrix gene cluster with breast cancer prognosis and endocrine therapy response.* Clinical Cancer Research, 2008. **14**(17): p. 5555-5564.
319. Bae, Y.K., et al., *Fibronectin expression in carcinoma cells correlates with tumor aggressiveness and poor clinical outcome in patients with invasive breast cancer.* Human Pathology, 2013. **44**(10): p. 2028-2037.
320. Barkan, D., J.E. Green, and A.F. Chambers, *Extracellular matrix: A gatekeeper in the transition from dormancy to metastatic growth.* European Journal of Cancer, 2010. **46**(7): p. 1181-1188.
321. Sceneay, J., M.J. Smyth, and A. Moller, *The pre-metastatic niche: finding common ground.* Cancer and Metastasis Reviews, 2013. **32**(3-4): p. 449-464.
322. Yao, E.S., et al., *Increased beta 1 integrin is associated with decreased survival in invasive breast cancer.* Cancer Research, 2007. **67**(2): p. 659-664.
323. To, W.S. and K.S. Midwood, *Plasma and cellular fibronectin: distinct and independent functions during tissue repair.* Fibrogenesis Tissue Repair, 2011. **4**: p. 21.
324. White, E.S., F.E. Baralle, and A.F. Muro, *New insights into form and function of fibronectin splice variants.* J Pathol, 2008. **216**(1): p. 1-14.
325. White, E.S. and A.F. Muro, *Fibronectin splice variants: understanding their multiple roles in health and disease using engineered mouse models.* IUBMB Life, 2011. **63**(7): p. 538-46.
326. Chauhan, A.K., et al., *Alternative splicing of fibronectin: a mouse model demonstrates the identity of in vitro and in vivo systems and the processing autonomy of regulated exons in adult mice.* Gene, 2004. **324**: p. 55-63.
327. Schwarzbauer, J.E. and D.W. DeSimone, *Fibronectins, their fibrillogenesis, and in vivo functions.* Cold Spring Harb Perspect Biol, 2011. **3**(7).
328. Pankov, R. and K.M. Yamada, *Fibronectin at a glance.* J Cell Sci, 2002. **115**(Pt 20): p. 3861-3.
329. Natali, P.G., et al., *Expression of fibronectin, fibronectin isoforms and integrin receptors in melanocytic lesions.* Br J Cancer, 1995. **71**(6): p. 1243-7.
330. Albrecht, M., et al., *Fibronectin in human prostatic cells in vivo and in vitro: expression, distribution, and pathological significance.* Histochem Cell Biol, 1999. **112**(1): p. 51-61.
331. Oyama, F., et al., *Coordinate oncodevelopmental modulation of alternative splicing of fibronectin pre-messenger RNA at ED-A, ED-B, and CS1 regions in human liver tumors.* Cancer Res, 1993. **53**(9): p. 2005-11.

332. Schwarzbauer, J.E., *Identification of the fibronectin sequences required for assembly of a fibrillar matrix.* J Cell Biol, 1991. **113**(6): p. 1463-73.
333. Leiss, M., et al., *The role of integrin binding sites in fibronectin matrix assembly in vivo.* Curr Opin Cell Biol, 2008. **20**(5): p. 502-7.
334. Dallas, S.L., Q. Chen, and P. Sivakumar, *Dynamics of assembly and reorganization of extracellular matrix proteins.* Curr Top Dev Biol, 2006. **75**: p. 1-24.
335. Larsen, M., et al., *The matrix reorganized: extracellular matrix remodeling and integrin signaling.* Curr Opin Cell Biol, 2006. **18**(5): p. 463-71.
336. Schwarzbauer, J.E., *Alternative splicing of fibronectin: three variants, three functions.* Bioessays, 1991. **13**(10): p. 527-33.
337. Singh, P., C. Carraher, and J.E. Schwarzbauer, *Assembly of fibronectin extracellular matrix.* Annu Rev Cell Dev Biol, 2010. **26**: p. 397-419.
338. Leahy, D.J., I. Aukhil, and H.P. Erickson, *2.0 angstrom crystal structure of a four-domain segment of human fibronectin encompassing the RGD loop and synergy region.* Cell, 1996. **84**(1): p. 155-164.
339. Krammer, A., et al., *A structural model for force regulated integrin binding to fibronectin's RGD-synergy site.* Matrix Biology, 2002. **21**(2): p. 139-147.
340. Bachman, H., et al., *Utilizing Fibronectin Integrin-Binding Specificity to Control Responses.* Advances in Wound Care, 2015. **4**(8): p. 501-511.
341. Carnemolla, B., et al., *The Inclusion of the Type-III repeat ED-B in the fibronectin molecule generates conformational modifications that unmask a cryptic sequence.* Journal of Biological Chemistry, 1992. **267**(34): p. 24689-24692.
342. Schwarzbauer, J.E., C.S. Spencer, and C.L. Wilson, *Selective Secretion of alternatively spliced fibronectin variants.* Journal of Cell Biology, 1989. **109**(6): p. 3445-3453.
343. Ffrenchconstant, C. and R.O. Hynes, *Alternative splicing of fibronectin is temporally and spatially regulated in the chicken-embryo.* Development, 1989. **106**(2): p. 375-388.
344. Oyama, F., et al., *Patterns of alternative splicing of fibronectin pre-mRNA in human adult and fetal tissues.* Biochemistry, 1989. **28**(3): p. 1428-34.
345. Rybak, J.N., et al., *The extra-domain A of fibronectin is a vascular marker of solid tumors and metastases.* Cancer Res, 2007. **67**(22): p. 10948-57.
346. Astrof, S., et al., *Direct test of potential roles of EIIIA and EIIIB alternatively spliced segments of fibronectin in physiological and tumor angiogenesis.* Molecular and Cellular Biology, 2004. **24**(19): p. 8662-8670.
347. Astrof, S., D. Crowley, and R.O. Hynes, *Multiple cardiovascular defects caused by the absence of alternatively spliced segments of fibronectin.* Developmental Biology, 2007. **311**(1): p. 11-24.
348. Mcdonald, J.A., et al., *Fibronectin cell-adhesive domain and an amino-terminal matrix assembly domain participate in its assembly into fibroblast pericellular matrix.* Journal of Biological Chemistry, 1987. **262**(7): p. 2957-2967.

349. Fogerty, F.J., et al., *Inhibition of binding of fibronectin to matrix assembly sites by anti-integrin (alpha 5 beta 1) antibodies.* Journal of Cell Biology, 1990. **111**(2): p. 699-708.
350. Wu, C.Y., A.E. Chung, and J.A. Mcdonald, *A novel role for alpha 3 beta 1 integrins in extracellular-matrix assembly.* Journal of Cell Science, 1995. **108**: p. 2511-2523.
351. Sechler, J.L., et al., *A novel RGD-independent fibronectin assembly pathway initiated by alpha 4 beta 1 integrin binding to the alternatively spliced V region.* Journal of Cell Science, 2000. **113**(8): p. 1491-1498.
352. Yang, J.T. and R.O. Hynes, *Fibronectin receptor functions in embryonic cells deficient in alpha 5 beta 1 integrin can be replaced by alpha v integrins.* Molecular Biology of the Cell, 1996. **7**(11): p. 1737-1748.
353. Wu, C.Y., et al., *Identification of a new biological function for the integrin alpha v beta 3:: Initiation of fibronectin matrix assembly.* Cell Adhesion and Communication, 1996. **4**(3): p. 149-158.
354. Johansson, S., et al., *Fibronectin-integrin interactions.* Front Biosci, 1997. **2**: p. d126-46.
355. Olorundare, O.E., et al., *Assembly of a fibronectin matrix by adherent platelets stimulated by lysophosphatidic acid and other agonists.* Blood, 2001. **98**(1): p. 117-24.
356. Zhong, C.L., et al., *Rho-mediated contractility exposes a cryptic site in fibronectin and induces fibronectin matrix assembly.* Journal of Cell Biology, 1998. **141**(2): p. 539-551.
357. Wierzbicka-Patynowski, I. and J.E. Schwarzbauer, *The ins and outs of fibronectin matrix assembly.* J Cell Sci, 2003. **116**(Pt 16): p. 3269-76.
358. Mao, Y. and J.E. Schwarzbauer, *Fibronectin fibrillogenesis, a cell-mediated matrix assembly process.* Matrix Biol, 2005. **24**(6): p. 389-99.
359. Mckeownlongo, P.J. and D.F. Mosher, *Binding of plasma fibronectin to cell-layers of human-skin fibroblasts.* Journal of Cell Biology, 1983. **97**(2): p. 466-472.
360. Sottile, J. and D.C. Hocking, *Fibronectin polymerization regulates the composition and stability of extracellular matrix fibrils and cell-matrix adhesions.* Molecular Biology of the Cell, 2002. **13**(10): p. 3546-3559.
361. Shi, F. and J. Sottile, *Caveolin-1-dependent beta 1 integrin endocytosis is a critical regulator of fibronectin turnover.* Journal of Cell Science, 2008. **121**(14): p. 2360-2371.
362. Sottile, J. and J. Chandler, *Fibronectin matrix turnover occurs through a caveolin-1-dependent process.* Molecular Biology of the Cell, 2005. **16**(2): p. 757-768.
363. Velling, T., et al., *Polymerization of type I and III collagens is dependent on fibronectin and enhanced by integrins alpha 11 beta 1 and alpha 2 beta 1.* Journal of Biological Chemistry, 2002. **277**(40): p. 37377-37381.
364. Sabatier, L., et al., *Fibrillin Assembly Requires Fibronectin.* Molecular Biology of the Cell, 2009. **20**(3): p. 846-858.

365. Twal, W.O., et al., *Fibulin-1 suppression of fibronectin-regulated cell adhesion and motility.* Journal of Cell Science, 2001. **114**(24): p. 4587-4598.
366. Dallas, S.L., et al., *Fibronectin regulates latent transforming growth factor-beta (TGF beta) by controlling matrix assembly of latent TGF beta-binding protein-1.* J Biol Chem, 2005. **280**(19): p. 18871-80.
367. Chung, C.Y. and H.P. Erickson, *Glycosaminoglycans modulate fibronectin matrix assembly and are essential for matrix incorporation of tenascin-C.* Journal of Cell Science, 1997. **110**: p. 1413-1419.
368. Huang, G.R., et al., *Fibronectin Binds and Enhances the Activity of Bone Morphogenetic Protein 1.* Journal of Biological Chemistry, 2009. **284**(38): p. 25879-25888.
369. Wijelath, E.S., et al., *Heparin-II domain of fibronectin is a vascular endothelial growth factor-binding domain - Enhancement of VEGF biological activity by a singular growth factor/matrix protein synergism.* Circulation Research, 2006. **99**(8): p. 853-860.
370. Todorovic, V., et al., *Latent TGF-beta binding proteins.* Int J Biochem Cell Biol, 2005. **37**(1): p. 38-41.
371. Muro, A.F., et al., *An essential role for fibronectin EDA in pulmonary fibrosis.* Am J Respir Crit Care Med, 2008. **177**(6): p. 638-45.
372. Saharinen, J. and J. Keski-Oja, *Specific sequence motif of 8-Cys repeats of TGF-beta binding proteins, LTBPs, creates a hydrophobic interaction surface for binding of small latent TGF-beta.* Molecular Biology of the Cell, 2000. **11**(8): p. 2691-2704.
373. Nunes, I., et al., *Latent transforming growth factor-beta binding protein domains involved in activation and transglutaminase-dependent cross-linking of latent transforming growth factor-beta.* J Cell Biol, 1997. **136**(5): p. 1151-63.
374. Sternlicht, M.D. and Z. Werb, *How MMPs regulate cell behavior.* Annual Review of Cell and Developmental Biology, 2001. **17**: p. 463-516.
375. Massova, I., et al., *Matrix metalloproteinases: structures, evolution, and diversification.* Faseb Journal, 1998. **12**(12): p. 1075-1095.
376. Egeblad, M. and Z. Werb, *New functions for the matrix metalloproteinases in cancer progression.* Nature Reviews Cancer, 2002. **2**(3): p. 161-174.
377. Nagase, H. and J.F. Woessner, *Matrix metalloproteinases.* Journal of Biological Chemistry, 1999. **274**(31): p. 21491-21494.
378. Piccard, H., P.E. Van den Steen, and G. Opdenakker, *Hemopexin domains as multifunctional liganding modules in matrix metalloproteinases and other proteins.* J Leukoc Biol, 2007. **81**(4): p. 870-92.
379. Knäuper, V., et al., *Biochemical characterization of human collagenase-3.* J Biol Chem, 1996. **271**(3): p. 1544-50.
380. Murphy, G., et al., *Assessment of the role of the fibronectin-like domain of gelatinase-a by analysis of a deletion mutant.* Journal of Biological Chemistry, 1994. **269**(9): p. 6632-6636.

381. Shipley, J.M., et al., *The structural basis for the elastolytic activity of the 92-kDa and 72-kDa gelatinases.* Journal of Biological Chemistry, 1996. **271**(8): p. 4335-4341.
382. Itoh, Y., et al., *Membrane type 4 matrix metalloproteinase (MT4-MMP, MMP17) is a glycosylphosphatidylinositol-anchored proteinase.* Journal of Biological Chemistry, 1999. **274**(48): p. 34260-34266.
383. Park, H.I., et al., *Identification and characterization of human endometase (matrix metalloproteinase-26) from endometrial tumor.* Journal of Biological Chemistry, 2000. **275**(27): p. 20540-20544.
384. Woessner, J.F., *Matrix Metalloproteinases and their inhibitors in connective-tissue remodeling.* Faseb Journal, 1991. **5**(8): p. 2145-2154.
385. Vanwart, H.E. and H. Birkedalhansen, *The cysteine switch - a principle of regulation of metalloproteinase activity with potential applicability to the entire matrix metalloproteinase gene family.* Proceedings of the National Academy of Sciences of the United States of America, 1990. **87**(14): p. 5578-5582.
386. Pei, D.Q. and S.J. Weiss, *Furin-dependent intracellular activation of the human stromelysin-3 zymogen.* Nature, 1995. **375**(6528): p. 244-247.
387. Strongin, A.Y., et al., *Mechanism of cell-surface activation of 72-kDa type-iv collagenase: isolation of activate form of membrane metalloprotease.* Journal of Biological Chemistry, 1995. **270**(10): p. 5331-5338.
388. Deryugina, E.I., et al., *MT1-MMP initiates activation of pro-MMP-2 and integrin alpha v beta 3 promotes maturation of MMP2 in breast carcinoma cells.* Experimental Cell Research, 2001. **263**(2): p. 209-223.
389. Lehti, K., et al., *Regulation of membrane-type-1 matrix metalloproteinase activity by its cytoplasmic domain.* Journal of Biological Chemistry, 2000. **275**(20): p. 15006-15013.
390. Morrison, C.J., et al., *Cellular activation of MMP2 (gelatinase A) by MT2-MMP occurs via a TIMP-2-independent pathway.* Journal of Biological Chemistry, 2001. **276**(50): p. 47402-47410.
391. Yu, Q. and I. Stamenkovic, *Localization of matrix metalloproteinase 9 to the cell surface provides a mechanism for CD44-mediated tumor invasion.* Genes & Development, 1999. **13**(1): p. 35-48.
392. Yu, Q. and I. Stamenkovic, *Cell surface-localized MMP-9 proteolytically activates TGF-beta and promotes tumor invasion and angiogenesis.* Genes & Development, 2000. **14**(2): p. 163-176.
393. Imai, K., et al., *Membrane-type matrix metalloproteinase 1 is a gelatinolytic enzyme and is secreted in a complex with tissue inhibitor of metalloproteinases 2.* Cancer Research, 1996. **56**(12): p. 2707-2710.
394. Gomez, D.E., et al., *Tissue inhibitors of metalloproteinases: Structure, regulation and biological functions.* European Journal of Cell Biology, 1997. **74**(2): p. 111-122.
395. Heath, J.K., J.J. Reynolds, and M.C. Meikle, *Osteopetrotic (gray-lethal) bone produces collagenase and timp in organ-culture - regulation by*

vitamin-A. Biochemical and Biophysical Research Communications, 1990. **168**(3): p. 1171-1176.
396. Koshikawa, N., et al., *Role of cell surface metalloprotease MT1-MMP in epithelial cell migration over laminin-5.* Journal of Cell Biology, 2000. **148**(3): p. 615-624.
397. Uria, J.A., et al., *Differential effects of transforming growth factor-beta on the expression of collagenase-1 and collagenase-3 in human fibroblasts.* Journal of Biological Chemistry, 1998. **273**(16): p. 9769-9777.
398. Shrivastava, A., et al., *An orphan receptor tyrosine kinase family whose members serve as nonintegrin collagen receptors.* Molecular Cell, 1997. **1**(1): p. 25-34.
399. Vogel, W., et al., *The discoidin domain receptor tyrosine kinases are activated by collagen.* Molecular Cell, 1997. **1**(1): p. 13-23.
400. Noe, V., et al., *Release of an invasion promoter E-cadherin fragment by matrilysin and stromelysin-1.* Journal of Cell Science, 2001. **114**(1): p. 111-118.
401. Kajita, M., et al., *Membrane-type 1 matrix metalloproteinase cleaves CD44 and promotes cell migration.* Journal of Cell Biology, 2001. **153**(5): p. 893-904.
402. Manes, S., et al., *Identification of insulin-like growth factor-binding protein-1 as a potential physiological substrate for human stromelysin-3.* Journal of Biological Chemistry, 1997. **272**(41): p. 25706-25712.
403. Whitelock, J.M., et al., *The degradation of human endothelial cell-derived perlecan and release of bound basic fibroblast growth factor by stromelysin, collagenase, plasmin, and heparanases.* Journal of Biological Chemistry, 1996. **271**(17): p. 10079-10086.
404. Levi, E., et al., *Matrix metalloproteinase 2 releases active soluble ectodomain of fibroblast growth factor receptor 1.* Proceedings of the National Academy of Sciences of the United States of America, 1996. **93**(14): p. 7069-7074.
405. Codony-Servat, J., et al., *Cleavage of the HER2 ectodomain is a pervanadate-activable process that is inhibited by the tissue inhibitor of metalloproteases-1 in breast cancer cells.* Cancer Research, 1999. **59**(6): p. 1196-1201.
406. Vecchi, M., et al., *Tyrosine phosphorylation and proteolysis - Pervanadate-induced, metalloprotease-dependent cleavage of the ErbB-4 receptor and amphiregulin.* Journal of Biological Chemistry, 1998. **273**(32): p. 20589-20595.
407. Nath, D., et al., *Shedding of c-Met is regulated by crosstalk between a G-protein coupled receptor and the EGF receptor and is mediated by a TIMP-3 sensitive metalloproteinase.* Journal of Cell Science, 2001. **114**(6): p. 1213-1220.
408. Fischer, A., *Mechanism of the proteolytic activity of malignant tissue cells.* Nature, 1946. **157**: p. 442.

409. Minn, A.J., et al., *Genes that mediate breast cancer metastasis to lung.* Nature, 2005. **436**(7050): p. 518-524.
410. Duffy, M.J., et al., *Metalloproteinases: role in breast carcinogenesis, invasion and metastasis.* Breast Cancer Research, 2000. **2**(4): p. 252-257.
411. Curran, S. and G.I. Murray, *Matrix metalloproteinases in tumour invasion and metastasis.* Journal of Pathology, 1999. **189**(3): p. 300-308.
412. Overall, C.M. and C. Lopez-Otin, *Strategies for MMP inhibition in cancer: Innovations for the post-trial era.* Nature Reviews Cancer, 2002. **2**(9): p. 657-672.
413. Coussens, L.M., B. Fingleton, and L.M. Matrisian, *Cancer therapy - Matrix metalloproteinase inhibitors and cancer: Trials and tribulations.* Science, 2002. **295**(5564): p. 2387-2392.
414. Fingleton, B., *Matrix metalloproteinase inhibitors for cancer therapy: the current situation and future prospects.* Expert Opinion on Therapeutic Targets, 2003. **7**(3): p. 385-397.
415. Lopez-Otin, C. and L.M. Matrisian, *Tumour micro environment - Opinion - Emerging roles of proteases in tumour suppression.* Nature Reviews Cancer, 2007. **7**(10): p. 800-808.
416. Heppner, K.J., et al., *Expression of most matrix metalloproteinase family members in breast cancer represents a tumor-induced host response.* American Journal of Pathology, 1996. **149**(1): p. 273-282.
417. Nielsen, B.S., et al., *Collagenase-3 expression in breast myofibroblasts as a molecular marker of transition of ductal carcinoma in situ lesions to invasive ductal carcinomas.* Cancer Res, 2001. **61**(19): p. 7091-100.
418. Crawford, H.C., et al., *The PEA3 subfamily of Ets transcription factors synergizes with beta-catenin-LEF-1 to activate matrilysin transcription in intestinal tumors.* Molecular and Cellular Biology, 2001. **21**(4): p. 1370-1383.
419. Sun, Y.B., et al., *p53 down-regulates human matrix metalloproteinase-1 (collagenase-1) gene expression.* Journal of Biological Chemistry, 1999. **274**(17): p. 11535-11540.
420. Sun, Y.B., et al., *Wild type and mutant p53 differentially regulate the gene expression of human collagenase-3 (hMMP-13).* Journal of Biological Chemistry, 2000. **275**(15): p. 11327-11332.
421. Polette, M., et al., *Gelatinase-A expression and localization in human breast cancers - an in-situ hybridization study and immunohistochemical detection using confocal microscopy.* Virchows Archiv-an International Journal of Pathology, 1994. **424**(6): p. 641-645.
422. Balbin, M., et al., *Loss of collagenase-2 confers increased skin tumor susceptibility to male mice.* Nature Genetics, 2003. **35**(3): p. 252-257.
423. Montel, V., et al., *Altered metastatic behavior of human breast cancer cells after experimental manipulation of matrix metalloproteinase 8 gene expression.* Cancer Research, 2004. **64**(5): p. 1687-1694.

424. Sarper, M., et al., *Loss of MMP8 in DCIS-associated myoepithelial cells contributes to tumour promotion through altered adhesive and proteolytic function.* Breast Cancer Research, 2017. **19**.
425. Gorrin-Rivas, M.J., et al., *Mouse macrophage metalloelastase gene transfer into a murine melanoma suppresses primary tumor growth by halting angiogenesis.* Clinical Cancer Research, 2000. **6**(5): p. 1647-1654.
426. Dong, Z.Y., et al., *Macrophage-derived metalloelastase is responsible for the generation of angiostatin in Lewis lung carcinoma.* Cell, 1997. **88**(6): p. 801-810.
427. Bergers, G., et al., *Effects of angiogenesis inhibitors on multistage carcinogenesis in mice.* Science, 1999. **284**(5415): p. 808-812.
428. Koolwijk, P., et al., *Proteolysis of the urokinase-type plasminogen activator receptor by metalloproteinase-12: implication for angiogenesis in fibrin matrices.* Blood, 2001. **97**(10): p. 3123-3131.
429. Savinov, A.Y., et al., *Matrix metalloproteinase 26 proteolysis of the NH2-terminal domain of the estrogen receptor beta correlates with the survival of breast cancer patients.* Cancer Research, 2006. **66**(5): p. 2716-2724.
430. Sternlicht, M.D., et al., *The stromal proteinase MMP3/stromelysin-1 promotes mammary carcinogenesis.* Cell, 1999. **98**(2): p. 137-146.
431. McCawley, L.J., et al., *A protective role for matrix metalloproteinase-3 in squamous cell carcinoma.* Cancer Research, 2004. **64**(19): p. 6965-6972.
432. Coussens, L.M., et al., *MMP-9 supplied by bone marrow-derived cells contributes to skin carcinogenesis.* Cell, 2000. **103**(3): p. 481-490.
433. Andarawewa, K.L., et al., *Dual stromelysin-3 function during natural mouse mammary tumor virus-ras tumor progression.* Cancer Research, 2003. **63**(18): p. 5844-5849.
434. Wu, E.X., et al., *Stromelysin-3 suppresses tumor cell apoptosis in a murine model.* Journal of Cellular Biochemistry, 2001. **82**(4): p. 549-555.
435. Boulay, A., et al., *High cancer cell death in syngeneic tumors developed in host mice deficient for the stromelysin-3 matrix metalloproteinase.* Cancer Research, 2001. **61**(5): p. 2189-2193.
436. Baserga, R., *The contradictions of the insulin-like growth factor 1 receptor.* Oncogene, 2000. **19**(49): p. 5574-5581.
437. Pendas, A.M., et al., *Diet-induced obesity and reduced skin cancer susceptibility in matrix metalloproteinase 19-deficient mice.* Molecular and Cellular Biology, 2004. **24**(12): p. 5304-5313.
438. Jost, M., et al., *Earlier onset of tumoral angiogenesis in MMP-19-deficient mice.* Cancer Res, 2006. **66**(10): p. 5234-41.
439. Gomm, J.J., et al., *Isolation of pure populations of epithelial and myoepithelial cells from the normal human mammary gland using immunomagnetic separation with Dynabeads.* Anal Biochem, 1995. **226**(1): p. 91-9.
440. O'Hare, M.J., et al., *Conditional immortalization of freshly isolated human mammary fibroblasts and endothelial cells.* Proc Natl Acad Sci U S A, 2001. **98**(2): p. 646-51.

441. Duffy, S.W., et al., *Mammographic density and breast cancer risk in breast screening assessment cases and women with a family history of breast cancer.* European Journal of Cancer, 2018. **88**: p. 48-56.
442. Place, A.E., S.J. Huh, and K. Polyak, *The microenvironment in breast cancer progression: biology and implications for treatment.* Breast Cancer Research, 2011. **13**(6).
443. Reisfeld, R.A., *The tumor microenvironment: a target for combination therapy of breast cancer.* Crit Rev Oncog, 2013. **18**(1-2): p. 115-33.
444. Lagios, M.D., *Heterogeneity of duct carcinoma in-situ (DCIS) - relationship of grade and subtype analysis to local recurrence and risk of invasive transformation.* Cancer Letters, 1995. **90**(1): p. 97-102.
445. Price, P., et al., *DCIS: predictors of local recurrence and progression in patients treated by surgery alone.* Br J Cancer, 1990. **61**(6): p. 869-72.
446. Hattar, R., et al., *Tamoxifen induces pleiotrophic changes in mammary stroma resulting in extracellular matrix that suppresses transformed phenotypes.* Breast Cancer Research, 2009. **11**(1).
447. Elosegui-Artola, A., et al., *Rigidity sensing and adaptation through regulation of integrin types.* Nat Mater, 2014. **13**(6): p. 631-7.
448. Thomas, G.J., et al., *AlphaVbeta6 integrin promotes invasion of squamous carcinoma cells through up-regulation of matrix metalloproteinase-9.* Int J Cancer, 2001. **92**(5): p. 641-50.
449. Leeman, M.F., S. Curran, and G.I. Murray, *The structure, regulation, and function of human matrix metalloproteinase-13.* Critical Reviews in Biochemistry and Molecular Biology, 2002. **37**(3): p. 149-166.
450. Masood, S., S.J. Sim, and L. Lu, *Immunohistochemical differentiation of atypical hyperplasia vs. carcinoma in situ of the breast.* Cancer Detect Prev, 1992. **16**(4): p. 225-35.
451. Kumar, S. and V. Weaver, *Mechanics, malignancy, and metastasis: The force journey of a tumor cell.* Cancer and Metastasis Reviews, 2009. **28**(1-2): p. 113-127.
452. Samuel, M.S., et al., *Actomyosin-mediated cellular tension drives increased tissue stiffness and beta-catenin activation to induce epidermal hyperplasia and tumor growth.* Cancer Cell, 2011. **19**(6): p. 776-791.
453. Hinz, B., et al., *Recent developments in myofibroblast biology paradigms for connective tissue remodeling.* American Journal of Pathology, 2012. **180**(4): p. 1340-1355.
454. Hijova, E., *Matrix metalloproteinases: their biological functions and clinical implications.* Bratisl Lek Listy, 2005. **106**(3): p. 127-32.
455. Yamamoto, Y., et al., *Quantitative diagnosis of breast tumors by morphometric classification of microenvironmental myoepithelial cells using a machine learning approach.* Scientific Reports, 2017. **7**.
456. Stylianopoulos, T., L.L. Munn, and R.K. Jain, *Reengineering the physical microenvironment of tumors to improve drug delivery and efficacy: from mathematical modeling to bench to bedside.* Trends in Cancer, 2018. **4**(4): p. 292-319.

SUPPLEMENTARY

	Tissue area % (range)		
	Epithelium	Stroma	Adipose
Normal	1% (1-6%)	9% (2-17%)	83 (79-95%)
DCIS			
Non-High Grade	5% (1-8%)	16% (7-31%)	79% (67-92%)
High Grade	12% (4-45%)	25% (8-63%)	62% (11-86%)
DCIS/IDC	14% (2-42%)	21% (4-33%)	65% (45-84%)

Supplementary Table S1. Tissue composition of the final serial section of DCIS and DCIS with associated invasion

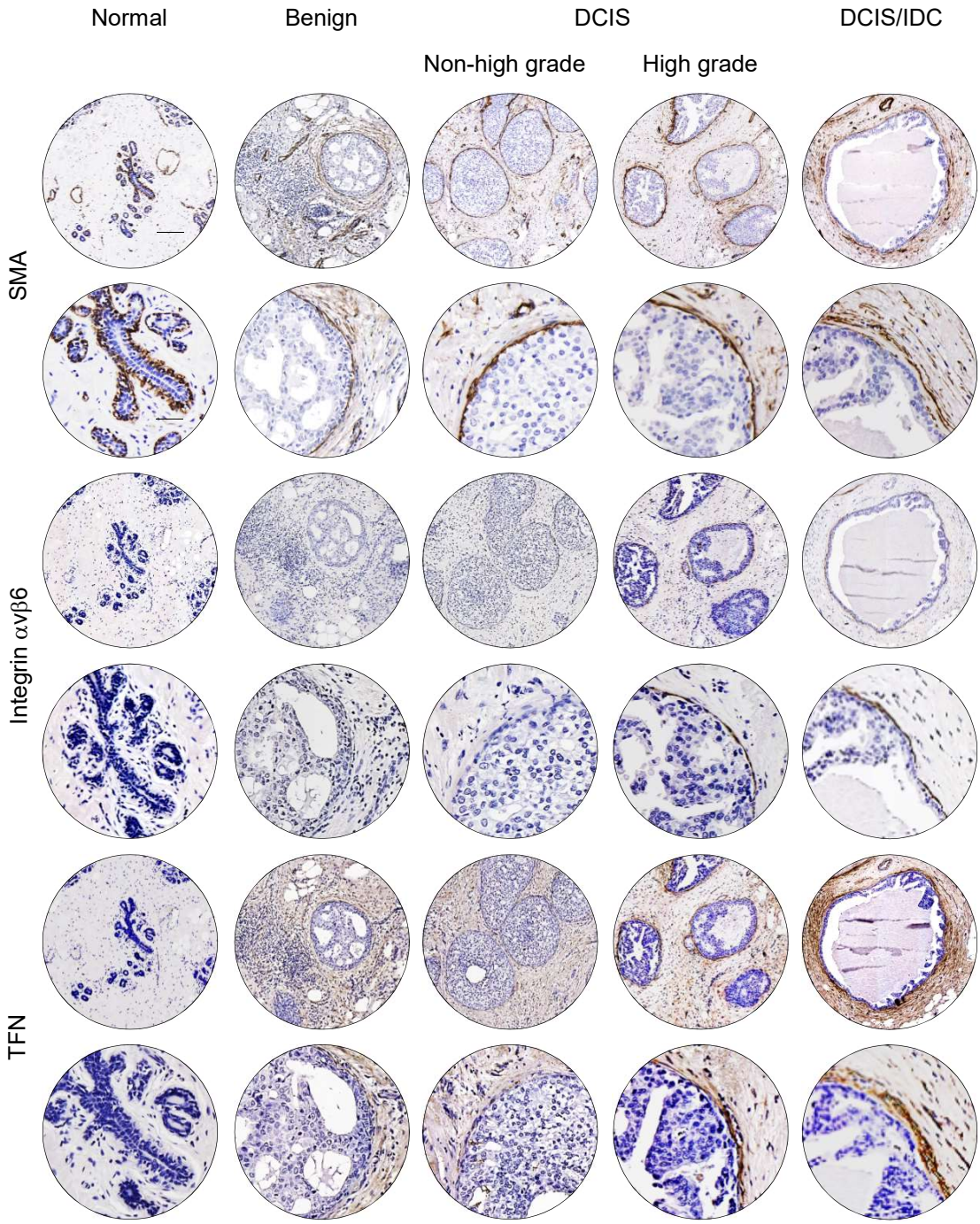

Supplementary Figure S1. DCIS progression is accompanied by upregulation of integrin αvβ6 by myoepithelial cells and increased periductal fibronectin deposition. Immunohistological staining of human breast tumour samples (staining for SMA; panel 1-2, integrin αvβ6; panel 3-4, and TFN; panel 5-6) featuring areas of normal, benign, DCIS (non-high grade and high grade) and DCIS/IDC. Magnification x5 and x20. Scale bar, 200μm and 100μm, respectively. Representative images are shown.

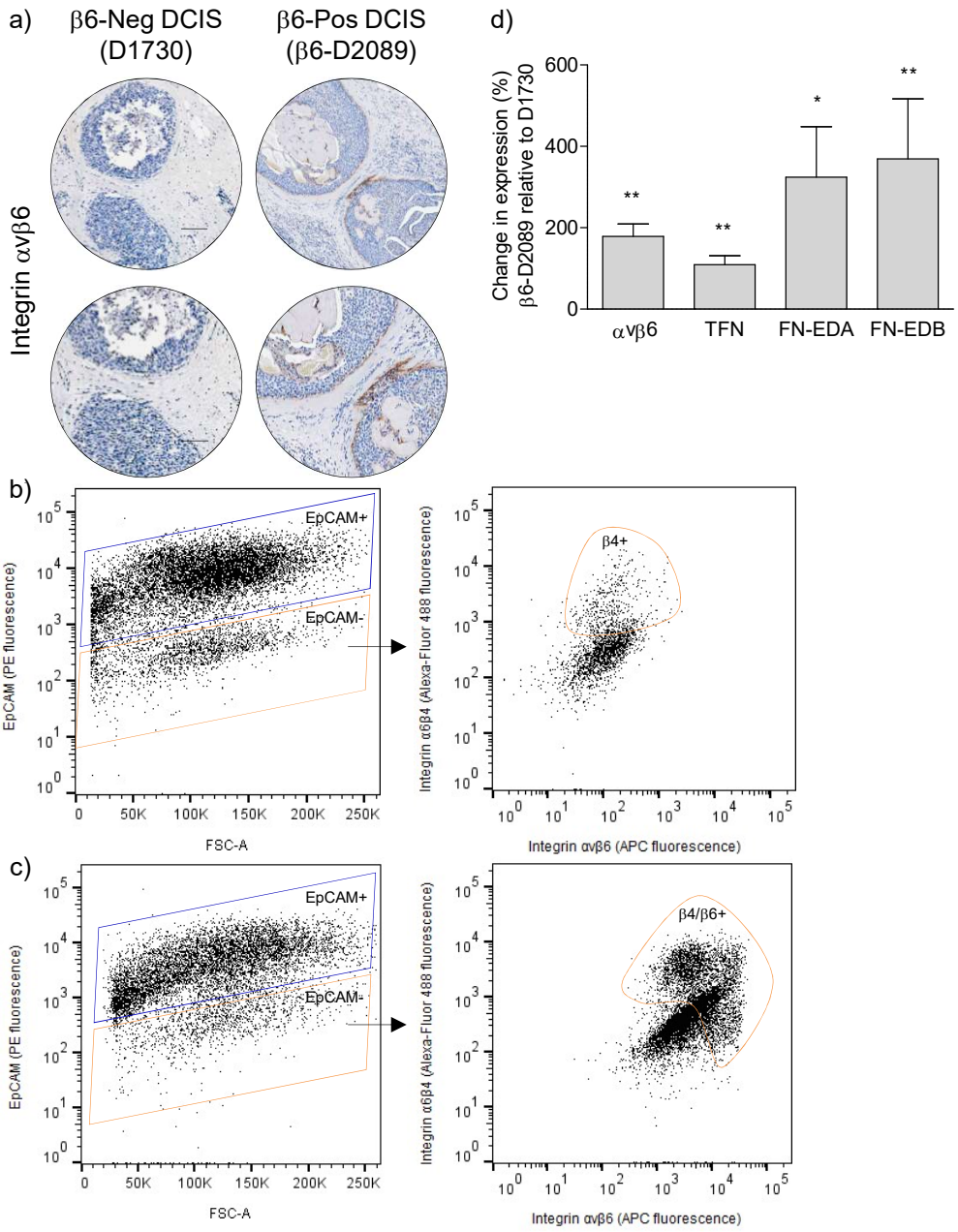

Supplementary Figure S2. Integrin αvβ6-positive primary DCIS-myoepithelial cells upregulate fibronectin expression. a) Immunohistochemical images of an integrin αvβ6-negative and integrin αvβ6-positive DCIS case is shown (additional patients in Supplementary Figure S2). Magnification x5 and x10. Scale bar, 200μm and 100μm, respectively. b, c) FACS plots of DCIS organoid samples; D1730 (b) and β6-D2089 (c) separated by the expression of EpCAM (phycoerythrin (PE) fluorescence; blue gate), integrin α6β4 and αvβ6 (Alexa-Fluor 488 and allophycocyanin (APC) fluorescence, respectively; orange gate). d) qRT-PCR analysis of integrin αvβ6, TFN, FN-EDA and FN-EDB mRNA levels in D1730 and β6-D2089. The values are presented as the mean percentage change in expression relative to D1730. Representative images are shown, and analyses is shown as a mean of 3 independent experiments ±SEM. p-value ≤0.001 ('***'), ≤0.01 ('**') and ≤0.05 ('*') were considered significant, 'ns' indicates not significant.

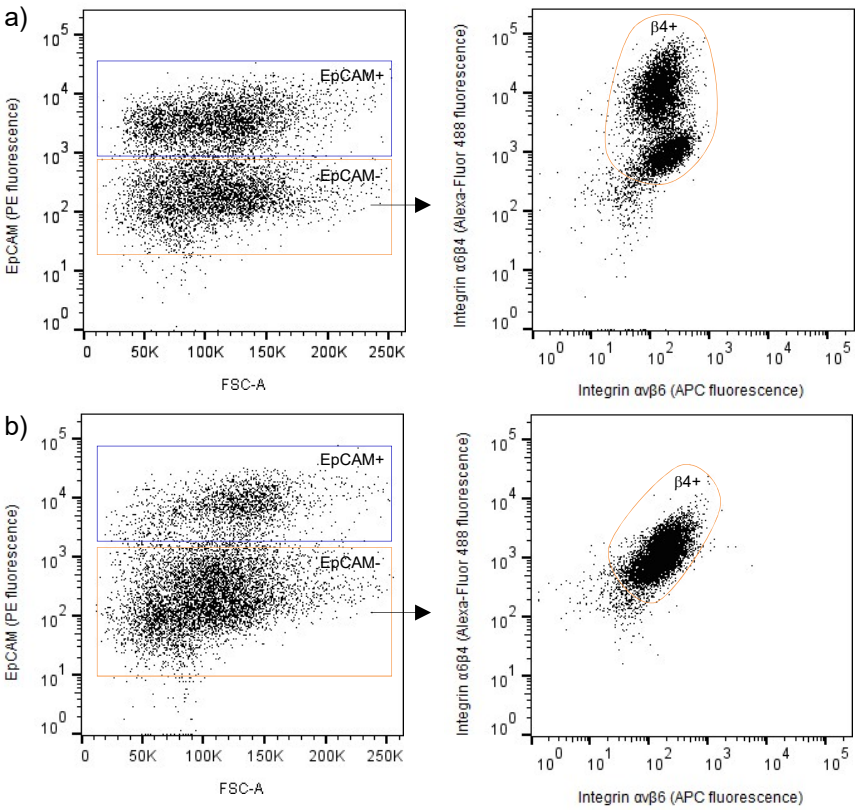

Supplementary Figure S3. Primary normal myoepithelial cells lack integrin αvβ6 expression. a, b) FACS plots of reduction mammoplasty organoid samples; N-1989 (a) and N-3002 (b) separated by the expression of EpCAM (phycoerythrin (PE) fluorescence; blue gate), integrin α6β4 and αvβ6 (Alexa-Fluor 488 and allophycocyanin (APC) fluorescence, respectively; orange gate).

Supplementary Figure S4. Integrin αvβ6-positive myoepithelial cell line upregulates MMP9 expression. Gelatin zymography for MMP9 expression in cCM from N-1089 and β6-1089, and 1μg/mL recombinant MMP9 (rMMP9; lane 1-3). No expression of MMP2 was detected in gelatin zymography (data not shown).

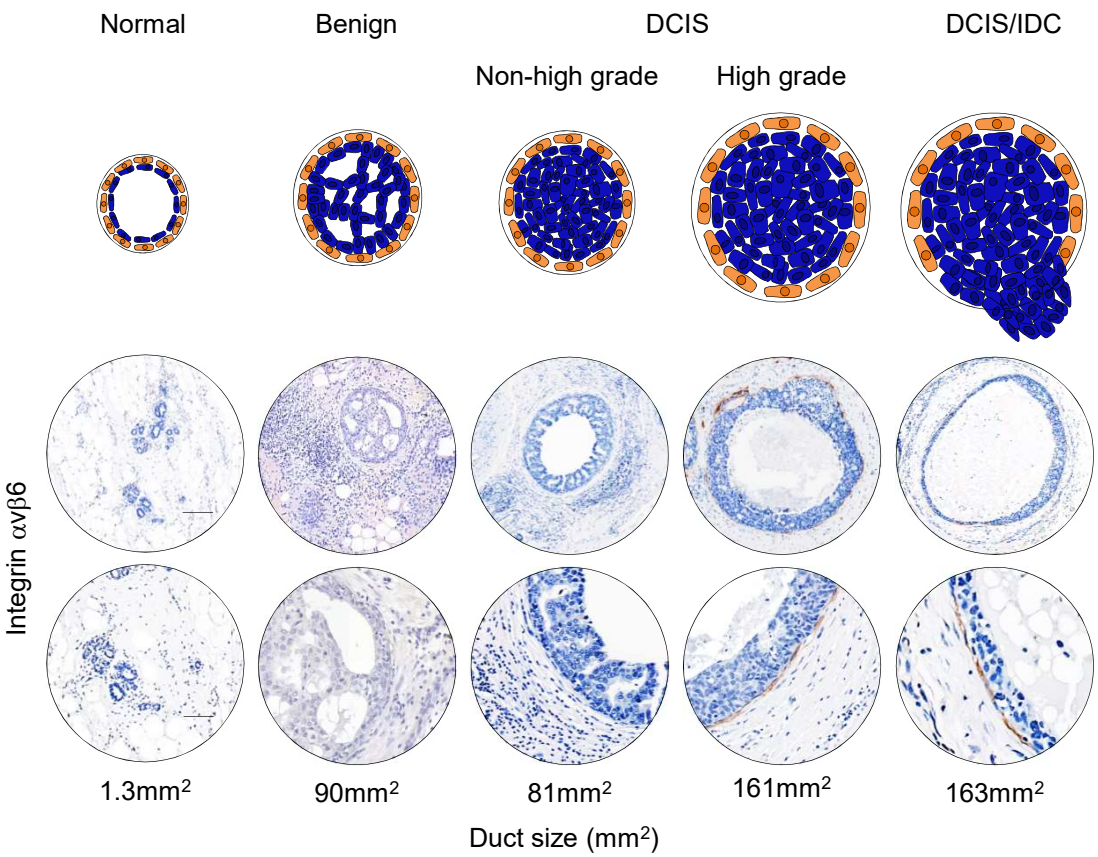

Supplementary Figure S5. Duct expansion in benign and DCIS lesions. a) Immunohistological staining of human breast tumour samples (staining for integrin αvβ6; panel 2-3) featuring normal breast, benign, DCIS (non-high grade and high grade) and DCIS/IDC ducts. Magnification x5 and x20. Scale bar, 200μm and 100μm, respectively. Representative images are shown.

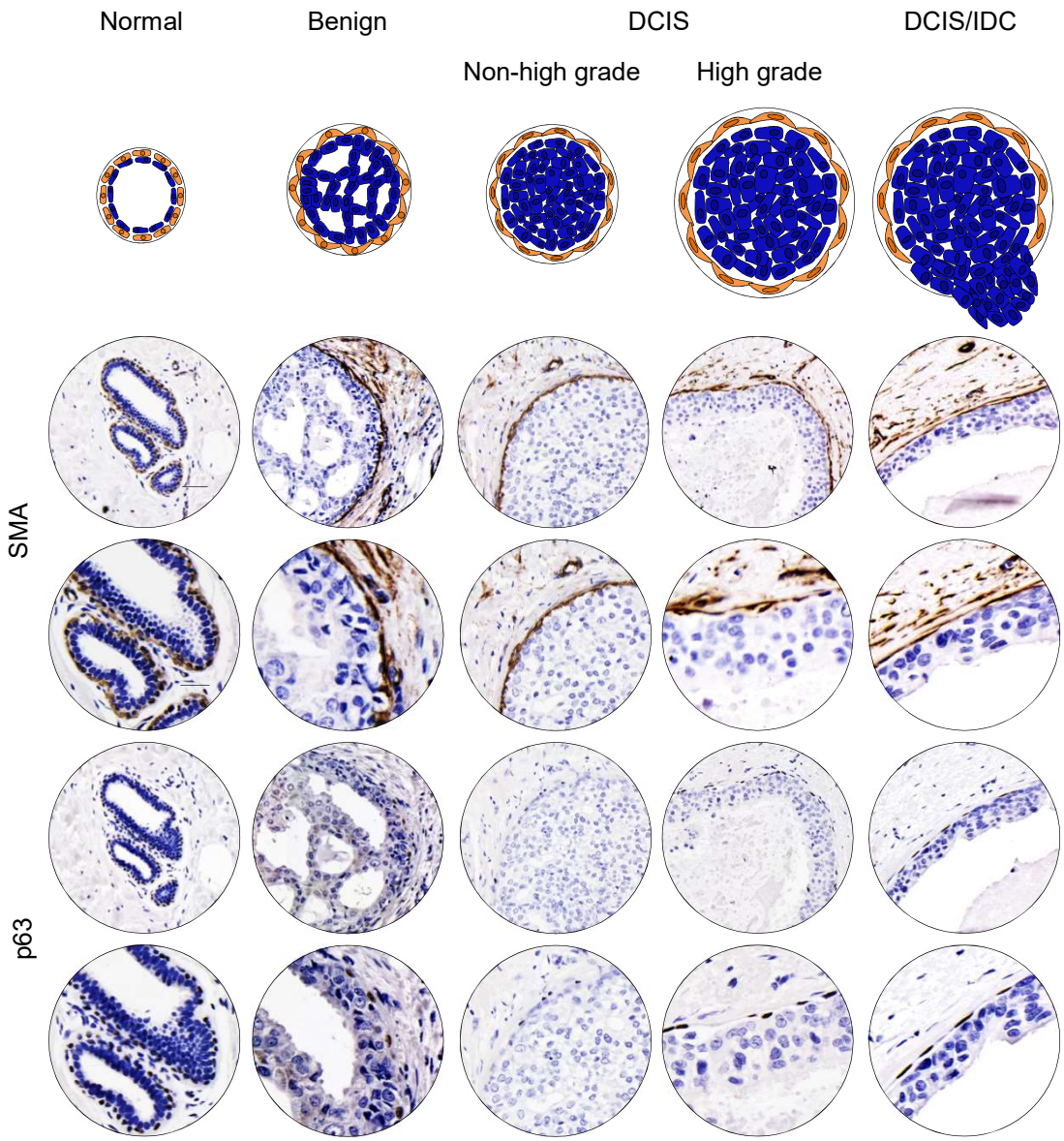

Supplementary Figure S6. Morphological changes in myoepithelial cells in benign and DCIS lesions. a) Immunohistological staining of human breast tumour samples (staining for SMA; panel 2-3 and p63; panel 4-5) featuring normal breast, benign, DCIS (non-high grade and high grade) and DCIS/IDC ducts. Magnification ×20 and x40. Scale bar, 50μm and 25μm, respectively. Representative images are shown.

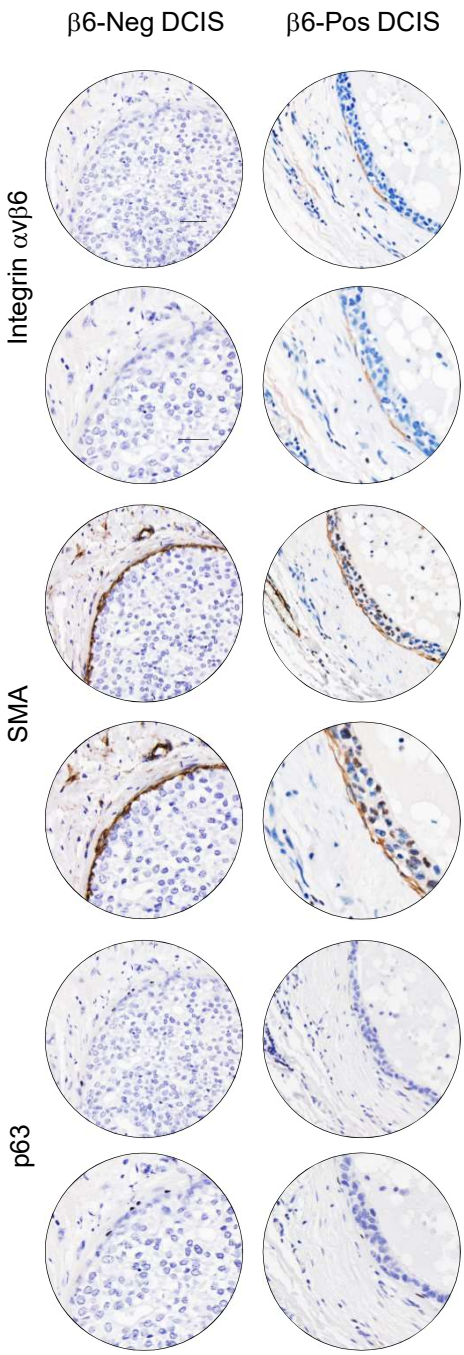

Supplementary Figure S7. Morphological changes in myoepithelial cells in DCIS correlate with integrin αvβ6 expression. a) Immunohistological staining of human breast tumour samples (staining for integrin αvβ6; panel 1-2, SMA; panel 3-4 and p63; panel 5-6) featuring DCIS ducts with and without the expression of integrin αvβ6. Magnification ×20 and x40. Scale bar, 50μm and 25μm, respectively. Representative images are shown.